Master of Science in Aerospace Engineering

# Onset Theory

(Strain Invariant Failure Theory)
Consistent Approach and Automation

Simon Baar

Delft University of Technology • Faculty of Aerospace Engineering • Department of Aerospace Structures and Materials



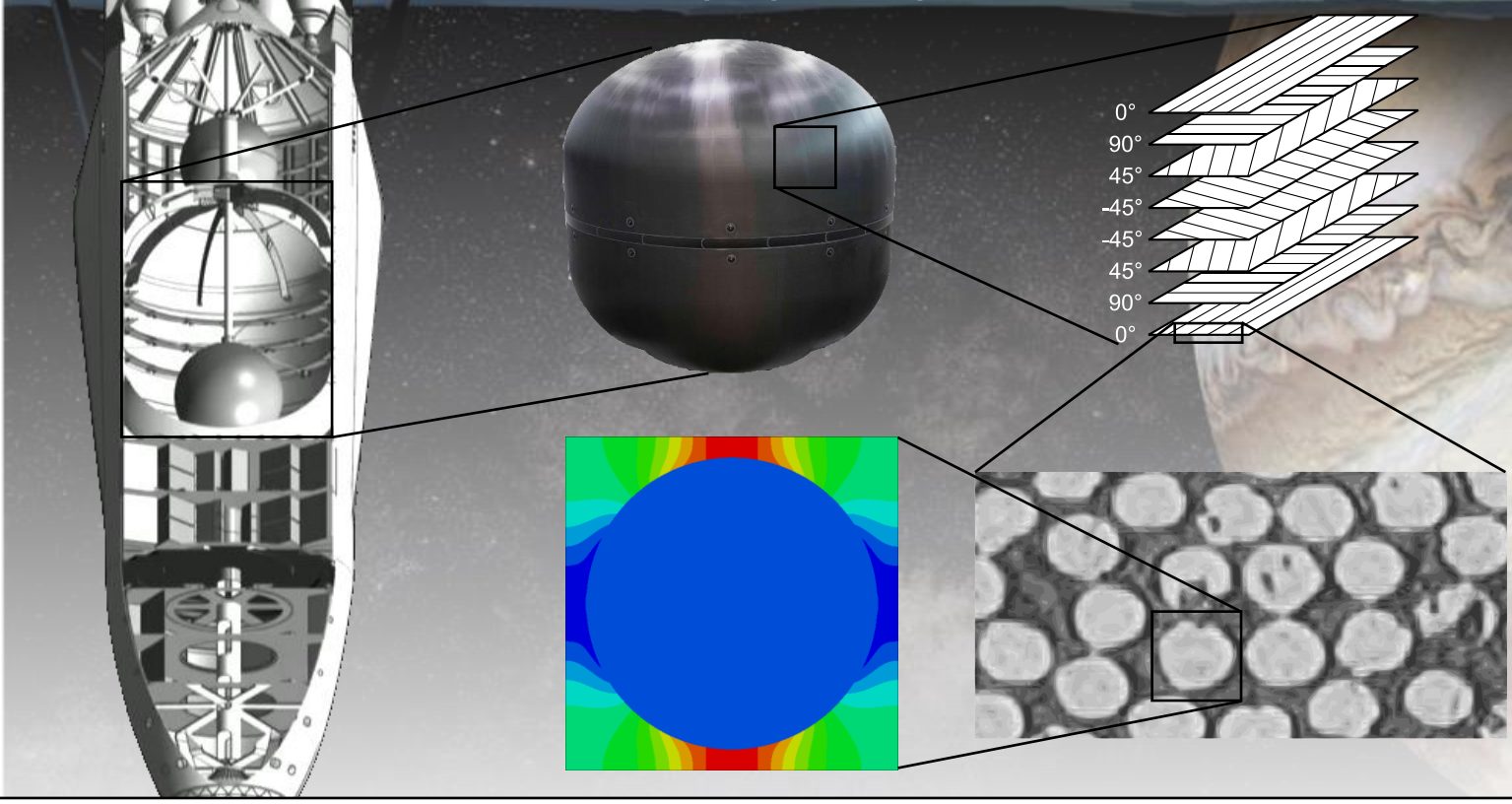


TU Delft

ATG europe

# Onset Theory (Strain Invariant Failure Theory)

## Consistent Approach and Automation

by

**Simon Baar**

in partial fulfillment of the requirements for the degree of

**Master of Science**

in Aerospace Engineering

at Delft University of Technology, Faculty of Aerospace Engineering, Department of Aerospace Structures and Materials

to be defended publicly on 27 February 2017 at 9:30am.

The work in this thesis was completed with significant support from ATG Europe B.V. (http://www.atg-europe.com/). Their cooperation is gratefully acknowledged.


Delft University of Technology

Faculty of Aerospace Engineering

Department of Aerospace Structures and Materials

**GRADUATION COMMITTEE**

Chair of Committee:

Dr. Sergio Turteltaub
Delft University of Technology

Committee Members:

Dr. Christos Kassapoglou
Daily Supervisor

Dr. Derek Gransden
Delft University of Technology

ir. Leonid Pavlov
ATG Europe, B.V.
Company Supervisor

# Abstract

Many composite failure criteria suffer from serious flaws related to prediction accuracy and the number of tests required to apply them, as found for example during the World Wide Failure Exercises. In 2001, Jon Gosse of Boeing Phantom Works developed a new criterion for matrix failure. Initially known as Strain Invariant Failure Theory (SIFT), it was soon extended through collaboration with John Hart-Smith to also include fiber failure. During this process, it was also renamed to Onset Theory.

Onset Theory predicts failure using micromechanically obtained strain invariants in the constituents of a composite. As a physics-based criterion, it is claimed to be applicable to all types of loading, boundary conditions, geometries, and layups. However, it has yet to see widespread application.

In this thesis, a consistent approach to Onset Theory has been developed. This addresses and resolves the contradictions found in literature regarding the exact details of the application of Onset Theory. In addition to that, failure envelopes are generated for comparison with laminate test data. Previously, finite element models were required for each specimen and state of strain. In this thesis, the entire process has been automated for ease and speed of applicability.

Using the consistent, automated approach, Onset Theory is shown to quite accurately predict failure in composite laminates under biaxial strains. This includes non-catastrophic matrix cracking preceding ultimate failure, without the necessity of performing a progressive failure analysis. Onset Theory also correctly captures trends in the difference between lamina and laminate failure. Most importantly, it only requires a single set of critical strain invariants (three in total), regardless of loading condition or stacking sequence. This means that extensive and expensive testing can be reduced significantly.

# Acknowledgments

Looking back, many coincidental events and chance encounters were not quite so coincidental or chance after all. I am grateful for that, and in particular for having been endowed with the skills that helped me reach this point. Things working out helped along the way, but things not working out sometimes helped even more. By getting a scholarship for my exchange year, I would have missed out on the best host family and friends I can possibly imagine. By knowing what I wanted to do after high school, I might not have ended up in Delft, missing out on more great friends (and the perfect field of studies). By not spending a somewhat miserable semester abroad, I would not have learned some very important lessons about myself and my motivation to get out of bed in the morning. By being accepted for some internships, I would not have ended up with the job I am about to start. I guess the lesson from all this is that everything in life happens for a reason.

This list could be continued endlessly. However, what is most important are the people involved. So – thank you, Christos, for providing me with countless hours of career and life advice, going far above and beyond the duties of a professor. It made me a better engineer and person. Thanks is also due to ATG Europe for providing me with this thesis opportunity. In particular, thank you, Leonid – not only for being the other party in one of those chance encounters, but also for providing awesome guidance (and a sufficient amount of mean comments…) to get me through this thesis successfully and with a smile. However, the medal for the meanest comments and surprise nerf gun attacks – besides some very useful life advice – goes to Samo. Just like everybody else at ATG, you made the experience of working here for almost a year a very pleasant one.

Other people I am very grateful to include Jon Gosse for clarifying some questions regarding Onset Theory, and Sergio and Derek for agreeing to be on my thesis committee (had they known how long this thesis would turn out to be, they probably would – and should – have refused…).

This page is almost full, so I have to wrap up. Thanks is due to my host family, as well as my friends all over the world, who continue to inspire me to do my best every day – while also keeping me in check if I run the risk of turning arrogant. Both of these are equally important. Finally, a big thank you to my parents for raising and supporting me in countless ways for those last almost 25 years. In particular, thanks for educating me such that I realize that not all of life's questions are to be approached with an engineering mindset.

Delft University of Technology — Simon Baar
February 18, 2017

"The hardest thing to explain is the glaringly evident which everybody has decided not to see."

—Ayn Rand, The Fountainhead

# Table of Contents



 

# List of Figures

# List of Matrices and Tables

# List of Symbols and Abbreviations

| | |
|---|---|
| $\boldsymbol{A}$ | Vector of thermal amplification factors |
| Directions 1, 2, 3 | Principal directions (e.g. for principal strains) |
| Directions 11, 22, 33 or $x$, $y$, $z$ | Directions in any orthogonal coordinate system. Used interchangeably. |
| $\boldsymbol{C}$ | Stiffness matrix |
| $C_{ij}$ | Component of stiffness matrix |
| $E_i$ | Young's modulus (in a certain direction) |
| $G_{ij}$ | Shear modulus (in a certain direction) |
| $\boldsymbol{I}$ | Identity matrix |
| IF | Interfiber (location in the matrix where fibers are closest together) |
| IS | Interstitial (location in the matrix where fibers are furthest apart) |
| $J_1$ | First invariant of the strain tensor |
| $J_2'$ | Second invariant of the strain deviator tensor |
| $\boldsymbol{M}$ | Matrix of mechanical amplification factors |
| $\boldsymbol{Q}$ | Reduced stiffness matrix (assuming plane stress) |
| QI | Quasi-isotropic |
| $\boldsymbol{S}$ | Compliance matrix |
| $\boldsymbol{T}$ | In-plane rotation matrix |
| $t$ | Thickness (typically of a ply) |
| $S_{ij}$ | Component of compliance matrix |

| | |
|---|---|
| SIFT | **S**train **I**nvariant **F**ailure **T**heory (also known as Onset Theory) |
| Superscript "*" | Critical value (e.g. $J_1^*$) |
| Superscript "f" | Fiber property |
| Superscript "m" | Matrix property |
| $u$, $v$, $w$ | Displacements in $x$-, $y$- and $z$-directions, respectively |
| $V_f$ | Fiber volume fraction |
| WWFE | **W**orld **W**ide **F**ailure **E**xercise |
| $x_0$, $x_1$, $y_0$, $y_1$, $z_0$, $z_1$ | Faces of a unit cell |
| $\alpha_i$ | Thermal expansion coefficient (in a certain direction) |
| $\gamma_{ij}$ | Engineering shear strain ($\gamma_{ij} = 2\epsilon_{ij}$, $i \neq j$) |
| $\Delta T$ | Temperature difference |
| $\boldsymbol{\epsilon}$ | Strain vector |
| $\epsilon_{eqv}$ | Equivalent (von Mises) strain |
| $\epsilon_i$ or $\epsilon_{ij}$ | Strain component (principal or in any orthogonal coordinate system, respectively) |
| $\boldsymbol{\Theta}$ | Unit cell rotation matrix |
| $\theta$ | Various angles |
| $\nu_{ij}$ | Poisson's ratio in a certain direction |
| $\boldsymbol{\Pi}$ | Poisson's effect matrix (usually with subscripts $\epsilon_x$, $\epsilon_y$ or biaxial) |
| $\rho$ | Density |
| $\boldsymbol{\sigma}$ | Stress vector |
| $\sigma_{ij}$ | Stress component |
| $\tau_{ij}$ | Engineering shear stress ($i \neq j$) |
| $\boldsymbol{\Omega}$ | Strain rotation matrix from laminate to ply coordinate system |
| # | Number |

# Chapter 1

# Introduction to Onset Theory

For several decades there has been an ongoing discussion on the validity of commonly used failure criteria for composites. John Hart-Smith in particular has been an adamant opponent of most existing theories, claiming that they are a *"plethora of meaningless smooth curves passed through unrelated data points"* (Hart-Smith, 1991, p. 1510). However, there has also been some less belligerent investigation, in particular as part of the World Wide Failure Exercise (WWFE). Its outcome was that there are indeed severe shortcomings with all present failure criteria (Hinton, Kaddour, & Soden, 2002). The authors therefore recommended to develop physics-based, more accurate failure criteria. They also identified the need to improve the accessibility of the criteria. A major point of criticism was that most theories are quite complex and require significant time and effort to be implemented in a form that is suitable for everyday design work.

In 2001, a new physics-based failure criterion was proposed by (Gosse & Christensen, 2001). Called Strain Invariant Failure Theory (SIFT), it attempts to predict failure at the level of constituents rather than for a homogenized ply. Since its original conception, SIFT has been renamed to Onset Theory (Pipes & Gosse, 2009). Both names will be used interchangeably in this thesis.

Section 1.1 in the current chapter provides an overview of the motivation and general ideas behind Onset Theory. Subsequently, the similarities and differences with other failure theories, as well as evidence supporting SIFT, are discussed in Sections 1.2 and 1.3. Finally, Sections 1.4 and 1.5 outline the purpose and scope of the present research.

Chapter 2 contains an overview of the information on Onset Theory found in literature. Various contradictions are discovered, which are resolved by developing a detailed, consistent approach in Chapter 3. This also addresses the first point of criticism raised by the authors of the WWFE, namely that composite failure theories are too complex to be usable. Subsequently, Chapter 4 covers the second point of criticism by developing a software tool to automatically apply SIFT in a manner suitable for everyday design work. Chapter 5 details verification efforts for theory and implementation. In Chapter 6 Onset Theory is validated using experimental data, while Chapter 7 contains further research enabled by the availability of an automated software tool. Chapter 8 contains the conclusions and recommendations resulting from the work done in the previous chapters.

## 1.1 Motivation and Basic Principle[1]

During the WWFE several composite failure criteria were evaluated, including Tsai-Wu, maximum strain, and maximum stress (which at the time were the most commonly used failure criteria (C. T. Sun, Quinn, Tao, & Oplinger, 1996, fig. 1)). Additional advanced failure criteria were also included in the comparison. Based on the results, the authors concluded that none of the theories was able to correctly predict either initial or final strength of multidirectional laminates (Hinton et al., 2002). The ultimate strength of a laminate could be predicted to within $\pm 50\%$ at best.

In the years since there has been little improvement. The second WWFE showed that the predictions by the best theories were within 10% of the experimental data in only 30% of the test cases (Kaddour & Hinton, 2013). Even after adjusting the criteria to match the test data, this number did not increase beyond 40%. In other words, in 60% of the cases predictions will be more than 10% off, even when using the best available failure theories and fine-tuning them to the test data. For the third WWFE, the comparison with experimental data does not seem to be available yet at the time of this writing, but there is a significant spread of predictions seen in (Kaddour, Hinton, Smith, & Li, 2013). This means that at least some theories have to be incorrect.

The result of the lack of credibility of existing failure theories leads to the reliance on expensive and extensive tests as the predominant means of designing and certifying composite structures. For example, (Paris, 2001) cites close to 10 000 coupons being tested by Boeing during the design of a composite helicopter. This process has to be repeated for every new material and structure.

The main issue with many failure criteria is that they are not physics-based. Instead of evaluating failure of the individual constituents of the composite, failure criteria such as Tsai-Wu use a smooth, interactive failure envelope for each ply, essentially curve-fitting test data. This works well as long as failure predictions are made close to the load conditions used to determine the envelope. However, in general fiber and matrix failure have to be considered separately (C. T. Sun et al., 1996).

Several attempts have been made to solve this issue. One of them is a new theory developed by Boeing about 15 years ago. Referred to initially as the Strain Invariant Failure Theory (SIFT) and later on as Onset Theory, it uses the first and second invariants of the strain tensor as criteria for failure. In fact, through the second invariant SIFT relies on the same mechanism as the von Mises yield criterion for metals. SIFT, as a failure theory for composites, adds the first invariant to the theory and uses micromechanics to identify individual constituent strains. Its fundamental proposition is that failure of a composite occurs if one of the strain invariants exceeds its critical value.

For other failure criteria failure is often characterized in terms of an interaction of the longitudinal and transverse tension and compression strengths of a lamina. Contrary to that Onset Theory takes into account two non-interactive fundamental failure modes for each of the constituents: failure due to dilatation (change in volume) through the first invariant, and failure in distortion (change in shape) through the second. The type of load by which they are triggered is considered irrelevant. In this way, SIFT attempts to investigate the underlying phenomena and failure mechanisms.

[1] A similar version of this section has been handed in for AE4010 Research Methodologies.

## 1.2 Comparison with Other Failure Theories

One of the most prominent distinguishing aspects of Onset Theory is the evaluation of failure at a constituent level rather than at the homogenized ply level, as stated before. This means that it predicts the actual failure mode and constituent which fails, instead of predicting an entire ply to be failed with no distinction between for example transverse matrix cracking and fiber breakage.

Another advantage of SIFT is its use of physics-based failure criteria which reduce to well-established failure criteria for isotropic materials. It is relatively complex due to the necessity to determine the local fiber and matrix strains. However, the underlying failure analysis is quite simple. In other words, the micromechanical enhancement explained in Subsection 2.1.4 is a (micro)structural analysis, similar to calculating strains in a skin/stringer combination made of different materials. Once the local strains are available, the failure theory works regardless of the material type (metal, carbon fiber, or epoxy matrix). While this type of general applicability is not a necessary requirement for a proper failure criterion, it would be expected from a true physics-based failure criterion.

Some of the input data for the micromechanical enhancement can be difficult to obtain. In particular, the full set of anisotropic elasticity constants for a single carbon fiber is not readily available. According to (Soden, Hinton, & Kaddour, 1998) they are in fact back-calculated (using micromechanics) from tests on a unidirectional lamina. However, this is still far more straightforward than the rather arbitrary determination of the $F_{12}$ interaction parameter in Tsai-Wu (see e.g. (Bergmann, 1998) for a discussion of this issue). Other criteria suffer from similar shortcomings. For example, (Puck, Kopp, & Knops, 2002) published "guidelines for the determination of the parameters in Puck's action plane strength criterion" (title of the paper), containing statements such as "validated data for $p_{\perp\perp}^{(-)}$ [...] do not exist", or "no clues concerning reasonable values for $p_{\perp\perp}^{(+)}$ exist apart from the presumption that all inclination parameters should be approximately of the same magnitude".

In particular for Tsai-Wu, the result of having unknown, unmeasurable parameters in the theory is that they are "tuned" to achieve good correlation with an existing database. This is true for phenomenological criteria in general. On the other hand, Onset Theory only uses a single reference strength per failure mode, rather than arbitrarily adjusting several parameters to match existing test data. The adjustment process also makes it very difficult for other researchers to reproduce results or apply a phenomenological criterion in general, because the required adjustment process is not based on physical reasoning but depends on the intuition of the researcher.

While phenomenological criteria show good results close to existing tests, they make new designs (in particular radically new ones) difficult because a new test database has to be created every time. SIFT, on the other hand, is in theory applicable to the *"general condition (all possible laminate stacking sequences, structural geometries, loading and boundary conditions)"* (Gosse, 2004a, p. 1).

This last statement, in fact, is the primary stipulated advantage of SIFT over any other failure criterion. Once the strain amplification factors have been computed and the critical invariants determined, no additional tests are required regardless of the structure being investigated.

In summary, this means that SIFT seems to be a very promising theory to predict failure of composites. Whether there is indeed any credibility to the theory is explored further in Section 1.3.

## 1.3 Supporting Evidence

Before any significant amount of effort is spent on the details of Onset Theory, it should be investigated whether there is any credible supporting evidence in the published literature so far.

One of the main arguments made by (Gosse & Christensen, 2001) during their development of Onset Theory is that the critical strain invariants do not change for various tests, whereas the critical values for failure criteria such as maximum strain vary significantly. However, this result would be expected from the original authors of the theory. What is of more interest is evidence provided by other researchers. If such evidence does not exist, the reasons should be explored carefully. While this could be the case due to the complexity of the theory or lack of awareness of the existence of the theory, it is quite likely to instead be an indicator that the theory is not performing (well).

Fortunately, there are three different types of evidence that lend credence to Onset Theory. First of all, there is indeed a number of researchers and research groups only loosely associated with the original authors, who do report good results using Onset Theory. Most of them did have some form of collaboration in place. However, this seems to mostly be about understanding the theory and obtaining critical invariants. This type of evidence is discussed in Subsection 1.3.1.

Secondly, several researchers showed that the two critical invariants for the matrix are independent of each other, based on series of tests. This is a crucial difference to other failure theories. Typically, the same test (e.g. longitudinal tensile strength) is repeated several times to obtain statistical information on the distribution of test results. The issue with this strategy is that it can at best confirm that the tests are carried out in a consistent manner. A theory for which the critical values are determined based on for example longitudinal tensile tests cannot be confirmed by retesting longitudinal tension. A different test would be needed. To this extent Onset Theory employs redundant testing. Several different tests are carried out for each critical invariant. This confirms or invalidates the theory (according to which the results should be identical) and also makes it possible to easily spot a faulty test without repeating the same test over and over again (Hart-Smith, 2010). Subsections 1.3.2 and 6.2.1 show how redundant testing results in evidence supporting Onset Theory.

Another form of redundancy, also confirming the propositions of SIFT, is visible in the results by (Z. Li, Guan, & He, 2011), who showed that the invariants for one constituent are independent of the other constituent. This is discussed in more detail in Subsection 6.2.1.

As the third type of evidence, it can be argued that there is some consistency in the critical values obtained years apart by researchers from different countries, as investigated in detail in Section 6.2.

Together with the other two arguments, it is clear that Onset Theory certainly deserves a detailed investigation. There are several different researchers who all report good correlation with test data, better than the one achieved with other common failure criteria; the critical matrix invariants are independent of each other, as shown by redundant (as opposed to repeated) testing; and the results are reproducible by different researchers. This is strong evidence for at least a certain level of credibility of the theory. The subsequent two sections contain more details on the supporting evidence.

### 1.3.1 Results by Independent Researchers

One of the noteworthy research groups is based at the National University of Singapore. In a series of PhD theses and published articles, predictions are made regarding progressive failure of a composite beam subject to 3-point bending (see e.g. (Tay, Tan, Tan, & Gosse, 2005)). These predictions matched the type and location of damage rather closely.

Another research group from the University of New South Wales (Australia) also investigated a variety of different complex structures (in particular T-joints and curved beams under 4-point bending (R. Li, Kelly, & Ness, 2003), as well as the bearing strength of bolted joints (Pearce & Kelly, 2012)) and also observed a good correlation between predictions and test data.

Neither of these publications have dedicated comparisons between predictions made using SIFT and predictions from other failure criteria. However, the PhD thesis of one of the researchers does contain additional information (Tan, 2005). SIFT and Tsai-Wu are combined with a damage progression algorithm called the "Element-Failure Method" (EFM). Using SIFT results in the good agreement reported in (Tay, Tan, Tan, et al., 2005). On the other hand, Tsai-Wu is judged to be unsuitable because it does not yield predictions comparable to the experimental results. On first glance, this seems like a very strong argument in favor of SIFT. However, it is unclear whether the discrepancy when using EFM in combination with Tsai-Wu is due to the EFM part or the Tsai-Wu part. EFM in combination with SIFT is the focus of the thesis. Therefore, it is likely that EFM is being fine-tuned such that in combination with SIFT it gives good correlation with the existing experimental data. This is further supported by the fact that the critical invariants are obtained from Jon Gosse, the original author of SIFT, even though the materials are different (Gosse used IM7/977-3, whereas the thesis is using T800H/924C). In addition to that, the strain amplification factors are also taken from Gosse. Both of these factors cast some doubt on the agreement between prediction and test in this thesis. In summary, this means that the EFM part of the failure prediction may simply be fine-tuned towards SIFT. What makes the comparison even less meaningful is the fact that the author acknowledges using Tsai-Wu strength data for a different material combination. Predictions for the T800H/924C material are made using strength values for T300/5208. This means that based on this article no conclusion can be drawn on the validity of SIFT as compared to Tsai-Wu. However, the fact that EFM in combination with SIFT yields good results is still a piece of supporting evidence for SIFT, because the fatal flaw in the comparison lies with the Tsai-Wu criterion.

The presumed fine-tuning of results to the individual test cases is a general point of criticism with all sources stated so far. They investigate single, rather complex test cases, requiring significant adjustments. The question is whether SIFT itself was successful, or whether it was simply working well enough to be fine-tuned – the exact process other failure theories are criticized for in Section 1.2.

Several researchers who are not part of a research group working in collaboration with Gosse have also shown close correspondence between predictions and tests. For example, (Ng, Felsecker, & Meilunas, 2004) found the maximum difference for a number of lamina and laminate tests (including matrix failures) to be less than 18%. In contrast, using Tsai-Wu resulted in very good values for the majority of test specimens (same accuracy as SIFT), but resulted in an error of 56% for a $[0_2, 90_{16}, 0_2]$ laminate (for which SIFT was within 16% of the test data). This is an example of the anticipated advantage of SIFT: while phenomenological failure criteria such as Tsai-Wu can yield

very good results for tests similar as the ones to which the criterion is "tuned", they can be extremely inaccurate outside of the scope of applicability of their "tuning parameters". A true physical failure criterion should be accurate for all conditions. This topic has also been addressed in Section 1.2.

Finally, (Tsai, Alper, & Barrett, 1999) – who were introduced to SIFT by Gosse before its official publication – investigated a variety of configurations of composite bolted joints, such as hot/cold temperatures and double lap joints with different laminates. Using the dilatational criterion for the adhesive (so that micromechanical enhancement as discussed in Subsection 2.1.4 is unnecessary), their conclusion was that the critical $J_1$ values were almost constant. Comparing, the $J_1$ strain at −65°F and 75°F for three different stacking sequences showed a difference of at most 11%. Contrary to that, the other criteria investigated (max. principle stress, von Mises stress, von Mises strain, max. principle strain, and max. peel stress) showed differences of at least 22% and up to 69%.

### 1.3.2 Redundant Testing and Independence of Matrix Invariants

As stated previously, SIFT employs redundant testing to confirm or invalidate the theory. The typical tests carried out to determine the critical matrix invariants are off-axis tension tests at angles varying from 10° to 90° (a 0° test would yield the fiber invariant). This choice is further discussed in Subsection 8.4.4. Besides (Pipes & Gosse, 2009), several other researchers have also shown that the invariants at failure are constant and independent of each other, with one or the other being critical. The switch of failure modes typically occurs around an angle of 20°-30°.

Figure 1.1 shows the matrix invariants at failure for several series of tests. The data for IM7/977-3 is taken from (Pipes & Gosse, 2009, Tables 1 and 2), the data for T300/Cycom 970 and T800s/3900-2 stems from (Tran, 2012, Tables 5-2 and 5-3), the results for IM7/5250-4 were found in (Ng et al., 2004, Table 5), and (Mao, 2011) contained results for E-glass/MTM57. For the critical invariant the average of several tests is used. (Note that this disagrees with only using the maximum result as done in the standard procedure (Hart-Smith, 2010). The purpose here is not to determine the invariant, but to show the consistency between redundant tests. There is therefore sometimes a minor difference between the critical invariants mentioned here and the results reported by the authors in literature.) Open circles indicate tests taken into account for the critical distortional invariant, while dots indicate tests taken into account for the critical dilatational invariant. Note that there are tests for which it is not clear whether the dilatational or distortional invariant caused failure. These tests are taken into account for both critical invariants.

As shown in Figure 1.1, the maximum error is 18.25% (for the critical dilatational invariant of T800s/3900-2). Note that three of the five tests produced identical results, while the other two gave quite different answers. This casts some doubt on their validity. Typical errors for the dilatational invariant are between 5% and 6%, while errors for the distortional invariant are at most 2.87%. This is also due to the typically lower number of tests involved in the distortional invariant.

Clearly, there is very little scatter in the results. Since four different authors observed this behavior for five different materials, the proposition made in Onset Theory that failure occurs once either the dilatational or distortional invariant achieves its critical value, with no interactions between the invariants, seems very plausible.

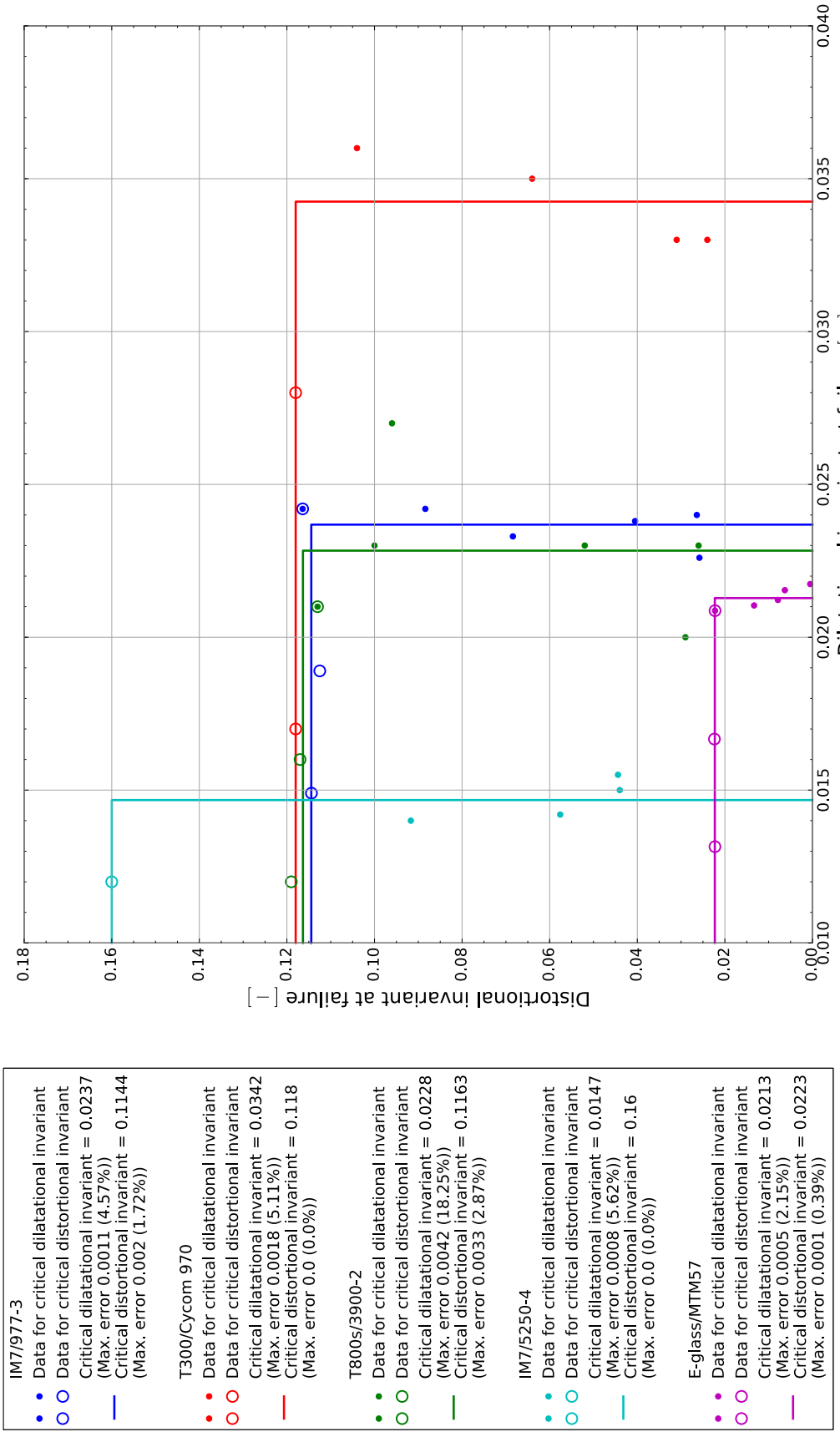


Figure 1.1: Matrix invariants at failure. Sources: (Pipes & Gosse, 2009) for IM7/977-3, (Tran, 2012) for T300/Cycom 970 and T800s/3900-2, (Ng et al., 2004) for IM7/5250-4, and (Mao, 2011) for E-glass/MTM57. The distortional invariant uses different definitions, as discussed in Subsection 6.2.3. Cycom 970 may be rubber toughened (Subsection 6.2.2).

## 1.4 Purpose of Research[1]

From an academic perspective, the basic principle outlined in Section 1.1 already satisfies the question regarding the relevance of SIFT. SIFT promises to improve the understanding of composite failures and to help move away from "curve fitting" to physics based failure criteria. However, SIFT is of course also relevant to industry. Inaccurate failure criteria mean at best added mass due to safety factors and at worst unanticipated failure, while also requiring expensive and time consuming tests. As outlined in Section 1.2 Onset Theory has shown some promising results in the past.

The purpose of the present research can be summarized as follows, with the points discussed in turn in the subsequent paragraphs.

- Development of a consistent approach to Onset Theory
- Development of failure envelope predictions
- Automation of theory (to simplify its application and enable the subsequent goals)
- Validation of theory and sensitivity studies regarding the input parameters
- Further research (in particular regarding trends found in failure envelopes)

In general, development efforts on a new composite failure criterion consist of validating the results and carrying out further research. However, before performing either of these tasks it has to be ensured that the procedure to apply the failure criterion is well-established and consistent. While studying the available literature, it was found that there are significant discrepancies and contradictions in several key aspects of the theory. Therefore, the first main point of focus of the present research is the development of a consistent approach to Onset Theory. Addressing and resolving the existing issues (as found in Chapter 2) is covered in Chapter 3. The need for a consistent approach is also clear based on claims being made by researchers without support by hard evidence. Typically their validity is asserted for the cases investigated. Clearly, there is a need to carry out research in order to prove or refute these claims. In addition to that, until a fundamental proof is found, they should be verified for each new study case. Note that due to the complexity of some of those claims this is only possible if the approach is automated (see third bullet point). One example are the location and number of interrogation points, as explained in Subsection 2.2.7 and Section 3.4.

Besides developing a consistent approach to Onset Theory, failure envelopes are generated automatically. While some developments in this direction exist (such as the analytical prediction of the full state of strain, see Section 3.2), they are not covered in literature. Although Onset Theory has shown promising results in the past, as discussed in Section 1.3 fine-tuning of the results very likely occurred for many of the single, rather complex test cases involved. By predicting standard in-plane failure envelopes, Onset Theory can be compared to tests data such as the WWFE (to which it has not yet been applied), as well as to other failure theories. This topic is also covered in Chapter 3.

A third aspect is automation of the theory. Although SIFT was developed 15 years ago it still has to see widespread application. Part of the issue is the number and complexity of the steps involved.

[1] A similar version of parts of this section has been handed in for AE4010 Research Methodologies.

Unlike commonly used failure criteria, where strength values are substituted into a simple equation, SIFT requires micromechanical finite element models. These models need to be fully parametrized for any combination of constituent properties and fiber volume fraction. In order to make SIFT more usable this step has to be as simple as possible. Therefore, Chapter 4 discusses the development of a software tool to quickly and consistently apply Onset Theory. This tool enables various research initiatives, both within this thesis and possibly also in the future by ATG Europe and TU Delft.

Prediction of failure envelopes and automation together create two possibilities. First of all, as mentioned above the prediction of failure envelopes enables straightforward comparison of theory and test data. In addition to that, it provides an opportunity to conduct quantitative and qualitative sensitivity studies regarding the input parameters used in SIFT, far more visual and intuitive than any other approach. One example would be to determine cases where the predictions made by Onset Theory differ significantly from those made by other failure criteria. Neither of these topics has been discussed thoroughly in literature. They are covered in the respective sections of Chapter 6.

Finally, the availability of a consistent, easy to apply approach to Onset Theory opens up opportunities for further research. Covered in the last section of Chapter 6, these research opportunities concern commonalities between envelopes for different ply orientations and materials, as well as an investigation into random fiber arrays.

In summary, the purpose of this thesis is to resolve the contradictions present in various sources regarding Onset Theory. Using the resulting consistent approach, further development is carried out in order to enable the prediction of failure envelopes. These are a much more suitable tool for validation and further research. Through the automation of the entire process, the criticism of the WWFE related to a lack of usable composite failure criteria is addressed. The consistent approach to Onset Theory, in combination with the failure envelopes generated, is then used for comparison to test data and research. This research includes an investigation of the sensitivity of the failure predictions to the input parameters, as well as possible trends found in the failure envelopes.

## 1.5 Scope of Research

Several limitations are placed on Onset Theory in general and this thesis in particular. Some of them are inherent to SIFT, while other promising topics had to be excluded due to time constraints.

First of all, SIFT only predicts the onset of damage (which is why it has been renamed to Onset Theory). Ultimate failure may or may not, depending on the structure and the applied load, require a subsequent progressive failure analysis. Several approaches have been investigated in literature, such as the Element-Failure Method in (Tay, Tan, Tan, et al., 2005) or Maximum Energy Retention in (Gosse, 2004a). A rather simplistic, unverified possibility is also suggested in Subsection 8.4.3. However, the present research will not focus on these approaches for a number of reasons.

In industry the point where irreversible damage occurs is defined as the ultimate load of a composite. This means that progressive failure analysis is relevant from an academic perspective (and certainly also from a damage tolerance point of view), but is less crucial for preliminary design work. The reason why damage beyond the onset of failure is not accepted is that a real structure experiences random loads. This is different from a laboratory situation where the load state is quite simple and

does not change after damage occurs. While progressive damage analysis might be possible in a laboratory, in a real structure the (unknown) load following the onset of damage may cause catastrophic failure. One example would be a change in load direction, resulting in fiber buckling in compression after (non-catastrophic) matrix cracking. Related to this are issues such as vibrational behavior or stiffness (deflection) limits. In an experiment, a specimen could be carrying loads beyond initial failure, but at the expense of large deflections. This is not acceptable in a real structure.

In addition to that, it is implausible to investigate progressive damage before the problem of predicting initial damage has been solved satisfactorily. Progressive damage analysis can only work once it is credibly known when the damage starts.

Besides excluding progressive failure analysis, determining the critical invariants is also outside the scope of this thesis. Modeling and conducting the tests – while most likely quite straightforward, using the procedure outlined in Subsection 8.4.4 – would presumably not have yielded large knowledge gains. This decision was made based on the large number of available critical invariants summarized in Section 6.2, as well as the findings regarding trends in their values. Since validation is not the primary focus of this thesis, the effort involved in determining the critical invariants would be disproportionate.

This leads to the last major limitation on the scope of the thesis. While some validation effort is carried out in Section 6.3, systematic validation is deferred to further research (see the introduction to Section 8.4). As stated previously, the intent of this thesis is to develop a consistent, easily applicable approach to Onset Theory. The lack of available reliable test data in literature showcases the difficulty of carrying out these tests appropriately. Professional researchers with decades of experience and large budgets for experiments did not manage to develop a truly reliable testing strategy. It seems unlikely that this problem would be solved in this thesis. With the theory well-established and automatically applicable, it is possible to specifically search for load states that confirm or disprove Onset Theory (i.e. where SIFT differs significantly from other failure theories). However, carrying out the required experiments is beyond the scope of this thesis.

# Chapter 2

# Overview of Literature on Onset Theory

The purpose of this chapter is to provide an overview of the literature on Onset Theory. There is consensus on the general steps of the theory, as presented in Section 2.1. However, for the details of each step the literature contains significant contradictions and gaps. This is explored in Section 2.2.

## 2.1 Accepted Fundamental Principles

Onset Theory was first proposed by (Gosse & Christensen, 2001) and further developed by (Buchanan, Gosse, Wollschlager, Ritchey, & Pipes, 2009) as well as (Ritchey, Dustin, Gosse, & Pipes, 2011) (apparently meant as an extension of the second article). (Hart-Smith, 2010) gives another excellent overview of SIFT, including extensive elaboration on the choices made. Since no contradictions were found for the topics in the present section, it is based on all of these sources.

The fundamental proposition behind SIFT is that failure of any material occurs once the critical value of either the dilatational or the distortional strain is exceeded. The dilatational strain is the first invariant of the strain tensor; the distortional strain is the second invariant of the deviatoric strain tensor (i.e. the strain tensor excluding volumetric effects). Using invariants means that the result of the evaluation is independent of the choice of coordinate system.

### 2.1.1 Strain Invariants and Failure Criteria

Typically, the dilatational strain is taken to be given by

$$\begin{aligned} J_1 &= \epsilon_1 + \epsilon_2 + \epsilon_3 \\ &= \epsilon_{11} + \epsilon_{22} + \epsilon_{33}. \end{aligned} \tag{2.1}$$

$\epsilon_{11}$, $\epsilon_{22}$ and $\epsilon_{33}$ are components of any strain tensor using an orthogonal basis (i.e. not necessarily the principal strains $\epsilon_1$, $\epsilon_2$ and $\epsilon_3$).

Both here and in the remainder of this research, directions 11, 22 and 33 will be used interchangeably with $x$, $y$ and $z$ (respectively), whereas directions 1, 2 and 3 refer to the principal directions.

Note that this equation is in fact a reduced version of the dilatational strain; its full expression is $J_1 + J_2 + J_3 = (\epsilon_{11} + 1)(\epsilon_{22} + 1)(\epsilon_{33} + 1) - 1$. However, because $J_2$ is related to the square of strains, and $J_3$ is related to the cube of strains, these terms are negligible for small strains.

For the distortional strain, several versions are used in literature, all related to each other through a direct algebraic operation. The most common version is to use the equivalent strain (also known as von Mises strain due to its resemblance to the well-known von Mises yield criterion for isotropic materials). This version of the distortional strain, see e.g. (Hart-Smith, 2010, Eqn. 4), is given by

$$\begin{aligned} \epsilon_{eqv} &= \sqrt{\frac{1}{2}[(\epsilon_1 - \epsilon_2)^2 + (\epsilon_1 - \epsilon_3)^2 + (\epsilon_2 - \epsilon_3)^2]} \\ &= \sqrt{\frac{1}{2}[(\epsilon_{11} - \epsilon_{22})^2 + (\epsilon_{11} - \epsilon_{33})^2 + (\epsilon_{22} - \epsilon_{33})^2] + \frac{3}{4}[\gamma_{23}^2 + \gamma_{13}^2 + \gamma_{12}^2]}. \end{aligned} \tag{2.2}$$

Note that the second equation uses engineering shear strains, e.g. $\gamma_{23} = 2\epsilon_{23}$ (technically $\gamma_{2233} = 2\epsilon_{2233}$ because any orthogonal coordinate system is acceptable, with directions denoted as 11, 22 and 33). This is also why a factor $\frac{3}{4}$ appears in front of the shear terms, instead of a factor 3.

As mentioned above, various formulations of the distortional strain are found in literature. One option would be using the invariant of the deviatoric strain tensor ($J_2'$) directly rather than the equivalent strain. The relationship between the equivalent strain and the underlying invariant is given by $J_2' = \frac{1}{3}\epsilon_{eqv}^2$. This fact is pointed out by (Tay, Tan, & Liu, 2006) (who do use the equivalent strain, but acknowledge its origin by mentioning the invariant itself as well).

On the other hand, (Pipes & Gosse, 2009) not only mention but actually use an expression which already includes the square root, but does not include the factor 3 found in the equivalent strain. This definition – $\sqrt{\frac{1}{6}[(\epsilon_1 - \epsilon_2)^2 + (\epsilon_1 - \epsilon_3)^2 + (\epsilon_2 - \epsilon_3)^2]}$ – is equal to $\sqrt{J_2'} = \frac{1}{\sqrt{3}}\epsilon_{eqv}$.

In summary, this means that there are at least three possible definitions of the distortional invariant. For the sake of completeness, there is also a fourth definition that seems plausible. This definition (the last one in the list below), while not stated directly in literature, still seems to be used by some of the sources in the list of critical invariants in Section 6.2.

Table 2.1: Possible definitions of the distortional invariant

| | |
|---|---|
| Definition #1 | $\epsilon_{eqv} = \sqrt{3J_2'} = \sqrt{\frac{1}{2}[(\epsilon_1 - \epsilon_2)^2 + (\epsilon_1 - \epsilon_3)^2 + (\epsilon_2 - \epsilon_3)^2]}$ |
| Definition #2 | $\frac{1}{\sqrt{3}}\epsilon_{eqv} = \sqrt{J_2'}$ |
| Definition #3 | $\epsilon_{eqv}^2 = 3J_2'$ |
| Definition #4 | $\frac{1}{3}\epsilon_{eqv}^2 = J_2'$ |

While none of these conflicting definitions pose a serious problem because the critical values can easily be converted, their presence still tends to lead to confusion or incorrect results if critical values based on a different definition are used. This will become particularly relevant in Section 6.2.

Using an asterisk to indicate the critical value, the failure criteria are then simply defined as

$$J_1 > J_1^* \tag{2.3}$$

$$\epsilon_{eqv} > \epsilon_{eqv}^* \tag{2.4}$$

One aspect which should be mentioned briefly here is the type of invariants used. Some researchers opt to use stress invariants instead of strain invariants. However, as discussed in detail in Subsection 2.2.1, strain invariants should be used in combination with strain-based test data.

### 2.1.2 Included Constituents and Failure Modes

Simply switching to the use of strain invariants as failure criterion alone would be unlikely to create a large improvement over existing failure criteria. However, in SIFT an additional step takes place: failure is investigated at the constituent level rather than on a per-ply basis.

For a typical composite, the constituents are fiber and matrix. The matrix can fail due to either the dilatational or the distortional strain exceeding their respective critical values. Regarding the fibers, the situation is more complicated. Carbon fibers do not appear to fail due to dilatation (Hart-Smith, 2010). However, for glass fibers the situation is not as clear, and the same source states that dilatation definitely occurs for boron fibers. In summary, this means that for typical carbon/epoxy composites, three failure modes are relevant: $J_1$-failure of the matrix, $\epsilon_{eqv}$-failure of the matrix, and $\epsilon_{eqv}$-failure of the fiber; for other materials, all four invariants may have to be taken into account.

One aspect that has not yet been touched upon is the failure of the interface (sizing) between fibers and matrix. (Hart-Smith, 2010) argues that this interface is a material aspect, rather than a structural one: “It is the responsibility of the materials and processes groups to ensure that the potential interface problems are not allowed to become a task for the structures engineers to deal with” (Hart-Smith, 2010, p. 4272). In essence, his point is that no composite should ever fail in the sizing first, because that would mean that the matrix and fiber are unable to achieve their full strength. While in theory composites with such a weak interface could be produced, they would not be very useful. Their analysis is outside the scope of SIFT as currently investigated.

Hart-Smith makes an additional argument related to the fact that the critical invariants are established based on tests of a cured composite rather than the individual constituents. This means that the interface is inherently included in the measured critical values, assuming the production process results in a repeatable and durable interface. This also means that if the interface does not influence the failure load, then the failure prediction based on SIFT will also not change if the interface is changed. On the other hand, if the failure load does change with a change in interface (which should not be the case based on the previous paragraph, because this would indicate the interface being the weak link), then this will in turn be included in the critical invariants, and the failure predictions will change accordingly. Note that this latter case would probably limit SIFT to a certain test data base because whether or not interface failure occurs would depend on the type of loading, so the critical invariants would be different depending on the occurrence of interface failure.

In conclusion, this means that interface (sizing) failure is not of particular interest for the scope of SIFT investigated at this point.

### 2.1.3 Unit Cells (Representative Volume Elements)

As explained in Subsection 2.1.2, SIFT investigates failure separately for fiber and matrix. The constituent strains are obtained using micromechanical analysis. This aspect is quite unique to Onset Theory, although there are some other theories (e.g. multicontinuum theory (Mayes & Hansen, 2004) or micromechanics of failure (Ha, Jin, & Huang, 2008)) which also employ micromechanics.

Ideally, a composite would be modeled completely in terms of its constituents. In that case, one would simply generate a pseudo-random distribution of fibers and use it for further analysis. However, doing so is computationally infeasible. Therefore, so-called representative volume elements, also known as unit cells, are commonly used to characterize a composite based on the properties of its constituents. In general, this is quite successful (C. T. Sun & Vaidya, 1996).

Unit cells are finite element models of a single complete fiber and its surroundings. Instead of the true, random microstructure, they represent one of several commonly found geometrical configurations, also known as fiber array types. Typical fiber array types are the square and hexagonal unit cells shown in Figure 2.1. Another commonly used unit cell uses a diamond arrangement (Figure 2.2). Note that all fibers are assumed to be circular. Based on Figure 2.1, this seems reasonable.

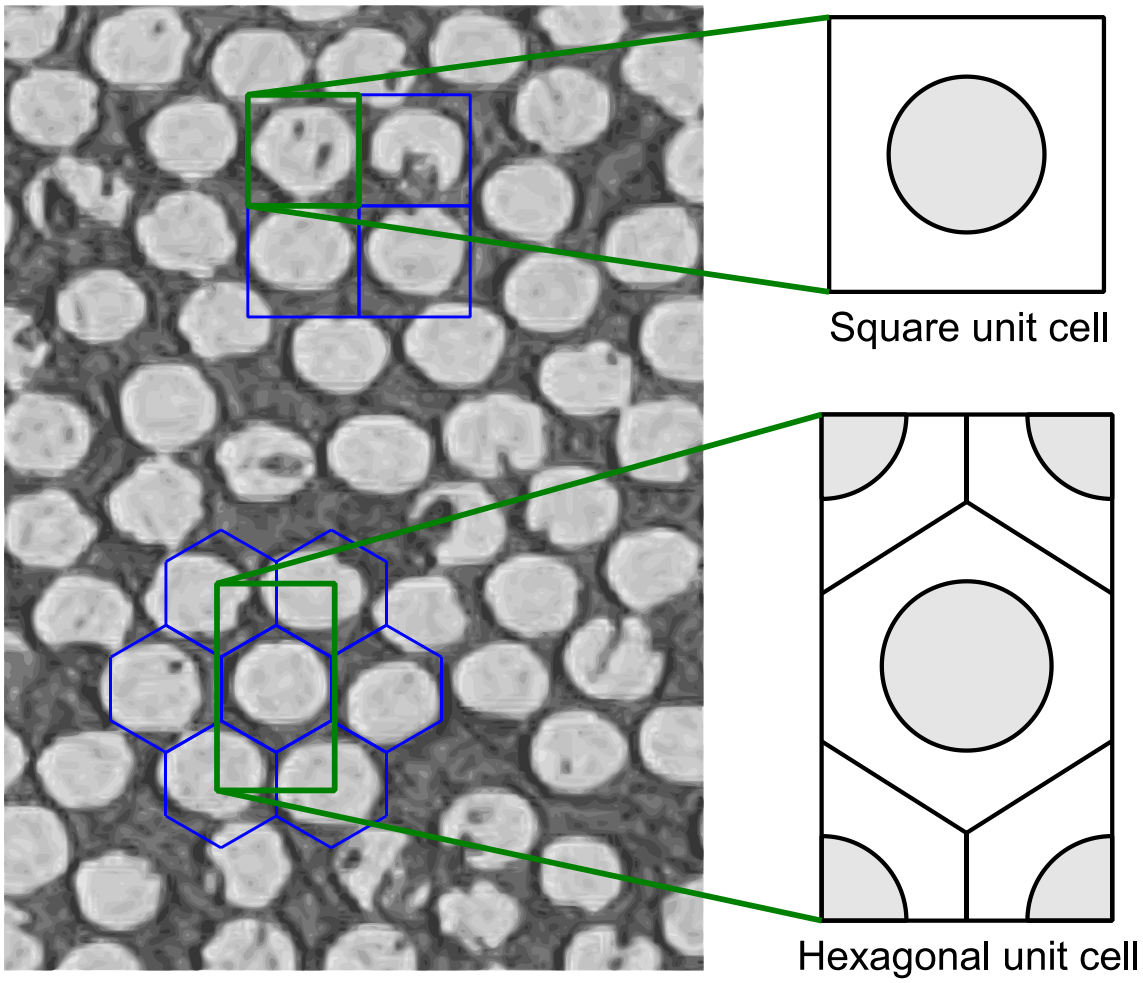


Figure 2.1: Square and hexagonal geometrical configurations represented by unit cells. Microscopy image taken from (Hrstka, Kučerová, Lepš, & Zeman, 2003, fig. 4).

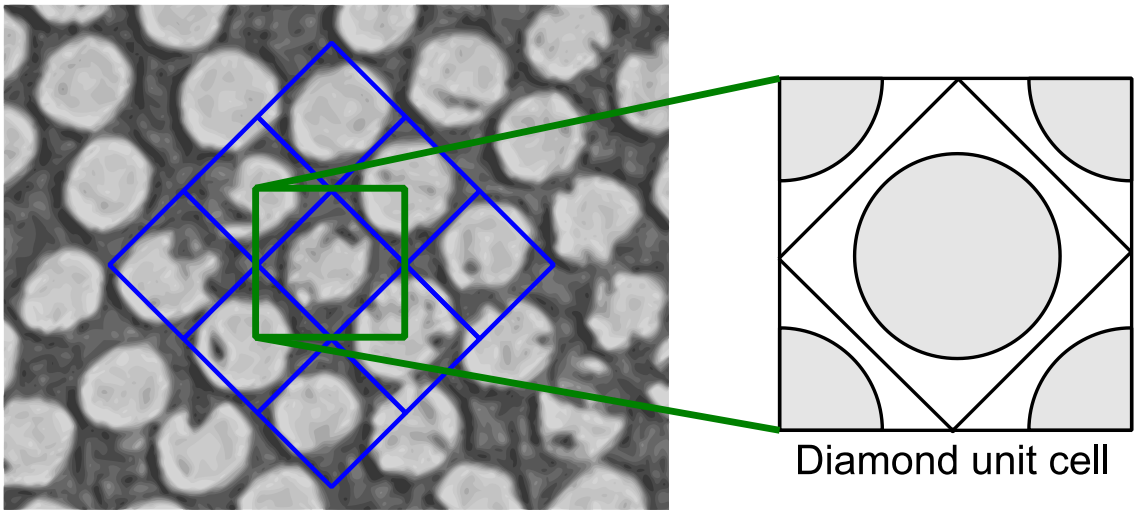


Figure 2.2: Diamond geometrical configuration represented by unit cell. Microscopy image taken from (Hrstka et al., 2003, fig. 4)

Both of these figures show several interesting features of unit cells quite clearly. First of all, even though the regular unit cells do correspond to the microstructure to some extent, they fail to do so accurately even for the few cells highlighted. Even with rotated unit cells, various fiber array types, and varying fiber volume fraction, it will still not be possible to capture the entire microstructure properly, besides violating the assumption (discussed below) that the entire composite is made up of a single repeated unit cell. These issues are addressed in Subsection 2.2.6 and Section 3.3.

Another noteworthy point is the fact that the hexagonal and diamond unit cells do not in fact have hexagonal and diamond cross sections, but rectangular and square ones, encompassing a single complete fiber and several quarter fibers. The exact reason for this choice is unknown, but literature quite consistently uses this type of unit cell. Presumably this is related to the simplicity of referring to and applying boundary conditions on perpendicular faces at the $x_0$, $x_1$, $y_0$ and $y_1$, using a simple in-plane x-y coordinate system with subscripts 0 and 1 referring to the faces of the unit cell.

Disregarding the conceptual questions arising when modeling a composite using unit cells, the fundamental assumption is that the entire composite is made up of a single unit cell, repeated as many times as necessary in all directions. This means that all unit cells experience the same stress and strain for any given uniform loading on the outside of the composite. Within this model, loading the unit cell results in the same answer as loading the composite. This is the origin of referring to the unit cells as "representative" volume elements. By modeling a single unit cell, which is computationally feasible, the response of the entire composite can be approximated. Similarly, the local strains in the constituents can be predicted given some applied load.

Micromechanical analysis is a crucial step in the analysis and prediction of failure of composites. This is due to the fact that the local strain in the constituents can differ significantly from the applied global strain. One example of this would be simple amplification by some factor, leading to failure occurring earlier than anticipated if amplification was not taken into account. However, there are far more crucial cases. (Gosse & Christensen, 2001) found that failure of a ply in compression was initiated by tensile failure of the matrix, leading to loss of support for the fibers. This tensile failure cannot be explained except through micromechanical amplification of the global strain state.

### 2.1.4 Micromechanical Enhancement[1]

In order to streamline the process from ply to constituent strains, a method called micromechanical enhancement is used. Instead of solving a finite element model with the actual strains as boundary conditions every time failure is evaluated, the response of a unit cell to applied unit strains is stored in forms of matrices. For this purpose so-called "amplification factors" or "influence functions" are used. They provide a mapping from applied global to local constituent strains.

There are two different types of amplification factors. Due to a mismatch in stiffness coefficients of the two constituents, an applied mechanical strain will cause nonuniform strains in the unit cell. This is captured by the mechanical amplification factors contained in the matrix $\boldsymbol{M}$. On the other hand, there are strains introduced due to the different coefficients of thermal expansion of fiber and matrix. These are taken into account through the thermal amplification factor vector $\boldsymbol{A}$.

The resulting principle can thus be formulated in form the following equation (based on e.g. (Tran, 2012, Eqn. 3-7) with a change from tensor component notation to matrix/vector notation):

$$\boldsymbol{\epsilon}_{local} = \boldsymbol{M}\boldsymbol{\epsilon}_{global} + \boldsymbol{A}\Delta T \tag{2.5}$$

In this equation, $\boldsymbol{\epsilon}_{local}$ is the strain at a certain point in one of the constituents, used in the failure criteria presented in Subsection 2.1.1. Similarly, $\boldsymbol{\epsilon}_{global}$ is the global strain applied to the ply. The contributions taken into account are discussed in Section 2.2.2, while Section 3.2 explains how to actually determine this parameter. Finally, $\Delta T$ is the applied temperature difference. Typically the difference between curing and application temperatures is used. However, since temperature effects typically relax over time, a sensitivity study is carried out regarding this parameter. More information can be found in Section 7.4.

In order to determine the amplification factors, unit cells are employed. In total, there are seven possible independent states of strain which can be applied to a unit cell. This includes normal loads in three directions, shear loads in three directions, and a temperature difference. Each of these causes a different state of strain in the unit cell. Note that each type of load case requires a specific set of boundary conditions. Subsections 2.2.3 to 2.2.5 contain a more detailed discussion of this aspect.

To determine the amplification factors, one of the seven independent global states of strain is applied, and the local strain at certain points in the unit cell (known as "interrogation points") is evaluated. Note that the amplification factors differ for each point in the unit cell, as discussed in Subsection 2.2.7. Since linear behavior is assumed (see Subsection 2.1.6), the results can be stored as a simple scaling factor for applying a strain of that particular type. The response to a combined strain state is then the combined response to all individual components. Based on the six mechanical amplification factor vectors, the matrix $\boldsymbol{M}$ is assembled, while the thermal amplification factor vector yields the vector $\boldsymbol{A}$. The purpose of this vector is discussed in more detail in Subsection 3.2.4.

Using regular matrix math, it is clear that the strains in the unit cell for e.g. an applied strain vector of $[0 \quad 0 \quad 1 \quad 0 \quad 0 \quad 0]^T$ determine the third column of $\boldsymbol{M}$. Similarly, a temperature difference of

[1] A similar version of parts of this section has been handed in for AE4010 Research Methodologies.

$\Delta T = 1$ (in the appropriate units) determines $\boldsymbol{A}$. The strain response used to extract the amplification factors should be the mechanical strain. Section 2.2.2 contains details on this topic. A temperature difference will cause both residual strains and free thermal contraction. This contraction has to be removed in order to obtain the correct strain amplification factors (Buchanan et al., 2009).

In this context it is crucial to ensure that the order of strain components is consistent. For example, (Buchanan et al., 2009) follow the standard convention of using $[\epsilon_x \quad \epsilon_y \quad \epsilon_z \quad \gamma_{yz} \quad \gamma_{xz} \quad \gamma_{xy}]^T$, whereas (Tran, Kelly, Prusty, Pearce, & Gosse, 2013) use $[\epsilon_x \quad \epsilon_y \quad \epsilon_z \quad \gamma_{xy} \quad \gamma_{yz} \quad \gamma_{xz}]^T$. While this is no issue as long as all definitions are consistent, it can lead to confusion when comparing results. Most importantly, it has to be avoided to apply a strain amplification factor matrix to a strain vector that follows a different convention. This would lead to incorrect results because for example $\gamma_{xy}$ is amplified as if it were $\gamma_{yz}$. The order of components is also relevant when rotating the laminate strains to the localized ply strains to draw the failure envelopes (Subsection 3.2.3), as well as when rotating the unit cells (Section 3.3). In this thesis the standard convention will be used everywhere.

The result of the finite element analysis is thus a set of amplification factor matrices and vectors for each interrogation point. Note that the analysis does not have to be rerun for every interrogation point; based on one analysis, the state of strain at each interrogation point can be determined.

Finally, failure is assumed to occur if one of the failure criteria predicts failure at any interrogation point. This defines the onset of failure. For damage tolerance or progressive damage analysis, it seems worthwhile to investigate how the results change if damage is assumed to occur once e.g. 10% of the interrogation points predict failure. However, this is beyond the scope of the present research.

### 2.1.5 Clarifying Examples and General Trends

In order to clarify some of the principles outlined previously, this section contains some example failure envelopes. Note that they are purely intended to show some of the trends seen. They are simple in-plane $\epsilon_{11}$ vs $\epsilon_{22}$ envelopes, completely disregarding out-of-plane effects, Poisson's ratios, curing strains, and other aspects involved in drawing actual failure envelopes (see Section 3.2). Only a single set of amplification factors (i.e. only one interrogation point) is used, instead of determining the – usually piecewise – minimum of several failure envelopes (one for each interrogation point).

The failure envelopes also ignore any coupling effects, both between normal strains and between normal and shear strains, and only use amplification for a single term. Typically there would be coupling effects between $\epsilon_{11}$, $\epsilon_{22}$ and $\epsilon_{33}$ (applied global to local) because of the amplification factors. Coupling between normal and shear strains is less common, but does occur. This is relevant, as discussed in Section 3.4. For the "standard" interrogation points as outlined in Subsection 2.2.7 (such as the interfiber and interstitial locations), the following terms are typically nonzero:

$$\boldsymbol{M} = \begin{bmatrix} 1 & 0 & 0 & 0 & 0 & 0 \\ x & x & x & 0 & 0 & 0 \\ x & x & x & 0 & 0 & 0 \\ 0 & 0 & 0 & x & 0 & 0 \\ 0 & 0 & 0 & 0 & x & 0 \\ 0 & 0 & 0 & 0 & 0 & x \end{bmatrix} \qquad \boldsymbol{A} = \begin{bmatrix} x \\ x \\ x \\ 0 \\ 0 \\ 0 \end{bmatrix}$$

This means that the mechanical amplification factor from an applied strain in fiber direction to the resulting strain in fiber direction is 1 (which is self-evident because there is no change in the unit cell in depth direction, meaning that the strains are by definition identical to the applied strains). Similarly, applied strains in the two transverse directions do not cause a strain along the fiber. Beyond that, there are significant cross-couplings between the strains in the three normal directions. On the other hand, the shear strains do not typically influence each other or the normal strains. Note again that this behavior is limited to certain "special" points. For the general case this is not true. Finally, an applied thermal load causes normal strains in all directions, but no shear strains.

Including the coupling terms, as well as not making any of the other assumptions stated above, means that the trends seen in actual failure envelopes will be far more involved and can only be addressed numerically (see Section 4.3). Using the stated assumptions, the failure criteria reduce to

$$\epsilon_{11,local} + \epsilon_{22,local} > J_1^* \rightarrow \epsilon_{22,local} = J_1^* - \epsilon_{11,local}$$

$$\sqrt{\frac{1}{2}\left[(\epsilon_{11,local} - \epsilon_{22,local})^2 + {\epsilon_{11,local}}^2 + {\epsilon_{22,local}}^2\right]} > \epsilon_{eqv}^*$$

$$\rightarrow \epsilon_{22,local} = \frac{1}{3}\left(\epsilon_{11,local} \pm \sqrt{6{\epsilon_{eqv}^*}^2 - 8\epsilon_{11,local}^2}\right)$$

Note the use of subscripts "local" for every strain component. The strains used in the failure criteria are not the same as the global applied strains plotted. No subscript refers to global applied strains.

Figure 2.3 shows the effect of micromechanical amplification, as well as changing critical invariants and temperatures, on $J_1$-failure. The blue line represents a trivial envelope with $J_1^* = 1$, $\boldsymbol{M} = \boldsymbol{I}$ (the identity matrix), and $\Delta T = 0$. For that $\Delta T$ the thermal amplification factors $\boldsymbol{A}$ are irrelevant.

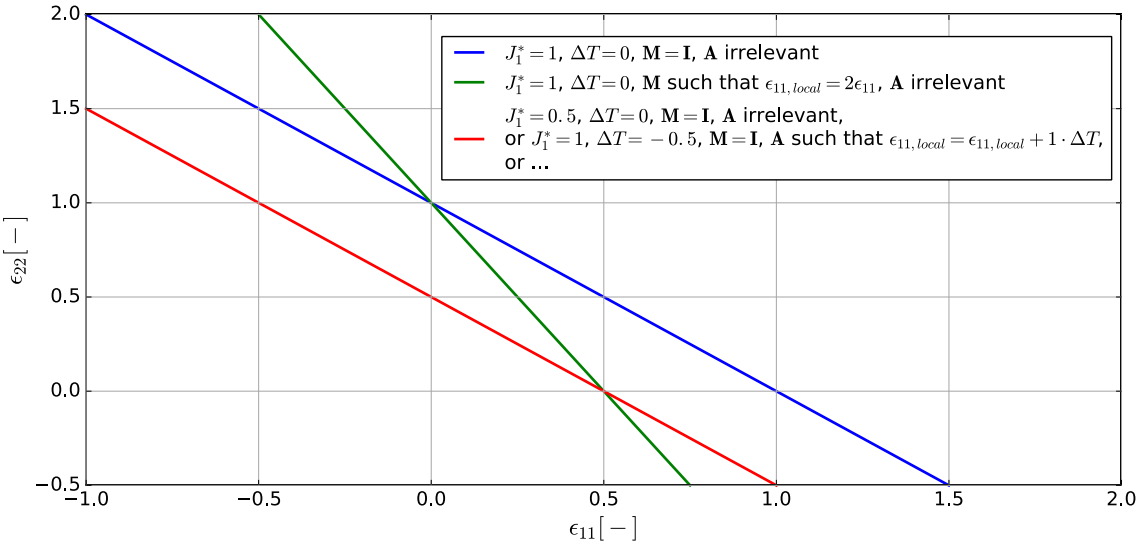


Figure 2.3: Effect of amplification factors and critical invariants on $J_1$-failure (pseudo-values)

If everything else is the same, but $\boldsymbol{M}$ is changed such that an applied strain $\epsilon_{11}$ is amplified twofold, the failure envelope changes to the green line (the equation becomes $\epsilon_{22,local} = J_1^* - \epsilon_{11,local} = J_1^* - 2\epsilon_{11}$, and, since there is no amplification of $\epsilon_{22}$, the failure envelope can be plotted as $\epsilon_{22} = J_1^* - 2\epsilon_{11}$). The $y$-intercept remains the same, but the slope of the line changes. This corresponds to

$$\boldsymbol{M} = \begin{bmatrix} 2 & 0 & 0 & 0 & 0 & 0 \\ 0 & 1 & 0 & 0 & 0 & 0 \\ 0 & 0 & 1 & 0 & 0 & 0 \\ 0 & 0 & 0 & 1 & 0 & 0 \\ 0 & 0 & 0 & 0 & 1 & 0 \\ 0 & 0 & 0 & 0 & 0 & 1 \end{bmatrix}.$$

Finally, the red line represents one of several options. Compared to the blue line, the critical invariant could have been changed to $J_1^* = 0.5$. Alternatively, a temperature difference of $\Delta T = -0.5$ might have been applied, with $\boldsymbol{A} = [1 \quad 0 \quad 0 \quad 0 \quad 0 \quad 0]^T$ (i.e. an applied temperature difference of 1 leads to a strain $\epsilon_{11,local} = 1$, corresponding to $\epsilon_{22} = \epsilon_{22,local} = J_1^* - \epsilon_{11,local} = J_1^* - \epsilon_{11} - \Delta T$). Obviously, there are many other possible combinations of $\boldsymbol{M}$, $\boldsymbol{A}$, $\Delta T$ and $J_1^*$.

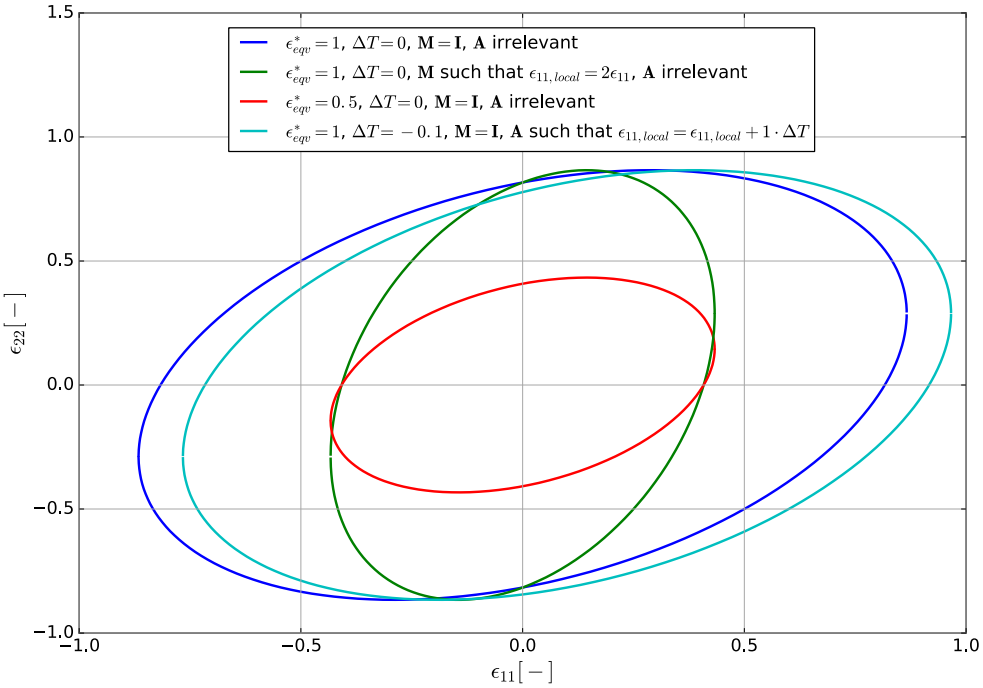


Figure 2.4: Effect of amplification factors and critical invariants on $\epsilon_{eqv}$-failure (pseudo-values)

For the closed $\epsilon_{eqv}$-failure envelope, the effects are mostly the same as for the $J_1$-cutoff, as shown in Figure 2.4. The blue line shows the envelope without any amplification, using $\epsilon^*_{eqv} = 1$. In that case, $\epsilon_{11,local} = \epsilon_{11}$ and $\epsilon_{22,local} = \epsilon_{22}$, and the $y$-intercept is located at $\epsilon_{22} \approx \pm 0.8165$. An amplification of $\epsilon_{11}$ by a factor of 2 (green line) does not change the $y$-intercept but compresses the failure envelope in $x$-direction. For the red line, reducing the invariant by a factor of 2 shrinks the entire envelope by that same factor. (This gives the same $x$-intercept as amplifying $\epsilon_{11}$ by a factor of 2.)

Unlike for $J_1$-failure, thermal effects will now be different from changing the invariant. Changing the invariant changes the size of the failure envelope while keeping it centered at the origin. On the other hand, a change in thermal effects will now shift the envelope. This is shown in the cyan line, where a temperature difference of $\Delta T = 1$ is assumed to cause a local strain $\epsilon_{11,local} = 1$. At an applied temperature difference of $\Delta T = -0.1$, this means the line is shifted to the right by 0.1 compared to the original blue line. Because the material is in compression already (in $\epsilon_{11,local}$), it can take less applied compression and more applied tension (in $\epsilon_{11}$) before failing.

For the complete failure envelope of a composite, all three envelopes ($\epsilon_{eqv}$-failure of fiber and matrix, and $J_1$-failure of the matrix, see Subsection 2.1.2) have to be taken into account. For typical values of the invariants and amplification factors, the result is that (for the $\epsilon_{11}$ vs $\epsilon_{22}$ envelope) $\epsilon_{eqv}$-failure of the matrix does not occur. The result is thus a truncation of the elliptical fiber failure envelope in the tension-tension quadrant due to matrix dilatational failure. On the other hand, for envelopes involving $\gamma_{12}$ terms, matrix distortional failure is one of the dominant failure modes. As stated in the introduction, the sum of the various effects influencing actual failure modes is tremendous and cannot be taken into account analytically. Further details can be found in Section 4.3.

Finally, for a homogeneous isotropic material (e.g. a metal – see also Section 3.1) the trivial case of $\boldsymbol{M}$ being identity and $\boldsymbol{A}$ being zero occurs. Since there is only one constituent, and considering that metals do not fail due to a change in volume alone – that is, $J_1$ failure does not occur – SIFT reduces to the von Mises yield criterion, although formulated in strain space. For metals, strain and stress based formulations are identical (unlike for polymers, as discussed in Subsection 2.2.1). This means that Onset Theory is consistent with well-established knowledge for metals.

### 2.1.6 Assumptions and Limitations

In addition to the limitations discussed in Section 1.5, a number of other assumptions should also be discussed. First of all, the fundamental assumption when modeling a composite using unit cells is that the strain in a unit cell is the same as the applied (average lamina) strain (Subsection 2.1.3). Relaxing this assumption would mean investigating a model involving multiple different unit cells. This quickly approaches modeling the entire composite in terms of fibers and matrix, which has been discarded as computationally infeasible. Analyzing multi-cell models, although very interesting, is not really part of SIFT as implemented here. It is discussed to some extent in Section 7.5.

Another limitation is the use of linear-static finite element analysis only. This is based on for example (Tran, Kelly, Prusty, Gosse, & Christensen, 2012, p. 749), who state that *"when constrained by the fibers in unidirectional laminates, the matrix has been observed to deform elastically in strain space but anelastically in stress space"*. They elaborate further in (Tran et al., 2013, p. 4), stating that *"anelastic behaviour is reversible provided the critical strain invariants have not been realized"*. Note that this also points to the use of strains rather than stresses, as discussed in Subsection 2.2.1. Using nonlinear analysis would render using matrix algebra for the micromechanical enhancement impossible. The superposition of responses to independent states of strain would not be valid anymore. Therefore, the present research is limited to linear analyses.

One final point that has to be stressed here is that Onset Theory as implemented in this thesis does not predict ply interface failures, such as delaminations. This is also discussed by (Ritchey et al., 2011). Using unit cells that contain only a single fiber direction, and assuming that the entire structure consists of those unit cells repeated indefinitely in all directions (with the strain being identical everywhere), means an inherent inability to investigate locations where the strains are not uniform. In particular, this is the case at the interface of one ply to the next. To investigate those locations, unit cells containing multiple fiber orientations should be analyzed to determine the appropriate strain amplification factors. This is discussed in Subsection 8.4.1. Onset Theory as investigated here is purely intended as an improved ply failure criterion.

## 2.2 Contested Details

As stated in the introduction to this chapter, only the general steps of the theory are well-known and widely accepted. Due to different assumptions and direct contradictions discrepancies are found in literature regarding the details of each step. The following subsections present these contradicting opinions. Corresponding investigations to determine the correct approach, where deemed necessary based on the literature review, are carried out in Chapter 3.

### 2.2.1 Using Stresses or Strains

One of the central aspects of SIFT is the use of strain invariants. There are several very important reasons to also use strain-based test data. An overview is found in (Tran, 2012, pp. 59–61).

To paraphrase, the stress at yield of a polymer is shown to be strongly affected by the amount of dilatation versus distortion applied. On the other hand, the strains are affected to a much smaller extent. This is related to the independence of the matrix invariants, as discussed in Subsection 1.3.2. As shown by various researchers, the dilatational and distortional strain invariants are independent of each other. This is not the case for stress invariants, which will become relevant in the second half of this subsection where the use of stress invariants instead of strain invariants is discussed.

Note that in their original article (Gosse & Christensen, 2001) do mention that the equivalent strain excludes the effects of pressure on yield. However, this has not been mentioned or raised as an issue anywhere else. It seems likely that this was an initial thought before a thorough investigation took place. Investigating the influence of hydrostatic pressure on yield in polymers (in other words, the coupling between dilatational and distortional failure modes under triaxial loads) is not considered to be of particular importance for this thesis since the focus is on biaxial laminate failure.

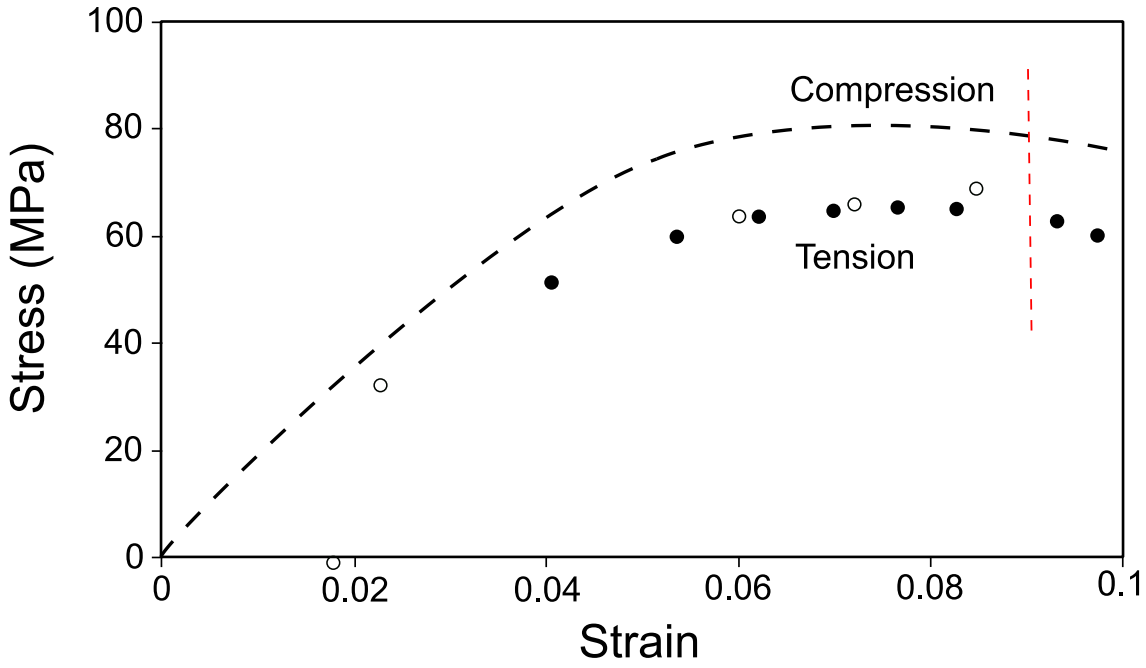


Figure 2.5: Stress-strain curves of polycarbonate at $T = 300K$ and $\dot{\epsilon} = 0.01\frac{1}{s}$. Adapted from (Tran, 2012, fig. (3-6)).

Another aspect that points towards the use of strains rather than stresses is the claim made by (Tran, 2012, p. 60) based on Figure 2.5. He claims that *"for polymeric resins the strain for the onset of irreversible behavior is the same in tension and compression whereas the stress is different in these two load cases"*. Note that this applies to pure resins, not to composites. As for the coupling of dilatational and distortional behavior, the difference in yield stresses in tension and compression is discussed in the second half of this subsection.

Finally, according to Tran there is little dependency of the failure strain on the strain rate, whereas the stress is once again strongly dependent. (Caruthers & Medvedev, 2009) – the original source on which Tran's overview is based – also mention a dependency of the stress at yield on temperature.

The strain rate influence can be confirmed using the data by (Koerber, Xavier, & Camanho, 2010). Comparing the ultimate stresses and strains for various off-axis tension coupons at quasi-static and dynamic loads ((Koerber et al., 2010, Tables 3 and 4), the average ratio of stresses is 1.4, while the average ratio of strains is 1.16 (calculating the ratio such that it is always larger than 1).

The inaccuracy of using stress-based data has also been confirmed in the experimental work by (Ng et al., 2004). Using the failure stress, the maximum difference between test and prediction was 58%. Using the failure strain, this value decreased to 18%. The authors therefore also concluded that failure strains rather than failure stresses should be used in SIFT.

A final argument that can be made based on literature is that the matrix behavior is linear in strain space up until failure, but anelastic in stress space. This was discussed in Subsection 2.1.6.

Based on this discussion, it is clear that failure strain data is to be preferred over failure stress data. Any validation based on failure stress data would suffer from large uncertainties and inaccuracies. Note that is somewhat problematic given the fact that most test data is given in terms of stresses. The available test data is discussed in Section 6.1.

Some researchers (Ha et al., 2008; C. H. Wang, 2005; J. Wang & Chiu, 2011) opted for the use of stress invariants in place of strain invariants. One of the reason seems to be that they consider a stress-based failure criterion to be easier to use; however, in general they do not seem to state a specific reason for their choice (beyond the fact that they consider the two formulations equivalent).

There are two options when using stress invariants. First of all, one could use strain-based test data to avoid the issues involved with stress-based test data, and subsequently convert the data to stress space. However, this causes issues related to the uncertainty in lamina-level stiffness properties. In order to convert a strain-based failure prediction to stress space, the stiffness matrix for the particular unit cell that is most critical in the failure prediction should be used. Using measured lamina-level stiffness properties introduces an additional level of inaccuracy. Although their use is not fully avoided in this thesis (see Subsections 3.2.1 and 3.2.2), their effect should be kept to a minimum. I should be noted here that the conversion between strain and stress space does offer some interesting possibilities for progressive failure analysis, as investigated in Subsection 8.4.3.

What seems more likely is that these researchers elect to use stress-based test data. This causes an issue commonly raised which seems worth addressing here as well. Because of the use of stresses instead of strains, there is an influence of the hydrostatic component of the stress on yield (in other words, there is a coupling between dilatational and distortional behavior, and the yield stresses in

tension and compression are different, as discussed previously in this subsection). This effect, which is only present in stress space, is not captured by the von Mises yield criterion. Therefore, all of these researchers found it necessary to replace the von Mises criterion by a criterion that includes an interaction effect between the distortional and dilatational behavior. Using this type of criterion (typically a Drucker-Prager type failure criterion) shifts the stress space failure envelope towards the compression/compression quadrant. This is visualized in Figure 2.6. (The "failure regions of interest" are indicated as such because the tension quadrant will be truncated by the $J_1$ matrix failure criterion (Eqn. (2.1)) and is thus not active for the most part.)

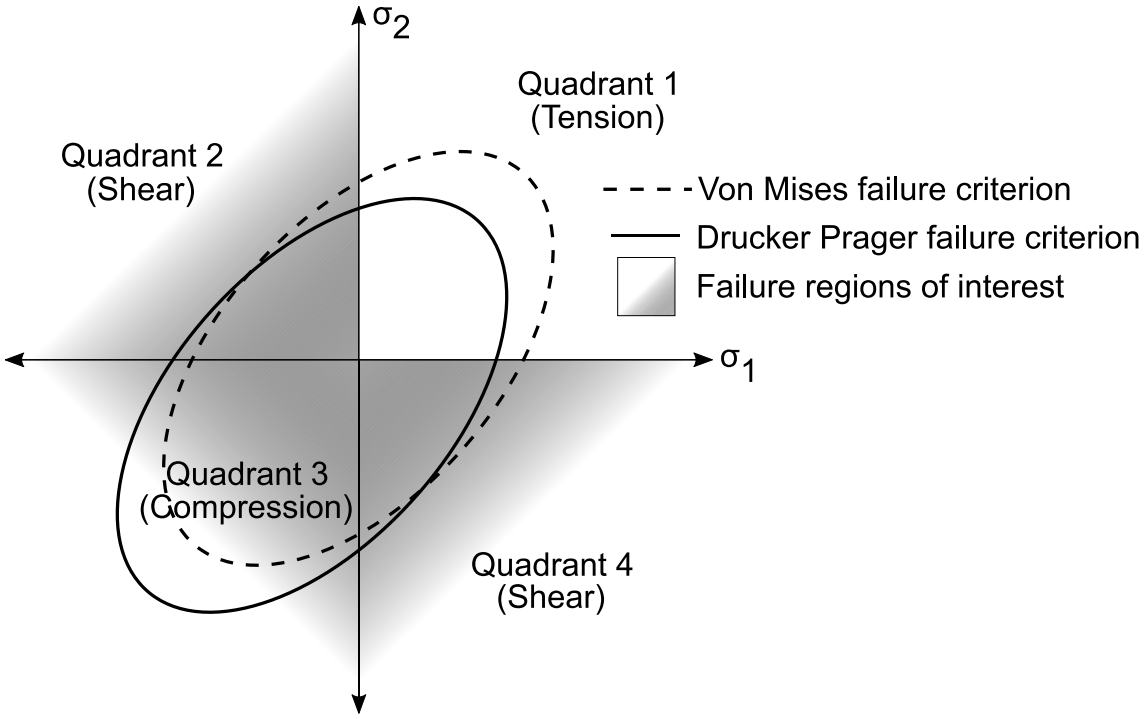


Figure 2.6: Visualization of shifted stress space failure envelope (Chowdhury, Wang, Chiu, & Yan, 2016, fig. 8)

It seems as if the main reason why researchers used a Drucker-Prager type criterion is that they tried to employ SIFT in stress space. Presumably, using the Drucker-Prager yield criterion mitigates some of the problematic effects of doing so. However, the use of stress-based data – even if a Drucker-Prager type criterion is used – still shows a lack of awareness of the other issues involved with stress-based data, such as nonlinearity or dependency on strain rate and temperature.

In summary, it is more straightforward and less error prone to use SIFT in strain space. This means that strain invariants should be used, in combination with strain-based test data.

### 2.2.2 Contributions to Applied Strain

So far, the contributions taken into account for the applied strain have not yet been specified properly. The present section provides an overview of the reasoning and choices made for this thesis.

The first topic that should be addressed is the type of strains used in the failure criteria. Both the article by (Buchanan et al., 2009) and the one by (Ritchey et al., 2011) stress that mechanical

strains rather than total strains should be used, meaning that the effect of free thermal contraction has to be removed. For mechanical loads total and mechanical strains are identical because there is no free thermal contraction. However, for example for a cube of homogeneous material experiencing heating without any restrictions on its expansion, the dilatational failure criterion in Eqn. (2.3) based on the total strain (defined as $\Delta L/L$) would predict failure. This is clearly not the case. The use of the mechanical strain is also clear from the verification calculations in Subsection 5.2.1.

The local strain $\boldsymbol{\epsilon}_{local}$, as discussed in Subsection 2.1.4, contains several contributions. First among these are of course the direct mechanical strains due to an external load, taken into account through $\boldsymbol{\epsilon}_{global}$. However, there are additional contributions due to thermal and chemical shrinkage during curing, as well as hygroscopic (i.e. moisture ingression) effects (Hart-Smith, 2010).

Regarding thermal effects, Section 3.2 established the correct procedure to include thermal strains, including curing strains (as verified in Subsections 5.2.1 and 5.2.2). As discussed in Subsection 3.2.4, there are two types of strains due to the temperature difference: a macro-level one ($\boldsymbol{\epsilon}_{curing}$) and a micro-level one ($\boldsymbol{A}\Delta T$). Both effects need to be taken into account for both invariants.

It is worth mentioning that thermal stresses are commonly assumed to relax over time. However, according to (Hart-Smith, 2014) this does not mean they can be ignored, because every rapid change in temperature will reintroduce thermal stresses. This means that the real thermal effects will be in between the extremes of no thermal effects and theoretical thermal effects based on the difference between curing and application temperatures. For a further investigation see Section 7.4.

Regarding moisture absorption, a similar derivation as in Subsection 3.2.2 is possible, using coefficients of expansion due to moisture absorption in place of the thermal expansion coefficients. However, (Hart-Smith, 2010) argues that the strains due to moisture absorption would be benign because they relieve some of the strains due to thermal shrinkage. Since they cannot be quantified accurately, he neglects them, arguing that the resulting failure prediction will, if anything, be conservative.

(Hart-Smith, 2010) also briefly discusses chemical shrinkage, but only in the context of $J_1$. For this case, he argues that it can be omitted because it is present in both the critical and any calculated value. His choice to limit the discussion to the dilatational invariant is based on the fact that the matrix typically fails in dilatation, while the fiber does not undergo chemical shrinkage during curing. For the distortional matrix invariant chemical shrinkage could not simply be removed from both sides of the equation because the expression is far more complex than the summation used for the dilatational invariant. It is not clear how to include this effect for distortional matrix failure.

In summary, moisture absorption and chemical shrinkage do not appear to be extremely relevant. Previous researchers obtained good results without taking these factors into account, as discussed in Section 1.3. In addition to that, moisture absorption has is presumably beneficial since it reduces residual thermal strains, leading to conservative predictions. Chemical shrinkage, on the other hand, will not influence the dilatational matrix invariant or the distortional fiber invariant, as argued above. The distortional matrix invariant is typically not relevant for failure predictions, since for laminates fiber failure usually occurs before the matrix reaches its distortional limit. This is also seen in Section 6.3. Therefore, in the context of this thesis these two effects are neglected.

### 2.2.3 Boundary Conditions for Normal Load Cases

In order to apply unit strains to the representative volume elements, as discussed in Subsection 2.1.4, boundary conditions for the faces of the unit cell need to be chosen. Three categories of loads are applied: normal loads, shear loads, and a thermal load. They are discussed in turn in this subsection, Subsection 2.2.4, and Subsection 2.2.5.

For the normal load cases, there is a significant contradiction between different sources. In general, there are two options. Given an applied load (say along the fiber), the remaining faces can be forced to remain in place (from here on called "fixed boundary conditions"), or they can be allowed to freely, uniformly translate normal to their original position ("movable boundary conditions").

The former of these approaches is used by one of the original authors of SIFT, namely Gosse (see e.g. (Ritchey et al., 2011, p. 612) or any other article published in collaboration with Gosse): for an applied strain in the "1" direction, the displacement in $y$- and $z$-directions is forced to be 0 at the $y$- and $z$-faces, respectively. On the other hand, the other original author (Hart-Smith) seems to indicate that the other faces be allowed to float freely (Hart-Smith, 2010). This behavior is also evident in (Jin, Huang, Lee, & Ha, 2008, fig. 5 (a)), where the initial and final $z$-boundaries of the unit cell are clearly not at the same location for tensile loading in $y$-direction (see Figure 2.7).

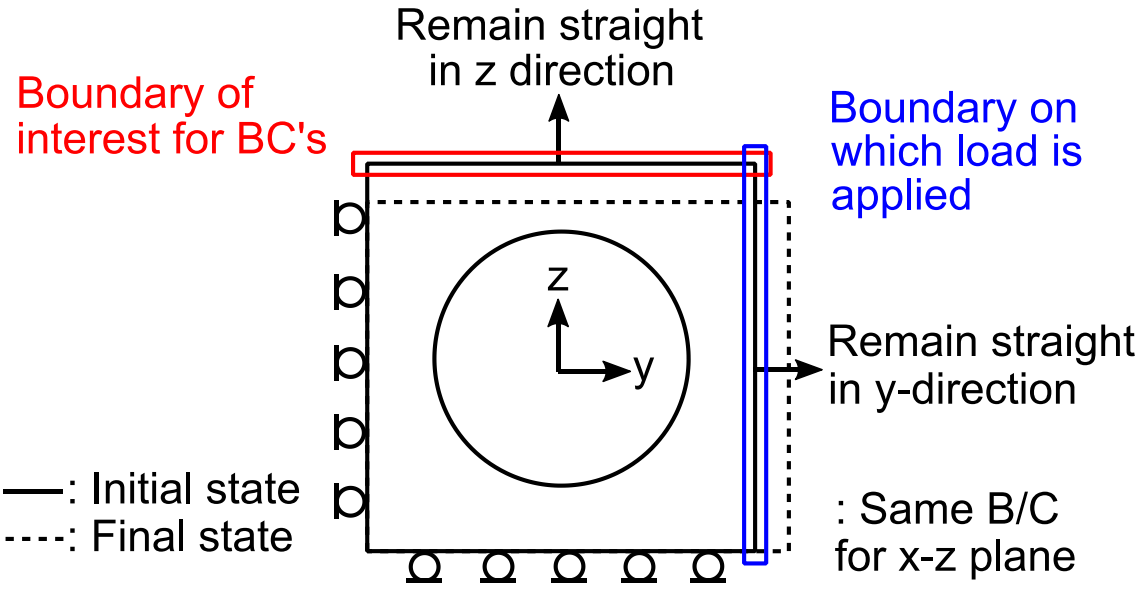


Figure 2.7: Indication of boundaries discussed for the normal load cases. Adapted from (Jin et al., 2008, fig. 5 (a)) (modifications in red and blue).

The same figure also shows the boundaries being discussed. Marked in blue is the boundary on which the load is applied (in this case a transverse tensile strain). The red region is the boundary of interest for the boundary conditions. Indicated in the figure is a movable boundary condition: the boundary is moving from the initial to the final state, with the only requirement being that it remain straight in z-direction. If fixed boundary conditions were implemented, this boundary would be fixed in place (i.e. the initial and final state would coincide at the location of the current initial state).

In summary, there are thus two possible sets of boundary conditions. The fixed boundary conditions would mean fixing all faces of the unit cell in normal direction, with the exception of one of the

faces in the direction of the applied unit strain. As an example, for an applied strain of $\epsilon_{11}$ the boundary conditions would be $u = 0$ at $x_0$, $u = 1$ at $x_1$, $v = 0$ at $y_0$ and $y_1$, $w = 0$ at $z_0$ and $z_1$, where the faces of the unit cell are located at $x_0$, $x_1$, $y_0$, $y_1$, $z_0$ and $z_1$, and $u$, $v$ and $w$ are displacements in the $x$-, $y$- and $z$-directions, respectively. The fiber is running along the $x$-direction.

On the other hand, for the movable boundary conditions the situation would be more complex. For an applied strain of $\epsilon_{11}$ the only displacement boundary conditions would be $u = 0$ at $x_0$ and $u_1$ at $x_1$. The other faces should be forced to remain flat, but are allowed to translate normal to their original location. For the practical implementation in Abaqus, see Subsection 4.2.2.

All of these boundary conditions assume a basic unit cell size of 1, such that an applied displacement of $u = 1$ results in a strain $\epsilon_{11} = 1$. In practical applications measures need to be taken to avoid numerical inaccuracies. This is discussed in Subsection 4.2.6.

The discrepancy in possible boundary conditions needs to be resolved in order to obtain a consistent approach regarding the application of SIFT. Section 3.5 contains a full list of boundary conditions for the normal load cases, based on the results of the discussion in Section 3.1.

### 2.2.4 Boundary Conditions for Shear Load Cases

Regarding the shear load cases, there is essentially agreement in literature. The only point of attention is the difference between pure shear and simple shear, see for example (Buchanan et al., 2009). The applied strain should be e.g. $\gamma_{yz} = 1$. However, this is not achieved by applying a displacement of $v = 1$ on $z_1$. The result would be simple shear, whereas the desired deformation is pure shear (which does not involve any dilatational deformation of the unit cell). Therefore, the set of boundary conditions to apply $\gamma_{yz} = 1$ is $v = 0.5$ at $z_1$ and $w = 0.5$ at $y_1$ (assuming a unit strain applied to a unit cell of size 1, as for the normal load cases). All other movement should be constrained, using $u = 0$ at every face, $w = 0$ at $y_0$, and $v = 0$ at $z_0$. The same definitions as for the normal load cases are used. Figure 2.8 shows the nonzero displacement boundary conditions used to apply $\gamma_{yz} = 1$, as well as the loaded and unloaded states (represented by dashed and solid lines, respectively).

No constraints on warping of the faces due to the loading are required. This can be deduced from the deformed shape seen in (Jin et al., 2008, fig. 5b) or the lack of a constraint in $y$-direction on the $y$-faces in (Ritchey et al., 2011, Eqn. 11d). In fact, though this took place before the development of SIFT, (C. T. Sun & Vaidya, 1996) investigated unit cells under shear and concluded that straight edges are overly restrictive.

Based on the preceding discussion there is agreement on the details of applying shear loading, including letting the faces warp. Therefore, a detailed investigation of this point does not seem relevant. As for the normal load cases, Section 3.5 contains a full list of the required boundary conditions.

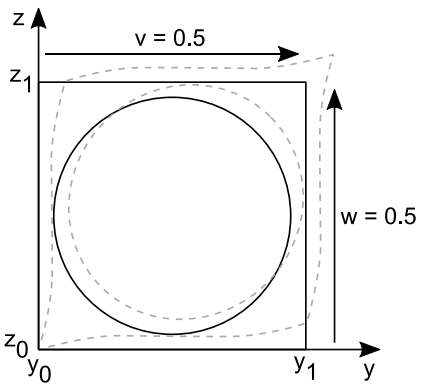


Figure 2.8: Applied displacement and deformed shape for $\gamma_{yz}$ shear loading (exact shapes taken from finite element results)

### 2.2.5 Boundary Conditions for Thermal Load Case[1]

For the boundary conditions for the thermal load case an inconsistency was found in literature. The issue is similar to the one encountered for the normal load cases. (R. Li et al., 2003) and (Tay, Tan, & Tan, 2005) use fixed boundary conditions, which are also used by (Yudhanto, 2005) and (McNaught, 2009). On the other hand, (Buchanan et al., 2009), (X. S. Sun, Tan, & Tay, 2011) and (Ritchey et al., 2011) use movable boundary conditions. This choice is also in (Tran, 2012). Finally, (Xia, Zhang, & Ellyin, 2003) propose periodic boundary conditions for the unit cells.

Comparing these three options, it is clear that the more recent literature allows free uniform translation to the surfaces. In addition to that, Tan and Tay, who used fixed boundary conditions previously (Tay, Tan, & Tan, 2005), switched to using movable boundary conditions (X. S. Sun et al., 2011). Finally, the original authors of SIFT (Buchanan et al., 2009) also uses this approach, while acknowledging and discarding the periodic boundary conditions suggested by (Xia et al., 2003).

In conclusion, this means that an investigation of the thermal load case would serve to increase confidence in the choice of using movable boundary conditions. This is addressed in Subsection 3.1.1.

### 2.2.6 Fiber Array Types and Representativeness of Unit Cells

As discussed in Subsection 2.1.3 micromechanical analysis relies on unit cells. Several issues were raised, related to the geometrical configurations (fiber array types) that should be taken into account as well as whether the unit cells are in fact representative of the true random microstructure.

One of the strongest claims made regarding the fiber array types used is found in (Hart-Smith, 2010, p. 4305). He states that *"four standard fiber arrays can provide bounds on all of the possible random arrays […]; the square array, the diamond array, and the two hexagonal arrays"*. (By "two hexagonal arrays", hexagonal unit cells with long edges in horizontal and vertical orientation are meant). While this point is not directly found in (Buchanan et al., 2009) (or (Ritchey et al., 2011), which can be regarded as a follow up article), the authors only mention square and hexagonal fiber arrays, which is even more limiting than square, diamond and hexagonal, as investigated by Hart-Smith. They also do not mention random arrays. Similarly, (Tran, Kelly, Prusty, & Pearce, 2011, p. 1) assert that *"the square and hexagonal arrangements […] have been shown to give bounding magnification factors and are assumed to exist somewhere in the random distribution of fibers in the laminate"*.

Note that whether or not a certain regular unit cell gives bounding amplification factors is only one part of the story. Even if this was the case, it does not mean that the strain in each unit cell is the same. If the amplification factors for a certain cell are very large, but at the same time the cell is extremely stiff and (in the real microstructure) surrounded by very compliant cells with lower amplification factors, then these other cells would experience the majority of the strain, resulting in larger overall local strains. The problematic assumption that the strains in a unit cell are the same as the average lamina strains was discussed previously in Subsection 2.1.3. However, there does not seem to be a computationally feasible way to avoid using unit cells.

[1] A similar version of parts of this section has been handed in for AE4010 Research Methodologies.

Some investigation of the differences between various (regular) unit cells has been carried out in the master thesis by (Yudhanto, 2005), However, this research took place before the procedure was fully established, meaning that the results are not really applicable. For example, only the diagonal terms of the amplification factor matrix are used, so there is no coupling between strain components.

The only thorough investigation of other fiber array types, as well as random fiber arrays, has been carried out by a research group around Prof. Ha of Hanyang University, Korea. In a series of articles, they compare the local strains obtained from regular arrays to those originating from random arrays.

Worth mentioning in this context is that they extend the regular arrays to cover all rotated versions of the square and hexagonal arrays (the diamond array being a rotated square array), see for example (Ha et al., 2008). Note also that most of the results are based on local stresses rather than strains.

Unfortunately, there does not seem to be a consistent answer. In (Hobbiebrunken, Hojo, Jin, & Ha, 2008, p. 3112), the conclusion is that *"periodic unit-cells are not suitable in a microscopic failure analysis where the magnitude and distribution of microscopic stresses is important"*. Similarly, (Oh, Jin, & Ha, 2006, p. 777), state that *"the analysis with the periodic fiber array […] could not predict the real microscopic behavior accurately due to the random arrangement of fibers in real composite materials"*. On the other hand, according to (Jin, Oh, & Ha, 2007, p. 609), *"the regular array can provide a convenient way to investigate the residual stresses of a real unidirectional composite under thermal loading"*, and according to (Huang, Jin, & Ha, 2008, p. 1870), *"the cumulative frequency distributions of stress invariants in random and regular arrays due to various loading types and various loading angles show good agreement, which validates the effectiveness of regular arrays"*.

Clearly, this is not truly conclusive. Based on the research presented above, it can be ventured that there is a difference between the engineering and numerical points of view. SIFT is concerned with noticeable failure. If the majority of the random distribution fails when the regular arrays fail, then local failure of a single point in a random array is irrelevant, provided the failure does not progress catastrophically. This is hinted at by (Huang et al., 2008), mentioning good agreement of the cumulative frequency distributions. It could be an explanation for the contradiction between the results obtained by Prof. Ha and the use of unit cells in SIFT for convenience in terms of modeling effort and computing time. In an article published after Prof. Ha's research (Buchanan et al., 2009), his work is cited without mentioning unit cells not being sufficiently accurate.

Rotating the arrays seems advisable, and an investigation of random fiber arrays (focusing on the contrast between local numerical differences and global behavior) would be very valuable. The aspect of rotating the fiber arrays is covered in Section 3.3. As stated before, random fiber array (multi-cell) models are outside of the scope of this thesis. Section 7.5 contains some discussion.

### 2.2.7 Location of Interrogation Points

As stated in Section 2.1.4, the failure criteria are evaluated at several points in the unit cell. Two sets of interrogation points can be distinguished: those in the matrix phase, and those in the fiber phase. For the matrix phase, (Buchanan et al., 2009) and all other articles involving Gosse (the original author of SIFT) state that the most critical points are the interstitial (where fibers are furthest apart) and interfiber (where they are closest) locations. Figure 2.9 indicates those points.

This choice of three points (two interfiber, one interstitial, regardless of fiber array) is based on a series of finite element calculations which showed these points to cause the maximum values of the invariants for the cases investigated. However, (Buchanan et al., 2009) do state that increasing the number of interrogation points may improve the accuracy of the results. In addition to that, there is no guarantee that the chosen locations will be the most critical ones for every single case.

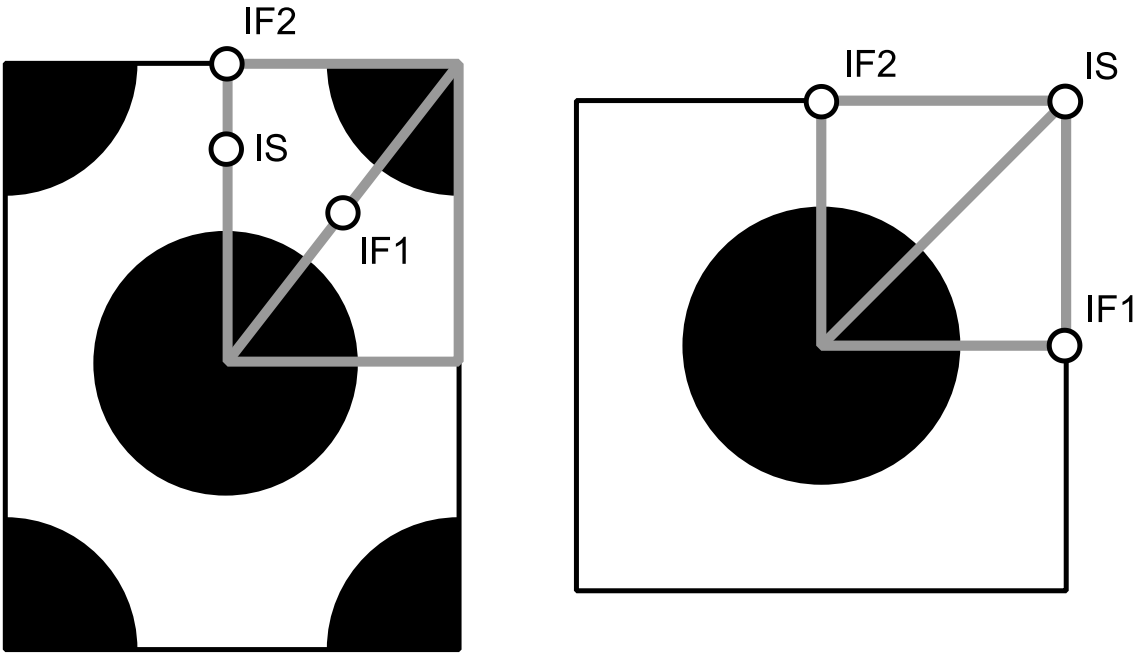


Figure 2.9: Interrogation points in the matrix phase (Buchanan et al., 2009, fig. 3). Interstitial = IS, interfiber = IF.

Regarding the interrogation points in the fiber, very little information is available. (Yudhanto, Tay, & Tan, 2006) use the center of the fiber, as well as points on the fiber boundary at 0°, 45°, and 90° (as measured from the horizontal), for the square array. This is in agreement with (X. Li, Guan, Li, & Liu, 2014) (see Figure 2.10) and (Tay et al., 2006) (Figure 2.11).

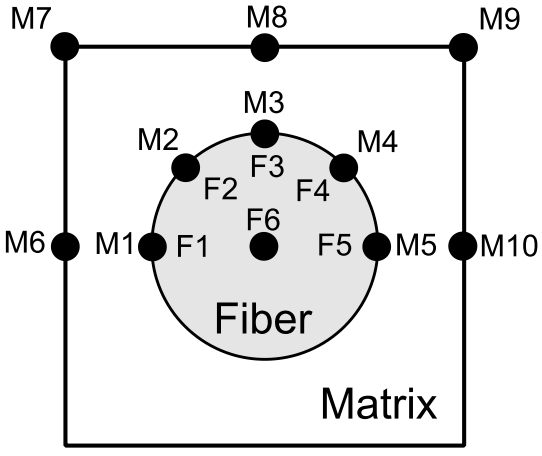


Figure 2.10: Interrogation points used by (X. Li et al., 2014, fig. 2 (a)) for the square array

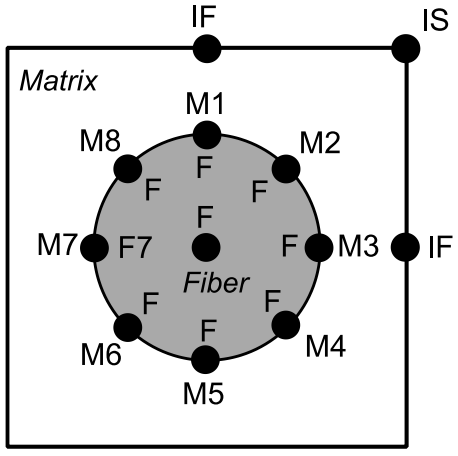


Figure 2.11: Interrogation points used by (Tay et al., 2006, fig. 2 (a)) for the square array

(X. Li et al., 2014) use points at 0°, 30°, 60° and 90° on the fiber edge for the hexagonal array (see Figure 2.12). Note that they do not use the standard points in the matrix (they use two interstitial

and one interfiber points). On the other hand, Figure 2.13 shows that (Tay et al., 2006) use points at 0°, 45°, and 90° on the fiber edge for the hexagonal array, just like for the square array.

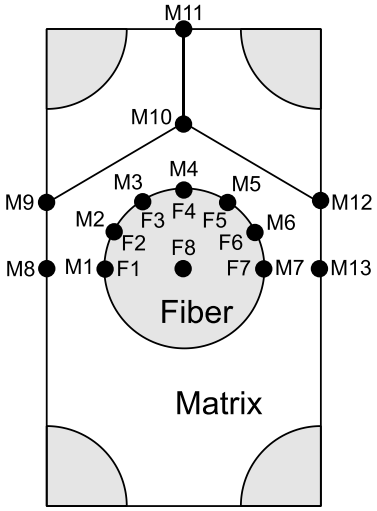


Figure 2.12: Interrogation points used by (X. Li et al., 2014, fig. 2 (b)) for the hexagonal array

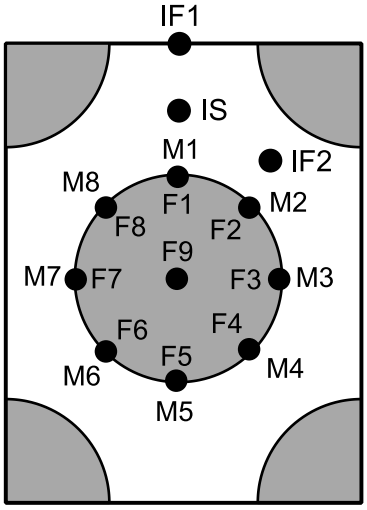


Figure 2.13: Interrogation points used by (Tay et al., 2006, fig. 2 (b)) for the hexagonal array

Another aspect that should be considered is symmetry of the unit cell. (Buchanan et al., 2009) use interrogation points in a single quarter of the unit cell only, as seen in Figure 2.9. (X. Li et al., 2014), however, use points in one half of the unit cell (Figure 2.10 and Figure 2.12). Finally, Figure 2.11 shows that (Tay et al., 2006) use points in a single quarter for the interfiber and interstitial locations, but elected to investigate points around the entire circumference of the fiber (i.e. in all four quarters). This is also the case for the hexagonal array (Figure 2.13).

In summary, the results above mean that both the necessity of including interrogation points in two quarters of the unit cell (or even the entire unit cell) and the exact location and number of points clearly require additional evidence. There does not seem to be any literature available which investigates this aspect in detail. Therefore, an investigation is carried out in Section 3.4.

# Chapter 3

# Development of Consistent Approach

In the previous chapter, a thorough literature study revealed several discrepancies regarding the details of the steps that need to be taken to apply Onset Theory. The present chapter focuses on the development of a consistent approach by investigating and resolving these contradictions.

The contradicting statements regarding the boundary conditions (see Subsections 2.2.3 to 2.2.5) are investigated in Section 3.1. Based on the choices made, an analytical approach to determine the full state of strain is developed in Section 3.2. Sections 3.3 and 3.4 discuss rotated unit cells and the required locations of interrogation points, respectively. Section 3.5 summarizes the complete consistent approach to Onset Theory.

## 3.1 Investigation of Boundary Conditions on Unit Cell

In Subsections 2.2.3 to 2.2.5, contradiction statements regarding the required boundary conditions on the unit cell were discovered. For the normal load cases, there were two distinct schools of thought, one fixing the faces in place (fixed boundary conditions), with the other one allowing the faces to translate uniformly normal to their original location (movable boundary conditions). Similarly, for the thermal load case the same two schools of thought existed, although based on the more recent literature movable boundary conditions seem to be the correct choice. The present section investigates movable and fixed boundary conditions with a focus on normal load cases, while also seeking to increase confidence in the selection of movable boundary conditions for the thermal load case. Subsection 3.1.1 contains a thought experiment, resulting in the insight that in fact fixed and movable boundary conditions are equivalent for the normal load cases, provided appropriate adjustments are made. The details of this consolidation are discussed in Subsection 3.1.2.

### 3.1.1 Thought Experiment

In Section 2.2.2 it was established that the elastic strain should be used in Onset Theory. Based on this, a thought experiment was carried out, assuming a unit cell containing a single homogeneous isotropic material (i.e. a unit cell representing a metal). For this case, the correct resulting state of

strain under normal and thermal loads is known and can be related back to the desired states of strain required for the micromechanical enhancement process (Subsection 2.1.4).

An applied temperature difference is used to determine the thermal strain amplification vector $\boldsymbol{A}$. As will be discussed in Subsection 3.2.4, $\boldsymbol{A}$ represents the micro-level strains due to the mismatch between thermal expansion coefficients of fiber and matrix. In case of a metal, there is only a single material, meaning that there are no mismatches, and $\boldsymbol{A}$ should be zero. If a temperature difference is applied to a homogeneous cube of material, it will contract according to its thermal expansion coefficient. The desired elastic strain free state is achieved by not restricting this movement in anyway. In that case, the only strains will be thermal. This means that the correct choice of boundary conditions for a unit cell of a composite is also to allow the boundaries to move, although they should be forced to remain flat in order to ensure compatibility between neighboring unit cells. Since this is the definition of movable boundary conditions, it is clear that using the type of boundary condition found in the more recent literature is indeed the correct choice.

Contrary to that, the micromechanical enhancement process for mechanical strains (represented through the mechanical amplification matrix $\boldsymbol{M}$) relies on unit strains in a single direction being applied to the unit cell (as also discussed in Subsection 2.1.4). Relating this back to the postulated cube of metal, applying a unit strain in some direction will result in Poisson's contractions in the other two directions if the movement of the faces is not restricted. These Poisson's contractions are elastic strains, violating the assumption of a strain in a single direction being applied when determining the amplification factors. This means that applying the full set of global strains (including strains due to a Poisson's contracting) to the movable boundary conditions takes the Poisson's effect into account twice, resulting in an overconservative prediction. On the other hand, when using fixed boundary conditions, it is crucial to indeed use the full set of strain. Otherwise those strain components not directly measured, but caused by Poisson's effects, are not taken into account (meaning unconservative predictions). Assuming the unknown strains to be zero is incorrect.

In other words, for the movable boundary conditions the Poisson's effect is taken into account implicitly by the unit cell and has to be removed from the external applied strains. Contrary to that, the fixed boundary conditions do not take the Poisson's effect into account at all, meaning that it has to be included explicitly in the external applied strains. These two approaches are, in fact, equivalent. The next subsection discusses consolidating the respective formulations, as well as explaining the selection of boundary chosen for this thesis.

### 3.1.2 Consolidation of Boundary Conditions for Normal Load Cases

To formalize the principle stated in the previous section, suppose only a strain $\epsilon_x$ is applied to the same cube of metal. The resulting state of strain for this case is $[\epsilon_x \quad -\nu_{12}\epsilon_x \quad -\nu_{13}\epsilon_x \quad 0 \quad 0 \quad 0]^T$. For the movable boundary conditions, applying only $\epsilon_x$ will result in the correct state of strain because the Poisson's strains are taken into account implicitly by the unit cell. On the other hand, for the unit cell using fixed boundary conditions, the Poisson's effect needs to be taken into account in the applied strain vector. This means that for a metal using fixed boundary conditions the mechanical amplification factor matrix $\boldsymbol{M}$ is equal to the identity matrix.

In terms of equations, this means that for the fixed boundary conditions

$$\begin{bmatrix} \epsilon_x \\ -\nu_{12}\epsilon_x \\ -\nu_{13}\epsilon_x \\ 0 \\ 0 \\ 0 \end{bmatrix} = \begin{bmatrix} 1 & 0 & 0 & 0 & 0 & 0 \\ 0 & 1 & 0 & 0 & 0 & 0 \\ 0 & 0 & 1 & 0 & 0 & 0 \\ 0 & 0 & 0 & 1 & 0 & 0 \\ 0 & 0 & 0 & 0 & 1 & 0 \\ 0 & 0 & 0 & 0 & 0 & 1 \end{bmatrix} \begin{bmatrix} \epsilon_x \\ -\nu_{12}\epsilon_x \\ -\nu_{13}\epsilon_x \\ 0 \\ 0 \\ 0 \end{bmatrix}, \tag{3.1}$$

whereas for the movable boundary conditions

$$\begin{bmatrix} \epsilon_x \\ -\nu_{12}\epsilon_x \\ -\nu_{13}\epsilon_x \\ 0 \\ 0 \\ 0 \end{bmatrix} = \begin{bmatrix} 1 & -\nu_{21} & -\nu_{31} & 0 & 0 & 0 \\ -\nu_{12} & 1 & -\nu_{32} & 0 & 0 & 0 \\ -\nu_{13} & -\nu_{23} & 1 & 0 & 0 & 0 \\ 0 & 0 & 0 & 1 & 0 & 0 \\ 0 & 0 & 0 & 0 & 1 & 0 \\ 0 & 0 & 0 & 0 & 0 & 1 \end{bmatrix} \begin{bmatrix} \epsilon_x \\ 0 \\ 0 \\ 0 \\ 0 \\ 0 \end{bmatrix} \tag{3.2}$$

(where principle discussed for an applied strain of $\epsilon_x$ is applied to the other normal strains as well).

This concept can be extended to a composite unit cell. If the full state of strain is applied to the unit cell using fixed boundary conditions, the outcome should be the same as applying a strain in a single direction to the unit cell using movable boundary conditions. For example, for T800s/3900-2 (see Section D.2 for the material properties) the following sets of amplification factors were determined for one interrogation point (located at $(x, y, z) = (0.1,0.5,0.303)$, i.e. a location somewhere in the fiber on the line of horizontal symmetry):

$$\begin{bmatrix} 1 & 0 & 0 & 0 & 0 & 0 \\ -0.02745 & 0.6934 & -0.00407 & 0 & 0 & 0 \\ -0.02262 & -0.01175 & 0.7557 & 0 & 0 & 0 \\ 0 & 0 & 0 & 0.367 & 0 & 0 \\ 0 & 0 & 0 & 0 & 0.4655 & 0 \\ 0 & 0 & 0 & 0 & 0 & 0.4168 \end{bmatrix}$$

Matrix 3.1: Example amplification factors using fixed boundary conditions

$$\begin{bmatrix} 1 & -0.01186 & -0.01186 & 0 & 0 & 0 \\ -0.2027 & 0.695 & -0.2319 & 0 & 0 & 0 \\ -0.2118 & -0.2602 & 0.7599 & 0 & 0 & 0 \\ 0 & 0 & 0 & 0.367 & 0 & 0 \\ 0 & 0 & 0 & 0 & 0.4655 & 0 \\ 0 & 0 & 0 & 0 & 0 & 0.4168 \end{bmatrix}$$

Matrix 3.2: Example amplification factors using movable boundary conditions

Note that the shear terms are identical since the present discussion only concerns the normal load cases. In addition to that, the following deformations were extracted (by manually inspecting the finite element model) from the unit cell using movable boundary conditions:

- For an applied strain of $\epsilon_x = 1$, the resulting strains were $\epsilon_y = \epsilon_z = -0.2543$
- For an applied strain of $\epsilon_y = 1$, the resulting strains were $\epsilon_x = -0.1186$ and $\epsilon_z = -0.3291$
- For an applied strain of $\epsilon_z = 1$, the resulting strains were $\epsilon_x = -0.1186$ and $\epsilon_y = -0.3291$

If now, for example, a strain vector of $[1 \quad -0.2543 \quad -0.2543 \quad 0 \quad 0 \quad 0]^T$ – which is the full external state of strain – is passed through the mechanical amplification factors based on fixed boundary conditions (Matrix 3.1), the resulting state of strain is

$$\begin{bmatrix} 1 & 0 & 0 & 0 & 0 & 0 \\ -0.02745 & 0.6934 & -0.00407 & 0 & 0 & 0 \\ -0.02262 & -0.01175 & 0.7557 & 0 & 0 & 0 \\ 0 & 0 & 0 & 0.367 & 0 & 0 \\ 0 & 0 & 0 & 0 & 0.4655 & 0 \\ 0 & 0 & 0 & 0 & 0 & 0.4168 \end{bmatrix} \begin{bmatrix} 1 \\ -0.2543 \\ -0.2543 \\ 0 \\ 0 \\ 0 \end{bmatrix} = \begin{bmatrix} 1 \\ -0.2027 \\ -0.2118 \\ 0 \\ 0 \\ 0 \end{bmatrix}.$$

This is identical to the result obtained from the movable boundary conditions if a strain vector of $[1 \quad 0 \quad 0 \quad 0 \quad 0 \quad 0]^T$ is applied (i.e. the first column of Matrix 3.2). Carrying out the same calculation for applied strains of $\epsilon_y$ and $\epsilon_z$ yields the second and third columns of Matrix 3.2. Clearly, at least for this case fixed and movable boundary conditions are indeed equivalent.

In order to increase confidence, the amplification factors for all interrogation points were compared. Note that only a single set of adjustment factors (the resulting strains outlined above) were required. Terms that were zero in one case and very small, but nonzero, in the other (due to the numerical cutoff described in Subsection 4.2.6) and other similar numerical issues were excluded. For the square array the maximum difference in any term was 1.1%, with an average of 0.022% across all terms for all interrogation points (excluding cases with zero difference to avoid skewing the statistics). Similarly, for the hexagonal array the maximum difference was 7.3%, with an average of 0.08%.

This means that fixed and movable boundary conditions for the normal load cases are, in fact, identical. The only difference is related to the way in which Poisson's strains are taken into account. As stated previously, for the movable boundary conditions the Poisson's effect has to be removed from the external applied strain, whereas for the fixed boundary conditions it has to be added manually to all strains that are not measured directly (instead of assuming those strains to be zero).

For an applied strain in a single direction, it is simpler to use movable boundary conditions. All other strains will automatically be included by the unit cell. However, once biaxial strains are known (e.g. the typical case of measuring $\epsilon_x$ and $\epsilon_y$ for a laminate), the situation becomes much more complex because the Poisson's strains due to $\epsilon_y$ have to be removed from $\epsilon_x$ and vice versa. For the case of the full state of strain being known (for example from a finite element analysis), coupling effects between all three normal strain components would have to be removed. This would become quite challenging and also very difficult to understand conceptually.

For the fixed boundary conditions the approach is much more intuitive. The full set of applied strains needs to be used, obtained either through measurement or otherwise through approximation using analytical calculations. Therefore, it was chosen to use fixed boundary conditions for the micromechanical enhancement, and to establish unknown strains using the process developed in Section 3.2. This is also in agreement with the majority of literature, including the articles by Gosse.

## 3.2 Full State of Strain for Failure Envelope Generation

With the decision made to use fixed boundary conditions, evaluating failure for a known full state of strain is straightforward. Most investigations in literature employ a detailed finite element model, loaded both mechanically and thermally, to determine the full state of strain. However, for research purposes, comparison to laminate test data, or sensitivity studies, failure envelopes are more useful. Using finite elements for all strain combinations would be far too time consuming. Therefore, this section focuses on analytical evaluation of the full state of strain.

As discussed in Subsection 2.1.5 real failure envelopes involve various factors, including out-of-plane effects, Poisson's ratios, and curing strains. These topics are covered in Subsections 3.2.1 and 3.2.2. Subsection 3.2.3 reviews classical lamination theory regarding strain rotations from the laminate to the ply coordinate system, followed by Subsection 3.2.4 presenting a summary of the full state of strain.

Other challenges mentioned are coupling effects between strain components, as well as amplification factors differing between interrogation points. These are covered in Section 4.3 because they only influence the practical implementation, with no additional theoretical investigation required.

The generation of failure envelopes in this section assumes thin, flat, orthotropic plies and laminates, without changes in thickness direction (i.e. a state of plane stress without bending loads). Typically, symmetric balanced laminates are assumed, although the expressions are not limited to those cases.

### 3.2.1 Poisson's Effects

An important aspect of the full state of strain is the out-of-plane strain due to the Poisson's effect. Neglecting this component and using only the direct strains (e.g. $\epsilon_{11}$ and $\epsilon_{22}$ for the common case of in-plane normal strain envelopes) would be unconservative, as discussed in Subsection 3.1.2. Parts of the following derivation are based on classical lamination theory. The corresponding equations can be found in any standard textbook and will only be briefly summarized here.

The relationship between stresses and strains is given by Matrix 3.3 and its inverse (Matrix 3.4).

$$\boldsymbol{\sigma} = \boldsymbol{C}\boldsymbol{\epsilon} \rightarrow \begin{bmatrix} \sigma_x \\ \sigma_y \\ \sigma_z \\ \tau_{yz} \\ \tau_{xz} \\ \tau_{xy} \end{bmatrix} = \begin{bmatrix} C_{11} & C_{12} & C_{13} & 0 & 0 & 0 \\ C_{12} & C_{22} & C_{23} & 0 & 0 & 0 \\ C_{13} & C_{23} & C_{33} & 0 & 0 & 0 \\ 0 & 0 & 0 & C_{44} & 0 & 0 \\ 0 & 0 & 0 & 0 & C_{55} & 0 \\ 0 & 0 & 0 & 0 & 0 & C_{66} \end{bmatrix} \begin{bmatrix} \epsilon_x \\ \epsilon_y \\ \epsilon_z \\ \gamma_{yz} \\ \gamma_{xz} \\ \gamma_{xy} \end{bmatrix}$$

Matrix 3.3: Definition of stiffness matrix for an orthotropic material (e.g. (Kassapoglou, 2013, Eqn. 3.4))

$$\boldsymbol{\epsilon} = \boldsymbol{S}\boldsymbol{\sigma} \rightarrow \begin{bmatrix} \epsilon_x \\ \epsilon_y \\ \epsilon_z \\ \gamma_{yz} \\ \gamma_{xz} \\ \gamma_{xy} \end{bmatrix} = \begin{bmatrix} S_{11} & S_{12} & S_{13} & 0 & 0 & 0 \\ S_{12} & S_{22} & S_{23} & 0 & 0 & 0 \\ S_{13} & S_{23} & S_{33} & 0 & 0 & 0 \\ 0 & 0 & 0 & S_{44} & 0 & 0 \\ 0 & 0 & 0 & 0 & S_{55} & 0 \\ 0 & 0 & 0 & 0 & 0 & S_{66} \end{bmatrix} \begin{bmatrix} \sigma_x \\ \sigma_y \\ \sigma_z \\ \tau_{yz} \\ \tau_{xz} \\ \tau_{xy} \end{bmatrix}$$

Matrix 3.4: Definition of compliance matrix for an orthotropic material

The stiffness matrix is obtained by inverting the compliance matrix, i.e. $\boldsymbol{C} = \boldsymbol{S}^{-1}$. The compliance matrix (for an individual ply), in turn, is determined from the basic material properties using

$$\boldsymbol{S} = \begin{bmatrix} \frac{1}{E_1} & -\frac{\nu_{12}}{E_1} & -\frac{\nu_{13}}{E_1} & 0 & 0 & 0 \\ -\frac{\nu_{12}}{E_1} & \frac{1}{E_2} & -\frac{\nu_{23}}{E_2} & 0 & 0 & 0 \\ -\frac{\nu_{13}}{E_1} & -\frac{\nu_{23}}{E_2} & \frac{1}{E_3} & 0 & 0 & 0 \\ 0 & 0 & 0 & \frac{1}{G_{23}} & 0 & 0 \\ 0 & 0 & 0 & 0 & \frac{1}{G_{13}} & 0 \\ 0 & 0 & 0 & 0 & 0 & \frac{1}{G_{12}} \end{bmatrix}.$$

Matrix 3.5: Content of compliance matrix based on ply material properties (e.g. (Kassapoglou, 2013, Eqn. 3.10))

For a state of plane stress, as assumed in the ply of a thin laminate, the third row of Matrix 3.3 leads to $0 = C_{13}\epsilon_x + C_{23}\epsilon_y + C_{33}\epsilon_z$. From this, the out-of-plane Poisson's effect is calculated as

$$\epsilon_z = -\frac{C_{13}\epsilon_x + C_{23}\epsilon_y}{C_{33}}. \tag{3.3}$$

Note that calculating the Poisson's effect as $\epsilon_z = -\nu_{13}\epsilon_x - \nu_{23}\epsilon_y$ (which seems correct at first glance) does not work because of the coupling between loads in $x$- and $y$-directions.

Similarly, for uniaxial loading (e.g. in $x$-direction), the standard equations

$$\epsilon_z = \frac{S_{13}}{S_{11}} = -\nu_{13}\epsilon_x \tag{3.4}$$

and

$$\epsilon_y = \frac{S_{12}}{S_{11}} = -\nu_{12}\epsilon_y \tag{3.5}$$

hold (following from the first three rows of Matrix 3.4). This is relevant for envelopes involving one normal strain component and one shear component. Similarly, if $\epsilon_y$ is applied uniaxially and the other two boundaries are stress free, the relations become

$$\epsilon_x = \frac{S_{12}}{S_{22}\epsilon_y} = -\nu_{12}\frac{E_2}{E_1} \tag{3.6}$$

and

$$\epsilon_z = \frac{S_{23}}{S_{22}}\epsilon_y = -\nu_{23}\epsilon_y \tag{3.7}$$

Out-of-plane loads are rather uncommon and thus not included here. The derivation would be equivalent. This type of calculation is only an approximation (similar to the curing strains in Subsection 3.2.2) because the laminate being tested may not actually be flat. Many biaxial test facilities employ cylindrical laminates, with the two strain components being the hoop and axial strains.

It is important to understand the use of ply and laminate properties. For the out-of-plane direction, the ply Poisson's ratio (in the ply coordinate system) should be used. This is due to the fact that in that direction the stress is assumed to be zero (plane stress conditions), meaning that each ply

experiences a strain according to its own Poisson's ratios (it is not restricted in its movement by the other plies). On the other hand, for cases where in-plane Poisson's effects need to be taken into account (for example for failure envelopes involving only one of $\epsilon_x$ and $\epsilon_y$, or for uniaxial tests with an unknown nonzero transverse strain), laminate properties (in the laminate coordinate system) should be used because of the assumption of in-plane strain compatibility made in classical lamination theory. The relevant parameters can be determined using once again classical lamination theory:

$$E_{1,laminate} = Q_{11,laminate} - \frac{Q_{12,laminate}^2}{Q_{22,laminate}} \tag{3.8}$$

$$E_{2,laminate} = Q_{22,laminate} - \frac{Q_{12,laminate}^2}{Q_{11,laminate}} \tag{3.9}$$

$$\nu_{12,laminate} = \frac{Q_{12,laminate}}{Q_{22,laminate}} \tag{3.10}$$

where $\boldsymbol{Q}_{laminate}$ is given by Eqn. (3.11).

In the following sections, the Poisson's effects are usually included in form of a matrix multiplication, using the Poisson's effect matrices shown below. The full relationship is shown in Eqn. (3.19).

$$\boldsymbol{\Pi}_{biaxial,out-of-plane} = \begin{bmatrix} 1 & 0 & 0 & 0 & 0 & 0 \\ 0 & 1 & 0 & 0 & 0 & 0 \\ -\frac{C_{13}}{C_{33}} & -\frac{C_{23}}{C_{33}} & 0 & 0 & 0 & 0 \\ 0 & 0 & 0 & 1 & 0 & 0 \\ 0 & 0 & 0 & 0 & 1 & 0 \\ 0 & 0 & 0 & 0 & 0 & 1 \end{bmatrix}$$

Matrix 3.6: Out-of-plane Poisson's effect matrix for biaxial known strains

$$\boldsymbol{\Pi}_{biaxial,in-plane} = \begin{bmatrix} 1 & 0 & 0 & 0 & 0 & 0 \\ 0 & 1 & 0 & 0 & 0 & 0 \\ 0 & 0 & 1 & 0 & 0 & 0 \\ 0 & 0 & 0 & 1 & 0 & 0 \\ 0 & 0 & 0 & 0 & 1 & 0 \\ 0 & 0 & 0 & 0 & 0 & 1 \end{bmatrix} = \boldsymbol{I}$$

Matrix 3.7: In-plane Poisson's effect matrix for biaxial known strains

$$\boldsymbol{\Pi}_{longitudinal,out-of-plane} = \begin{bmatrix} 1 & 0 & 0 & 0 & 0 & 0 \\ 0 & 1 & 0 & 0 & 0 & 0 \\ -\nu_{13} & 0 & 0 & 0 & 0 & 0 \\ 0 & 0 & 0 & 1 & 0 & 0 \\ 0 & 0 & 0 & 0 & 1 & 0 \\ 0 & 0 & 0 & 0 & 0 & 1 \end{bmatrix}$$

Matrix 3.8: Out-of-plane Poisson's effect matrix for uniaxial longitudinal strain known

$$\boldsymbol{\Pi}_{\epsilon_x,in-plane} = \begin{bmatrix} 1 & 0 & 0 & 0 & 0 & 0 \\ -\nu_{12} & 0 & 0 & 0 & 0 & 0 \\ 0 & 0 & 0 & 0 & 0 & 0 \\ 0 & 0 & 0 & 1 & 0 & 0 \\ 0 & 0 & 0 & 0 & 1 & 0 \\ 0 & 0 & 0 & 0 & 0 & 1 \end{bmatrix}$$

Matrix 3.9: In-plane Poisson's effect matrix for uniaxial $\epsilon_x$ known

$$\mathbf{\Pi}_{transverse,out-of-plane} = \begin{bmatrix} 1 & 0 & 0 & 0 & 0 & 0 \\ 0 & 1 & 0 & 0 & 0 & 0 \\ 0 & -\nu_{23} & 0 & 0 & 0 & 0 \\ 0 & 0 & 0 & 1 & 0 & 0 \\ 0 & 0 & 0 & 0 & 1 & 0 \\ 0 & 0 & 0 & 0 & 0 & 1 \end{bmatrix}$$

Matrix 3.10: Out-of-plane Poisson's effect matrix for uniaxial transverse strain known

$$\mathbf{\Pi}_{\epsilon_y,in-plane} = \begin{bmatrix} 0 & -\nu_{12}\dfrac{E_2}{E_1} & 0 & 0 & 0 & 0 \\ 0 & 1 & 0 & 0 & 0 & 0 \\ 0 & 0 & 1 & 0 & 0 & 0 \\ 0 & 0 & 0 & 1 & 0 & 0 \\ 0 & 0 & 0 & 0 & 1 & 0 \\ 0 & 0 & 0 & 0 & 0 & 1 \end{bmatrix}$$

Matrix 3.11: In-plane Poisson's effect matrix for uniaxial $\epsilon_y$ known

It should be stressed here that the out-of-plane matrix depends on the resulting state of strain in the ply coordinate system. This means that a 90° ply, loaded in uniaxial $\epsilon_x$, should be using $\mathbf{\Pi}_{\epsilon_x,in-plane}$ for in-plane effects, but $\mathbf{\Pi}_{transverse,out-of-plane}$ for out-of-plane loads. Contrary to that, if a 90° ply is loaded in uniaxial $\epsilon_y$, $\mathbf{\Pi}_{\epsilon_y,in-plane}$ and $\mathbf{\Pi}_{longitudinal,out-of-plane}$ should be used. For angles other than 0° or 90°, $\mathbf{\Pi}_{biaxial,out-of-plane}$ should be used.

One additional topic that needs to be addressed is the type of material properties used. In Subsection 3.1.2, the transverse displacements of the unit cell for an applied unit strain were extracted manually from the finite element model. Since the size of the unit cell is 1, a displacement directly translates into a strain of the same magnitude. The Poisson's ratio is equal to the ratio of measured to applied strain, which means that it is just the measured strain (which, in turn, is equal to the measured displacement) because the applied strain is a unit strain.

However, at the present state of development of the theory all ply material properties (including those used in Matrix 3.5, as well as all out-of-plane Poisson's effect matrices) need to be determined using experimental methods. This means that regardless of the fiber array type, the same (measured) Poisson's ratio is used. The in-plane Poisson's effect matrices are based on laminate properties, which are in turn calculated based on measured ply properties.

It may be beneficial to extract the stiffness properties from the micromechanical models. On one hand, using calculated ply stiffness properties based on a certain fiber array type holds the advantage of reducing the required experimental input data. It also adheres to the assumption of the particular type of unit cell repeating indefinitely in all directions, as discussed in Subsection 2.1.3. On the other hand, if experimental data is used an additional degree of realism is introduced compared to using theoretical calculations. This is also similar to the discrepancy between model and reality that is accepted when assuming the measured ply strains to be identical to the unit cell strains (Subsection 2.1.6). Making the same assumption for the Poisson's effects is more consistent.

It is also not clear how the process of extracting properties from the finite element model would work for the rotated unit cells investigated in Subsection 3.3. In this thesis, measured properties will be used because they are typically readily available in literature for most common composites.

### 3.2.2 Curing Strains

Similarly to the derivation of the Poisson's effects, parts of the derivation of the mechanical strains due to the temperature difference between curing and application temperatures (subsequently referred to as "curing strains") is based on classical lamination theory. These parts will only be covered briefly. First, the thermal expansion coefficients of the laminate are calculated. Then, the curing strains are determined as the strains required to overcome the mismatch between laminate and ply thermal expansion coefficients.

The approach of using the difference between the free thermal expansion of a ply and the thermal expansion of the laminate to determine the curing strains is based on the article by (Ritchey et al., 2011), which – together with (Buchanan et al., 2009) – seems to be the only source addressing this topic in detail. However, neither of these two articles discuss generating failure envelopes.

The derivation of the thermal expansion coefficients consists of two steps. First, the laminate stiffness matrix needs to be calculated. Subsequently, the thermal expansion coefficients can be derived.

Calculating the stiffness matrix starts by once again assuming plane stress. Based on that, the stiffness matrix (Matrix 3.3) can be simplified by setting $\sigma_z$, $\tau_{yz}$ and $\tau_{xz}$ to zero. From this a direct result is that $\gamma_{yz}$ and $\gamma_{xz}$ are also zero. Additionally, the expression for $\epsilon_z$ in terms of $\epsilon_x$ and $\epsilon_z$ derived in Eqn. (3.3) can be substituted. Three equations remain: $\sigma_x = C_{11}\epsilon_x + C_{12}\epsilon_y + C_{13}\left(-\frac{C_{13}\epsilon_x + C_{23}\epsilon_y}{C_{33}}\right)$, $\sigma_y = C_{12}\epsilon_x + C_{22}\epsilon_y + C_{23}\left(-\frac{C_{13}\epsilon_x + C_{23}\epsilon_y}{C_{33}}\right)$, and $\tau_{xy} = C_{66}\gamma_{xy}$.

The reduced stiffness matrix in the ply coordinate system (denoted "$\boldsymbol{Q}_{ply}$") is therefore given by

$$\begin{bmatrix}\sigma_x\\ \sigma_y\\ \tau_{xy}\end{bmatrix} = \boldsymbol{Q}_{ply}\begin{bmatrix}\epsilon_x\\ \epsilon_y\\ \gamma_{xy}\end{bmatrix} \rightarrow \boldsymbol{Q}_{ply} = \begin{bmatrix} C_{11} - \frac{C_{13}^2}{C_{33}} & C_{12} - \frac{C_{13}C_{23}}{C_{33}} & 0 \\ C_{12} - \frac{C_{13}C_{23}}{C_{33}} & C_{22} - \frac{C_{23}^2}{C_{33}} & 0 \\ 0 & 0 & C_{66}\end{bmatrix}.$$

Matrix 3.12: Definition and content of reduced stiffness matrix (e.g. (Kassapoglou, 2013, Eqns. 3.16 and 3.17))

In the laminate coordinate system, the ply stiffness matrix can be determined using the in-plane rotation matrix according to $\boldsymbol{Q}_{ply,rotated} = \boldsymbol{T}^T\boldsymbol{Q}_{ply}\boldsymbol{T}$, where $\boldsymbol{T}$ is the in-plane part of Matrix 3.14:

$$\boldsymbol{T} = \begin{bmatrix} c^2 & s^2 & cs \\ s^2 & c^2 & -cs \\ -2cs & 2cs & c^2 - s^2\end{bmatrix}$$

Matrix 3.13: In-plane rotation matrix. $c = \cos\theta$ and $s = \sin\theta$, where $\theta$ is the angle between ply and laminate coordinate systems (e.g. (Ritchey et al., 2011, Eqn. 17).

Due to the assumption of strain compatibility, the laminate in-plane stiffness matrix can be calculated as the weighted average of the ply stiffness matrices. In other words, since the width cancels,

$$\boldsymbol{Q}_{laminate} = \frac{\sum \boldsymbol{Q}_{ply,rotated} t_{ply}}{\sum t_{ply}} = \frac{\sum \boldsymbol{T}^T\boldsymbol{Q}_{ply}\boldsymbol{T} t_{ply}}{\sum t_{ply}}. \tag{3.11}$$

It should be noted that, provided the ply thickness is the same for all plies, its actual value does not matter for the calculation of the reduced stiffness matrix.

Similar steps are taken to arrive at the thermal expansion coefficients. First of all, the in-plane thermal expansion coefficients of the ply in terms of the basic material properties are given by

$$\boldsymbol{\alpha}_{ply} = \begin{bmatrix} \alpha_1 \\ \alpha_2 \\ 0 \end{bmatrix} \tag{3.12}$$

(where the third component refers to shear, which – due to the orthogonality of a ply – is zero). Note that these coefficients are assumed to be constant with temperature, similar to the assumption of linear analysis made in Subsection 2.1.6. In the laminate coordinate system, the properties are

$$\boldsymbol{\alpha}_{ply,rotated} = \boldsymbol{T}^{-1}\boldsymbol{\alpha}_{ply}. \tag{3.13}$$

Finally, in order to determine the laminate thermal expansion coefficients, once more strain compatibility is enforced. Since this means that the net force needs to be equal to the sum of forces, the following equation holds: $\boldsymbol{Q}_{laminate}\boldsymbol{\epsilon}_{laminate}t_{laminate} = \sum \boldsymbol{Q}_{ply,rotated}\boldsymbol{\epsilon}_{ply,rotated}t_{ply}$ (where the width is again canceled). Substituting $\epsilon = \alpha\Delta T$ for both laminate and ply, and rearranging, yields

$$\boldsymbol{\alpha}_{laminate} = \frac{\boldsymbol{Q}^{-1}_{laminate}}{t_{laminate}} \sum \boldsymbol{Q}_{ply,rotated}\boldsymbol{\alpha}_{ply,rotated}t_{ply}$$

which can be substituted to yield

$$\boldsymbol{\alpha}_{laminate} = \frac{\boldsymbol{Q}^{-1}_{laminate}}{t_{laminate}} \sum \boldsymbol{T}^T\boldsymbol{Q}_{ply}\boldsymbol{\alpha}_{ply}t_{ply}. \tag{3.14}$$

Note that for balanced laminates, the shear term of the thermal expansion factors should be zero.

With the thermal expansion coefficients of the laminate known, the in-plane curing strains are calculated as the strains required to remove the discrepancy between the thermal expansion of the laminate and the free thermal expansion of a ply, in other words (in the ply coordinate system)

$$\boldsymbol{\epsilon}_{curing,in-plane} = \begin{bmatrix} \epsilon_{x,curing,in-plane} \\ \epsilon_{y,curing,in-plane} \\ \epsilon_{xy,curing,in-plane} \end{bmatrix} = (\boldsymbol{T}\boldsymbol{\alpha}_{laminate} - \boldsymbol{\alpha}_{ply})\Delta T. \tag{3.15}$$

Note that there are no direct curing strains in out-of-plane direction, because each ply is free to deform according to its own coefficient of thermal expansion. However, the in-plane mechanical strains will still cause an out-of-plane mechanical strain due to the Poisson's effect according to Eqn. (3.3) and have to be added separately. This means that the final vector of curing strains is found to be

$$\boldsymbol{\epsilon}_{curing} = \begin{bmatrix} \epsilon_{x,curing,in-plane} \\ \epsilon_{y,curing,in-plane} \\ -\dfrac{C_{13}\epsilon_{x,curing,in-plane} + C_{23}\epsilon_{y,curing,in-plane}}{C_{33}} \\ 0 \\ 0 \\ \epsilon_{xy,curing,in-plane} \end{bmatrix}. \tag{3.16}$$

This can be more easily expressed using the biaxial Poisson's effect matrix $\boldsymbol{\Pi}_{biaxial,out\ of\ plane}$ (the multiplication by $\boldsymbol{\Pi}_{biaxial,in-plane}$ can be omitted for the reason that $\boldsymbol{\Pi}_{biaxial,in-plane} = \boldsymbol{I}$):

$$\boldsymbol{\epsilon}_{curing} = \boldsymbol{\Pi}_{biaxial,out\ of\ plane} \begin{bmatrix} \epsilon_{x,curing,in-plane} \\ \epsilon_{y,curing,in-plane} \\ 0 \\ 0 \\ 0 \\ \epsilon_{xy,curing,in-plane} \end{bmatrix}. \tag{3.17}$$

Similar to the fact that the actual value of $t_{ply}$ does not matter provided all layers have the same thickness, changing the layup also does not have any effect as long as the ply percentages stay the same. This means that [0,90,90,0], [0,0,90,90,0,0] and [90,0,0,90] all give the same results because from an in-plane thermal point of view they are identical.

The same comments as in Subsection 3.2.1 hold for the curing strains. These expressions are only an approximation assuming flat laminates, adhering to the assumptions of classical lamination theory. Additionally, as for the Poisson's effects the thermal expansion coefficients are experimentally determined values rather than being extracted from the micromechanical models. The suggestion to research the drawbacks and benefits of doing so also holds for this case.

In addition to that, curing strains – similar to the direct temperature effects taken into account through $\boldsymbol{A}\Delta T$ in Eqn. (2.5) – may relax over time. This is addressed in Section 7.4.

### 3.2.3 Rotation from Laminate to Ply Coordinate System

If a finite element software is used, typically the rotation from laminate to ply coordinate system is carried out automatically, using the material orientation defined for the ply. However, in order to determine failure envelopes this process has to be carried out manually. Matrix 3.14 shows the full 3D strain rotation matrix, using the standard convention for the order of strain components ($[\epsilon_x \quad \epsilon_y \quad \epsilon_z \quad \gamma_{yz} \quad \gamma_{xz} \quad \gamma_{xy}]^T$, as discussed in Subsection 2.1.4). $\boldsymbol{\epsilon}_{ply} = \boldsymbol{\Omega}\boldsymbol{\epsilon}_{laminate}$, where

$$\boldsymbol{\Omega} = \begin{bmatrix} c^2 & s^2 & 0 & 0 & 0 & cs \\ s^2 & c^2 & 0 & 0 & 0 & -cs \\ 0 & 0 & 1 & 0 & 0 & 0 \\ 0 & 0 & 0 & c & -s & 0 \\ 0 & 0 & 0 & -s & c & 0 \\ -2cs & 2cs & 0 & 0 & 0 & c^2 - s^2 \end{bmatrix}$$

Matrix 3.14: Strain rotation matrix from laminate to ply coordinate system. $c = \cos\theta$ and $s = \sin\theta$, where $\theta$ is the angle between ply and laminate coordinate systems.

This matrix can be found in any textbook covering classical lamination theory. The rotation between $\epsilon_x$, $\epsilon_y$ and $\gamma_{xy}$ is defined by the standard in-plane rotation matrix, found for example in (Kassapoglou, 2013, Eqn. 3.36). $\epsilon_z$ is not affected by a rotation about the $z$-axis. Finally, the out-of-plane shear strains $\gamma_{yz}$ and $\gamma_{xz}$ only experience a rotation for one of their components ($x$ or $y$, but not $z$), meaning that the regular cosine and sine rotation terms (readily derived from a simple sketch) are sufficient. Since the $z$-direction is not affected, there is no coupling between normal and shear components, unlike for the in-plane strains.

### 3.2.4 Summary of Full State of Strain

The full procedure to analyze a laminate, experiencing a temperature difference and mechanical strains, can be summarized using Eqn. (2.5) ($\boldsymbol{\epsilon}_{local} = \boldsymbol{M}\boldsymbol{\epsilon}_{global} + \boldsymbol{A}\Delta T$) as a starting point.

$\boldsymbol{\epsilon}_{global}$ consists of the summation of applied mechanical strains and curing strains, in other words

$$\boldsymbol{\epsilon}_{global} = \boldsymbol{\epsilon}_{applied} + \boldsymbol{\epsilon}_{curing}. \tag{3.18}$$

All strains are in the ply coordinate system. $\boldsymbol{\epsilon}_{curing}$ is determined from Eqn. (3.17), and

$$\boldsymbol{\epsilon}_{applied} = \boldsymbol{\Pi}_{out-of-plane}\boldsymbol{\Omega}\boldsymbol{\Pi}_{in-plane}\boldsymbol{\epsilon}_{applied,laminate}. \tag{3.19}$$

In this equation, the in-plane Poisson's effects are added using the appropriate in-plane Poisson's effect matrix (Matrix 3.7, Matrix 3.9, or Matrix 3.11). Subsequently, the laminate strains are rotated to the ply coordinate system using Matrix 3.14, followed by adding the Poisson's effects according to the appropriate choice of Matrices 3.6, 3.8, or 3.10.

Note that the effect of the curing strains is simply to shift the failure envelope. They can be determined by any means (including a finite element analysis, if desired), and added afterwards.

It seems worth mentioning that there are two distinct types of strains due to temperature differences: macro-level strains due to the mismatch in thermal expansion coefficients of laminate and ply, and (as discussed in Subsection 2.1.4) micro-level strains due to the mismatch between fiber and matrix, which are taken into account through the thermal amplification vector.

## 3.3 Investigation of Fiber Array Types and Rotated Unit Cells

In Subsection 2.2.6, several contradicting claims were found regarding the types of unit cells that should be taken into account in the micromechanical enhancement process. (Hart-Smith, 2010) in particular asserted that square, diamond, and two hexagonal unit cells (vertical and horizontal) are sufficient. Contrary to that, (Ha et al., 2008) suggest using a square and hexagonal fiber arrays, rotated by in between 0° and 180°. The purpose of the present section is to investigate those points. The first question is whether square, diamond, and both hexagonal unit cells can indeed be obtained by rotating square and hexagonal fiber arrays. Secondly, the required rotation angles for the unit cells need to be established. Based on this, a conclusion can be drawn on whether the fiber arrays Hart-Smith claims to be sufficient indeed give the most conservative results.

Hart-Smith's argumentation is mostly based on the severity of strain amplification factors. Since the development efforts in this thesis resulted in a software tool capable of automatically generating failure envelopes, a more visual means of determining the most critical fiber array is available. This approach will be employed in the subsequent sections. With the exception of the aspect being investigated (required fiber array types and rotation angles), the full procedure outlined in Section 3.5 will be used.

### 3.3.1 Equivalence of Vertical and Horizontal Hexagonal Unit Cells

The first investigation concerns the equivalence of vertical and horizontal hexagonal unit cells. It also explains the basic principle behind using rotated unit cells.

For vertical and horizontal hexagonal unit cells, it is self-evident that a strain applied in the direction of the long side of the vertical unit cell should cause the same response of the unit cell as a strain applied in the direction of the long side of the horizontal unit cell, with the only difference being the coordinate systems used. In other words, assuming that the long side of the vertical unit cell is located in $y$-direction and the long side of the horizontal unit cell is located in $z$-direction, a strain of $\epsilon_y = 1$ applied to the vertical cell should be identical to a strain of $\epsilon_z = 1$ applied to the horizontal cell. This indeed noticeable since the strain amplification factors for equivalent points in the vertical and horizontal hexagonal unit cells contain the same terms in different arrangements.

Based on this, it should be possible to obtain the response of the horizontal unit cell by rotating the applied strain (in the horizontal coordinate system) such that $\epsilon_z$ becomes $\epsilon_y$ (in other words, rotating to the vertical coordinate system), applying the result to the vertical cell, and rotating the result back to the horizontal coordinate system. This principle can be formalized as follows:

$$\boldsymbol{\epsilon}_{local,horizontal} = \boldsymbol{M}_{horizontal}\boldsymbol{\epsilon}_{global} = \boldsymbol{\Theta}_{90^\circ}{}^{-1}\boldsymbol{M}_{vertical}\boldsymbol{\Theta}_{90^\circ}\boldsymbol{\epsilon}_{global} \tag{3.20}$$

where

$$\boldsymbol{\Theta}_{90^\circ} = \begin{bmatrix} 1 & 0 & 0 & 0 & 0 & 0 \\ 0 & 0 & 1 & 0 & 0 & 0 \\ 0 & 1 & 0 & 0 & 0 & 0 \\ 0 & 0 & 0 & -1 & 0 & 0 \\ 0 & 0 & 0 & 0 & 0 & -1 \\ 0 & 0 & 0 & 0 & 1 & 0 \end{bmatrix}.$$

This matrix is a mathematical way of expressing a switch of $y$- and $z$-components due to a rotation of 90°. It is a specific version (using a rotation angle of 90°) of the more general rotation matrix

$$\boldsymbol{\Theta} = \begin{bmatrix} 1 & 0 & 0 & 0 & 0 & 0 \\ 0 & c^2 & s^2 & cs & 0 & 0 \\ 0 & s^2 & c^2 & -cs & 0 & 0 \\ 0 & -2cs & 2cs & c^2 - s^2 & 0 & 0 \\ 0 & 0 & 0 & 0 & c & -s \\ 0 & 0 & 0 & 0 & s & c \end{bmatrix},$$

Matrix 3.15: Unit cell rotation matrix. $c = \cos\theta$ and $s = \sin\theta$, where $\theta$ is the unit cell rotation angle.

obtained similarly to Matrix 3.14, albeit for a rotation about the $x$-axis (along the fiber) rather than the $z$-axis.

Performing the calculation is straightforward. For example, for a point corresponding to M13 of Figure 2.12 and using the material properties from Section B.2, the vertical unit cell returns

$$\begin{bmatrix} 1 & 0 & 0 & 0 & 0 & 0 \\ -0.1503 & 0.9514 & -0.5344 & 0 & 0 & 0 \\ 0.5983 & 0.5277 & 2.793 & 0 & 0 & 0 \\ 0 & 0 & 0 & 1.404 & 0 & 0 \\ 0 & 0 & 0 & 0 & 4.684 & 0 \\ 0 & 0 & 0 & 0 & 0 & 0.3125 \end{bmatrix},$$

while the horizontal unit cell returns

$$\begin{bmatrix} 1 & 0 & 0 & 0 & 0 & 0 \\ 0.5983 & 2.793 & 0.5277 & 0 & 0 & 0 \\ -0.1503 & -0.5344 & 0.9514 & 0 & 0 & 0 \\ 0 & 0 & 0 & 1.404 & 0 & 0 \\ 0 & 0 & 0 & 0 & 0.3125 & 0 \\ 0 & 0 & 0 & 0 & 0 & 4.684 \end{bmatrix}.$$

Evidently these are the same matrices, except for a switch in $y$- and $z$-components.

Instead of comparing responses for some applied strain vector, $\boldsymbol{\epsilon}_{global}$ is dropped on both sides of Eqn. (3.20), resulting in $\boldsymbol{M}_{horizontal} = \boldsymbol{\Theta}_{90°}{}^{-1}\boldsymbol{M}_{vertical}\boldsymbol{\Theta}_{90°}$. Performing this calculation for the amplification factors shown above is trivial and indeed produces identical results.

Since this expression will be used for square and diamond unit cells as well (see Subsection 3.3.2), it is written in more general form as

$$\boldsymbol{M} = \boldsymbol{\Theta}^{-1}\boldsymbol{M}'\boldsymbol{\Theta}. \tag{3.21}$$

In this expression, $\boldsymbol{M}'$ refers to the mechanical amplification factor matrix of the "base" unit cell (in this case vertical hexagonal), while $\boldsymbol{M}$ is the same property for the "derived" unit cell (in this case horizontal). This equation means that the mechanical strain amplification factors for the horizontal hexagonal unit cell can be obtained from the vertical one without any additional finite element analyses. (Of course, this relationship could also be inverted. In this thesis the vertical hexagonal unit cell was chosen as the "standard". Whenever a hexagonal unit cell is referred to in subsequent sections, the vertical one is meant, although it is in fact not important which one is used.)

For the thermal amplification factors, a similar equation can be derived. Since the thermal amplification factors are already a vector in the vertical coordinate system ($\Delta T$ is a scalar), only a single rotation is required (from the vertical back to the horizontal coordinate system). This is given by

$$\boldsymbol{A} = \boldsymbol{\Theta}^{-1}\boldsymbol{A}'. \tag{3.22}$$

It should be mentioned here that the properties of interest for the application of Onset Theory are invariants. Therefore, the inverse rotation ($\boldsymbol{\Theta}^{-1}$) in Eqns. (3.21) and (3.22) is technically not needed. However, it is still included in case the actual strain amplification factors for a rotated unit cell are of interest. In this thesis the inverse rotation is irrelevant since only invariants are used.

### 3.3.2 Equivalence of Square and Diamond Unit Cells

A similar comparison can be carried out for the square and diamond unit cells. Using once again the material properties from Section B.2, amplification factors for the square array were extracted at a point corresponding to IF1 in Figure 2.9 and an equivalent point in the diamond unit cell.

Unlike for the hexagonal unit cells in the previous section, it is not immediately obvious that one set of amplification factors can be obtained from the other since on first glance the terms are completely different. Therefore, the calculations are discussed in detail below.

Matrices 3.16 to 3.19 show the strain amplification factors obtained from the square and diamond unit cells, while Matrices 3.20 and 3.21 show the results of Eqns. (3.21) and (3.22) (with $\theta = 45°$).

$$\begin{bmatrix} 1 & 0 & 0 & 0 & 0 & 0 \\ -0.2731 & 0.4741 & -0.5336 & 0 & 0 & 0 \\ 0.8041 & 1.036 & 3.083 & 0 & 0 & 0 \\ 0 & 0 & 0 & 1.94 & 0 & 0 \\ 0 & 0 & 0 & 0 & 6.816 & 0 \\ 0 & 0 & 0 & 0 & 0 & 0.1201 \end{bmatrix}$$

Matrix 3.16: Mechanical amplification factors for the square array

$$\begin{bmatrix} -6439 \\ -8295 \\ 12560 \\ 0 \\ 0 \\ 0 \end{bmatrix} \cdot 1\text{e-}8$$

Matrix 3.17: Thermal amplification factors for the square array

$$\begin{bmatrix} 1 & 0 & 0 & 0 & 0 & 0 \\ 0.2655 & 1.985 & 0.04513 & -0.2599 & 0 & 0 \\ 0.2655 & 0.04513 & 1.985 & -0.2599 & 0 & 0 \\ -1.077 & -2.089 & -2.089 & 1.528 & 0 & 0 \\ 0 & 0 & 0 & 0 & 3.468 & -3.348 \\ 0 & 0 & 0 & 0 & -3.348 & 3.468 \end{bmatrix}$$

Matrix 3.18: Mechanical amplification factors for the diamond array

$$\begin{bmatrix} -6439 \\ 2132 \\ 2132 \\ -20850 \\ 0 \\ 0 \end{bmatrix} \cdot 1\text{e-}8$$

Matrix 3.19: Thermal amplification factors for the diamond array

$$\begin{bmatrix} 1 & 0 & 0 & 0 & 0 & 0 \\ 0.2655 & 1.985 & 0.04487 & -0.2598 & 0 & 0 \\ 0.2655 & 0.04487 & 1.985 & -0.2598 & 0 & 0 \\ -1.077 & -2.089 & -2.089 & 1.527 & 0 & 0 \\ 0 & 0 & 0 & 0 & 3.468 & -3.348 \\ 0 & 0 & 0 & 0 & -3.348 & 3.468 \end{bmatrix}$$

Matrix 3.20: Mechanical amplification factors for the square array, rotated by 45° using Eqn. (3.21)

$$\begin{bmatrix} -6439 \\ 2132.5 \\ 2132.5 \\ -20855 \\ 0 \\ 0 \end{bmatrix} \cdot 1\text{e-}8$$

Matrix 3.21: Thermal amplification factor for the square array, rotated by 45° using Eqn. (3.22)

Clearly, the results from rotated square and diamond unit cell are essentially identical. The small differences (the maximum is 0.57% in terms (3,2) and (2,3) of Matrix 3.20) can be traced back to the rounding procedure described in Subsection 4.2.6. Used there to avoid numerical inaccuracies during the convergence study, it does introduce some minor inaccuracies in this context.

Multiple points in the square and diamond unit cells show this behavior. For further confirmation, failure envelopes are generated as well. Figure 3.1 shows that the two envelopes are indeed identical.

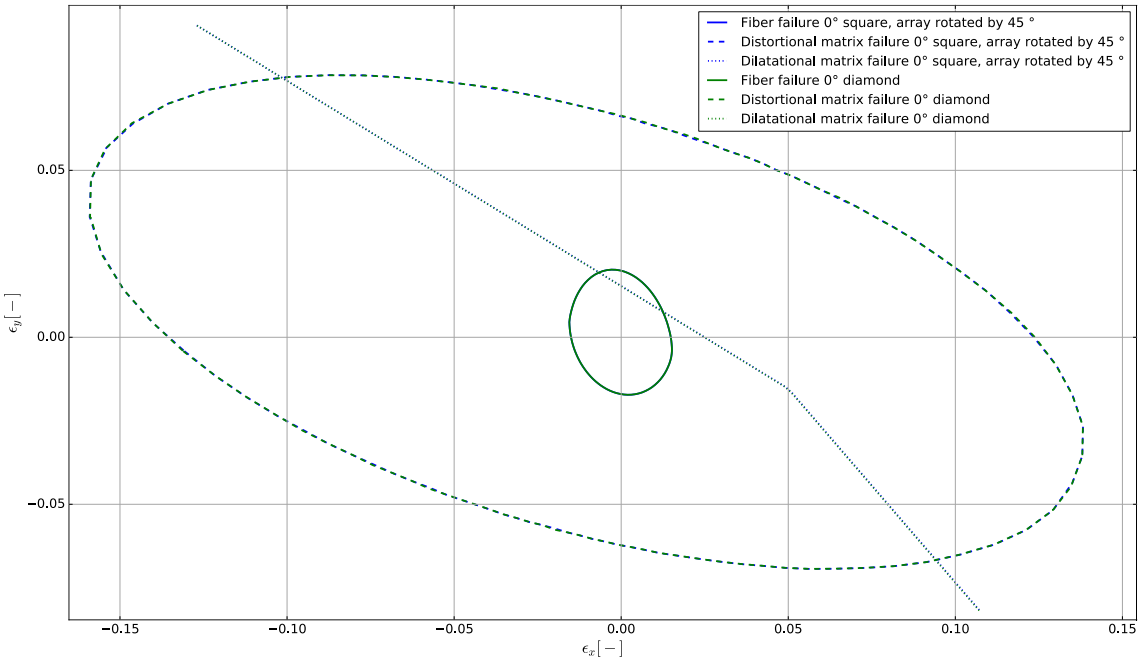


Figure 3.1: Comparison of failure envelopes based on diamond and rotated square fiber arrays. The invariants are $J_1^{*m} = 0.0225$, ${\epsilon^*_{eqv}}^m = 0.204$ and ${\epsilon^*_{eqv}}^f = 0.02$, combined with the material properties from Section B.2.

### 3.3.3 Required Rotation Angles

Based on the preceding two sections, it is clear that the diamond and horizontal hexagonal unit cells are rotated versions of the square and vertical hexagonal unit cells, respectively. This means that all unit cells mentioned by for example Hart-Smith (square, diamond, and vertical and horizontal hexagonal) can be obtained by using a square unit cell rotated by 0° and 45° and a horizontal unit cell rotated by 0° and 90°. The question is thus whether other rotation angles prove to be more critical than these four possibilities. If that is the case, using only those four unit cells is insufficient.

(Ha et al., 2008) use rotation angles between 0° and 180°. However, due to the rotational symmetry of the unit cell values of up to 90° for the square unit cell and up to 60° for the hexagonal unit cell should be sufficient. In addition to that, since interrogation points in one half of the unit cell are taken into account (see Section 3.4), these ranges are further reduced by a factor of 2. In other words, the required ranges of rotation angles are 0° to 45° for the square unit cell and 0° to 30° for the hexagonal unit cell.

During the development process, this behavior was confirmed, with rotation angles of 0°, 90°, 180°,… for the square unit cell yielding identical results. Increasing the angle, 15°, 75°, 105°,… gave identical results. Further increments of 15° yielded the patterns 30°, 60°, 120°,… and 45°, 135°, 225°,…. At this point another increment of 15° would end up in the pattern based on 30°, showing that indeed a range of 0° to 45° is sufficient for the square unit cell. For the hexagonal unit cell, equivalent patterns were established for base angles of 0°, 15° and 30°.

The question thus is which of the rotation angles between 0° to 45° for the square unit cell and 0° to 30° for the hexagonal unit cell are most critical. This was investigated by directly comparing the failure envelopes for multiple rotation angles. The material used was T800s/3900-2 (see Section D.2

for the material properties), with the critical invariants $J_1^{*m} = 0.024$, ${\epsilon^*_{eqv}}^m = 0.2$ and ${\epsilon^*_{eqv}}^f = 0.02$ (i.e. the default values from Subsection 6.2.5).

Figure 3.2 shows an example for the hexagonal unit cell. Rotation angles of 0°, 15° and 30° are used for an $\epsilon_x$ vs $\epsilon_y$ failure envelope. The fiber failure envelope is entirely defined by 0° and 30° rotations (corresponding to the vertical and horizontal hexagonal unit cells), with relatively small differences between the two except for dilatational matrix failure. This failure mode is purely defined by the 30° rotation. However, the distortional matrix failure is defined by the 15° rotation for the part of the envelope shown (the present view is an enlarged version of the entire envelope in order to show the relevant details; in other parts of the envelope, 0° and 30° rotations are critical).

This means that technically using only vertical and horizontal hexagonal unit cells would be unconservative for distortional matrix failure. However, for the envelope shown this failure mode is always preceded by fiber or dilatational matrix failure, which will both be catastrophic for a single ply. The same result was obtained for other ply angles and strain combinations (for example $\epsilon_y$ vs $\gamma_{xy}$).

Although the intermediate angles did not seem to be particularly critical, another analysis was carried out using more refined angles. This meant steps of 7.5° instead of 15°, in other words rotation angles of 0°, 7.5°, 15°, 22.5°, 30°, 37.5° and 45° for the square array and 0°, 7.5°, 15°, 22.5° and 30° for the hexagonal array. The purpose was in particular to establish whether one of those finer intermediate angles resulted in a more critical fiber or dilatational matrix failures.

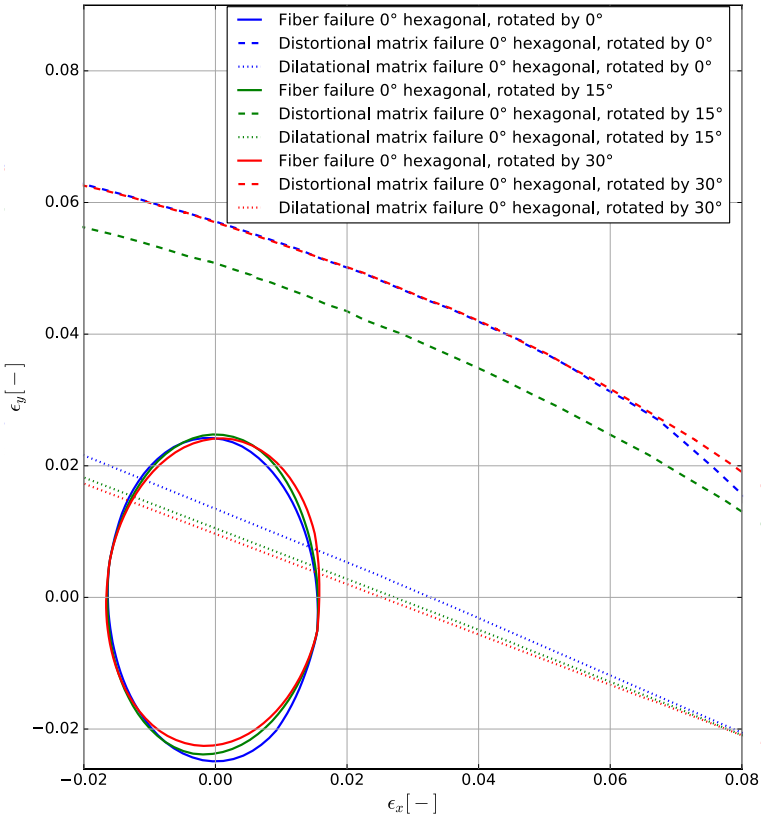


Figure 3.2: Comparison of various rotation angles for the hexagonal unit cell

Figure 3.3 shows the $\epsilon_y$ vs $\gamma_{xy}$ envelopes resulting from smaller increments in rotation angles for the square unit cell. The results are similar to the ones discussed previously for the hexagonal fiber array. The overall critical failure prediction is fully defined by a rotation angle of 0°, with a rotation angle of 7.5° being very similar. For distortional matrix failure, the finer intermediate angles (e.g. 22.5°) did indeed lead to even slightly more conservative predictions than the intermediate angles of 15° and 30°. These differences may very well be within the accuracy of the numerical approach to determine the failure envelopes (Subsection 4.3.1), as well as numerical cutoffs used in the micromechanical enhancement process (Subsection 4.2.6). In addition to that, in all cases these failures are preceded by catastrophic fiber failures.

In general, during the analysis of various combinations of ply angles, strain components on the $x$- and $y$-axes of the envelope, and rotation angles, no cases were found where angles other than 0° for the square fiber array and 0° and 90° for the hexagonal fiber array were critical for the overall failure prediction. This means that based on this analysis not even the diamond array is relevant. On the other hand, increments of 7.5° did result in more critical failure envelopes for distortional matrix value, although these were preceded by other failure modes. In order to ensure that the most conservative envelope is included even for other materials, critical invariants, or combinations of the parameters investigated here (ply angles and strain components on the $x$- and $y$-axes), 7.5° will be used as increments in this thesis.

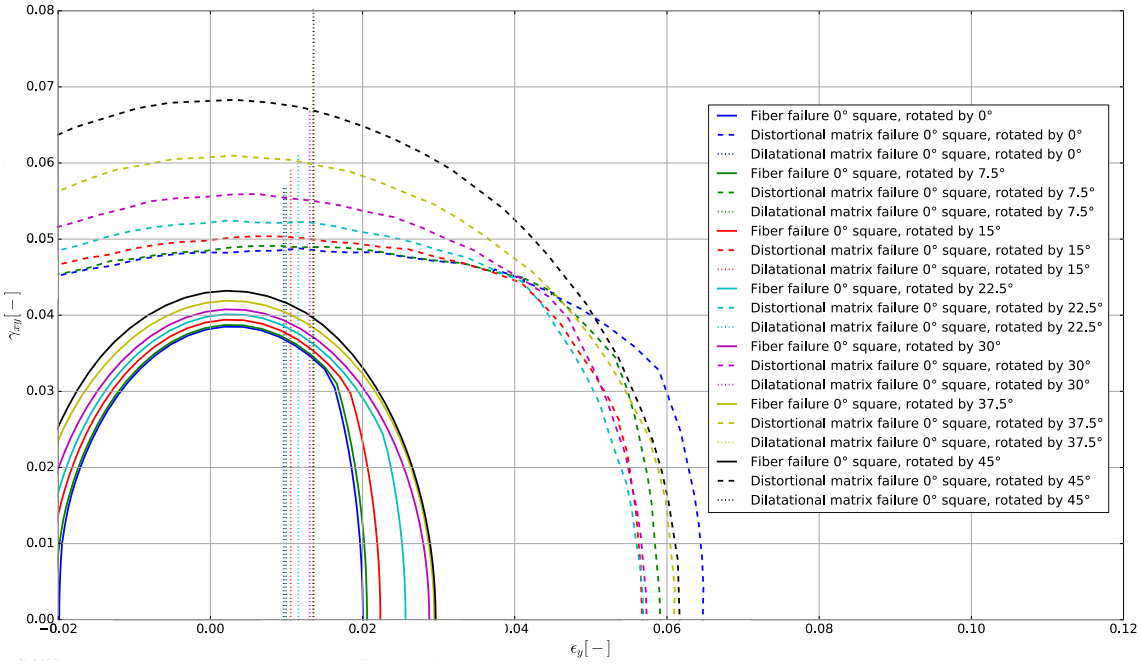


Figure 3.3: Comparison of various rotation angles for the square unit cell

In this context it should be mentioned that (Hart-Smith, 2007, Slide 63) shows the diamond array being more critical than the square array. However, this result was obtained in stress space. Hart-Smith is using the stiffness matrix based on the particular unit cell to convert between strain and stress spaces. Since according to him the transverse stiffness of the diamond array is about 20% lower than the one for the square array, the diamond array becomes more critical. In the present thesis, as discussed at the end of Subsection 3.2.1, the same stiffness matrix is used (based on

measured ply properties) regardless of the unit cell. Additionally, with the exception of the suggested progressive failure analysis (Subsection 8.4.3), only strain-based envelopes will be used based on the reasoning found in Subsection 2.2.1. In order to ensure conservatism, the diamond unit cell (in form of a square unit cell rotated by 45°) will be included for all analyses in this thesis. However, at this point it does not seem to be the critical unit cell for any combination of parameters investigated.

### 3.3.4 Summary of Required Fiber Array Types and Rotation Angles

In summary, this means two things. First of all, only a square and a hexagonal array need to be used, rotated by 0°, 7.5°, 15°, 22.5°, 30°, 37.5° and 45° for the square array and 0°, 7.5°, 15°, 22.5° and 30° for the hexagonal array. Based on the analysis in the preceding subsections, no rotation is necessary for the square array, and only 0° and 30° are needed for the hexagonal array. The additional rotation angles are included in order to provide confidence for corner cases not investigated here. The resulting computational time is still reasonable (see also Subsection 4.3.2). Note that the diamond unit cell is identical to the square unit cell, rotated by 45°, while the horizontal hexagonal unit cell is identical to the vertical one, rotated by 30°.

The second conclusion regards the claim by (Hart-Smith, 2010) that square, diamond, and both hexagonal unit cells are sufficient for conservative failure predictions. Based on Subsection 3.3.3, these claims are mostly correct. Although some rotated unit cells result in more conservative failure envelopes for distortional matrix failure, this type of failure is preceded by distortional matrix failure in all cases investigated. In fact, the diamond unit cell is also not critical, at least in strain space.

(Buchanan et al., 2009) and (Ritchey et al., 2011) (both involving Gosse, the original author of Onset Theory) imply that only a square and one hexagonal unit cell is sufficient. This is not the case because both hexagonal unit cells define parts of the envelope. It does stand to reason that Gosse is aware of this fact, given that he also collaborated with Prof. Ha, who used rotated unit cells with rotation angles between 0° and 180° (see e.g. (Ha et al., 2008)). Regarding this approach, it was found that this range contains duplicate angles and can be reduced.

## 3.4 Investigation of Required Interrogation Points

As examined in Subsection 2.2.7, different researchers sample their strain amplification factors at different locations in fiber and matrix. In order to determine the correct choices, Subsection 3.4.1 examines which points contribute to the most conservative failure envelope for a variety of cases. The failure envelopes are determined using the full procedure outlined in Section 3.5, with the exceptions specified in the following subsection. Subsequently, the symmetry of the unit cell is considered in Subsection 3.4.2. This is particularly relevant for the rotated failure envelopes (Section 3.3).

### 3.4.1 Critical Interrogation Points

The example used is once again T800s/3900-2 (see Section D.2 for the material properties), with the critical invariants $J_1^{*m} = 0.024$, ${\epsilon^*_{eqv}}^m = 0.2$ and ${\epsilon^*_{eqv}}^f = 0.02$ (i.e. the default values from Subsection 6.2.5). In this subsection, a dense grid of interrogation points in one half of the unit cell is

taken into account (see e.g. Figure 4.1). Both square and hexagonal cells are investigated. The purpose is to determine whether the "standard" interrogation points discussed in Subsection 2.2.7 are sufficient, or whether other points need to be taken into account. The reason for selecting points in one half of the unit is discussed in detail in Subsection 3.4.2. In order to reduce the amount of information at least somewhat, only unit cell rotation angles of 0° are taken into account. As discussed in Subsection 3.3.3 these cover the majority of critical cases (although a hexagonal unit cell, rotated by 30°, will also be critical for some parts of the envelope). The purpose is not to obtain the true conservative failure envelope, but to determine which points are critical in general. During the investigation of rotated unit cells, it was found that the fiber failure envelope is entirely dominated by the 0° rotations, while for the matrix cutoffs the 30° rotation of the hexagonal unit cell is most critical in some locations.

Figure 3.4 shows the contributions to the fiber failure envelope. Clearly, the envelope is almost entirely determined by IP13Fiber, IP57Fiber, and IP170Fiber of the square array. All other contributions are quite minor. Although there are some pieces of the envelope that where other interrogation points appear to be more critical, this is most likely due to the numerical accuracy of the process described in Section 4.3. Note that this numerical accuracy is also the cause of the gaps in the contributions. For the pieces in between, it is not clear which interrogation point is most critical. They are filled in with straight lines for the final envelope.

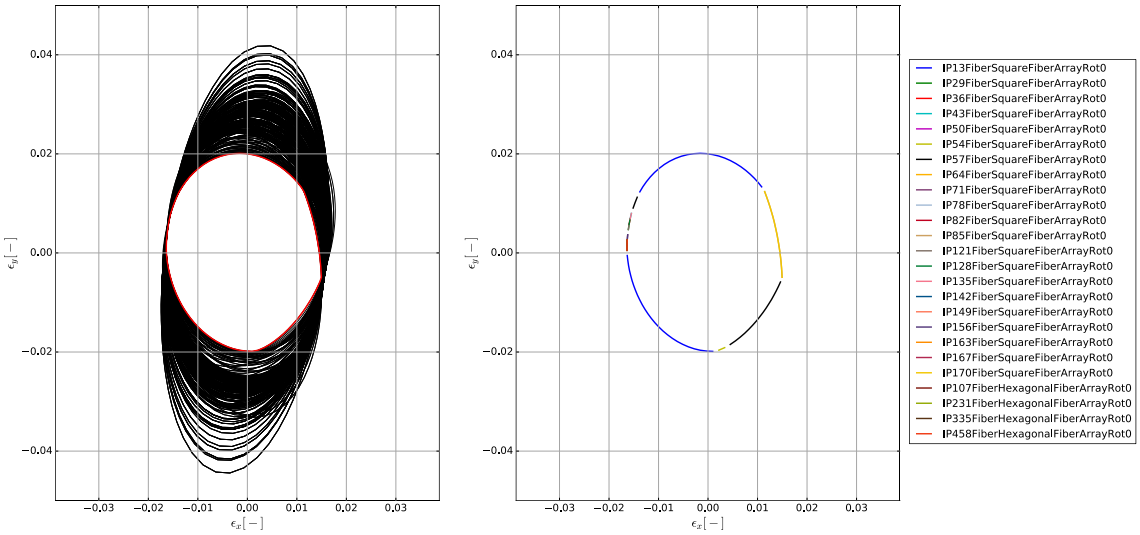


Figure 3.4: Contributions to fiber failure envelope

Based on Figure 3.5, these three interrogation points correspond to the center of the fiber, as well as points at 90° and 270° (measured from a horizontal line, originating at the center of the unit cell and pointing to the right) on the fiber/matrix boundary. It should be mentioned that the envelope for IP85Fiber (at 0° on the fiber/matrix boundary) exactly overlaps with the one for IP170Fiber (at 270°). This overlap is not visible in the plot because the lines coincide. Symmetry of the unit cell is discussed further in Subsection 3.4.2.

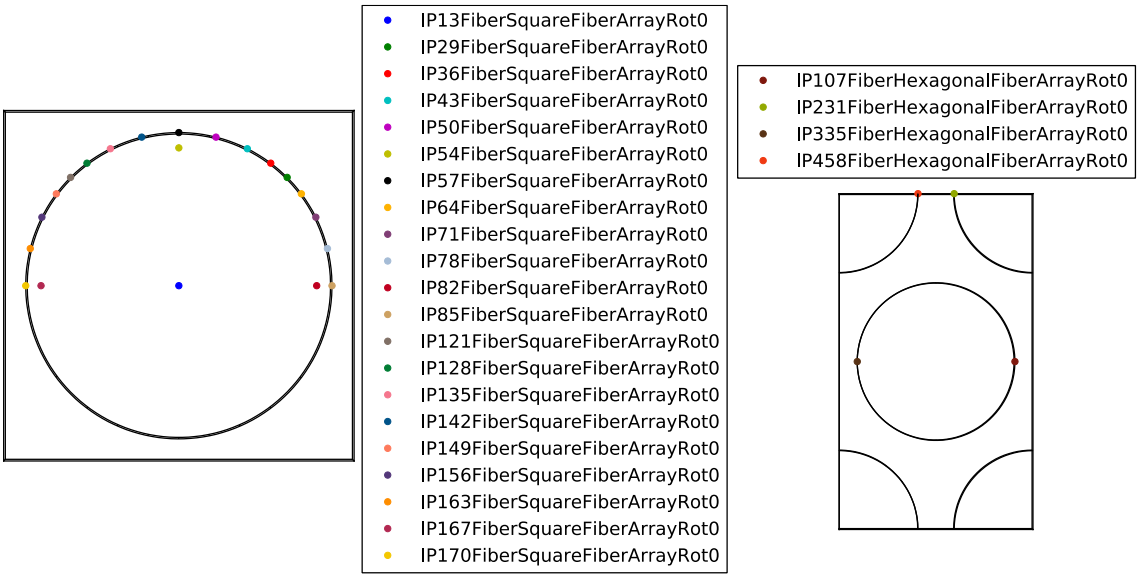


Figure 3.5: Location of critical interrogation points for fiber failure envelope

Similar results are found for an envelope involving a shear strain. In that case, the envelope is almost exclusively defined by IP13Fiber and IP57Fiber, with only a very minor numerical inaccuracy.

The same investigation is carried out for the distortional matrix failure envelope (Figure 3.6). In that case, the envelope is mostly defined by IP37Matrix of the hexagonal array and IP93Matrix of the square array. Minor contributions are IP181Matrix of the square array, as well as IP423Matrix and IP437Matrix of the hexagonal array. The remaining contributions are either two small to discern or coincide with the points mentioned already.

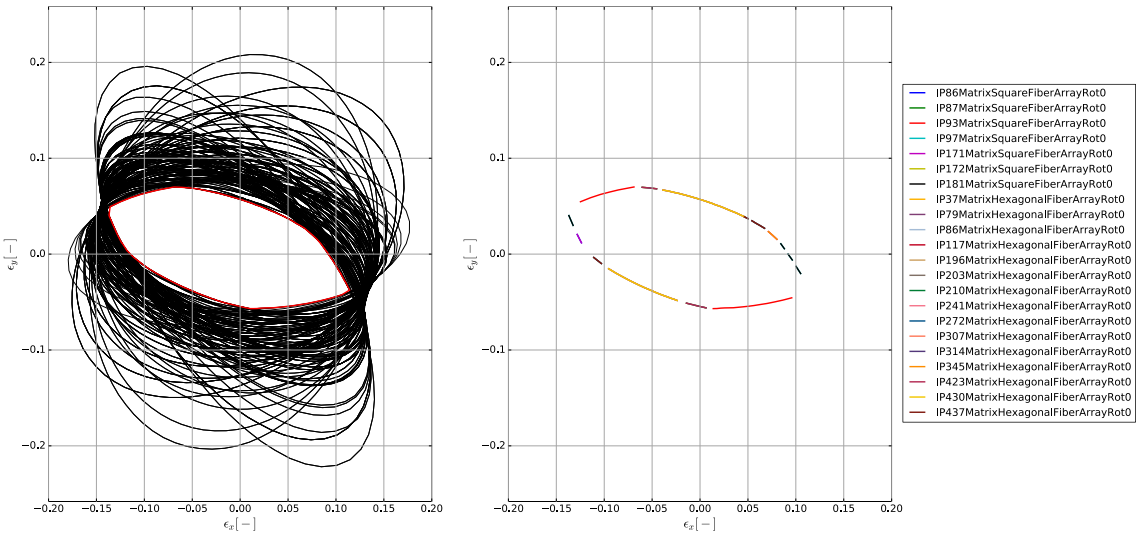


Figure 3.6: Contributions to distortional matrix failure envelope

Using Figure 3.7, it is found that the critical locations correspond to the interfiber locations, as defined in for example Figure 2.9. In addition to that, some points on the fiber/matrix interface also appear to play a role. However, these are the minor contributions mentioned above.

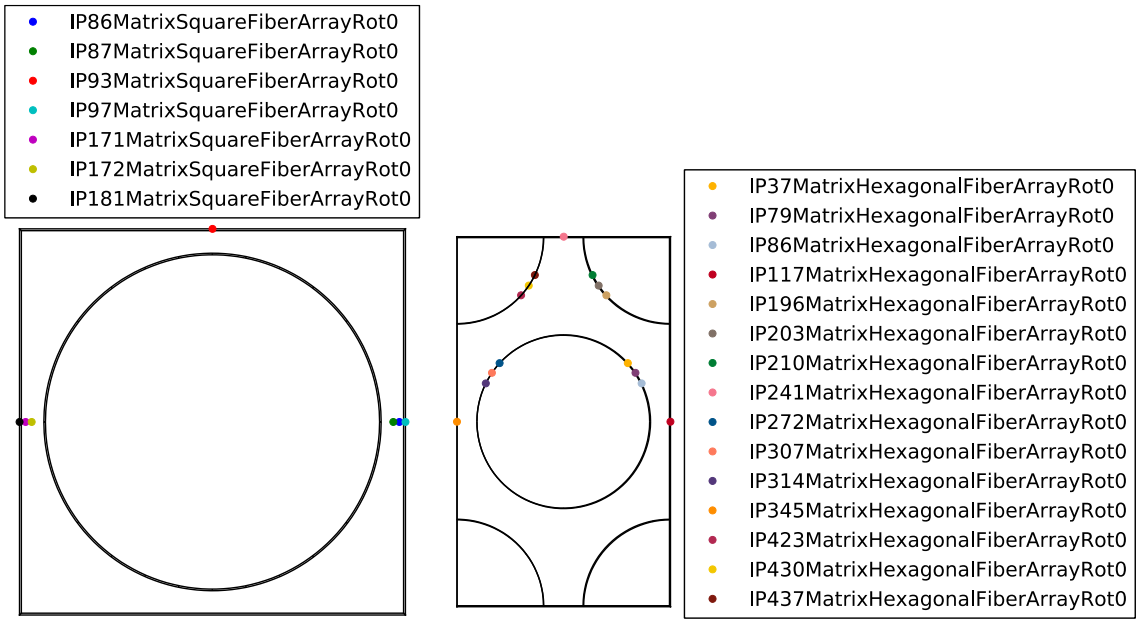


Figure 3.7: Location of critical interrogation points for distortional matrix failure envelope

For the dilatational matrix cutoff, the only relevant point is IP57Matrix of the square array. This corresponds to point M1 in Figure 2.11 (i.e. a point at 90° on the fiber/matrix boundary). All other parts of the cutoff are also defined by points on the fiber/matrix boundary.

As for the fiber envelope, the matrix envelopes for strain combinations involving shear do not yield significantly different results. Once again the same points are relevant, although their relative importance changes somewhat. In particular, the points on the fiber/matrix boundary of the hexagonal array (IP423Matrix etc.) become slightly more important for distortional matrix failure.

The preceding investigation does seem to indicate that only the interfiber points of the square and hexagonal arrays are relevant for distortional matrix failure, if minor contributions possibly related to numerical inaccuracies are excluded. On the other hand, the interstitial location (see e.g. Figure 2.9) – claimed to be relevant by all researchers – does not seem to play a role.

Regarding the fiber failure envelope, the fiber center and points at 0° and 90° on the fiber/matrix boundary are most important.

### 3.4.2 Symmetry of the Unit Cell

One question that can be raised is how symmetry of the unit cell influences the required interrogation points. As mentioned in the previous subsection, the failure envelopes for some points overlap.

Since both square and hexagonal unit cells are doubly symmetric (in horizontal and vertical directions), intuitively using interrogation points in a single quarter of the unit cell should be sufficient. This approach is also chosen by many other researchers, as discussed in Subsection 2.2.7. However, there are two reasons why using a single quarter is insufficient.

The first argument is based on the response of the unit cell to shear strains. Figure 3.8 shows the strain component $\epsilon_{33}$ in the matrix of a square unit cell for an applied shear strain of $\gamma_{23}$. In the

top right and top left quarter of the unit cell, the magnitude of the values is identical, but the sign of the strain is different. This means that in equation Eqn. (2.2) (the equivalent strain), for terms such as $(\epsilon_{11} - \epsilon_{33})^2$ the value will be either added or subtracted, resulting in different failure predictions. Similar results are obtained for other strain combinations, as well as for the fiber phase. (Note that this switch in sign also occurs for the shear strains; however, these terms are squared individually in the equation for the equivalent strain, meaning that their sign does not matter.)

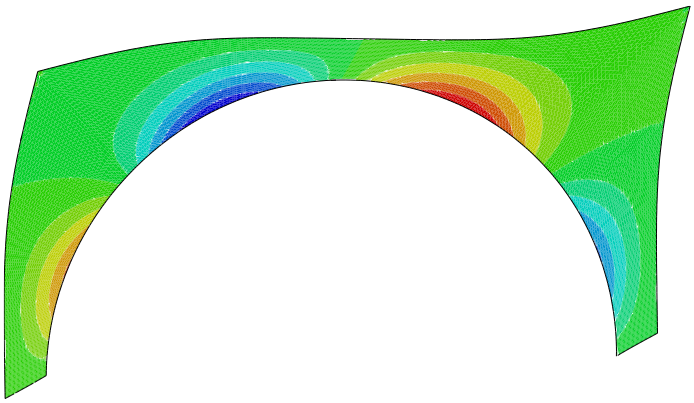

Figure 3.8: Resulting $\epsilon_{33}$ in the matrix for applied $\gamma_{23}$. Only the upper half of the unit cell is shown. The fiber has been removed for the visualization.[1]

It should be mentioned that this argument only holds for the additional interrogation points used in Subsection 3.4.1. The "standard" interrogation points found in literature (points at the fiber center, 0°, 45° or 90° on the fiber boundary, or the interfiber and interstitial locations defined in Figure 2.9) are not affected by this behavior because there are no coupling terms between shear and normal strains. This was also discussed in Subsection 2.1.5.

The second argument is related to the rotation of unit cells, as examined in Subsection 3.3. If a square array is rotated with interrogation points in a single quarter only, it fails to reproduce the diamond unit cell. This is shown in Figure 3.9.

Finally, note that the lower half of the unit cell is an antisymmetric copy of the upper half. Since resulting strains of both signs are already present in the upper half, the lower half could be replaced with symmetry boundary conditions. However, runtime of the micromechanical models is not critical at this point (see Subsection 4.2.7). Therefore, the symmetry approach was not pursued further in this thesis. Note that for the interrogation points, indeed only half of the unit cell is used, as also shown in Figure 4.1.

[1] The small white triangles visible on some screens / print outs are caused by a rendering problem in the Abaqus vector graphics export and do not carry any meaning

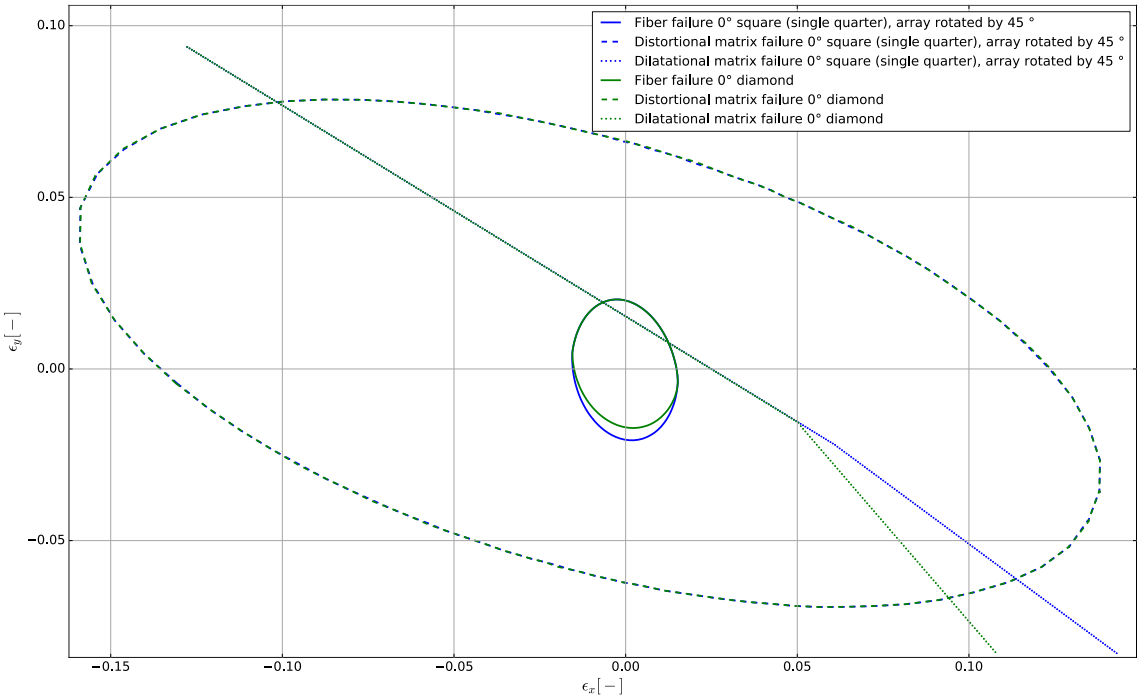


Figure 3.9: Comparison of failure envelopes based on diamond and rotated square fiber arrays (interrogation points in a single quarter). Material properties and invariants as indicated in Figure 3.1.

### 3.4.3 Summary of Required Interrogation Points

Based on Subsection 3.4.1, the interfiber locations (see e.g. Figure 2.9 for definitions of the standard locations) define distortional matrix failure, while points at 0° and 90° on the fiber boundary determine dilatational matrix failure and fiber failure. For fiber failure, the center of the fiber is also important. This result mostly supports the claims in literature regarding the critical points, although the interstitial location was not found to play a role.

This conclusion is also supported by the comparison between failure envelopes in Subsections 5.2.3 to 5.2.5, where envelopes generated using all interrogation points do not differ significantly from Hart-Smith's envelopes, although according to (Hart-Smith, 2010) he only seems to be taking interfiber and interstitial locations into account for the matrix (see also Subsection 2.2.7 for a definition of those locations). It is not clear which point(s) he is using for the fiber, but since he is performing the calculations analytically, it is very likely that only very few points are taken into account.

For this thesis the decision was made to use a dense grid of interrogation points (see e.g. Figure 4.1) in order to ensure that the most conservative behavior is captured regardless of the combination of input parameters (e.g. constituent material properties, ply rotation angle, and so on), and to include corner cases missed in the present investigation. In that case, interrogation points in one half of the unit cell need to be taken into account, rather than just one quarter as done by most researchers. This is relevant in order to capture the different sign of the shear terms. In addition to that, the interrogation points in a second quarter of the unit cell are also relevant for rotated unit cells, as examined in Section 3.3. Although it was concluded there that most likely rotation is not necessary, for this thesis it was decided to include rotations to ensure conservative predictions.

## 3.5 Summary of Consistent Approach

This section summarizes all relevant assumptions, processes, equations, and input data required to apply Onset Theory. It is meant as a quick guide for implementation, without containing any explanations or derivations. References to the (sub)sections discussing the various aspects are included.

### 3.5.1 Assumptions and Limitations

The following assumptions are made during the application of Onset Theory as used in this thesis:

- only onset of damage is considered (i.e. no progressive failure analysis) (Section 1.5);
- Onset Theory is only used as a ply failure criterion, with no prediction of ply interface failures such as delaminations (Subsection 2.1.6);
- only strain-based data is used (Subsection 2.2.1);
- measured ply properties are used, rather than ply properties extracted from the unit cell (Subsection 3.2.1);
- all analyses are linear static (Subsection 2.1.6);
- material properties (in particular thermal expansion factors) are constant with temperature (Subsection 3.2.2);
- the strain in a unit cell is the same as the strain in the ply, implying that the entire lamina consists of a single type of unit cell, repeated in all directions (Subsection 2.1.6);
- the fibers are assumed to be circular (Subsection 2.1.3);
- moisture absorption and chemical shrinkage are neglected (Subsection 2.2.2);
- failure of the fiber/matrix interface is not taken into account (Subsection 2.1.2);
- the fiber only failure in distortion, not in dilatation (Subsection 2.1.2);
- the order of strain components is $[\epsilon_{11} \quad \epsilon_{22} \quad \epsilon_{33} \quad \gamma_{23} \quad \gamma_{13} \quad \gamma_{12}]^T$ (Subsection 2.1.4);
- plies and laminates are thin, flat, and orthotropic, placing them in a state of plane stress (introduction to Section 3.2);
- there are no changes in thickness direction of the laminate, meaning no bending loads (introduction to Section 3.2);
- and finally, typically symmetric balanced laminates are considered, although the expressions should not be limited to this class of laminates (introduction to Section 3.2).

### 3.5.2 Micromechanical Enhancement

In order to obtain the strain amplification factors required to convert between global and local strains (used in Subsection 3.5.3), micromechanical analyses are carried out. Two fiber array are investigated: a square array and a hexagonal one (typically with the long side in vertical, i.e. $y$-

direction, although this is not relevant). Each interrogation point in the fiber arrays yields a mechanical amplification factor matrix $\boldsymbol{M'}$ and a thermal amplification factor vector $\boldsymbol{A'}$.

Based on these base values, values for rotated unit cells are calculated using Eqns. (3.21) and (3.22):

$$\boldsymbol{M} = \boldsymbol{\Theta^{-1}} \boldsymbol{M'} \boldsymbol{\Theta}$$

$$\boldsymbol{A} = \boldsymbol{\Theta^{-1}} \boldsymbol{A'}.$$

Based on Matrix 3.15,

$$\boldsymbol{\Theta} = \begin{bmatrix} 1 & 0 & 0 & 0 & 0 & 0 \\ 0 & c^2 & s^2 & cs & 0 & 0 \\ 0 & s^2 & c^2 & -cs & 0 & 0 \\ 0 & -2cs & 2cs & c^2 - s^2 & 0 & 0 \\ 0 & 0 & 0 & 0 & c & -s \\ 0 & 0 & 0 & 0 & s & c \end{bmatrix},$$

where $c = \cos\theta$ and $s = \sin\theta$, with $\theta$ being each one of the values 0°, 7.5°, 15°, 22.5°, 30°, 37.5° and 45° for the square array and 0°, 7.5°, 15°, 22.5° and 30° for the hexagonal array (Subsection 3.3.4). This means that for each interrogation point in the square array, seven sets of amplification factors are obtained, while for the hexagonal array, there are five sets per interrogation point.

Regarding the interrogation points, every point in the unit cell returns different strain amplification factors. In order to ensure sufficient coverage, a large number of interrogation points is taken into account (see for example Figure 4.1). As discussed in Subsection 3.4.3, interrogation points in one half of the unit cell need to be included.

During the micromechanical analyses, three different types of external loads are considered, resulting in seven load cases in total: normal strains ($\epsilon_{11}$, $\epsilon_{22}$ and $\epsilon_{33}$), shear strains ($\gamma_{23}$, $\gamma_{13}$ and $\gamma_{12}$), and a thermal load ($\Delta T$). For the normal strains, fixed boundary conditions will be used (Subsection 3.1.2), while for the thermal load, movable boundary conditions are used (Subsection 3.1.1). "Fixed" in this context means fixing the faces of the unit cell in place (with the exception of the applied displacement), while "movable" refers to allowing uniform translation of the face normal to its original position (see also Subsection 2.2.3 for a discussion of these two types of boundary conditions). For the shear cases, pure shear needs to be applied. During this type of loading the faces of the unit cell are allowed to warp (Subsection 2.2.4).

The basic dimension of the unit cell (both sides of the square cell, and the short side of the hexagonal cell) is 1, although the depth of the unit cell (length in $x$-direction) is irrelevant (Subsection 4.2.3). Based on geometrical considerations, the long side of the hexagonal unit cell (assumed to align with the $y$-direction, in accordance with Subsection 3.3.1) has a length of $\sqrt{3}$ (Subsection 4.2.6).

Using this basic dimension, the locations of the faces for the square unit cell are $x_0 = y_0 = z_0 = 0$ and $x_1 = y_1 = z_1 = 1$. For the hexagonal unit cell, $x_0$, $y_0$, $z_0$, $x_1$ and $z_1$ are in the same location, but $y_1 = \sqrt{3}$. In Subsection 4.2.4, the fiber radius and maximum volume fraction were derived to be $r = \sqrt{\frac{V_f}{\pi}}$ and $V_{f,max} = \frac{\pi}{4}$ for the square unit cell, and $r = \sqrt{\frac{\sqrt{3}V_f}{2\pi}}$ and $V_{f,max} = \frac{\pi}{2\sqrt{3}}$ for the hexagonal unit cell.

For the displacements in $x$-, $y$- and $z$- directions, $u$, $v$ and $w$ are used, respectively. The fiber is running along the $x$-direction.

In terms of equations, the boundary conditions for the seven load cases are thus

- $\epsilon_{11} = 1$: $u = 0$ at $x_0$, $u = 1$ at $x_1$, $v = 0$ at $y_0$ and $y_1$, $w = 0$ at $z_0$ and $z_1$
- $\epsilon_{22} = 1$: $u = 0$ at $x_0$ and $x_1$, $v = 0$ at $y_0$, $v = 1$ at $y_1$, $w = 0$ at $z_0$ and $z_1$
- $\epsilon_{33} = 1$: $u = 0$ at $x_0$ and $x_1$, $v = 0$ at $y_0$ and $y_1$, $w = 0$ at $z_0$, $w = 1$ at $z_1$
- $\gamma_{23} = 1$: $u = 0$ at all faces, $w = 0$ at $y_0$, $w = 0.5 \cdot y_1$ at $y_1$ (meaning $w = 0.5$ for the square unit cell and $w = 0.5\sqrt{3}$ for the hexagonal unit cell), $v = 0$ at $z_0$, $v = 0.5$ at $z_1$ (technically $v = 0.5 \cdot z_1$, but $z_1 = 1$ for both unit cells)
- $\gamma_{13} = 1$: $v = 0$ at all faces, $w = 0$ at $x_0$, $w = 0.5 \cdot x_1$ at $x_1$ (taking into account the fact that the depth of the unit cell may not be 1), $u = 0$ at $z_0$, $u = 0.5$ at $z_1$
- $\gamma_{12} = 1$: $w = 0$ at all faces, $v = 0$ at $x_1$, $v = 0.5 \cdot x_1$ at $x_1$, $u = 0$ at $y_0$, $u = 0.5 \cdot y_1$ at $y_1$
- $\Delta T = 1$: $u = 0$ at $x_0$, $v = 0$ at $y_0$, $z = 0$ at $z_0$. The faces at $x_1$, $y_1$ and $z_1$ are forced to remain flat, but may translate normal to their original location. See Subsection 4.2.2 for an example of how to implement this in Abaqus.

For each of these load cases, the strain response of the unit cell at one of the interrogation points is extracted. The mechanical load cases determine the columns of $\boldsymbol{M}'$ (e.g. the response for $\epsilon_{11} = 1$ is the first column), while the thermal load case determines $\boldsymbol{A}'$. During this step, it is important to ensure that the strain amplification factors, the columns of $\boldsymbol{M}'$, and the rows of $\boldsymbol{M}'$ and $\boldsymbol{A}'$ all follow the standard convention for the order of strain components (described in Subsection 3.5.1).

Since the basic dimension of the unit cell is unity, an applied unit displacement results in a unit strain. Therefore, the strain responses for the stated boundary conditions can be used directly as the columns of $\boldsymbol{M}'$ and $\boldsymbol{A}'$, with the exception of the mechanical amplification factors for $\epsilon_{22}$ in case of the hexagonal unit cell. These factors need to be multiplied by $\sqrt{3}$, see Subsection 4.2.6). Similar adjustments need to be made if the depth of the unit cell is reduced (Subsection 4.2.3). For the shear load cases the dimensions of the unit cell are included in the boundary conditions. In addition to that, typically smaller displacements and larger temperatures are applied in order to avoid numerical issues, meaning that the strain amplification factors need to be scaled accordingly (see again Subsection 4.2.6).

### 3.5.3 Full State of Strain for Failure Envelope Generation

Failure is evaluated for fiber and matrix separately (depending on whether fiber or matrix amplification factors are used) according to Eqns. (2.1) to (2.4):

$$\epsilon_{11} + \epsilon_{22} + \epsilon_{33} > J_1^*$$

$$\sqrt{\frac{1}{2}[(\epsilon_{11} - \epsilon_{22})^2 + (\epsilon_{11} - \epsilon_{33})^2 + (\epsilon_{22} - \epsilon_{33})^2] + \frac{3}{4}[\gamma_{23}^2 + \gamma_{13}^2 + \gamma_{12}^2]} > \epsilon_{eqv}^*$$

where the strains are the components of $\boldsymbol{\epsilon}_{local}$ (the order was defined in Subsection 3.5.1), given by Eqn. (2.5):

$$\boldsymbol{\epsilon}_{local} = \boldsymbol{M}\boldsymbol{\epsilon}_{global} + \boldsymbol{A}\Delta T.$$

$\boldsymbol{M}$ and $\boldsymbol{A}$ were defined in Subsection 3.5.2. Every combination of interrogation point, fiber array and unit cell rotation angle needs to be used, with failure assumed to occur if predicted by at least one combination.

Based on Eqn. (3.18),

$$\boldsymbol{\epsilon}_{global} = \boldsymbol{\epsilon}_{applied} + \boldsymbol{\epsilon}_{curing}.$$

Using Eqn. (3.19),

$$\boldsymbol{\epsilon}_{applied} = \mathbf{\Pi}_{out-of-plane}\mathbf{\Omega}\mathbf{\Pi}_{in-plane}\boldsymbol{\epsilon}_{applied,laminate}$$

where $\mathbf{\Pi}_{out-of-plane}$ and $\mathbf{\Pi}_{in-plane}$ are the appropriate choices of Matrices 3.6 to 3.11 based on the applied loads. Note that the use of the out-of-plane Poisson's ratio will differ for each ply, depending on the state of strain in that particular ply's coordinate system. For cases other than 0° and 90° plies, $\mathbf{\Pi}_{biaxial,out-of-plane}$ should be used.

Measured ply properties in the ply coordinate system are used for the out-of-plane matrices, while laminate properties (derived from measured ply properties) in the laminate coordinate system are used for the in-plane matrices.

$$\mathbf{\Pi}_{biaxial,out-of-plane} = \begin{bmatrix} 1 & 0 & 0 & 0 & 0 & 0 \\ 0 & 1 & 0 & 0 & 0 & 0 \\ -\frac{C_{13}}{C_{33}} & -\frac{C_{23}}{C_{33}} & 0 & 0 & 0 & 0 \\ 0 & 0 & 0 & 1 & 0 & 0 \\ 0 & 0 & 0 & 0 & 1 & 0 \\ 0 & 0 & 0 & 0 & 0 & 1 \end{bmatrix} \quad \mathbf{\Pi}_{biaxial,in-plane} = \begin{bmatrix} 1 & 0 & 0 & 0 & 0 & 0 \\ 0 & 1 & 0 & 0 & 0 & 0 \\ 0 & 0 & 1 & 0 & 0 & 0 \\ 0 & 0 & 0 & 1 & 0 & 0 \\ 0 & 0 & 0 & 0 & 1 & 0 \\ 0 & 0 & 0 & 0 & 0 & 1 \end{bmatrix}$$

$$\mathbf{\Pi}_{longitudinal,out-of-plane} = \begin{bmatrix} 1 & 0 & 0 & 0 & 0 & 0 \\ 0 & 1 & 0 & 0 & 0 & 0 \\ -\nu_{13} & 0 & 0 & 0 & 0 & 0 \\ 0 & 0 & 0 & 1 & 0 & 0 \\ 0 & 0 & 0 & 0 & 1 & 0 \\ 0 & 0 & 0 & 0 & 0 & 1 \end{bmatrix} \quad \mathbf{\Pi}_{\epsilon_x,in-plane} = \begin{bmatrix} 1 & 0 & 0 & 0 & 0 & 0 \\ -\nu_{12} & 0 & 0 & 0 & 0 & 0 \\ 0 & 0 & 1 & 0 & 0 & 0 \\ 0 & 0 & 0 & 1 & 0 & 0 \\ 0 & 0 & 0 & 0 & 1 & 0 \\ 0 & 0 & 0 & 0 & 0 & 1 \end{bmatrix}$$

$$\mathbf{\Pi}_{transverse,out-of-plane} = \begin{bmatrix} 1 & 0 & 0 & 0 & 0 & 0 \\ 0 & 1 & 0 & 0 & 0 & 0 \\ 0 & -\nu_{23} & 0 & 0 & 0 & 0 \\ 0 & 0 & 0 & 1 & 0 & 0 \\ 0 & 0 & 0 & 0 & 1 & 0 \\ 0 & 0 & 0 & 0 & 0 & 1 \end{bmatrix} \quad \mathbf{\Pi}_{\epsilon_y,in-plane} = \begin{bmatrix} 0 & -\nu_{12}\frac{E_2}{E_1} & 0 & 0 & 0 & 0 \\ 0 & 1 & 0 & 0 & 0 & 0 \\ 0 & 0 & 1 & 0 & 0 & 0 \\ 0 & 0 & 0 & 1 & 0 & 0 \\ 0 & 0 & 0 & 0 & 1 & 0 \\ 0 & 0 & 0 & 0 & 0 & 1 \end{bmatrix}$$

$E_1$, $E_2$ and $\nu_{12}$ for the laminate are given by Eqns. (3.8) to (3.10) (with $\boldsymbol{Q}_{laminate}$ defined below):

$$E_{1,laminate} = Q_{11,laminate} - \frac{Q_{12,laminate}^2}{Q_{22,laminate}},$$

$$E_{2,laminate} = Q_{22,laminate} - \frac{Q_{12,laminate}^2}{Q_{11,laminate}}, \text{ and}$$

$$\nu_{12,laminate} = \frac{Q_{12,laminate}}{Q_{22,laminate}}.$$

For rare triaxial states of load, $\mathbf{\Pi}$ should be omitted. $\mathbf{\Omega}$ is given by Matrix 3.14:

$$\boldsymbol{\Omega} = \begin{bmatrix} c^2 & s^2 & 0 & 0 & 0 & cs \\ s^2 & c^2 & 0 & 0 & 0 & -cs \\ 0 & 0 & 1 & 0 & 0 & 0 \\ 0 & 0 & 0 & c & -s & 0 \\ 0 & 0 & 0 & -s & c & 0 \\ -2cs & 2cs & 0 & 0 & 0 & c^2 - s^2 \end{bmatrix}$$

where $c = \cos\theta$ and $s = \sin\theta$, with $\theta$ being the ply angle.

The components of $\boldsymbol{\epsilon}_{applied,laminate}$ are mechanical strains (not total strains), following the same convention as the components of $\boldsymbol{\epsilon}_{local}$. Typically four of the six components are zero, while the remaining two are mapped to the two axes of the failure envelope to be plotted.

The other contribution to $\boldsymbol{\epsilon}_{global}$ is determined from Eqn. (3.17):

$$\boldsymbol{\epsilon}_{curing} = \boldsymbol{\Pi}_{biaxial,out\ of\ plane} \begin{bmatrix} \epsilon_{x,curing,in-plane} \\ \epsilon_{y,curing,in-plane} \\ 0 \\ 0 \\ 0 \\ \epsilon_{xy,curing,in-plane} \end{bmatrix}$$

where according to Eqn. (3.15)

$$\begin{bmatrix} \epsilon_{x,curing,in-plane} \\ \epsilon_{y,curing,in-plane} \\ \epsilon_{xy,curing,in-plane} \end{bmatrix} = \boldsymbol{\epsilon}_{curing,in-plane} = (\boldsymbol{T}\boldsymbol{\alpha}_{laminate} - \boldsymbol{\alpha}_{ply})\Delta T.$$

The rotation matrix is Matrix 3.13:

$$\boldsymbol{T} = \begin{bmatrix} c^2 & s^2 & cs \\ s^2 & c^2 & -cs \\ -2cs & 2cs & c^2 - s^2 \end{bmatrix}.$$

$\boldsymbol{\alpha}_{laminate}$ is determined using Eqn. (3.14), stating that

$$\boldsymbol{\alpha}_{laminate} = \frac{\boldsymbol{Q}^{-1}_{laminate}}{t_{laminate}} \sum \boldsymbol{T}^T \boldsymbol{Q}_{ply} \boldsymbol{\alpha}_{ply} t_{ply}.$$

The ply thermal expansion factors are

$$\boldsymbol{\alpha}_{ply} = \begin{bmatrix} \alpha_1 \\ \alpha_2 \\ 0 \end{bmatrix}$$

(Eqn. (3.12)). $\boldsymbol{T}$ was stated previously. $\boldsymbol{Q}_{laminate}$ was derived in Eqn. (3.11) to be

$$\boldsymbol{Q}_{laminate} = \frac{\sum \boldsymbol{T}^T \boldsymbol{Q}_{ply} \boldsymbol{T} t_{ply}}{\sum t_{ply}},$$

while according to Matrix 3.12

$$\boldsymbol{Q}_{ply} = \begin{bmatrix} C_{11} - \dfrac{C_{13}^2}{C_{33}} & C_{12} - \dfrac{C_{13}C_{23}}{C_{33}} & 0 \\ C_{12} - \dfrac{C_{13}C_{23}}{C_{33}} & C_{22} - \dfrac{C_{23}^2}{C_{33}} & 0 \\ 0 & 0 & C_{66} \end{bmatrix}.$$

The $C_{ij}$ terms are found from Matrix 3.3:

$$\boldsymbol{C} = \begin{bmatrix} C_{11} & C_{12} & C_{13} & 0 & 0 & 0 \\ C_{12} & C_{22} & C_{23} & 0 & 0 & 0 \\ C_{13} & C_{23} & C_{33} & 0 & 0 & 0 \\ 0 & 0 & 0 & C_{44} & 0 & 0 \\ 0 & 0 & 0 & 0 & C_{55} & 0 \\ 0 & 0 & 0 & 0 & 0 & C_{66} \end{bmatrix}$$

which results from Matrix 3.4

$$\boldsymbol{S} = \begin{bmatrix} S_{11} & S_{12} & S_{13} & 0 & 0 & 0 \\ S_{12} & S_{22} & S_{23} & 0 & 0 & 0 \\ S_{13} & S_{23} & S_{33} & 0 & 0 & 0 \\ 0 & 0 & 0 & S_{44} & 0 & 0 \\ 0 & 0 & 0 & 0 & S_{55} & 0 \\ 0 & 0 & 0 & 0 & 0 & S_{66} \end{bmatrix}$$

according to $\boldsymbol{C} = \boldsymbol{S}^{-1}$. Finally, the content of the compliance matrix is determined from the basic material properties as follows (Matrix 3.5):

$$\boldsymbol{S} = \begin{bmatrix} \frac{1}{E_1} & -\frac{\nu_{12}}{E_1} & -\frac{\nu_{13}}{E_1} & 0 & 0 & 0 \\ -\frac{\nu_{12}}{E_1} & \frac{1}{E_2} & -\frac{\nu_{23}}{E_2} & 0 & 0 & 0 \\ -\frac{\nu_{13}}{E_1} & -\frac{\nu_{23}}{E_2} & \frac{1}{E_3} & 0 & 0 & 0 \\ 0 & 0 & 0 & \frac{1}{G_{23}} & 0 & 0 \\ 0 & 0 & 0 & 0 & \frac{1}{G_{13}} & 0 \\ 0 & 0 & 0 & 0 & 0 & \frac{1}{G_{12}} \end{bmatrix}.$$

### 3.5.4 Required Input Data

The required input data to plot a failure envelope for an arbitrary laminate is therefore

- $E_1$, $E_2$, $E_3$, $\nu_{12}$, $\nu_{13}$, $\nu_{23}$, $G_{12}$, $G_{13}$, $G_{23}$, $\alpha_1$, $\alpha_2$ and $\alpha_3$ of the fiber material, the matrix material, and the ply;
- the volume fraction $V_f$;
- the applied temperature difference $\Delta T$;
- the stacking sequence;
- the ply thickness $t_{ply}$ (in case it differs between plies, otherwise it is not needed);
- the critical invariants $J_1^*$ for the matrix and $\epsilon_{eqv}^*$ for fiber and matrix (typical values are ${J_1^*}^m = 0.024 \pm 15\%$, ${\epsilon_{eqv}^*}^m = 0.2 \pm 10\%$, and ${\epsilon_{eqv}^*}^f = 0.02 \pm 10\%$, as found in Subsection 6.2.5);
- and the choice of strain components for the $x$- and $y$-components of the failure envelope.

# Chapter 4

# Automation and Practical Aspects

The purpose of this chapter is to investigate the practical aspects involved in implementing the consistent approach to Onset Theory developed in the previous chapter and summarized in Section 3.5 in an automated manner. In particular, this consists of a description of the two main software tools developed: the micromechanical enhancement software (Section 4.2) and the failure envelope prediction software (Section 4.3).

Both software tools are written in Python, using version 3.5 or higher (with the exception of commands executed in Abaqus, as described in Subsection 4.2.1). Besides the limitation on the minimum Python version (various features of the 3.x release line are used, so Python 2.7.x will not suffice to run the software), there are no particular operating system or hardware requirements. Python is free software, available via https://www.python.org/.

During this thesis, a relatively powerful (by 2016 standards) desktop computer was used, offering a quad-core Intel Xeon processor and 16GB of memory. Together with the typical file size generated by Abaqus, this implies a 64-bit operating system (in this case Windows 7). Any reported runtimes refer to this computer. ATG Europe's providing of this system is gratefully acknowledged.

As a final note, verification of the software is not part of this chapter. For a comparison of the results obtained using the developed tools with results found in literature, please see Chapter 5.

## 4.1 Purpose of Automation

One aspect separate from the topics addressed so far is automation. Clearly, Onset Theory is quite complex and involves a series of computational steps to arrive at a failure prediction. Some of these steps are rather tedious. It therefore seems plausible that automation would be employed on a large scale. Another benefit of this would be that the approach used could be standardized, eliminating the uncertainties and discrepancies involved (see Section 2.2).

About a decade ago, some researchers were simply relying on amplification factors provided by Gosse, regardless of whether these had been derived for the material combination they were investigating (Tan, 2005). There is some indication that more recently, automation is available for parts

of the process. For example, (R. Li, Kelly, & Mikulik, 2007) modify an existing micromechanical model of a square unit cell to obtain strain amplification factors. However, these approaches are not documented or publicly available. Having an in-house software capable of automatically carrying out all required tasks is crucial for application and further research by TU Delft and ATG Europe.

In addition to that, none of the published literature contains information on a fully automated process capable of investigating the issues listed in Sections 3.3 to 3.1, or of rapidly generating failure envelopes based on classical lamination theory as done in Section 3.2. All approaches found in literature rely on extensive (and expensive in terms of time) finite element simulations of a laminate, with many elements per ply. An automated approach would be far preferable, facilitating for example the investigation of the sensitivity to input parameters.

One additional aspect that should also be addressed by the automated software tools is the criticism raised by the authors of the WWFE that failure theories are too time-consuming and difficult to apply for everyday use, as discussed in Chapter 1. Therefore, the developed software should be "simple" to use. Defining "simple" in this context is somewhat difficult. Most likely, Onset Theory will never be as straightforward to use as failure criteria that do not involve micromechanics. "Simple" will therefore be understood to mean that no expert level dedicated knowledge of SIFT should be needed to apply the failure criterion.

## 4.2 Micromechanical Enhancement Software

One of the most important steps of Onset Theory is to amplify the average ply strain to obtain the individual constituent strains. In order to do so, micromechanical models of unit cells have to be generated, the correct boundary conditions applied, and the strain response extracted. This procedure has been discussed in detail in Chapter 2. The present section investigates some of the practical details encountered during automation of the method of micromechanical enhancement, while Section A.1 contains an overview of the final software layout and a sample input file.

### 4.2.1 Software Choice and Related Practical Matters

The first step to take is to select an appropriate finite element software. For this thesis, Dassault Systemes' Abaqus (http://www.3ds.com/products-services/simulia/products/abaqus/) was selected. The main reason is its very powerful, Python-based scripting interface. Virtually all tasks possible in the graphical user interface can also be performed through Python commands.

Running Abaqus requires a very expensive software license. As with the computer mentioned in the introduction to this chapter, thanks is due to ATG Europe for providing the license.

At the time of writing of this thesis, Abaqus 2016 is being used. Previously Abaqus 6.14-2 was used. The software tool developed should be compatible with any version of Abaqus that provides the required API commands. Since the ones used are fairly common, this should usually be the case. Migrating from Abaqus 6.14-2 to Abaqus 2016 did not require any changes in the software tool.

There is one difficulty associated with the choice of Abaqus. While the scripting interface is Python based, it uses an Abaqus-internal implementation of Python. This implementation is using the 2.7.x

release line. It is also quite difficult to install additional modules. Therefore, some additional steps had to be taken to communicate between "outside" Python 3.5 and "inside" Abaqus Python 2.7. Abaqus Python scripts are invoked by invoking the "inside" Python interpreter with the required arguments, using a subprocess spawned from "outside" Python. Data is transferred from "outside" to "inside" Python using the "pickle" module also used for storing results (see Subsection 4.2.7). These steps are implemented in a dispatch layer, as indicated in the flowcharts in Section A.1.

One other practical matter is that in order to use the mechanical strain (see Section 2.2.2), the elastic strain output "EE" should be used. According to the Abaqus Analysis User's Guide, subsection "strain output", the total strain ("E") comprises the elastic strain "EE" and the thermal strain "THE" (amongst other components). Since the thermal strain should not be included, "EE" remains. For the mechanical load cases, there is no difference between total and elastic strains. However, for the thermal load case it is important to ensure that the correct strain measure is used.

### 4.2.2 Application of Boundary Conditions

There are three different types of boundary conditions, as outlined in Section 3.5. First of all, there are displacement boundary conditions (both to fix faces in place and to apply the displacements required to cause the desired state of strain). Applying these in Abaqus is straightforward.

The second type of boundary condition is the applied temperature difference required to determine the thermal amplification factor vectors. In Abaqus, this is handled by applying a so-called predefined field, taking care to apply the same temperature difference to the entire unit cell.

Finally, for the thermal amplification factors the faces need to be kept planar, but allowed to translate uniformly normal to their original position. A number of different modeling approaches was attempted before the successful strategy was found. Coupling of faces failed because it resulted in overconstrained edges. Excluding the edges meant that the faces behaved correctly, but the edges themselves warped. A second attempt was made using the planar constraint tool offered by Abaqus, creating an analytical rigid surface placed in frictionless contact with the face. However, the complexity of this approach was too high. Eventually the choice was made to use equation constraints. A reference node is created for each face to be constrained. Once the reference nodes are available, an equation can be written that sets the movement of all nodes of a face equal to the movement of the reference node. This is easy to implement and results in the desired uniform movement.

There is a minor disadvantage to using equation constraints in Abaqus. Unlike other types of constraints, they apply to all solution steps. It is therefore not possible to have the step for the thermal load case in the same model as the mechanical load cases. This meant that separate models had to be created. In order to reduce the performance loss due to model generation, a base model containing the geometry, interrogation points, and mesh was created and copied to apply the different types of loads. As for the other tasks described in this section this entire process is automated.

As a side note, although in Subsection 2.2.4 it was found that there is no need to keep the faces of the unit cell planar for the shear load cases, if this does turn out to be required the suggestion is to create a local coordinate system on the faces and specify the equation constraint in that coordinate system. This still allows the faces to tilt, while forcing them to remain flat.

### 4.2.3 Meshing Strategy and Unit Cell Size

Before analyzing the finite element model, the unit cell has to be meshed. Initially a number of unsuccessful attempts were made. These will be briefly outlined below, followed by a description of the chosen appropriate meshing strategy chosen.

As a starting point, two meshing strategies were investigated. One followed a relatively structured approach, creating radial partitions from the center of the fiber. This was similar to typical meshes found in literature. The other approach was selected because of its ease of implementation in Abaqus and consisted of simply specifying the global element size, resulting in an unstructured mesh.

Based on convergence studies (see Subsection 4.2.5) it became clear that using an unstructured mesh was unacceptable due to multiple factors, including irregularity of the elements and movement of the interrogation points (using the closest available node) from mesh to mesh.

However, there were also issues related to the structured approach. Convergence of the mesh was not achieved before the runtime grew unacceptably large. Therefore, another means to improve the mesh refinement was required. This means increasing the number of nodes in the region of interest without a corresponding increase in the overall number of nodes.

Based on the nature of the applied load and the uniformity of the unit cell, there is no variation in results along the fiber. For axial loads in all directions and shear loads in the $y$-$z$-plane this is self-evident, and shear loads in the $x$-$z$- and $x$-$y$-plane also show this behavior (as can be easily verified by running the appropriate simulation). (C. T. Sun & Vaidya, 1996) in fact suggested using two-dimensional plane strain analysis for the investigation of transverse shear loading in the $y$-$z$-plane.

For reasons of simplicity it was decided to retain a single element in the depth direction. That way only a single model is required, rather than three-dimensional models for most of the analyses and two-dimensional ones for the others. In order to prevent excessively high aspect ratios the unit cell size in depth direction is reduced to one tenth of its basic dimension. Verification studies showed that varying either the depth or the number of elements in depth direction does not influence the results (which can be expected given that there is no change in depth direction). Therefore, using a reduced depth unit cell is in fact not required, but is thought to make this simplification even safer. This modeling approach is similar to the one chosen by (Ritchey, 2012, fig. 1.1).

Reducing the unit cell to a single element in depth direction causes a massive decrease in the number of nodes. For example, during the verification studies a full depth unit cell containing 169 619 nodes was replaced by a reduced depth consisting of 9 963 nodes with an identical mesh on the $x_0$- and $x_1$-faces, causing a 60-fold decrease in runtime. This reduction was in fact more than expected, presumably due to the fact that each element had fewer elements attached (two of its faces were free). All resulting amplification factors were identical.

An issue that was only briefly mentioned above in the discussion of the unstructured mesh is movement of the interrogation points. Initially the location of the interrogation points was specified, and the closest node was chosen to sample the resulting strains. However, this means that the actual interrogation point location varies slightly from mesh to mesh unless it is ensured that there is a fixed node at each interrogation point. Typically, this movement is irrelevant. However, there are

some points (in particular on the fiber/matrix interface) where the gradient zone is rather significant, meaning that the movement of the interrogation point can prevent convergence. The solution is to partition the unit cell such that each interrogation point is located at the corner of a partition, which will necessarily have a node.

In order to maintain some flexibility in the number of interrogation points it was decided to keep the software tool parametric in the sense of the number of interrogation points along certain paths (e.g. radially in the fiber or the matrix, or along the edge of the unit cell) being variable. The software contains default settings based on a number of verification studies.

Regarding the element type, it was decided to use quadratic brick elements (C3D20 in Abaqus). This enhances the analysis accuracy without imposing further restrictions on the meshing strategy and interrogation point partitions, as discussed above. An investigation of full and reduced integration revealed the difference between these two element types to be negligible. Since quadratic elements are used, shear locking is not considered an issue, and full integration elements were chosen.

The final meshing strategy therefore consists of creating a full cross section, reduced depth unit cell, containing partitions such that each interrogation point coincides with a corner of a partition.

This ensures that the interrogation points do not move regardless of the mesh chosen. Subsequently, the mesh is generated by specifying the global element size, with the exception of the depth direction (where a single element is enforced). Provided a reasonable number and distribution of interrogation points is used, this will generate a structured mesh based on the partitions created previously.

Figure 4.1 shows the partitions created in the final meshing strategy for the hexagonal fiber array. Whenever a number of nodes is mentioned in this thesis (e.g. in Subsection 4.2.5), this type of mesh is referred to, comprising quadratic full integration elements. Note that in theory it would be sufficient to model only half of the unit cell due to symmetry (see Section 3.4). However, because the runtime is sufficiently low to not be an issue, it was decided to retain the full cross section.

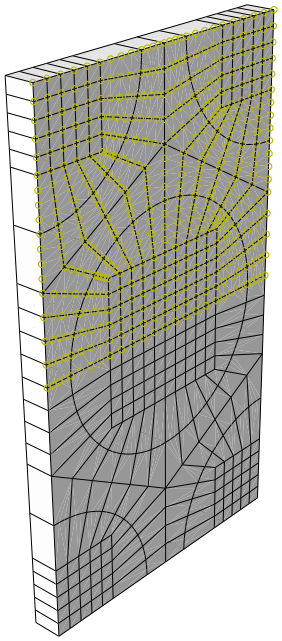

Figure 4.1: Partitions in final meshing strategy for a hexagonal fiber array. The mesh itself is not shown. Yellow circles refer to interrogation points.[1]

[1] The thin white lines visible on some screens / print outs are caused by a rendering problem in the Abaqus vector graphics export and do not carry any meaning.

### 4.2.4 Fiber Radius and Maximum Volume Fraction

One aspect that has not been addressed yet is the size of the fiber as a function of the volume fraction. Since there are no changes in thickness direction, the volume fraction is identical to the cross-sectional area fraction. Using a base dimension of unity, the square unit cell has a total cross-sectional area of 1. The fiber has an area of $\pi r^2$ (where $r$ is the radius of the fiber). Equating this to the volume (area) fraction results in $r = \sqrt{\frac{V_f}{\pi}}$. Since the unit cell is regular, the fiber will be centered at $(y, z) = (0.5{,}05)$. The maximum volume fraction is reached once the diameter of the fiber is equal to the size of the unit cell (i.e. $r = \frac{1}{2}$). This corresponds to a volume fraction of $V_{f,max} = \frac{\pi}{4} \approx 0.785$.

Similarly, for the hexagonal unit cell the cross-sectional area is $\sqrt{3}$. Since there are in total two fibers in the unit cell (a complete center one and four quarter fibers in the corners), the expression becomes $2\pi r^2 = \sqrt{3}V_f$. This can be solved to yield $r = \sqrt{\frac{\sqrt{3}V_f}{2\pi}}$. The maximum value in this case is achieved once two fibers touch each other. This is the case once the diameter of the fiber is equal to the diagonal length of the unit cell, given by $\sqrt{0.5^2 + \left(\frac{\sqrt{3}}{2}\right)^2} = 1$ (i.e. once again $r = \frac{1}{2}$). In other words, the maximum value is given by a volume fraction of $\frac{1}{2} = \sqrt{\frac{\sqrt{3}V_{f,max}}{2\pi}} \rightarrow V_{f,max} = \frac{\pi}{2\sqrt{3}} \approx 0.907$. For the hexagonal unit cell, the fiber is centered at $(y, z) = (\frac{\sqrt{3}}{2}, 05)$, assuming a vertical unit cell (see Subsection 3.3.1).

### 4.2.5 Convergence Study

In order to ensure that the meshes used are converged for all amplification factors, a convergence study is carried out based on each individual value of the mechanical amplification factor matrix and thermal amplification factor vector for each interrogation point. The chosen convergence measure is the normalized difference of the values for subsequent mesh refinement levels, defined as

$$\Delta_{ij} = \frac{|M_{ij} - N_{ij}|}{\max(|M_{ij}|, |N_{ij}|)} \tag{4.1}$$

where $M_{ij}$ and $N_{ij}$ are values of the amplification factor matrix or vector for the previous and current refinement levels, respectively. This definition returns similar error measures for each set of values, even though the mechanical amplification factors are orders of magnitude larger than the thermal ones. It also works consistently regardless of the order or sign of the values, as well as when one of the two values is zero. For the special case of $M_{ij} = N_{ij} = 0$, by definition $\Delta_{ij} = 0$.

However, one word of caution is necessary. If two meshes are relatively similar, then the change will be (close to) 0% regardless of convergence. At first this seems to be the same behavior as during a convergence study where the actual values are used. However, in that case a much finer mesh will cause the two points to more or less coincide and lie on a common convergence curve of all meshes investigated. The chosen measure, on the other hand, would not have a smooth convergence curve; instead, the curve would suddenly drop to 0% and then increase again. This can cause confusion. Therefore, in this thesis the number of nodes is approximately doubled for each subsequent mesh.

In addition to ensuring convergence between two different mesh sizes, element result averaging for an individual mesh is also taken into account. At a node, results are available based on each of the adjacent elements. The results from the attached elements are averaged. Note that for nodes at the interface, only elements with the material of interest for the amplification factors should be taken into account. That means that for each node at the interface, there will be two sets of amplification factors, one for the fiber and one for the matrix. One set will be included in the determination of the fiber failure envelope, while the other is considered for the matrix failures.

In the present work, the meshes are considered converged once no value of any of the amplification factor matrices or vectors changes by more than 5% when increasing the mesh size by a factor of 2. Both of the meshes in this comparison should be acceptable in terms of element result averaging, meaning that the maximum averaging error at a node for any value of any amplification factor should be below 5%. These settings can be adjusted as desired. The convergence study is run automatically in the background every time and will not be explicitly mentioned elsewhere in this thesis. Appendix C contains an example convergence study for the verification case from Subsection 5.1.1.

Mesh convergence was typically achieved at a mesh size of at most approximately 500 000 nodes. Sometimes even such a fine mesh was supposedly not converged or acceptable. It is advisable to manually investigate those cases. Typically the cause is the numerical cutoff (see Subsection 4.2.6). For example, if a node has attached elements with values just above and below the cutoff, the averaging error will be very large. Similarly, if the result for two subsequent mesh sizes are just above and below the cutoff, the averaging error will be 100%. Those and other cases are still acceptable provided the values are indeed sufficiently small to have no influence on the results.

### 4.2.6 Avoiding Numerical Issues

There are two separate steps taken to avoid numerical issues in the finite element calculations and subsequent postprocessing. First of all, Onset Theory calls for the application of unit strains to the unit cell. However, applying a displacement of 1 to a unit cell of size 1 would result in massively distorted elements. In order to avoid any possible issues the actual applied displacement is of magnitude 1e-3. This means that the resulting amplification factors have to be scaled appropriately. This is only possible because all simulations are linear, as discussed in Subsection 2.1.6.

The scaling factors need to be determined depending on the corresponding dimension of the unit cell. For a square unit cell, the appropriate scaling factor is 1000 in $x$- and $y$-directions, but modified by a factor of 10 in $x$-direction to take the reduced depth of the unit cell into account (see Subsection 4.2.3). For the hexagonal unit cell it is important to note that the scaling factor for the long side of the unit cell is $\sqrt{3} \cdot 1000$. Assuming a length of 1 for the short side, the long side has a length of $\sqrt{3}$ as determined from simple trigonometry. If a displacement of 1e-3 is applied, this means an applied strain of $\frac{0.001}{\sqrt{3}}$. To scale this to back to an applied unit strain the factor $\sqrt{3}$ is required.

A similar approach is taken for the thermal amplification factors, where for a temperature difference of 1° the resulting strains would be extremely small and might suffer from precision errors. Therefore, a difference of 100° is used and the thermal amplification factors are divided accordingly afterwards.

In postprocessing, a second measure is taken to avoid numerical issues in the convergence calculations (Subsection 4.2.5). For small results close to 0 the percentage difference could potentially be extremely large, even though the actual values are negligible. As an example, results for two subsequent mesh sizes of 1e-13 and 1e-16 would mean a calculated error of 99.9%. Therefore, the choice was made to remove values with a magnitude smaller than 0.1% of the largest magnitude value in the matrix. In addition to that, every value is rounded to four significant digits to avoid excessively long output. Both the numerical cutoff and the number of significant digits were determined based on a series of convergence studies. They are set to default values in the software.

### 4.2.7 Storage Module

While the runtime of the micromechanical enhancement software is quite short (a typical convergence study takes about ten minutes, using four-core parallelization on the system described at the beginning of this chapter), it is still advisable to devise a storage module to avoid rerunning analyses.

The Python module "pickle" is used because it is available in any standard Python distribution (including the Abaqus-internal one). It is also cross-compatible between Python versions and simple to use. Intermediate results are stored for each mesh size for each fiber array type. Additionally the converged results for each fiber array type are stored. This holds the dual advantage of facilitating rerunning the convergence study with adjusted convergence criteria without having to rerun the actual finite element analysis (unless finer meshes are required), while also providing quick access to the final results once convergence is established.

For the converged results for each fiber array type, the same structure as for the failure envelope prediction software (see Section 4.3) is used, providing easy data exchange between the two tools.

## 4.3 Failure Envelope Prediction Software

The second software tool automatically generates failure envelopes. With the theoretical aspects having been discussed in Section 3.2, this section focuses on the practical details of the implementation. Subsection 4.3.1 addresses failure envelopes based on a single interrogation point, while Subsection 4.3.2 explains how to combine individual envelopes into a common one. As for the micromechanical enhancement software, software flowcharts as well as a sample input file are presented in Section A.2, also containing visualizations of the approaches described in the following subsections.

### 4.3.1 Approach for Single Interrogation Point

For a single interrogation point, there is a single set of amplification factors (mechanical and thermal). This means that for a given state of ply strain, the invariants can be calculated and compared to their respective critical values. However, this is only useful for the evaluation of failure for a single state of strain and does not immediately lead to the ability to predict entire failure envelopes.

Initially, an attempt was made to solve for the failure envelopes analytically. For the equivalent strain, this meant deriving for example the equation for $\epsilon_{22}$ in terms of $\epsilon_{11}$ (ply strains) where the resulting local constituent strains – depending on the values of the amplification factors – caused

the strain invariant to be equal to its critical value. This process was successful initially and served as confirmation for the first steps of the numerical approaches outlined below, but quickly became prohibitively complex algebraically. In particular, this investigation took place before the full details of determining the full state of strain (see Section 3.2) were understood properly. Therefore, it did not include thermal strains, curing strains, or Poisson's effects. Taking those effects into account for the full envelope would not be feasible analytically, as discussed in Subsection 2.1.5 as well.

Since the analytical procedure failed, another approach had to be chosen. It was quickly realized that attempting to solve the failure envelope analytically was inherently flawed. Onset Theory is not an analytical failure criterion that returns a simple expression for the failure envelope, such as criteria like Tsai-Wu. Consequently it should not be treated as such. Instead, SIFT is based on evaluating a single set of strains and determine whether or not failure occurs. This means that the derivation of failure envelopes should be based on evaluating failure on a large number of points and choosing the set of points on the boundary between failure and no failure. The advantage of this process is that for a single point it is relatively straightforward to calculate the full state of strain in a ply, using the approach described in Section 3.2.

Initially, an algorithm was implemented that started at a single point on the failure envelope (i.e. points where the state switched from "not failed" to "failed") and then searched its vicinity for other points where the state switched, until returning to its starting point. However, this approach was too slow for reasonable levels of accuracy. Since it became apparent that evaluating many points at once using Python's built-in matrix libraries was significantly faster than evaluating points individually, the second attempt was to evaluate failure on a large grid of points and determine the convex hull (i.e. the outer bound) of all points where failure was predicted. In this case, the failure evaluations were much faster, but calculating the convex hull turned out to be inadmissibly slow. Therefore, the final choice was to evaluate failure on radial lines from the origin, and to use the points where the state switched from "not failed" to "failed". This is visualized in Figure A.8.

In that case, many points are still evaluated at once, unlike the first attempted algorithm that investigated point by point individually. At the same time, once a point is determined for a radial line, that point is known to be part of the envelope without a need to compute the convex hull.

Analytical and numerical solutions were identical for all cases within the scope of applicability of the analytical solution (e.g. no Poisson's effects, only 0° plies, and so on). For the correct procedure using the correct full state of strain derived in Section 3.2, the numerical solution could not be verified as easily since no analytical solution was available. However, the failure envelope prediction software as a whole is verified in Section 5.2.

The discussions so far were all related to closed failure envelopes (in other words, $\epsilon_{eqv}$-failure). For the matrix, $J_1$-failure has to be taken into account as well. In this case the situation is somewhat simpler because this cutoff is known to be a straight line. Therefore, determining two points on the cutoff is sufficient. Evaluating failure on a horizontal and a vertical line is usually sufficient to obtain these two points, except for cases where the cutoff is horizontal or vertical (such as envelopes involving $\gamma_{xy}$). These exceptions are addressed by evaluating failure on two horizontal or two vertical lines if the initial approach fails. Note also that there are cases (again for envelopes involving $\gamma_{xy}$)

where the $J_1$-cutoff consists of two lines, one for positive shear and one for negative shear. Again provisions are made accordingly. Figure A.9 shows the approach to determine $J_1$-failure numerically.

Regarding the $J_1$-cutoff, it should be noted that having two points is only sufficient for a single envelope. Given the procedure described in the next section to determine the combined cutoff for multiple interrogation points, additional points are generated in between the two points.

### 4.3.2 Approach for Multiple Interrogation Points

So far, the discussion was limited to a single interrogation point. If multiple interrogation points are taken into account, the failure envelope has to be generated for each one of them. The complete failure envelope then consists of the piecewise most conservative set of all individual envelopes.

Regardless of the type of failure ($\epsilon_{eqv}$-envelope or $J_1$-cutoff), the combined failure envelope is determined by merging the data points of all individual envelopes. Subsequently, failure is evaluated based on every interrogation points once more. However, in this case the dataset is the merged data of all individual envelopes, rather than a line from the origin. By filtering out all data points where any interrogation point causes failure, the most conservative failure envelope is left over. This can be explained as follows: the data points on an individual failure envelope represent the location where that particular interrogation point is on the verge of causing failure. If another interrogation point is more critical, these data points will be removed. Left over are therefore the points where one particular interrogation point is on the verge of causing failure, while all other interrogation points do not yet cause failure. This is by definition the inner (most conservative) failure envelope. Once again the approach is depicted for a pseudo-case in the appendix (Figure A.10).

For a real case, the process of selecting the final failure envelope from the contributions of the individual interrogation points is shown in Subsection 3.4.1. Similar to the convergence study for the strain amplification factors (Subsection 4.2.5), this process is carried out automatically in the background for every failure envelope shown in this thesis.

Combining all fiber array types and unit cell rotation angles (Section 3.3) with all interrogation points (Section 3.4) results in several thousands of combinations. Determining the individual envelopes for all of these combinations is quite slow. Therefore, Python's built-in multiprocessing toolbox is used to employ parallelization to improve the runtime. On the system described in the introduction to this chapter, generating a typical laminate failure envelope (excluding sensitivities) with four distinct ply angles takes approximately three minutes.

# Chapter 5

# Verification of Approach and Software

Chapter 4 contained a description of the two software tools developed to implement the consistent approach to Onset Theory. Before working on validation and research tasks, it is important to ensure that software and approach work correctly. For the micromechanical enhancement, this is a straightforward task because several quite reliable sources exist which report strain amplification factors. This is discussed in Section 5.1. On the other hand, verifying the failure envelope predictions proves more involved because only very few failure envelopes are found in literature, and there are significant doubts about their validity. Section 5.2 investigates the details of this topic.

## 5.1 Verification of Micromechanical Enhancement

The purpose of this section is to provide thorough verification of the micromechanical enhancement software. This is achieved by comparing results returned by the software tool to literature results. Several sources are used, both to have data for all four categories of amplification factors (fiber and matrix for square and hexagonal fiber arrays) and to provide confidence that there are no unidentified errors common to both literature and software. In general, it is noticeable that there is more (and more reliable) data available for the amplification factors in the matrix than for the ones in the fiber, and similarly for square fiber arrays as opposed to hexagonal ones. The reason is probably that SIFT was initially developed as a matrix failure criterion. However, there are several less reliable sources available, such as student theses. These will also be used for verification. While they are not published in peer reviewed journals, and there is a significant chance that the authors misunderstood or misapplied the theory, they do contain far more details than a scientific article.

It should be noted here that the Master thesis by (Yudhanto, 2005) contains various sets of amplification factors, covering all four categories described previously. However, these were derived before the proper procedure as outlined in (Buchanan et al., 2009) was established. For example, Yudhanto only uses the diagonal terms of the amplification factor matrices, and uses fixed boundary conditions for the thermal amplification factors (see Subsection 2.2.5). Therefore, his results are only used as the main source for verification if no other results are available (i.e. in Subsection 5.1.4).

### 5.1.1 Matrix Amplification Factors for Square Fiber Array

The first category of strain amplification factors to be verified are the matrix amplification factors for the square fiber array. (Buchanan et al., 2009) is used for this purpose, both because it was the first article by Gosse (SIFT's original author) describing the process of micromechanical enhancement and also because it showcases some typical problems encountered during this process.

Section B.1 contains the full data required to reproduce the results of this verification effort, including the input data for the micromechanical models (Table B.1), the literature results (Matrices B.1 to B.6), and the results obtained using the software tool developed during this thesis (Matrices B.7 to B.12). The locations – IF1, IS and IF2 – follow the choice of interrogation points by (Buchanan et al., 2009), as shown in Figure 2.9. Note that this example is also used for the example convergence study shown in Appendix C.

Comparing literature and software results yields the differences shown in Matrices 5.1 to 5.6. The method of calculating these difference is the same as described in Subsection 4.2.5. All values are in percent and rounded to two decimals.

$$\begin{bmatrix} 0 & 0 & 0 & 0 & 0 & 0 \\ 2.64 & 0.52 & 37.79 & 0 & 0 & 0 \\ 1.85 & 3.1 & 0.59 & 0 & 0 & 0 \\ 0 & 0 & 0 & 2.78 & 0 & 0 \\ 0 & 0 & 0 & 0 & 1.07 & 0 \\ 0 & 0 & 0 & 0 & 0 & 1.01 \end{bmatrix}$$

Matrix 5.1: Difference [%] in square array matrix mechanical strain amplification factors at IF1

$$\begin{bmatrix} 0.28 \\ 0.05 \\ 0.84 \\ 0 \\ 0 \\ 0 \end{bmatrix}$$

Matrix 5.2: Difference [%] in square array matrix thermal strain amplification factors at IF1

$$\begin{bmatrix} 0 & 0 & 0 & 0 & 0 & 0 \\ 0.74 & 0.83 & 2.09 & 0 & 0 & 0 \\ 2.9 & 3.7 & 0.09 & 0 & 0 & 0 \\ 0 & 0 & 0 & 1.85 & 0 & 0 \\ 0 & 0 & 0 & 0 & 0.44 & 0 \\ 0 & 0 & 0 & 0 & 0 & 0.44 \end{bmatrix}$$

Matrix 5.3: Difference [%] in square array matrix mechanical strain amplification factors at IS

$$\begin{bmatrix} 0.38 \\ 3.66 \\ 23.91 \\ 0 \\ 0 \\ 0 \end{bmatrix}$$

Matrix 5.4: Difference [%] in square array matrix thermal strain amplification factors at IS

$$\begin{bmatrix} 0 & 0 & 0 & 0 & 0 & 0 \\ 1.85 & 0.59 & 3.1 & 0 & 0 & 0 \\ 2.64 & 37.79 & 0.52 & 0 & 0 & 0 \\ 0 & 0 & 0 & 2.78 & 0 & 0 \\ 0 & 0 & 0 & 0 & 1.01 & 0 \\ 0 & 0 & 0 & 0 & 0 & 1.07 \end{bmatrix}$$

Matrix 5.5: Difference [%] in square array matrix mechanical strain amplification factors at IF2

$$\begin{bmatrix} 0.28 \\ 0.84 \\ 0.05 \\ 0 \\ 0 \\ 0 \end{bmatrix}$$

Matrix 5.6: Difference [%] in square array matrix thermal strain amplification factors at IF2

Comparing results, it is clear that the overall agreement is excellent. The maximum difference is 3.7%, with the exception of two terms. First of all, term (2,3) of the mechanical amplification factors at IF1 (Matrix 5.1) differs by 37.79%. Note that this is identical to term (3,2) of Matrix 5.5 due to symmetry. Secondly, term 3 of the thermal amplification factors at IS (Matrix 5.4) differs by 23.91%.

Regarding the latter one, as discussed in Section B.1 the likelihood of a print error is rather high. Terms 2 and 3 should be identical. Since the agreement with term 2 is quite good, the disagreement for term 3 is discarded as a point of concern.

Regarding term (2,3) of Matrix 5.1 (and term (3,2) of Matrix 5.5), the issue is probably caused by the lack of convergence of the literature results, as pointed out in Section B.1. One of the driving factors during the development of the meshing strategy, including reducing the depth of the unit cell (see Subsection 4.2.3 for a description of the final choice), was in fact convergence problems with those two particular terms.

An investigation was carried out of this individual interrogation point on a very coarse mesh of a full cube unit cell, containing 20 489 nodes (corresponding to a single element deep unit cell with 4 960 nodes – note that the 252 003 nodes were required for full convergence of all terms at all interrogation points according to the criteria used in this thesis). The meshing strategy was similar to the one shown in (Buchanan et al., 2009, fig. 2). In that case, all terms were within 6.4% of the converged values, with the exception of the problematic one. With a value of 0.05854 (instead of the 0.07776 resulting from full convergence), it was off by 24.72%. Although the result by Buchanan (0.125) exceeds the converged value rather than being too low, it is obvious that this particular term is problematic, with all other terms at this interrogation point being converged already for a very coarse mesh.

Unfortunately, (Buchanan et al., 2009) do not discuss how they ensured convergence of their mesh. It seems plausible that the results are not converged for every single value individually, but only for the equivalent strain of a column (see e.g. (Tran, 2012, fig. 3-13), who coauthored articles on SIFT with Gosse, such as (Tran, Kelly, et al., 2012)). The reason why this will lead to different results is that small unconverged values can be masked by larger values in the same column. In literature, the nonzero terms of the third column of the amplification factors at IF1 (Matrix B.1) are $\epsilon_{22} = 0.125$ and $\epsilon_{33} = 0.61$. Using the software the values are $\epsilon_{22} = 0.07776$ and $\epsilon_{33} = 0.6064$ (Matrix B.7). Looking at the individual terms, this means differences of 37.79% and 0.59%, as reported in Matrix 5.1. On the other hand, if the equivalent strain is calculated based on Eqn. (2.2), the results are $\epsilon_{eqv} = \sqrt{\frac{1}{2}[{\epsilon_{22}}^2 + {\epsilon_{33}}^2 + (\epsilon_{22} - \epsilon_{33})^2]} = \sqrt{\frac{1}{2}[0.125^2 + 0.61^2 + (0.125 - 0.61)^2]} = 0.558$ based on the literature values and 0.572 based on the software results. The resulting difference is much smaller, namely only 2.45%. A similar calculation for the $J_1$-strain reveals a difference of 6.94%. This means that the mesh will be (almost) converged when judging by the strain invariants, whereas the individual terms still show very large differences.

Of course, the value which will be used in failure calculations are in fact the strain invariants. That means that likely the lack of convergence of a single term will not influence the results much, unless it somehow becomes the only active amplification factor. The safest way is to ensure convergence of every term individually, as discussed in Subsection 4.2.5, although this does carry a penalty in terms of runtime because much finer meshes are required to converge each individual value.

In summary, this means that the few existing significant differences between software and literature results can be explained plausibly by a lack of convergence of the literature results. This is also supported by other comparisons, using the results reported in (Ritchey et al., 2011, Table 4) for IM7/8552, (Tran, 2012, Eqns. 3-17 to 3-19) for T800s/3900-2, and (Tran, 2012, Eqns. 3-20 to 3-22)

for T300/Cycom 970. While the terms that were problematic in the comparison with (Buchanan et al., 2009) still showed the lowest level of agreement, the difference to literature reduced to less than 15%. In general, the magnitude of deviations was very similar to the case presented in detail here. These other comparisons serve to increase confidence in the validity of the results, but otherwise do not show any distinct interesting feature and are thus not covered in detail.

As a side note, if comparison is attempted with the results by (Tran, 2012), it appears that a temperature difference of about $-160°$ is used when reporting the thermal amplification factors (rather than the $-140°$ stated). A consistent difference in results of between 10% and 15% was found for all interrogation points and both materials, which can be explained by an incorrect value of $\Delta T$. The curing temperature of Cycoml 970 according to the manufacturer's data sheets is 177° Celsius, resulting in a temperature difference of 157° to room temperature.

### 5.1.2 Matrix Amplification Factors for Hexagonal Fiber Array

The second category of strain amplification factors to be verified are the matrix amplification factors for the hexagonal fiber array. (Ritchey et al., 2011) is used because it was coauthored by Gosse and is thus deemed the most reliable source available. As for the matrix amplification factors for the square array, the full data required to reproduce the results is found in the appendix in Section B.2, presenting and discussing the input data (Table B.2), literature results (Matrices B.13 and B.14), and own results (Matrices B.17 and B.18).

Comparing literature and software tool results for the thermal amplification vector yields a vector of differences $[0.61 \quad 1.65 \quad 3.32 \quad 0 \quad 0 \quad 0]^T$ (all values in percent), meaning that the literature results are reproduced very closely.

For the mechanical amplification factors, all terms are identical with the exception of the second column ($y$-direction, referring to the long side of the hexagonal unit cell). For this column, the nonzero values in literature are $\epsilon_{22} = 0.6$ and $\epsilon_{33} = 0.3$, while the software tool returns values of $\epsilon_{22} = 1$ and $\epsilon_{33} = 0.5$. Both of these correspond to a difference of 40%.

This issue due to the way displacements are applied to the unit cell. As discussed in Subsection 4.2.6, for the long side of the hexagonal unit cell an additional factor of $\sqrt{3}$ is required to obtain an applied unit strain. Since $\sqrt{3} \cdot 0.6 = 1.04 \approx 1$ and $\sqrt{3} \cdot 0.3 = 0.52 \approx 0.5$ (which are the values obtained using the software tool), it seems very likely that this step was omitted in the literature results. The faultiness of this approach is also clear from the corresponding failure envelopes, where omitting the factor $\sqrt{3}$ for the hexagonal unit cell results in a completely different failure envelope than the square unit cell (scaled in $y$-direction by a factor of $\sqrt{3}$, as per the general trends discussed in Subsection 2.1.5). A final piece of evidence is the match in fiber strain amplification factors for the hexagonal fiber array, as shown in Subsection 5.1.4.

In summary, this means that just like for the matrix amplification factors for the square array the agreement with literature results is excellent with the exception of plausibly explainable cases.

### 5.1.3 Fiber Amplification Factors for Square Fiber Array

For the fiber amplification factors for the square fiber array, no complete or fully reliable results are available. The best source of results are the theses by (Mao, 2011) and (McNaught, 2009).

Of these two, the results by Mao could not be reproduced. During the investigation, it was found that the results reported do not seem plausible. For example, at location IS (all locations are again in correspondence with e.g. Figure 2.9), the three shear terms of the amplification factor matrix are 1.3659, 1.8438, and 1.1096 (Mao, 2011, Table 5-4). Due to symmetry of the unit cell and loading, at least two of these terms (corresponding to $\gamma_{xz}$ and $\gamma_{xy}$) should be identical. However, this is not the case. Similarly, the matrices on the fiber boundary at 0° and 90° (assuming a horizontal line through the fiber center, corresponding to e.g. points F3 and F5 of Figure 2.10) should be identical except for the arrangement of terms, whereas the reported matrices have different shear terms. Together with other similar problems, this means the results by Mao are not used for verification.

Therefore, the results by McNaught are used for verification purposes. Unfortunately, only the mechanical amplification factors are found in literature. A verification of the thermal amplification factors is not possible due to a lack of reference data.

For the three points chosen – McNaught made the same choice as Mao (i.e. center of the fiber, and points at 0° and 90° on the fiber/matrix boundary) – the comparison to literature yields the results shown in Matrices 5.7 to 5.9.

$$\begin{bmatrix} 0 & 0 & 0 & 0 & 0 & 0 \\ 0.45 & 2.34 & 1.52 & 0 & 0 & 0 \\ 0.45 & 1.52 & 0.82 & 0 & 0 & 0 \\ 0 & 0 & 0 & 26.14 & 0 & 0 \\ 0 & 0 & 0 & 0 & 1.57 & 0 \\ 0 & 0 & 0 & 0 & 0 & 1.57 \end{bmatrix}$$

Matrix 5.7: Difference [%] in square array fiber mechanical strain amplification factors at the center of the fiber

$$\begin{bmatrix} 0 & 0 & 0 & 0 & 0 & 0 \\ 5.22 & 0.76 & 14.86 & 0 & 0 & 0 \\ 2.51 & 2.64 & 0.16 & 0 & 0 & 0 \\ 0 & 0 & 0 & 20.8 & 0 & 0 \\ 0 & 0 & 0 & 0 & 1.32 & 0 \\ 0 & 0 & 0 & 0 & 0 & 4.11 \end{bmatrix}$$

Matrix 5.8: Difference [%] in square array fiber mechanical strain amplification factors at 0° on the fiber/matrix boundary

$$\begin{bmatrix} 0 & 0 & 0 & 0 & 0 & 0 \\ 2.51 & 0.16 & 2.64 & 0 & 0 & 0 \\ 5.22 & 14.86 & 0.76 & 0 & 0 & 0 \\ 0 & 0 & 0 & 20.8 & 0 & 0 \\ 0 & 0 & 0 & 0 & 4.11 & 0 \\ 0 & 0 & 0 & 0 & 0 & 1.32 \end{bmatrix}$$

Matrix 5.9: Difference [%] in square array fiber mechanical strain amplification factors at 90° on the fiber/matrix boundary

Not much is to be said about this comparison. Clearly, the overall agreement is quite good, with the exception of the (2,3) and (3,2) terms of the matrices at 0° and 90° on the fiber/matrix boundary, as well as the $\gamma_{yz}$ terms at all points. The former of these is presumably due to the same convergence issues discussed in Subsection 5.1.1. For the latter, the explanation is that (as stated in Section B.3) the $G_{23}$-term of the fiber is unknown and was assumed to be equal to $G_{12}$. Apparently McNaught used some other, unknown value.

Although not discussed in detail here because verification of the matrix amplification factors for the square array took place in Subsection 5.1.1 already, the mechanical matrix amplification factors reported by McNaught were also compared to results obtained from the software tool. There were no particular discrepancies. In case a comparison is attempted, the issues found were a sign error in literature (term (3,2) of point 5 as defined by McNaught), the terms typically problematic in terms of convergence (also discussed previously in Subsection 5.1.1), and term (3,2) of point 4, which was off by 140% with no plausible explanation found.

In summary, this means that the fiber amplification factors for the square array were also successfully verified, albeit using a literature source that cannot be considered fully reliable due to its being a student thesis rather than a peer reviewed journal article.

### 5.1.4 Fiber Amplification Factors for Hexagonal Fiber Array

The last category of amplification factors are the fiber amplification factors for the hexagonal fiber array. Only (C. H. Wang, 2005) contains a full amplification factor matrix. However, the results could not be verified because both the input data and the location of the interrogation point are unclear. Since no other literature data could be found, the last resort was to use the results by (Yudhanto, 2005), acknowledging the issues stated in the introduction to Section 5.1 (namely that only the diagonal terms of the mechanical amplification factors are available for verification).

Yudhanto reports values for four locations: points F1, F2, F3, and F9 in Figure 2.13, corresponding to points at 90°, 45° and 0° on the fiber boundary and the fiber center, respectively. Three volume fractions are included ($V_f = 0.5$, $V_f = 0.6$ and $V_f = 0.7$). Only $V_f = 0.5$ is used for the detailed comparison here. For the other volume fractions good agreement was reached as well (typically within about 15% of all values), with a slight trend towards larger differences at higher volume fractions. It seems questionable whether Yudhanto's results for those volume fractions are converged, given for example the different amplification factors in $y$- and $z$-directions at the fiber center.

$$\begin{bmatrix} 0 & & & & \\ & 1.47 & & ? & \\ & & 1.17 & & \\ & & & 3.53 & \\ & ? & & 1.07 & \\ & & & & 0.49 \end{bmatrix}$$

Matrix 5.10: Difference [%] in square array matrix mechanical strain amplification factors at the center of the fiber

$$\begin{bmatrix} 0 & & & & \\ & 0.47 & & ? & \\ & & 1.1 & & \\ & & & 5.67 & \\ & ? & & 1.07 & \\ & & & & 1.54 \end{bmatrix}$$

Matrix 5.11: Difference [%] in square array matrix mechanical strain amplification factors at 0° on the fiber/matrix boundary

$$\begin{bmatrix} 0 & & & & \\ & 0.03 & & ? & \\ & & 0.17 & & \\ & & & 4.27 & \\ & ? & & 0.08 & \\ & & & & 0.75 \end{bmatrix}$$

Matrix 5.12: Difference [%] in square array matrix mechanical strain amplification factors at 45° on the fiber/matrix boundary

$$\begin{bmatrix} 0 & & & & \\ & 0.27 & & ? & \\ & & 0.11 & & \\ & & & 0.19 & \\ & ? & & 0.11 & \\ & & & & 0.16 \end{bmatrix}$$

Matrix 5.13: Difference [%] in square array matrix mechanical strain amplification factors at 90° on the fiber/matrix boundary

Comparing literature (Matrices B.28 to B.31) with software tool results (Matrices B.32 to B.38) yields the differences shown in Matrices 5.10 to 5.13. Clearly, the agreement is excellent.

As a side note, amplification factors for the square fiber array and a volume fraction of $V_f = 0.6$ were also compared with software tool results. For points in the matrix, there was good agreement; in the fiber, all interrogation points showed excellent agreement except for those at 45° on the fiber/matrix boundary, which were completely different and contained significant off-axis terms.

Matrix amplification factors for the hexagonal array were also compared for all three volume fractions. Yudhanto's results seemed somewhat questionable, with for example terms (2,2) and (3,3) at IS (as defined in Figure 2.9) not being identical, and IF1 and IF2 containing different terms rather than being permutations of each other. Both of these indicate a lack of convergence. All in all, the agreement ranged from decent (within 20% or so) to very good (within 1%), depending from term to term. At a volume fraction of $V_f = 0.7$, there were significant differences with Yudhanto, and the software tool indicated a lack of convergence. The same argumentation as in Section B.2 can be followed, meaning that this should not be the cause for the differences. It however indicates that this volume fraction is particularly problematic, meaning that the literature results may also have had trouble with convergence.

### 5.1.5 Summary of Verification Efforts

Summarizing Subsections 5.1.1 to 5.1.4, it is clear that the software tool is working as expected. All four categories of amplification factors used in this thesis (fiber and matrix for square and hexagonal array) were verified by comparing results with published values from literature. For the most part there was excellent agreement, with plausible explanations found for the remaining values. In fact, the verification efforts led to the discovery of definite errors in literature, such as incorrect scaling of strains corresponding to the long side of the hexagonal unit cell in (Ritchey et al., 2011). While ensuring convergence can be difficult for all interrogation points according to the strict rules imposed by the automatic procedure (see Subsection 4.2.5), there do not seem to be any convergence issues of sufficient severity to impact the results. This means that the micromechanical enhancement software is safe to use for further research, in particular the generation of failure envelopes.

## 5.2 Verification of Failure Envelope Prediction

The second aspect involved in the consistent approach to Onset Theory is the prediction of failure envelopes using analytical means to establish the full set of strain. Several steps are carried out in order to verify whether theory and implementation work as expected. First of all, the calculations themselves are verified by comparing to literature results in Subsection 5.2.1. Secondly, Subsection 5.2.2 describes a finite element analysis carried out to further increase confidence in the analytical calculations. With the calculations verified, the entire approach to predict failure envelopes is put to the test. This is done for a ply under normal strains, a laminate under normal strains, and a ply under shear strain, in Subsections 5.2.3 to 5.2.5.

### 5.2.1 Analytical Calculation of Curing Strains and Poisson's Effects

In order to verify the calculation of Poisson's effects and curing strains – in other words the calculation of the full state of strain – as outlined in Section 3.2, the example calculations for the hexagonal fiber array from (Ritchey et al., 2011) are used (this is the same case as listed in Section B.2). However, in this case the micromechanical amplification factors (and thus the constituent properties) are not relevant. Curing strains and Poisson's effects are a ply-level structure effect. Table 5.1 contains the required ply material properties.

Table 5.1: Ply material properties used for analytical verification of the full state of strain (Ritchey et al., 2011, Table 1)

| | |
|---|---|
| $E_1$ [Pa] | 167.5e9 |
| $E_2$ [Pa] | 10.7e9 |
| $E_3$ [Pa] | 10.7e9 |
| $G_{12}$ [Pa] | 6.3e9 |
| $G_{13}$ [Pa] | 6.3e9 |
| $G_{23}$ [Pa] | 3.34e9 |
| $\nu_{12}$ [−] | 0.31 |
| $\nu_{13}$ [−] | 0.31 |
| $\nu_{23}$ [−] | 0.6 |
| $\alpha_1$ [$°C^{-1}$] | 0.41e-6 |
| $\alpha_2$ [$°C^{-1}$] | 35.1e-6 |
| $t$ [$m$] | 0.2e-3 |

Based on this, the first step is to calculate the ply compliance matrix. Its values are found to be

$$\boldsymbol{S} = \begin{bmatrix} 5.97 & -1.85 & -1.85 & 0 & 0 & 0 \\ -1.85 & 93.46 & -56.07 & 0 & 0 & 0 \\ -1.85 & -56.07 & 93.46 & 0 & 0 & 0 \\ 0 & 0 & 0 & 299.4 & 0 & 0 \\ 0 & 0 & 0 & 0 & 158.73 & 0 \\ 0 & 0 & 0 & 0 & 0 & 158.73 \end{bmatrix} \cdot \text{1e-12} \ \left[\frac{1}{Pa}\right].$$

Matrix 5.14: Compliance matrix for analytical verification of full state of strain

Through inversion, the ply stiffness matrix is then

$$\boldsymbol{C} = \begin{bmatrix} 172.8 & 8.6 & 8.6 & 0 & 0 & 0 \\ 8.6 & 17.1 & 10.5 & 0 & 0 & 0 \\ 8.6 & 10.5 & 17.1 & 0 & 0 & 0 \\ 0 & 0 & 0 & 3.3 & 0 & 0 \\ 0 & 0 & 0 & 0 & 6.3 & 0 \\ 0 & 0 & 0 & 0 & 0 & 6.3 \end{bmatrix} \cdot 1e9 \ [Pa]$$

Matrix 5.15: Stiffness matrix for analytical verification of full state of strain

The next step is to calculate the laminate reduced stiffness matrix, resulting in

$$\begin{bmatrix} 89.7 & 3.3 & 0 \\ 3.3 & 89.7 & 0 \\ 0 & 0 & 6.3 \end{bmatrix} \cdot 1e9 \ [Pa]$$

(for a [0/90/90/0] laminate)

and

$$\begin{bmatrix} 52.8 & 40.2 & 0 \\ 40.2 & 52.8 & 0 \\ 0 & 0 & 6.3 \end{bmatrix} \cdot 1e9 \ [Pa]$$

(for a [45/-45/-45/45] laminate).

Subsequently, the laminate thermal expansion coefficients are calculated. Since the two laminates are identical in terms of a thermal load because of symmetry, the expansion coefficients for both of them are $[3.04 \quad 3.04 \quad 0]^T \cdot$ 1e-6 $[-]$.

Based on this, the in-plane curing strains (in the ply coordinate system) for a temperature difference of $\Delta T = -100°C$ are then found to be $[-263 \quad 3206 \quad 0]^T \cdot$ 1e-6 $[-]$ (note that the last component is the shear component). These values are identical for all plies for the two laminates, again because of the thermal symmetry.

Finally, the out-of-plane curing strains, caused by the Poisson's ratio, are calculated. This leads to the final mechanical strain vector due to curing, $[-263 \quad 3206 \quad -1824 \quad 0 \quad 0 \quad 0]^T \cdot$ 1e-6 $[-]$.

The micro-level strains would then be calculated according to Eqn. (2.5): $\boldsymbol{\epsilon}_{local} = \boldsymbol{M}\boldsymbol{\epsilon}_{curing} + \boldsymbol{A}\Delta T$. All results are essentially identical to the ones found in literature, with the exception of minor differences due to rounding. Therefore, the literature values are not repeated.

In summary, it is clear that the calculations for the full state of strain are indeed implemented correctly according to the theory outlined in (Ritchey et al., 2011). The next step is to verify whether these analytical calculations are also supported by finite element results. This is in particular relevant because of the large magnitude of the curing strains (more than 3000 microstrain in transverse direction for a relatively small temperature difference of $\Delta T = -100°C$).

### 5.2.2 Finite Element Analysis of Curing Strains and Poisson's Effects

Finite element analysis was used for two distinct verification efforts. The main focus were square plates with layups of [0/90/90/0] and [45/-45/-45/45], analyzed under a thermal load and applied edge strains.

During all finite element analyses in this subsection it was made sure to use a sufficiently large plate to adhere to the assumption of a thin laminate. For the [0/90/90/0] laminate, this was ten times the thickness, while during the verification efforts for the [45/-45/-45/45] laminate plates up to 50 times the thickness were analyzed in order to exclude edge effects. Ultimately these efforts were only partially successful, as discussed below. Values are sampled close to the center of the plate. A relatively fine mesh was used, containing up to 50 000 quadratic brick elements (corresponding to 213 741 nodes) in the largest plate. The $x$- and $y$-faces of the laminate were kept planar in order to enforce strain compatibility. This was done using equation constrains, similar to the ones discussed in Subsection 4.2.2.

The first verification effort concerned the larger curing strains determined analytically in the previous section. In order to increase confidence in the results, a finite element analysis was carried out. This was also used to confirm whether there are indeed out-of-plane mechanical strains due to curing, based on the Poisson's effect. The finite element models confirmed the analytical predictions, both regarding the in-plane mechanical strains and also the resulting out-of-plane Poisson's strains. The mechanical strains were $\boldsymbol{\epsilon}_{curing} = [-263 \quad 3206 \quad -1824 \quad 0 \quad 0 \quad 0]^T \cdot$ 1e-6 $[-]$ in all plies of the [0/90/90/0] laminate, identical to the analytical results.

For the [45/-45/-45/45] laminate, some minor problems were encountered. Regardless of the size of the plate and the refinement of the mesh, the state of strain was not completely uniform, resulting in small deviations in the mechanical curing strains (in the order of a few tens of microstrains). For example, at the center of the plate the result for $\epsilon_x$ varied between $-266$e-6 and $-293$e-6, which is first of all clearly not a uniform result and secondly differs from the analytical predictions and the results for a [0/90/90/0] plate. However, these issues could be traced back to the edges of the plate not being lined up with the stiff and compliant directions of a ply. This was confirmed by modeling a circular plate with a [0/90/90/0] layup, which showed similar problematic behavior as a square [45/-45/-45/45] plate (for example, $\epsilon_x$ varied between $-265$e-6 and $-270$e-6). Increasing the size of the plate to obtain a higher size to thickness ratio, or refining the mesh, failed to remove this issue.

The purpose of the finite element model was to confirm the theory, which was successful given the exact match for the [0/90/90/0] laminate and the relatively small magnitude of the deviations for the [45/-45/-45/45] laminate. Investigating modeling issues involving edge effects was not the focus of this verification effort. Therefore, no further investigation was carried out.

A second finite element model was used to verify the ply by ply formulation of Poisson's effects based on a state of plane stress, as opposed to the discarded intuitive formulation (see Subsection 3.2.1). The thermal model is unsuited for this because the effects in $x$- and $y$-directions are identical, meaning that the coupling effects present in the ply by ply model and lacking in the intuitive formulation do not play a role. Therefore, mechanical strains of $\epsilon_x = 0.01$ and $\epsilon_y = 0.001$ are applied to the [0/90/90/0] laminate. For these in-plane strains, the intuitive formulation would predict an out-of-plane strain of $\epsilon_z = -0.31 \cdot 0.01 - 0.6 \cdot 0.001 = -3700$e-6 for the 0° plies, and of $\epsilon_z = -0.31 \cdot 0.001 - 0.6 \cdot 0.01 = -6310$e-6 in the 90° plies. On the other hand, the formulation based on plane stress would yield $\epsilon_z = -\frac{8.6}{17.1} \cdot 0.01 - \frac{10.5}{17.1} \cdot 0.001 = (-5601\text{e-}6)$ for the 0° plies and $\epsilon_x = (-6598\text{e-}6)$ for the 90° plies. The final strain results are put into brackets because they are based on the exact values rather than the rounded values shown in Matrix 5.15.

The finite element model showed out-of-plane strains of $-5601$e-6 in the 0° ply and $-6598$e-6 in the 90° ply, confirming the approach of calculating the Poisson's strains on a ply by ply basis using the formulation based on the assumption of plane stress.

In summary, the result of the finite element based verification efforts was that the analytical procedure indeed correctly predicts curing and out-of-plane Poisson's strains.

### 5.2.3 Ply Envelopes Involving Normal Strains

Very few failure envelopes are available in literature. The only source is (Hart-Smith, 2007). However, the envelopes he presents are incorrect (as will be discussed below).

The input data used can be found in Section B.5. Based on this, the micromechanical enhancement process is carried out and failure envelopes are generated. Hart-Smith's failure envelope has been sampled from (Hart-Smith, 2007, Slide 63).

Figure 5.1 shows the comparison of the correct failure envelope (established using the procedure outlined in Section 3.5) with Hart-Smith's envelope. There are significant discrepancies both in the fiber failure envelope and in particular also in the dilatational matrix cutoff. Hart-Smith does not

give the distortional matrix failure envelope. Note that the envelope plotted here only uses the square fiber array without any rotation of unit cells. It does, however, include the full set of interrogation points.

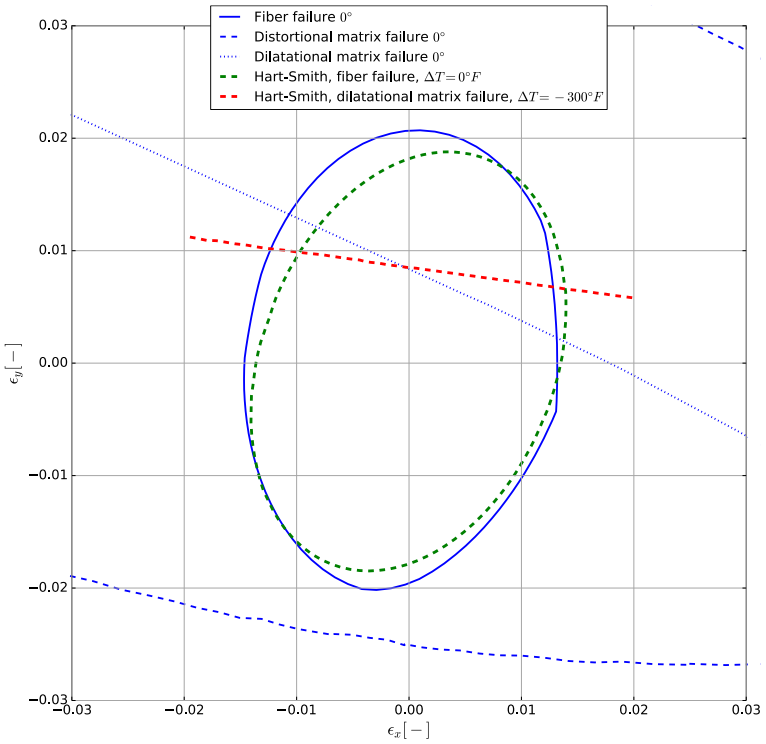


Figure 5.1: Comparison of correct normal strain ply failure envelope with Hart-Smith's envelope (Hart-Smith, 2007, Slide 63)

Since Hart-Smith uses movable boundary conditions (Subsection 2.2.3), the applied strains have to be adjusted (Subsection 3.1.2). Based on Eqn. (3.2) the unit cell will cause Poisson's effects according to Matrix 5.16. Therefore, the Poisson's effects in the applied strains have to be removed.

$$\mathbf{\Pi}_{movable} = \begin{bmatrix} 1 & -\frac{E_2}{E_1}\nu_{12} & -\frac{E_3}{E_1}\nu_{13} & 0 & 0 & 0 \\ -\nu_{12} & 1 & -\frac{E_3}{E_1}\nu_{23} & 0 & 0 & 0 \\ -\nu_{13} & -\nu_{23} & 1 & 0 & 0 & 0 \\ 0 & 0 & 0 & 1 & 0 & 0 \\ 0 & 0 & 0 & 0 & 1 & 0 \\ 0 & 0 & 0 & 0 & 0 & 1 \end{bmatrix}.$$

Matrix 5.16: Equivalent Poisson's effect matrix for movable boundary conditions

Figure 5.2 compares an envelope generated using $\mathbf{\Pi}_{movable}$ as the out of plane Poisson's effect matrix in Eqn. (3.19) (without any other changes to the procedure, in other words without adjusting the applied strains) with Hart-Smith's results. Clearly, the agreement has improved.

Note that as discussed in Subsection 3.1.2 measured ply properties rather than properties extracted from the unit cell were used to approximate the movable boundary conditions, resulting in an additional source of discrepancy. However, during the development process, the actual movable boundary conditions were used, resulting in a similar elongation.

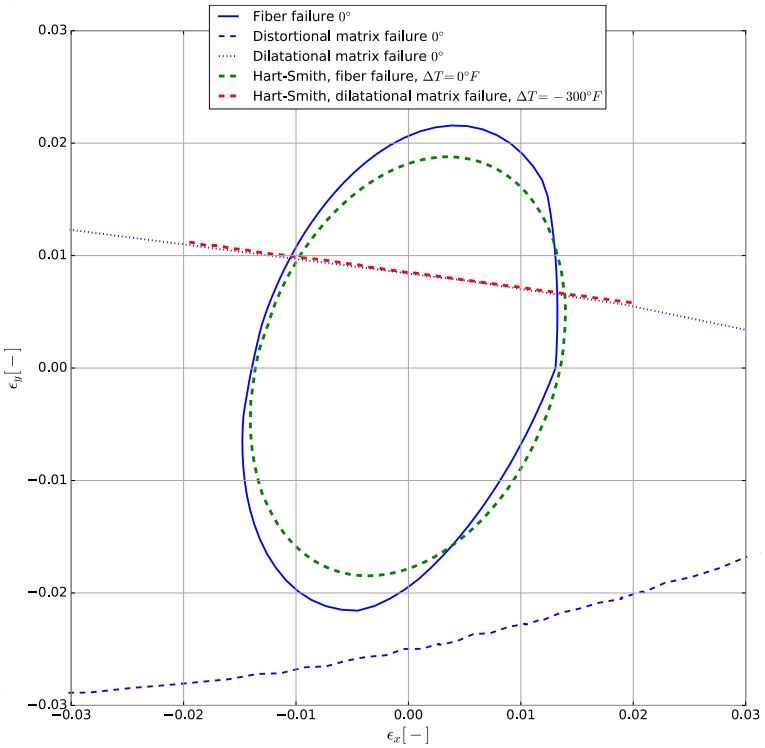


Figure 5.2: Comparison of normal strain ply failure envelope (using artificially introduced incorrect Poisson's effect) with Hart-Smith's envelope (Hart-Smith, 2007, Slide 63)

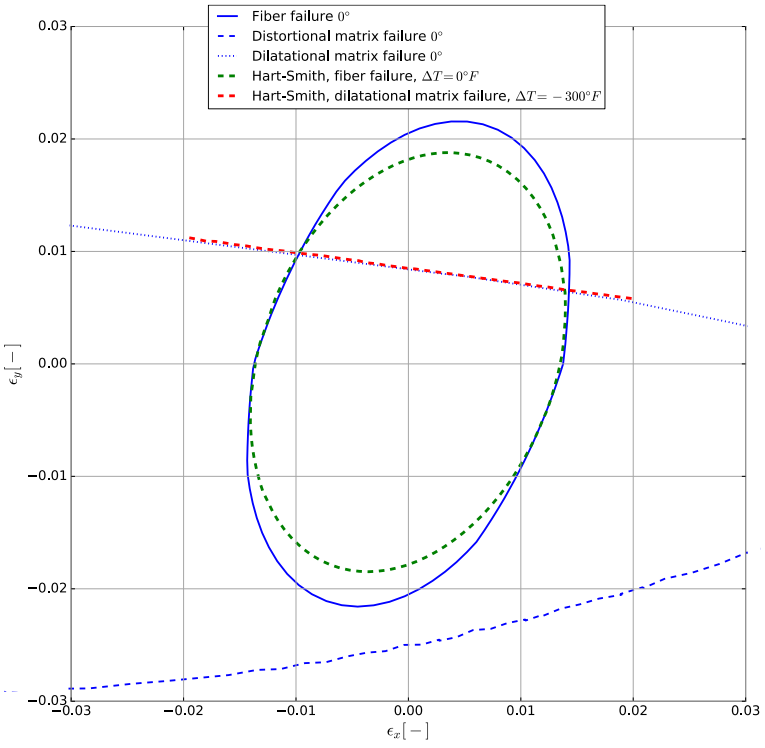


Figure 5.3: Comparison of normal strain ply failure envelope (using artificially introduced incorrect Poisson's effect and $\Delta T = 0$) for the fiber with Hart-Smith's envelope (Hart-Smith, 2007, Slide 63)

The final adjustment is due to the fact that for simplicity Hart-Smith assumes that the temperature difference experienced by the fiber is $\Delta T = 0$. The resulting failure envelope is shown in Figure 5.3. With the exception of the elongation of the fiber envelope along its major axis, the agreement is perfect. No explanation was found for this elongation. It is presumed that either slightly different input data is used, or one of the amplification factors used by Hart-Smith during his manual calculations was incorrect. The latter explanation seems more likely, because an incorrect amplification factor term would exactly result in scaling in a certain direction (see also Subsection 2.1.5).

Hart-Smith also shows envelopes for a diamond unit cell. The agreement between envelopes is essentially the same as here, using a square unit cell rotated by 45°. Additional errors are introduced because rotating the unit cell amplifies the impact of the difference between ply and unit cell properties when approximating the movable boundary conditions using the incorrect Poisson's mapping.

In summary, the approach to generate ply failure envelopes involving normal loads can be considered verified. At the same time, it has been discovered that Hart-Smith's application of SIFT is incorrect due to the use of movable boundary conditions without adequate adjustment of the applied strains.

Taking the correct Poisson's strains into account, as discussed in Section 3.5, would be quite tedious manually. This shows the major advantage of the consistent, automated approach developed in this thesis over Hart-Smith's manual calculations. It also facilitates including the temperature difference for the fiber (although the results indicate his assumption to be reasonable).

### 5.2.4 Laminate Envelopes Involving Normal Strains

The second comparison concerns a laminate failure envelope. Once again the only available source is Hart-Smith. The input data is the same as the one used in Subsection 5.2.3 (found in Section B.5), while the resulting envelope was sampled from (Hart-Smith, 2010, fig. 23).

In this section, the two issues with Hart-Smith's envelopes discovered in Subsection 5.2.3 (namely using incorrect boundary conditions for the micromechanical enhancement, and using $\Delta T = 0$ for the fiber) are already included. Figure B.1 shows the correct envelope.

Taking those errors into account results in Figure 5.4. Since there are still significant discrepancies, a further investigation was carried out. This revealed that Hart-Smith is neglecting the constraining environment of the other ply, causing the curing strains discussed in Subsection 3.2.2. The comparison resulting from excluding curing strains can be found in Figure 5.5. As discussed in Subsection 3.2.4, the effect of the curing strains is simply to shift the envelope. This shift occurs mostly in the transverse direction (of the ply) because of the respective stiffnesses of fiber and matrix.

Clearly, besides the elongation of the fiber envelope already discovered in Subsection 5.2.3, the two envelopes nearly coincide. This means that although an envelope involving curing strains could not be verified, the procedure of obtaining failure envelopes for rotated plies clearly works as well.

Unlike for the ply envelope in Subsection 5.2.3, Hart-Smith only provides a laminate envelope for the square array. The reason is that for each individual ply, the square array is more conservative than the diamond array. Therefore, the ply envelope (and thus also the laminate envelope) will be completely defined by the square array.

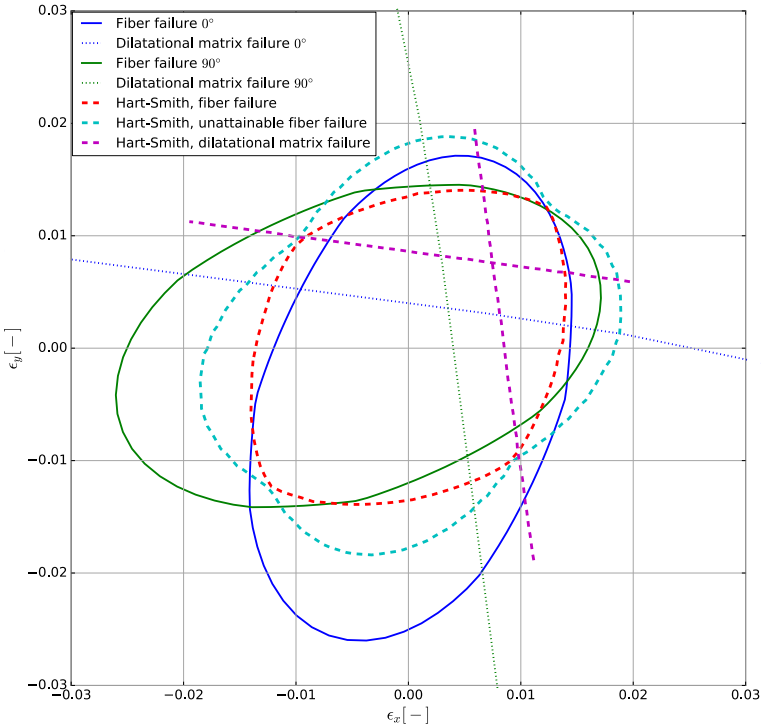


Figure 5.4: Comparison of normal strain [0/90/90/0] laminate failure envelope (using artificially introduced incorrect Poisson's effect and $\Delta T = 0$) for the fiber with Hart-Smith's envelope (Hart-Smith, 2010, fig. 23). Note that Hart-Smith calls the parts of the fiber failure envelope preceded by fiber failures in other directions “unattainable fiber failure”.

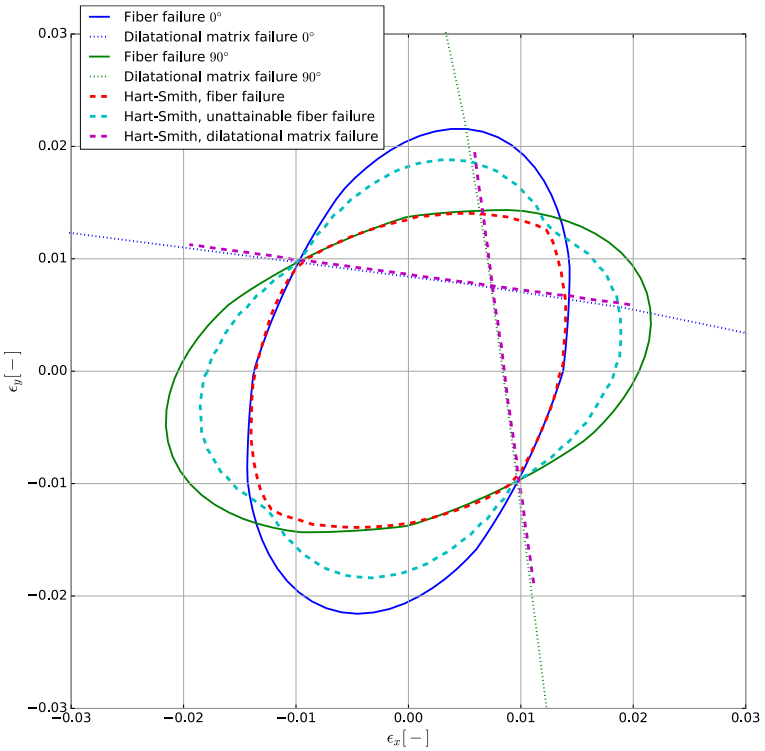


Figure 5.5: Comparison of normal strain [0/90/90/0] laminate failure envelope (using artificially introduced incorrect Poisson's effect and $\Delta T = 0$, as well as disregarding curing strains) for the fiber with Hart-Smith's envelope (Hart-Smith, 2010, fig. 23)

### 5.2.5 Ply Envelopes Involving Shear Strain

In order to also verify envelopes other than those containing purely normal strains, (Hart-Smith, 2007, Slide 69) is used, showing an $\epsilon_y$ vs $\gamma_{xy}$ envelope for a 0° ply. Figure 5.6 contains the comparison. The same input data as in the previous subsections is used.

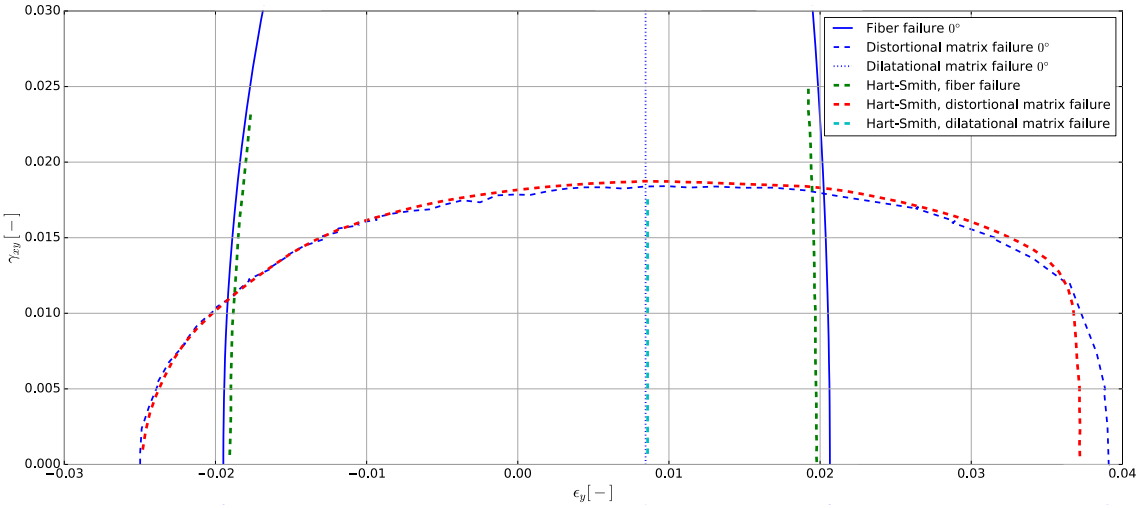


Figure 5.6: Comparison of shear strain ply failure envelope with Hart-Smith's envelope (Hart-Smith, 2007, Slide 69)

A couple of important points should be mentioned regarding this comparison. First of all, although there is clearly very good agreement between failure envelopes, this comparison suffers from inaccuracies due to the conversion between fixed and movable boundary conditions. This is related to the use of the ply Poisson's ratio instead of the Poisson's ratio computed from the unit cell (see also Subsection 3.1.2). A previous comparison carried out during the development process, using actual movable boundary conditions, showed even better agreement, with all lines essentially coinciding.

Secondly, note that unlike for the previous cases Hart-Smith is now taking the temperature difference into account for the fiber failure envelope. This is visible from the fact that the fiber failure envelope is not symmetric about $\epsilon_y = 0$ (which it should be because Eqn. (2.2) is quadratic in $\epsilon_{y,local}$, and for $\Delta T = 0$ Eqn. (2.5) linearly relates $\epsilon_{y,global}$ and $\epsilon_{y,local}$ without any offset).

Finally, for this envelope there is no difference between the correct approach (fixed boundary conditions, using the full state of strain as discussed in Subsection 3.5.3), and approximating the movable boundary conditions (using the incorrect Poisson's mapping from Subsection 5.2.3). This is the case because for a single 0° ply, the rotation matrix between laminate and ply coordinate systems can be omitted from Eqn. (3.19). In addition to that, only the second column of the Poisson's mapping is active. The second column of the multiplication of Matrices 3.10 and 3.11 ($\mathbf{\Pi}_{\epsilon_y,out-of-plane}\mathbf{\Pi}_{\epsilon_y,in-plane}$) contains the same components as the second column of the Poisson's mapping used to approximate the movable boundary conditions (Matrix 5.16), namely $\begin{bmatrix} -\frac{E_2}{E_1}\nu_{12} & 1 & -\nu_{23} & 0 & 0 & 0 \end{bmatrix}^T$. Since, finally, ply and laminate properties are identical, both approaches lead to the same result. The only differences between the literature failure envelope and the failure envelope plotted using this strategy are related to using the measured Poisson's ratio rather than the Poisson's ratio of the unit cell, as discussed previously.

Results for a diamond unit cell were also available. As for the ply envelope involving normal strains presented in Subsection 5.2.3, the agreement for the diamond unit cell is worse than for the square unit cell because rotating the unit cell (while not causing any error by itself) amplifies the impact of using ply properties rather than unit cell properties for the approximation of the movable boundary conditions. During the development process, a comparison between amplification factors using the actual movable boundary conditions for a diamond unit cell gave results essentially identical to those presented by Hart-Smith.

Finally, (Hart-Smith, 2007, Slide 70) also gives results for a 90° ply envelope involving $\epsilon_y$ and $\gamma_{xy}$, both for a square and for a diamond unit cell. These envelopes can be reproduced in the same manner discussed in this section and did not lead to additional findings. The same comments regarding the inaccuracy (introduced by using ply properties rather than unit cell properties to approximate the movable boundary conditions and amplified by rotating the unit cell to obtain the diamond fiber array) hold for the 90° envelope as well.

In addition to that, in the failure envelope for the 90° ply Hart-Smith also includes the results for a 0° ply envelope, as well as "failures in possible ±45° plies". As for the laminate envelope in Subsection 5.2.4, he does so by superimposing the individual envelopes without including curing strains.

### 5.2.6 Summary of Verification Efforts

Verification of the failure envelope predictions resulted in two core results. Most importantly, the approach of generating failure envelopes is working correctly. The discrepancies compared to the literature results could either be explained or were insignificant. This means that the entire approach towards Onset Theory, involving micromechanical enhancement and failure envelope prediction, can be considered verified. The next step will be to validate the theory and to carry out further research.

Secondly, the failure envelopes Hart-Smith shows are incorrect. There are three errors associated with them. Of minor importance is the fact that he is using $\Delta T = 0$ for the fiber envelopes for normal strain envelopes (Subsections 5.2.3 and 5.2.4). However, he is also making the crucial error of using movable boundary conditions without compensating for the added Poisson's effect appropriately (also Subsections 5.2.3 and 5.2.4), and he fails to include curing strains (Subsection 5.2.4). Both of these mean that the results he published regarding trends he found in SIFT – in particular in (Hart-Smith, 2010) – are suspect. It stands to reason that his results were based on analyses that contained the same flaws. Therefore, his claims should be investigated further. Efforts related to this are contained in Chapter 7.

# Chapter 6

# Validation of Onset Theory

In previous chapters a consistent procedure to apply Onset Theory was established, followed by automating the approach and verifying theory and implementation. The present chapter focuses on validation and research efforts. First of all, available test data is discussed in Section 6.1. Subsequently, the main input data not commonly available in literature (namely critical invariants) is listed in Section 6.2. During this process, certain trends are tentatively established which aid in the application of Onset Theory without requiring tests to be carried out to determine the critical invariants. Based on this, theory and test data are compared in Section 6.3. Finally, Section 6.4 compares Onset Theory and other failure theories to analyze advantages and disadvantages.

## 6.1 Test Data

One of the most extensive and presumably reliable sources for test data is the World Wide Failure Exercise (WWFE), carried out by (Soden, Hinton, & Kaddour, 2002). It is specifically meant for the benchmarking of failure criteria and contains a wealth of information. In fact, the application of Onset Theory to the WWFE benchmark problems has specifically been mentioned as a knowledge gap by (Hart-Smith, 2014). Evaluating SIFT in this way would provide significant additional credibility to the theory. Unfortunately, the vast majority of data used in the WWFE exercise is only available in stress space. Given the discussion in Subsection 2.2.1, this is inadmissible.

The only source that contains WWFE data is the article by (Swanson & Christoforou, 1986), who carried out tests on a quasi-isotropic (QI) laminate made of AS4/3501-6 in strain space. Additional data is contained in (Swanson & Nelson, 1986). This data is also contained in (Hart-Smith, 1989), who references (Swanson & Nelson, 1986).

Besides data for materials used in the WWFE, (Swanson & Qian, 1992) contains data for three laminates with various numbers of 0°, ±45° and 90° layers, made of T800/3900-2.

Finally, (Colvin & Swanson, 1990) have longitudinal vs transverse failure data for three different laminates consisting of IM7/8551-7, as well as transverse vs shear failure data for a single lamina.

For reference purposes, the full datasets are tabulated in Appendix D. In general, it can be stated that there is very little reliable strain-based failure data available. Note in particular that all test data has presumably been generated using the same facilities (all sources stem from the group around Swanson). This means that any flaws in their test facilities will instantaneously render almost all test data invalid. All in all, the lack of reliable data from multiple research facilities will make any validation tasks quite challenging.

## 6.2 Critical Invariants

Due to the relative novelty of Onset Theory, critical invariants for the material under investigation can be difficult to find. Therefore, a list of critical invariants found in literature has been compiled. It is meant as a starting point for other researchers to quickly identify realistic ranges of the values, as well as potential sources for critical invariants. Where possible, a critical review of the data is included. However, for many cases it proved difficult to verify whether the correct methodology (both experimental and in terms of modeling) has been used. In particular, some of the papers were only available in Korean or Chinese. This means that the only available information is the data found in equations, tables, and figures. Therefore, the list should not be trusted implicitly.

Appendix E contains all critical invariants found in literature, ordered essentially chronologically. This data is visualized in Figures 6.1 to 6.3. Results for the same materials from the same main author have been grouped together, such as the various articles involving Tran, or articles who cite (personal communication with) Gosse as their source. Note also that all references to "entries" in this section refer to Table E.2.

Some critical invariants are not included in this list, for a multitude of reasons. (Tsai et al., 1999) report invariants for various types of adhesives. This is not relevant for the topic of interest (failure of fiber/matrix composites). (Harman, Risborg, & Wang, 2008) omitted the essential step of micro-mechanically enhancing the applied strains, rendering the critical invariants they report for IM7/5250-4 meaningless. Finally, as discussed in Subsection 2.2.1, stress invariants are not considered in the present formulation of SIFT. This means the critical invariants reported particularly by (Ha et al., 2008), but also the matrix invariants given by (C. H. Wang, 2005), are also not included.

Acknowledging the lack of certainty regarding the information, as outlined in the first paragraph, it is still possible to draw a number of conclusions. They are related both to a confirmation of the theory (Subsection 6.2.1) and to trends of the critical invariants (Subsections 6.2.2 to 6.2.4).

### 6.2.1 General Observations

In Subsection 1.3.2, redundant testing for the matrix invariants was discussed as a means of verifying the validity of Onset Theory. For the most part, there is indeed very low spread of results for authors who report critical invariants for multiple specimens. Entries [1], [2], [5], 13], [17] and [18] of Figure 6.1 show this behavior (although it should be noted that entry [24,27,28,30] of the same figure shows very large spread, see annotation 4). The same observation can made regarding entries [17], [23,25,26], and [24,27,28,30] of Figure 6.2.

In addition to that, as mentioned in Section 1.3 one of the fundamental propositions of Onset Theory is that the critical invariants are independent of each other, both considering a single material (i.e. first and second matrix invariants) and the material combination (i.e. matrix and fiber invariants). The former of these claims was already discussed in Subsection 1.3.2, while the latter is based on (Z. Li et al., 2011, Table 3) (entries [20], [21] and [22]). Two fibers and two resins were investigated in all three possible combinations. For CCF300/5428, the matrix invariants were found to be $J_1^{*m} = 0.0319$ and ${\epsilon^*_{eqv}}^m = 0.195$, while for T700/5428 the results were $J_1^{*m} = 0.0313$ and ${\epsilon^*_{eqv}}^m = 0.202$. Similarly, for CCF300/5428 the fiber invariant was ${\epsilon^*_{eqv}}^f = 0.018$, whereas for CCF300/4228 the result was ${\epsilon^*_{eqv}}^f = 0.017$. This is very strong evidence in favor of the claim that the critical invariants are independent of the other material in the composite.

IM7/977-3 from [5] and IM7/K3B from [11] also yield almost identical fiber invariants. It would be very interesting to compare other cases as well (combinations of the same matrix with different fibers, or vice versa). Unfortunately no additional obvious cases are available in literature.

### 6.2.2 Observations Regarding Critical Dilatational Matrix Invariant

Figure 6.1 contains all values of the critical dilatational matrix invariant found in literature. A number of observations can be made, some of which are also included in Table E.2.

First of all, annotation 1 shows that the values for CCF300/5428 (entry [21]) and T700/5428 (entry [22]) are very similar, as discussed in the previous section.

For two cases, it is questionable whether the correct material is reported. As shown in annotation 2, the values in [19] for Cycom 970 are quite different from the ones for Cycom 970 in [23] and [26], but very similar to the ones for 3900-2 in [24]. All of this data was reported by the research group around Tran, leading to the belief that information has gotten mixed up in one publication. Exactly the same holds for the value in [6] for 977-3, being identical to the values for K3B in [13] but very different from the values for 977-3 in [14] (annotation 3). All of these sources cite Gosse.

As stated previously, redundant testing seems to result in consistent values for most cases. However, annotation 4 shows a very large spread of results. Values between 0.02 (for a 67° off-axis tension test) and 0.027 (35% of the smaller value; based on a 30° test) were determined (Tran, 2012).

Finally, there is some uncertainty regarding the values for T300/Cycom 970 in [23] and [26]. Highlighted in annotation 5, they are clear outliers compared to all other values. In (Tran et al., 2013) the authors discuss the fact that the material used was a rubber toughened resin. This could lead to progressive failure (failure strains beyond the onset of failure), which – as discussed in Section 1.5 – is not part of Onset Theory. Based on load/unload tests, they determined a critical invariant of 0.025, which is much closer to the other values.

It is difficult to make claims regarding the reproducibility of results across different researchers. A possible candidate would be 3900-2 by [24,27,28,30] and [31], but the spread of the former is too large to obtain any certainty.

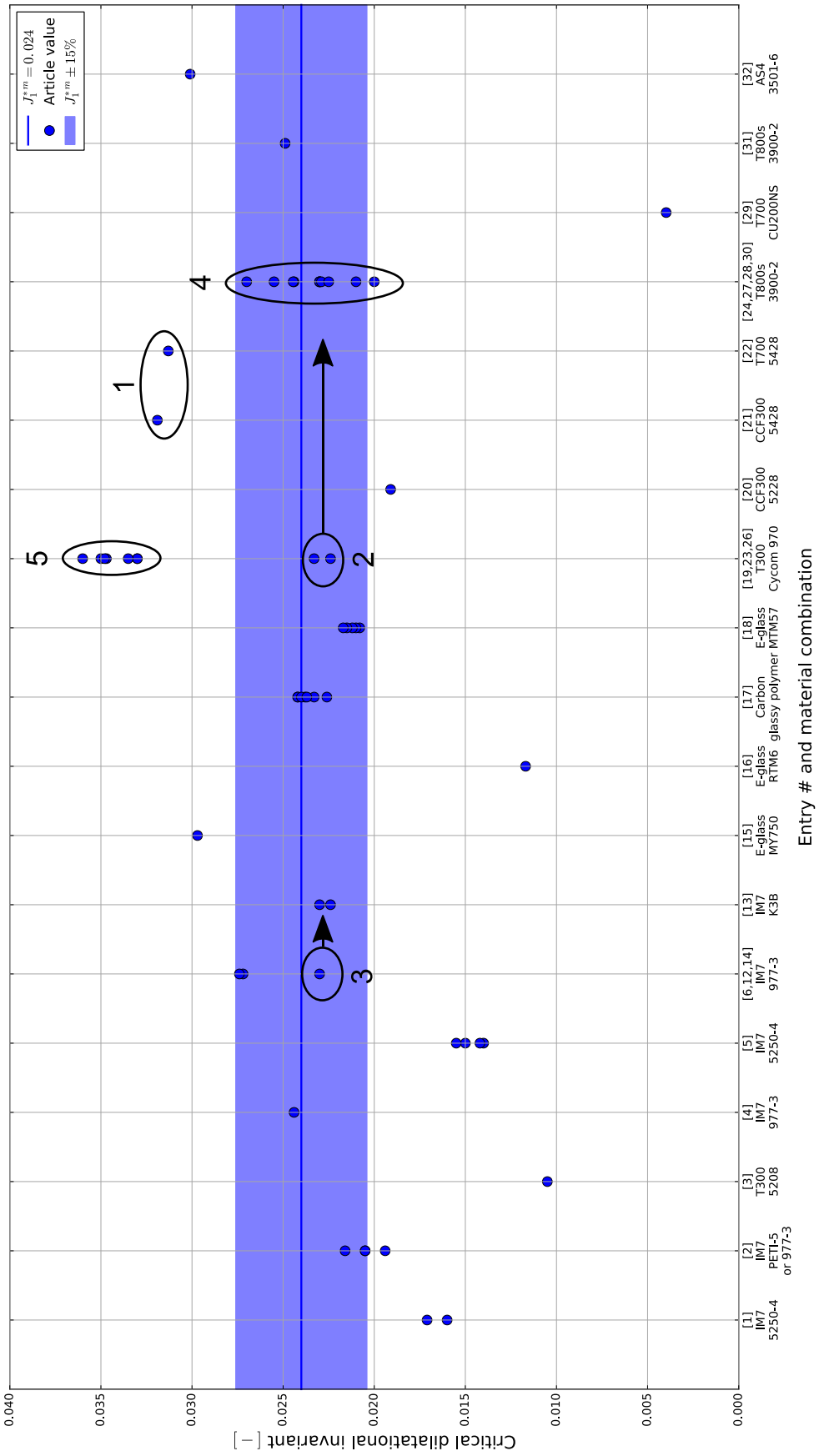


Figure 6.1: Overview of critical dilatational matrix invariants found in literature. Entry numbers refer to Table E.2. The transparent band refers to the suggested range of the critical invariant. Annotated points are discussed in the text

In general, the dilatational invariant seems to be rather difficult to determine given the large spread of results even for the same material. This could be related to the fact that typically a 90° tension test is used to determine this invariant. These coupons tend to fail prematurely (see e.g. (Hart-Smith, 2010, p. 33) for an in-depth discussion), explaining part of the scatter visible in Figure 6.1. On the other hand, if actual laminates are used, then dilatational matrix failure may not be catastrophic. Detection via acoustic emissions or changes in slope of the stress/strain curve are most likely not accurate enough to determine the true onset of failure.

Either way there seems to be some consistency in the critical values obtained from various material combinations. This is highlighted by the blue band in Figure 6.1, representing a value of the critical invariant between 0.0204 and 0.0276 (in other words 0.024 ± 15%). If the rubber toughened epoxy of [23,26] is moved to 0.025 as discussed above, then a significant part of the data is captured. Using the stated limits, 9 of 19 (groups of) entries are within bounds, 3 are somewhat outside (within 0.0191 and 0.0301) and 7 are at a larger distance. This means that the suggested range can only be considered a tentative suggestion. For the critical distortional invariants in Subsections 6.2.3 and 6.2.4 the results are more consistent.

### 6.2.3 Observations Regarding Critical Distortional Matrix Invariant

As for the previous section, the critical invariants from Table E.2 are presented visually in Figure 6.2. However, in this case four different colored bands are shown. This is related to the four possible definitions of the distortional invariant discussed in Subsection 2.1.1. Four definitions were found:

Table 6.1: Possible definitions of the distortional invariant (repeated from Table 2.1)

| | |
|---|---|
| Definition #1 | $\epsilon_{eqv}$ |
| Definition #2 | $\frac{1}{\sqrt{3}}\epsilon_{eqv}$ |
| Definition #3 | $\epsilon_{eqv}^2$ |
| Definition #4 | $\frac{1}{3}\epsilon_{eqv}^2$ |

For a value of ${\epsilon_{eqv}^*}^m = 0.2$ with a range between 0.18 and 0.22 (i.e. 0.2 ± 10%), the values in the resulting definitions become

Table 6.2: Suggested critical distortional matrix invariants using various definitions

| | |
|---|---|
| Definition #1 | 0.2 (range between 0.18 and 0.22) |
| Definition #2 | 0.115 (range between 0.104 and 0.127) |
| Definition #3 | 0.04 (range between 0.0324 and 0.0484) |
| Definition #4 | 0.0133 (range between 0.0108 and 0.016) |

Note how changing ${\epsilon_{eqv}^*}^m$ by 10% results in different percentage changes depending on the definition.

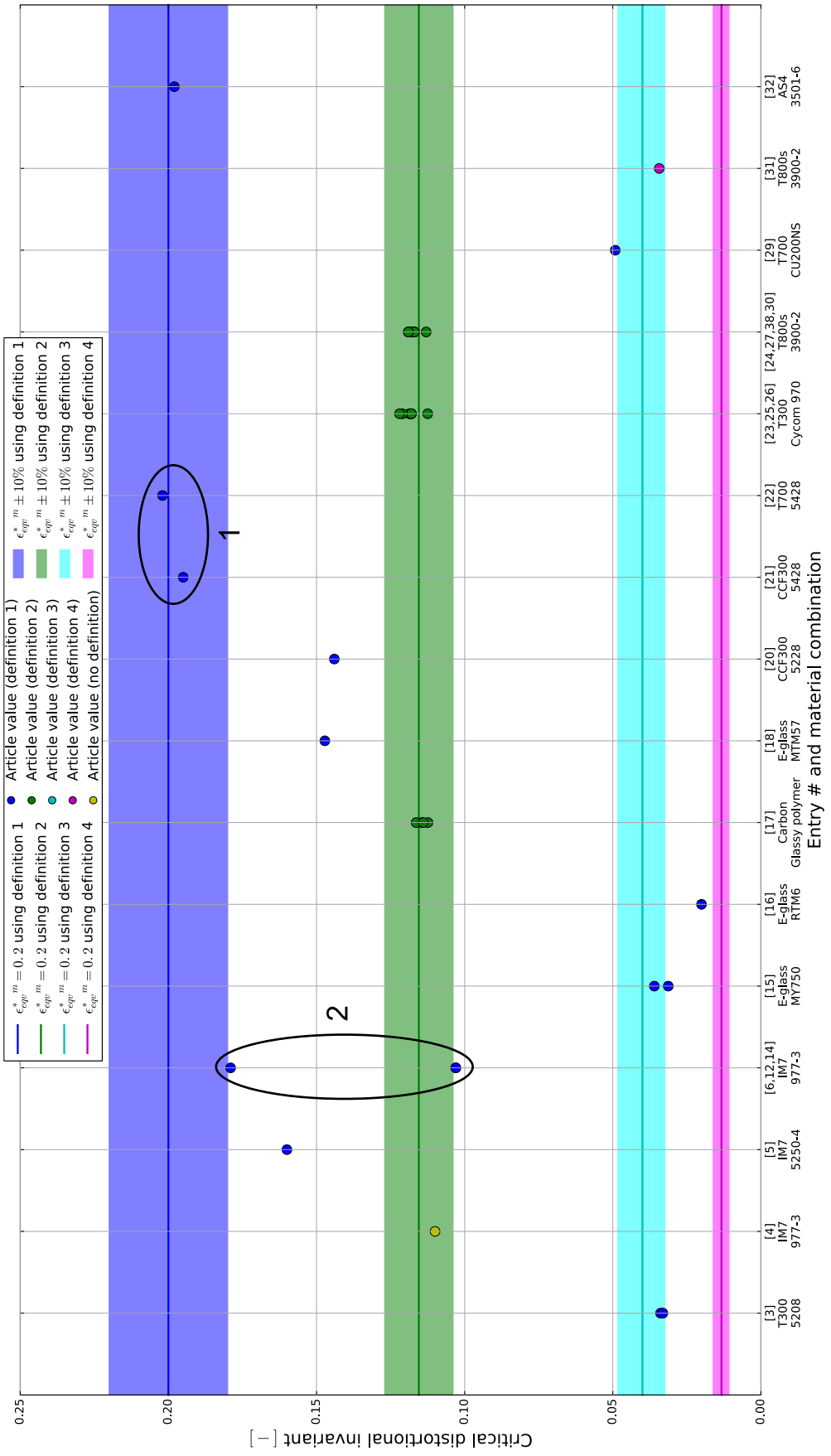


Figure 6.2: Overview of critical distortional matrix invariants found in literature. Entry numbers refer to Table E.2. The transparent bands refer to the suggested range of the critical invariant based on the definitions found in Subsection 2.1.1. Annotated points are discussed in the text.

The suggested value of ${\epsilon^*_{eqv}}^m = 0.2 \pm 10\%$ is determined based on the fact that there are serious doubts about whether the definitions stated in the articles are correct. As seen in Figure 6.2 a number of results (e.g. entries [3] or [15]), amongst others) are close to the suggested common value, but using a different definition than the one stated in the article. An incorrect definition seems far more likely than orders of magnitude of difference in the critical values. A particular example is highlighted in annotation 2. Entries [6], [12] and [14] all cite Gosse on the same material, but report different values of the critical invariant (0.103 and 0.179). These two values are almost exactly a factor $\sqrt{3}$ apart, which corresponds to the difference between definitions 1 and 2.

A number of minor observations can be made. First of all, as stated before and highlighted in annotation 1, CCF300/5428 (entry [21]) and T700/5428 (entry [22]) give almost identical results. Secondly, it is again rather difficult to make claims regarding the reproducibility of results by different researchers (beyond the fact that there seems to be significant similarity between invariants in general, regardless of the material). [4] and [6,12,4] return very similar results, but the definition used in [4] is unknown and [6,12,14] use two different definitions. [24,27,28,30] and [31] also return very similar results, provided it is accepted that the definition stated in [31] is incorrect and should in fact be definition 3.

More importantly, using the suggested range of ${\epsilon^*_{eqv}}^m = 0.2 \pm 10\%$, 7 of 16 entries are close to the definition stated in the article, 1 entry is close to the common value without any definition given in the article, 4 entries are close to a different definition than the one stated in the article, and 4 entries are far away from all definitions. As for the critical dilatational matrix invariant, this points to some consistency between the critical distortional matrix invariants for a variety of materials.

### 6.2.4 Observations Regarding Critical Distortional Fiber Invariant

The final set of invariants are the critical distortional fiber invariants, taken once again from Table E.2 and visualized in Figure 6.3. As in Figure 6.2 all four definitions are shown in form of colored bands. For a value of ${\epsilon^*_{eqv}}^f = 0.02$ with a range between 0.018 and 0.022 (i.e. $0.02 \pm 10\%$), the values in the resulting definitions become

Table 6.3: Suggested critical distortional fiber invariants using various definitions

| | |
|---|---|
| Definition #1 | 0.02 (range between 0.018 and 0.022) |
| Definition #2 | 0.0115 (range between 0.0104 and 0.0127) |
| Definition #3 | 0.0004 (range between 0.000324 and 0.000484) |
| Definition #4 | 0.000133 (range between 0.000108 and 0.00016) |

Since the suggested critical distortional fiber invariant is an order of magnitude smaller than the equivalent value for the matrix, definitions 3 and 4 effectively become meaningless because the resulting values are extremely small.

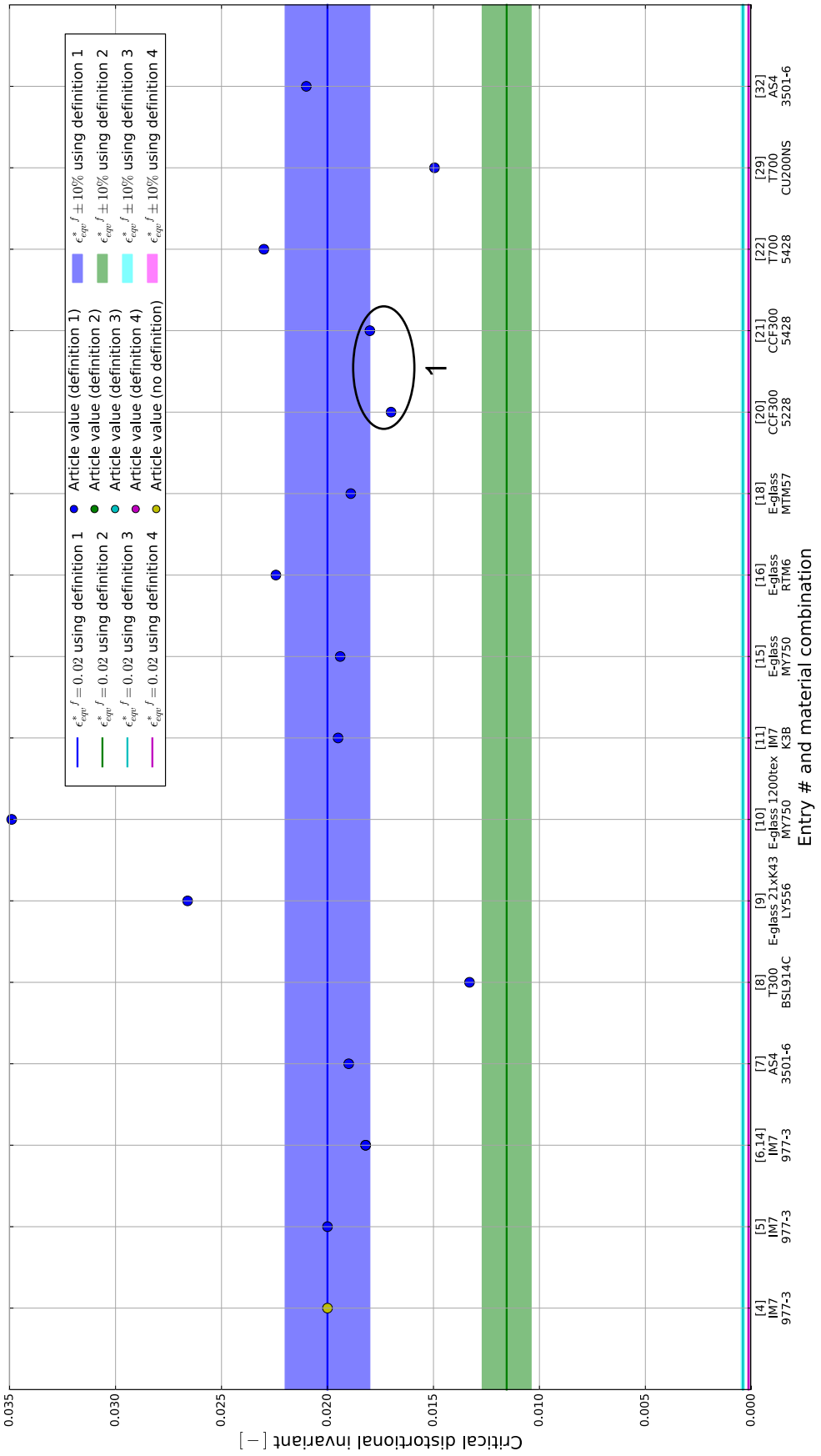


Figure 6.3: Overview of critical distortional fiber invariants found in literature. Entry numbers refer to Table E.2. The transparent bands refer to the suggested range of the critical invariant based on the definitions found in Subsection 2.1.1. Annotated points are discussed in the text.

A number of observations can be made. First of all, as discussed in Subsection 6.2.1 the results for CCF300/5228 and CCF300/5428 are almost identical (annotation 1).

Secondly, almost all values are close to the suggested common value using definition 1. This means that there are cases where there is a disconnect between the definition believed to have been used for $\epsilon^m_{eqv}$ and $\epsilon^f_{eqv}$. Particular examples include [6,12,14] and [15], where the fiber invariant is close to the common value using definition 1, while the matrix invariant appears to be using definitions 2 and 3, respectively. This disconnect can also be shown in the raw data. In [11] and [12], the critical values are ${\epsilon^*_{eqv}}^m = 0.179$ and ${\epsilon^*_{eqv}}^f = 0.0195$. For the same material combinations, citing the same source (Gosse), [14] reports ${\epsilon^*_{eqv}}^m = 0.103$ and ${\epsilon^*_{eqv}}^f = 0.0182$. This means the fiber invariant has only changed slightly, while the matrix invariant changed by a factor of $\sqrt{3}$, corresponding to the difference between definitions 1 and 2 (as discussed previously in Subsection 6.2.3, regarding annotation 2 of Figure 6.2). It appears that indeed the matrix and fiber definitions are not consistent.

Finally, regarding reproducibility, the values returned for IM7 in [4], [5] and [11] are almost identical. However, this is evidently part of a larger trend of consistency, since for example [6,14] reports a slightly different value for IM7 (which still falls into the suggested range of values).

Using ${\epsilon^*_{eqv}}^f = 0.02 \pm 10\%$, 9 of 16 entries are captured, while an additional 3 are only slightly outside the colored band. The remaining 4 entries are far away from the common value. It should be noted that entries [8], [9] and [10] were all determined by the same author, who is using strength test data (see Subsection 2.2.1 for a discussion of the necessity to use strain test data). In addition to that, during the verification efforts in Subsection 5.1.4 the micromechanical amplification factors could not be reproduced. As for the critical matrix invariants, this means that there appears to be some consistency between the critical values for a variety of materials.

### 6.2.5 Summary and Discussion

To summarize, based on the discussion in the preceding sections the following tentative values are suggested for the critical invariants of composites, regardless of the constituents:

$$J_1^{*m} = 0.024 \pm 15\%$$

$${\epsilon^*_{eqv}}^m = 0.2 \pm 10\%$$

$${\epsilon^*_{eqv}}^f = 0.02 \pm 10\%$$

Clearly, the consistency of in particular the critical invariant is a highly interesting result. Although this can at most be a tentative conclusion, it appears as if commonly used constituents all have very similar critical strain invariants. Since composites containing fibers ranging from IM7 or AS4 to E-glass will certainly have vastly different strengths (see for example (Soden et al., 1998) for some typical strength values), the similarity in critical strain invariants has to be due to stiffness effects. Either the same (global) failure strain results in different failure strengths, or due to the micromechanical enhancement process identical local failure strains correspond to different global failure strains. The former of these would be related to differences in the stiffness of the composite, while the latter would mean the individual constituent stiffnesses are the relevant factor (together with other factors such as the fiber volume fraction).

For the sake of completeness, the difference in tested strength could also be related to interface failure. However, as discussed in Subsection 2.1.2, this should not occur for useful composites. Even if it did it would most likely be reflected in the critical invariants, albeit at the cost of removing one of the main strengths of SIFT, namely its independence of the loading and boundary conditions.

In summary, it appears as if a first order failure approximation can be made without requiring strength tests of either the constituents or the ply. The only required input parameters are the stiffness properties of the constituents and the ply (using the current implementation; as discussed in Subsection 8.4.1 it is suggested to remove the necessity of including ply properties), as well as typical values for the critical invariants.

The suggested procedure to determine failure using Onset Theory would thus be to use the "generally applicable" invariants to obtain an approximation of the failure envelope, assuming that no test data is available. Subsequently, once test data is available, the invariants can be modified based on either dedicated tests to determine the critical invariants or by scaling the envelope through modifications of the critical invariant. Note that this scaling is not the same as the "fine-tuning" commonly done for many failure criteria, in particular Tsai-Wu. Unlike for those cases only the scale of the envelope is modified, while the shape of the failure envelope is the same. This means that once the envelope is fit to one point, the theory will be confirmed by the match with all other data points. This latter strategy is also discussed further in Subsection 8.4.4.

## 6.3 Comparison to Test Data

As discussed in Section 6.1, there are four sets of validation data available: failure strains in the normal strain plane for a QI laminate of AS4/3501-6, three different laminates of T800s/3900-2, and a QI laminate of IM7/8551-7, and a transverse load vs shear envelope for a uniaxial 90° specimen of IM7/8551-7. These four cases are presented in the following subsections, with the required input data summarized in the respective sections of Appendix D. The results are discussed in Subsection 6.3.5.

### 6.3.1 AS4/3501-6 Biaxial Strain Laminate Envelope

Typically, matrix cracking ($J_1$-failure) is not catastrophic for quasi-isotropic laminate under in-plane normal strains. Therefore, ultimate failure occurs once the fibers of some ply fail. Although this means there is another failure mode preceding ultimate failure, this is not a case of progressive failure analysis, as discussed below.

Two different values of $J_1^{*m}$ for AS4/3501-6 seem possible: 0.0301, and the default value of 0.024. Some tentative data is available for possible matrix cracking, although it is not clear how reliable this data is. See the discussion in Section D.1 for more details.

Figure 6.4 shows the comparison between prediction and test, using $J_1^{*m} = 0.024$. Suspected matrix cracking occurs essentially exactly when dilatational matrix failure is predicted for the 90° ply, meaning that the value of 0.0301 is most likely incorrect (although given the uncertainty in the test data there is not enough evidence to discard the literature value with certainty).

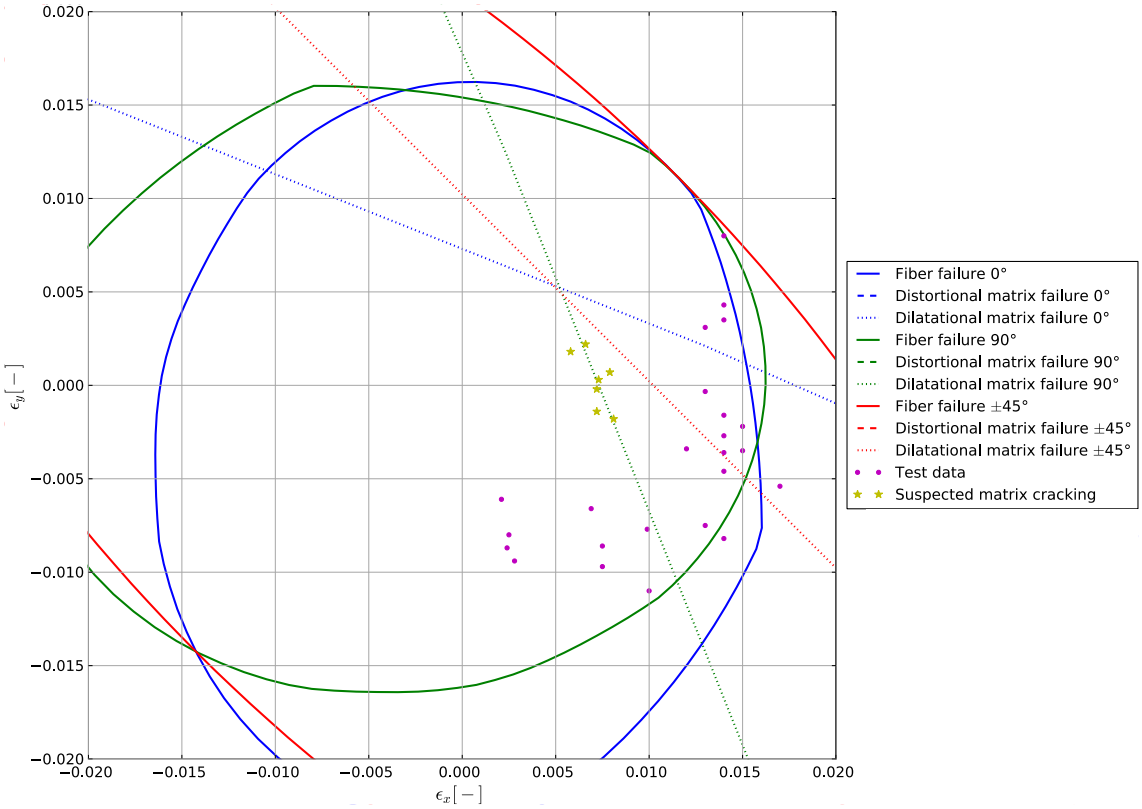


Figure 6.4: Comparison between prediction and biaxial strain test data for an AS4/3501-6 [90/±45/0]s laminate.

Clearly, the predictions of ultimate failure were not entirely accurate. In particular for strongly compression-dominated states of strain, the predictions were unconservative compared to the test data. The general trend was that the failure predictions formed an outer bound on the test data, with very few data points outside of the predicted envelope.

A perfect failure criterion, using the exact material properties from the test specimen, should predict the result achieved by a perfect test. In reality, some tests may even overachieve the perfect test results due to scatter in material properties. However, typically factors decreasing the test result (in particular for compression-dominated states of strain) will outweigh factors increasing the test result. One possibility that might be causing premature failures in compression are failure modes not included in Onset Theory at the present state of development, such as fiber kinking. This is one of the suggestions in Subsection 8.4.2. Other options include manufacturing flaws, test setup, instrumentation and measurement errors. In general, this means that an outer bound on the test data (as observed here) is only to be expected of a criterion predicting failure of a pristine structure.

Given the large scatter of the AS4/3501-6 test data, in particular for compression-dominated states of strain (on the same radial line – i.e. for the same strain ratio – in Figure 6.4, values between $\epsilon_y = -0.0061$ and $-0.0094$ are obtained, a difference of almost 55%, for very similar, small tensile values of $\epsilon_x$), imperfect tests indeed seem like a plausible explanation.

For a small number of specimen, falling short of or exceeding the predictions does not hold statistical significance. Therefore, more test data is needed to support or refute these hypotheses. This is

partially achieved through the comparison with test data for other materials in the following subsections. The results are discussed in Subsection 6.3.5.

In general, premature failures will certainly also occur in a production environment. However, the first step in creating accurate predictions for those cases would be to obtain perfect test data and a perfect failure criterion (or as nearly so as possible). Once this is available, effects such as premature failure can be added. Otherwise, the danger is that flaws in the criterion are compensated for by flaws in the test data for one case, but not for the next, leading to erratic predictions which are sometimes correct and sometimes not.

Besides possible issues with the test data, no sensitivities of any kind were taken into account for the failure predictions, and default values of the invariants were used. The predictions were also not tuned to the test data in any way. By reducing the critical fiber invariant, the envelope could be scaled down (without any change in shape, see also Subsection 2.1.5), providing a better match with test data. However, as stated above it is questionable whether this would result in more accurate predictions for the general case, or would simply mean including flaws of this particular set of test data in the critical invariant.

What is very interesting about this comparison is the near-perfect match between predicted matrix cracking and suspected matrix cracking. It should be stressed that no progressive failure analysis of any kind has been carried out. Since Onset Theory – unlike most other failure criteria – actually predicts the specific failure mode and constituent, it is not necessary to reduce ply properties in order to include a "first ply failure", based on which the remaining predictions are updated.

In strain space, with the exception of the curing strains a given ply's failure strain does not depend on the state of damage in (or, in fact, the existence of) another ply. This assumes that there are no strain concentrations or other effects due to failure in some ply. The analysis in this thesis is only a first order model which assumes identical strains in ply and laminate strains at all times. Related to this is the limitation that ply interface failure (such as delaminations) are not included in the theory as currently implemented. This was addressed in Subsection 2.1.6. Similar behavior would also occur due to interlaminar stresses at the edges of the specimens. Taking any of those effects into account would, first of all, require some way to determine those strains, and secondly appropriate unit cells to analyze the microstructural behavior at those locations.

Independence of the ply strains is another reason for the preference of strain-based over stress-based test data, as discussed in Subsection 2.2.1. For AS4/3501-6, matrix cracking in the 90° ply is predicted at a strain far below the ultimate strain of the laminate. This prediction matches the measured matrix cracking almost exactly. However, the fact that there are matrix cracks in the 90° ply does not influence fiber failure in the 0° ply.

Therefore, although there definitely is failure occurring before ultimate failure, this is not a case of progressive failure. Progressive failure would mean that a certain failure mode occurs, and that same failure mode continues to grow until final failure is reached in the same failure mode (or because of the initial failure, another failure starts, eventually cumulating in ultimate failure). An example would be growing delaminations, which are not included in Onset Theory as implemented in this thesis (see Subsection 2.1.6). In this case, the first failure mode is "ultimate failure" of one ply in that particular failure mode, but the laminate as a whole is still capable of carrying load. Ultimate

failure of the laminate then occurs once another, unrelated failure mode is triggered in another ply. This does not mean there was any progression of the first failure mode (which was already ultimate failure in that failure mode in that ply the moment it occurred).

Note that it can be argued that matrix cracking in the 90° ply will relieve the curing strains experienced by the 0° ply. This should definitely be investigated, as discussed in Subsection 8.4.3.

Finally, it should be mentioned that accepting matrix cracking as non-catastrophic is only possible for laboratory specimens. In a real-life structure experiencing various different states of load, the occurrence of matrix cracking would most likely lead to catastrophic failure the moment the structure is loaded in some other way (e.g. a simple reverse of sign of the load, leading to a tensile strain in the cracked matrix).

### 6.3.2 T800s/3900-2 Biaxial Strain Laminate Envelope

Test data for three different laminates is available for T800s/3900-2: a QI laminate, a laminate containing additional 0° plies, and a laminate containing additional ±45° plies. The comparison with failure predictions is shown in turn in the subsequent figures. Note that the only difference in predictions is due to the different curing strains developed in the laminates. In fact, for the $[0/\pm45/90]$s and $[0/(\pm45)_2/90]$s laminates, the curing strains and thus the failure predictions are identical because the effect of additional ±45° plies is equal in longitudinal and transverse directions.

The agreement is quite good for all three laminates, with the failure predictions essentially passing through the center of the scattered test data for the $[0/\pm45/90]$s and $[0/(\pm45)_2/90]$s laminates. Since the differences are rather small, they can easily be taken into account by allowing a small range of critical fiber invariants (which will scale the envelope up or down accordingly, with no change in shape). Although the default critical invariants appear to provide good predictions for different materials, and no sensitivity for any other parameter was taken into account either, this does not mean that (small) variations of the critical invariants can or should not be used as a simple means of including variations for example in the material properties.

For the laminate containing additional 0° plies (Figure 6.6), the agreement is not quite as good, with slightly unconservative predictions for most data points and a vastly overconservative prediction for another data point (at $\epsilon_x = 0.01498$ / $\epsilon_y = 0.01094$). Note that as for the AS4/3501-6 envelope no sensitivity is taken into account for any parameters, default critical invariants are used, and the prediction is not tuned to the test data in any way. For example, for Figure 6.5 a minor variation of the critical invariant by about 10% or so would already include almost all data points (the envelope simply increases or decreases by exactly the same amount as the critical invariant). This happens to coincide with the range of critical invariants suggested in Subsection 6.2.5 (although there, the range was based on multiple materials rather than just a single one).

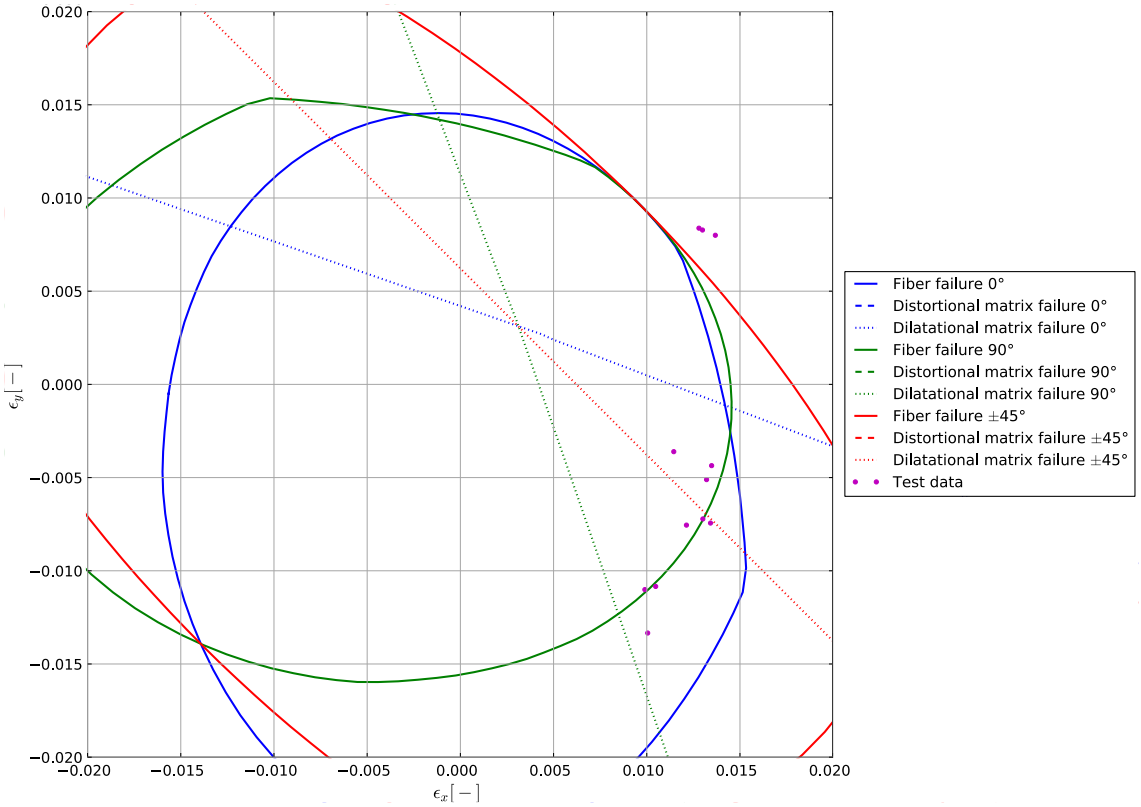


Figure 6.5: Comparison between prediction and biaxial strain test data for a T800s/3900-2 [0/±45/90]s laminate

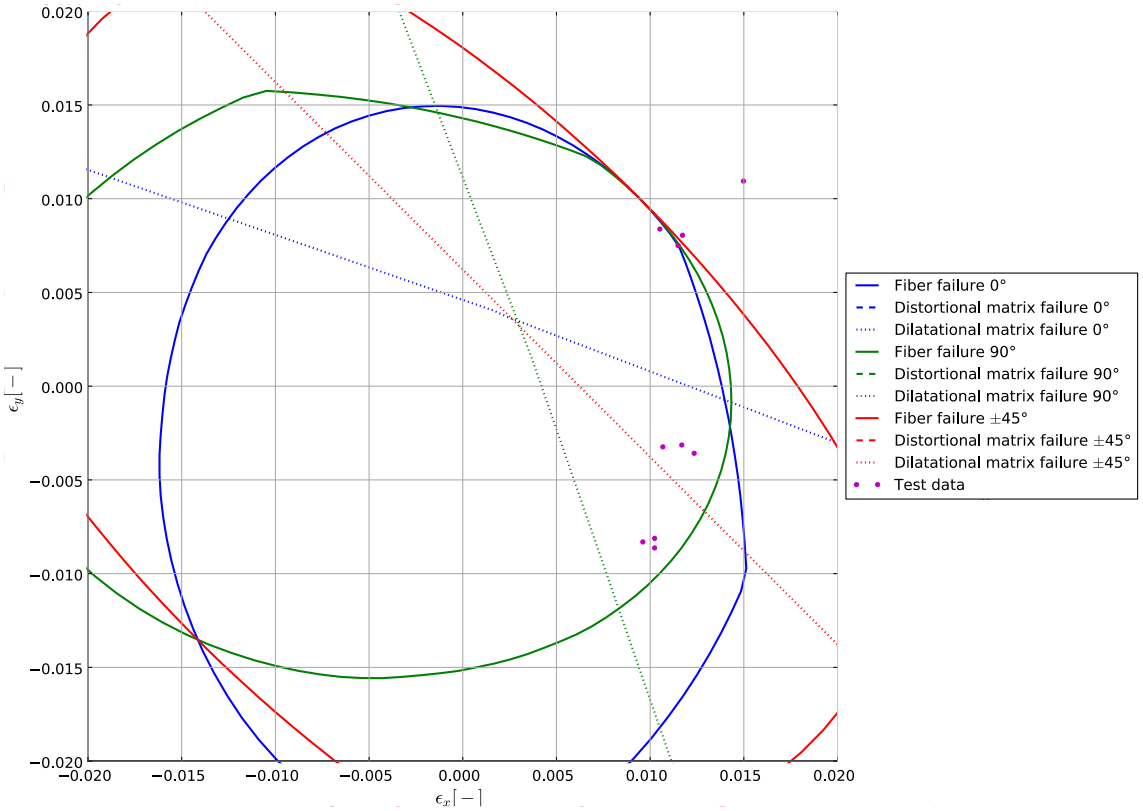


Figure 6.6: Comparison between prediction and biaxial strain test data for a T800s/3900-2 [$0_3$/±45/90]s laminate

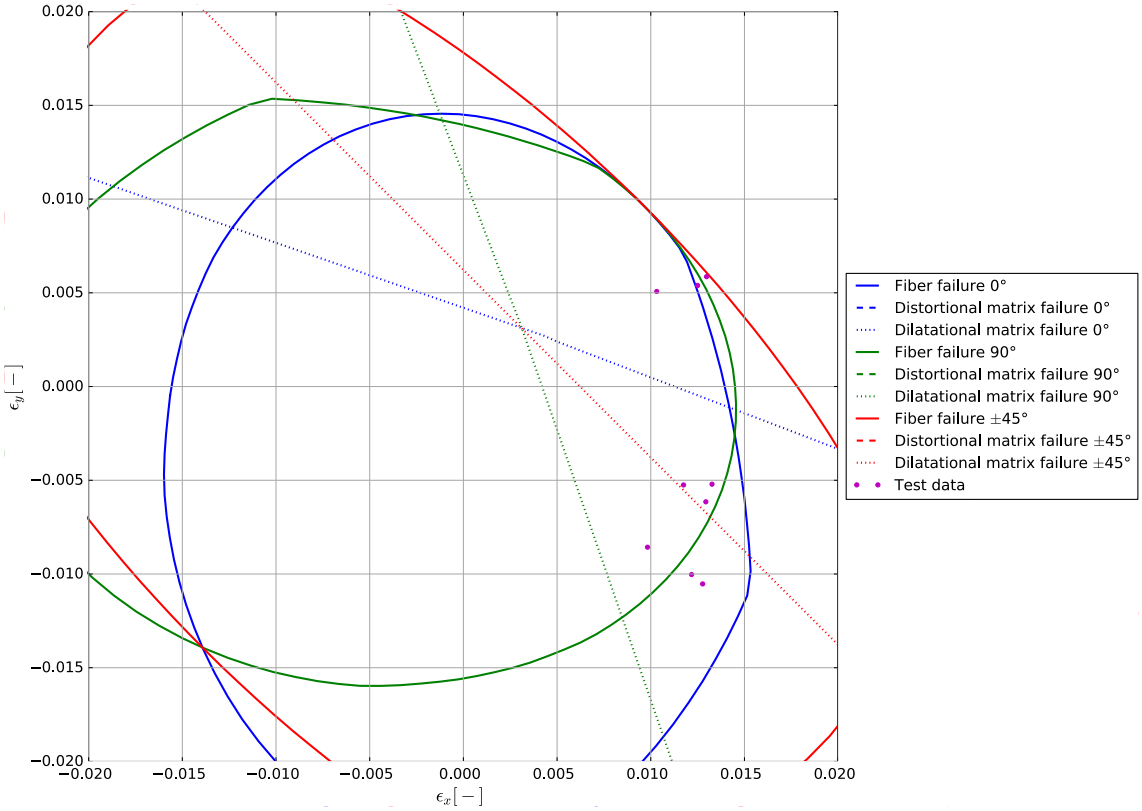


Figure 6.7: Comparison between prediction and biaxial strain test data for a T800s/3900-2 [0/(±45)$_2$/90]s laminate

### 6.3.3 IM7/8551-7 Biaxial Strain Laminate Envelope

For IM7/8551-7, test data is available for a [90/±45/0]s laminate under biaxial strain. Predictions were made using the input data in Section D.3, resulting in the comparison shown in Figure 6.8. The envelope shows similar behavior as the other envelopes, although it resembles an outer bound on the test data (argued above to be a reasonable expectation) more closely than the T800s/3900-2 predictions. It is not as unconservative as the envelope for AS4/3501-6 in some locations, although the measured predominantly uniaxial compressive strain (containing large scatter) does fail to reach the predicted values. Reasons for possible problems with severely compression-dominated loads were already discussed in Subsection 6.3.1.

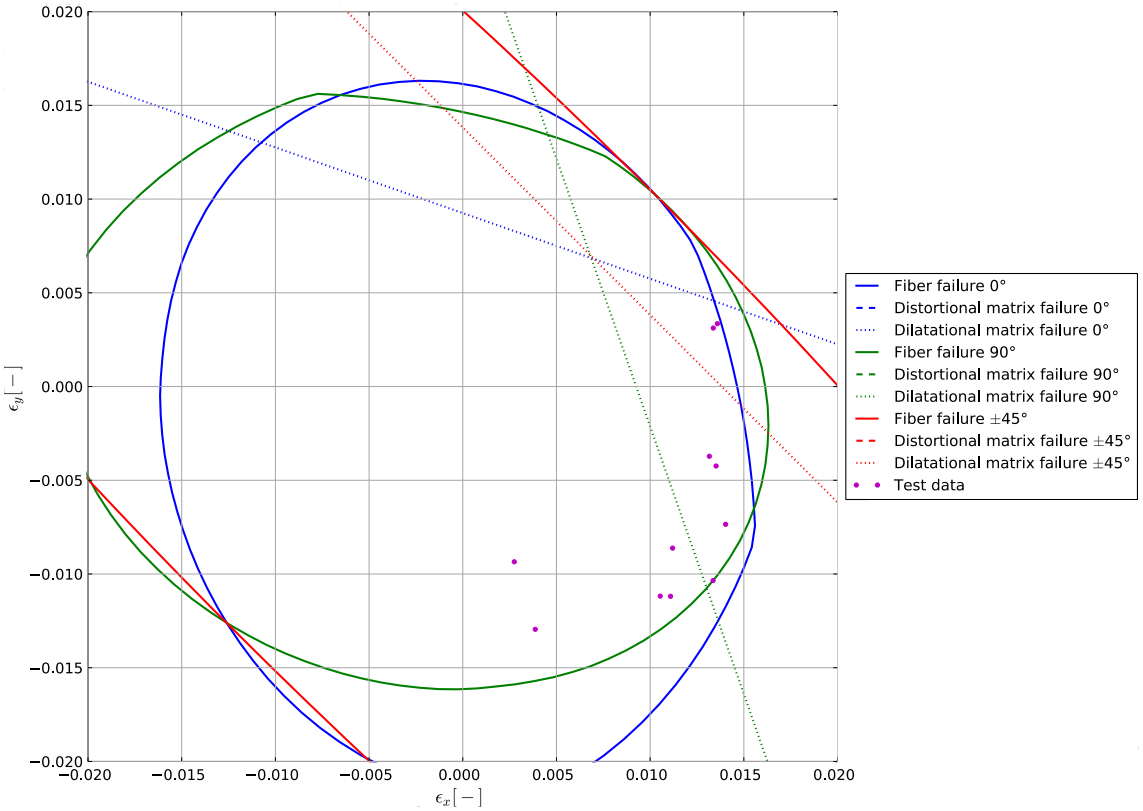


Figure 6.8: Comparison between prediction and biaxial strain test data for an IM7/8551-7 [90/±45/0]s laminate

### 6.3.4 IM7/8551-7 Shear Strain Uniaxial Specimen Envelope

The final validation case consists of a transverse vs shear strain failure envelope for a 90° IM7/8551-7 specimen. Figure 6.9 shows prediction and test data. This case is a noticeable diversion from the previous laminate specimens under biaxial strains. It is quite noticeable that Onset Theory completely fails to predict the test data in any way. With the exception of one data point (which seems to be a premature failure), the predictions of failure are conservative by almost a factor 2 compared to the test data. In addition to that, (Colvin & Swanson, 1990) state the failure modes observed during the test. All specimens failed in the matrix. For the transverse compression load states (it is not specified in the article, but assumed, that this includes the data points at nonzero shear strains, around transverse strains of $\epsilon_y = -3.1\%$ to $-3.2\%$), the fracture plane showed 45° shear failure, indicating distortional matrix failure. The transverse tension and in-plane shear failures (the states of strain where $\epsilon_y = -0.71\%$ and $-0.18\%$ were caused by pure shear stresses) had a perpendicular fracture plane, pointing to $J_1$-failure. Clearly, this is unrelated to the failure modes predicted by Onset Theory, with fiber failure occurring under predominantly transverse tensile or compressive strains (note that the specimen has an orientation of 90°, meaning that these translate into strains in fiber direction) and distortional matrix failure occurring under shear-dominated strains.

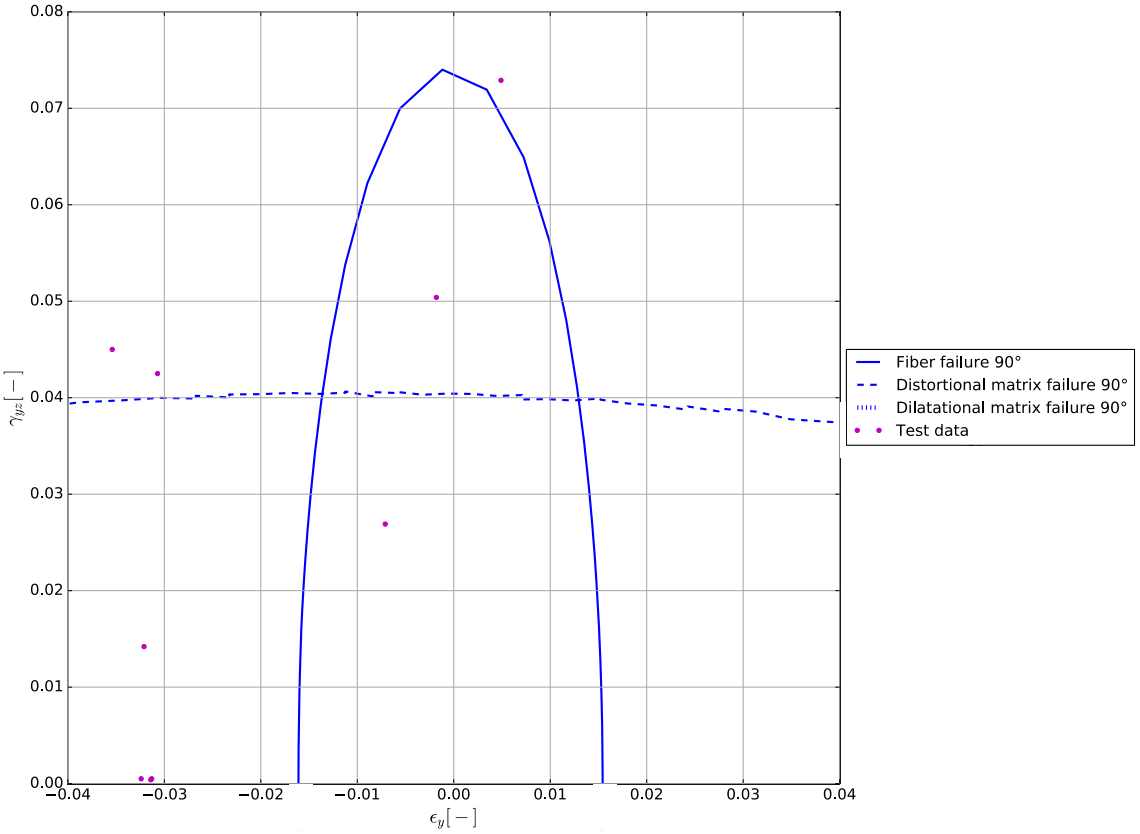


Figure 6.9: Comparison between prediction and transverse vs shear strain test data for an IM7/8551-7 90° specimen. The dilatational cutoff is not shown because matrix cracking under pure longitudinal loads occurs beyond the range shown in this plot.

This being said, there are several points casting some doubt on the test data. First of all, as mentioned above the states of strain where $\epsilon_y = -0.71\%$ and $-0.18\%$ were created by applying pure shear stress ($\sigma_y = 0$). For a 90° ply, there should not be any coupling between normal and shear strains. Some minor coupling strains could be expected (for example, for the pure compression cases with $\tau_{xy} = 0$, there is a shear strain on the order of a few hundreds of percent). However, the significant values seen for pure shear stress point to some problem with the test setup. One possibility could be a misalignment of specimens. Another possibility is related to the relatively large magnitude of applied shear. The specimen used is cylindrical, placed under axial loads in combination with torsion. If the torsion caused some form of torsional buckling (such that the cylinder simply crumbles, although there is no axial stress applied), the compressive strains for pure applied shear could be explained. This would also provide an explanation for the factor 2 difference between prediction and test for other data points at significant amounts of shear. It does, however, not provide any additional insight into why the pure axial compression specimens (where $\tau_{xy}$ and $\gamma_{xy}$ are both –nearly – zero) also exceed the predictions by almost a factor of 2.

In addition to that, (Kaddour & Hinton, 2012, Table 1) give values of the ultimate longitudinal compressive failure strain (note that the ply envelope in Figure 6.9 is for a 90° ply, meaning that $\epsilon_y$ refers to longitudinal strain) of 1.1% and of the shear failure strain of 5%. This is significantly closer

to the predictions than the values measured by (Colvin & Swanson, 1990) of around −3.15% and 7.29%, respectively, although the match would still not be very good.

Tentatively, a 0° envelope was also generated in case there was a reporting error on the ply orientation or strain component. However, this did not improve the agreement. There is some improvement if $\epsilon_y$ and $\gamma_{xy}$ are swapped in the test data, which could theoretically happen due to a reporting error. However, this can hardly be considered a serious argument, and the agreement remains quite bad.

Two final considerations regarding this envelope are that, first, based on load/unload tests (Colvin & Swanson, 1990) did notice damage before ultimate failure. However, it seems unlikely that there was fiber failure which remained undetected. This is therefore not a plausible explanation for the differences. The other point is that (Gosse & Christensen, 2001) mentioned $J_1$-failure under in-plane compression (although for a laminate rather than a ply). While some of the envelopes generated during the development process did indeed show this behavior, it always occurred at strains far beyond the point where failure was predicted based on other failure modes. However, these authors created finite element models of their laminates. It could therefore be that this failure mode was triggered by some aspect not captured in the present analytical process (e.g. free edge effects, or possibly even ply interface failures, which were excluded from the present analysis in Subsection 2.1.6).

In Subsection 6.4.1, additional problems with this set of test data are outlined. Due to this unreliability, it is not possible to draw any conclusions regarding the validity of Onset Theory for this case.

### 6.3.5 Discussion of Results

In the preceding subsections, six sets of data were compared with predictions. AS4/3501-6 included matrix cracking, T800s/3900-2 contained non-quasi-isotropic laminates, and IM7/8551-7 presented an envelope under strains other than biaxial in-plane ones.

Based on the observations made, some conclusions can be drawn. First of all, the agreement between predictions and test data is better for IM7/8551-7 than for AS4/3501-6, and yet again better for T800s/3900-2. This is partly due to less scatter in the data and partly due to the fact that the better matches do not include severely compression-dominated states of strain, which are problematic as discussed in Subsection 6.3.1. For example, for IM7/8551-7 under compression-dominated loads, the spread was less (between −0.00935 and −0.01295, as shown in Figure 6.8, compared to a range of −0.0061 and −0.0094 for AS4/3501-6 in Figure 6.4), and the achieved compression strain was significantly higher (and thus closer to predictions). For T800s/3900-2, the match is even better since strongly compression-dominated states of load are not included in the test data.

All three sets were generated by the same research group, but in different years (1986 for AS4/3501-6, 1990 for IM7/8551-7, 1992 for T800s/3900-2). Clearly, the agreement between predictions (using the same procedure for all three cases) and test data improves in chronological order. It does stand to reason that the test facilities and procedure has improved over the years, meaning that the full potential of the material is now being realized, rather than measuring incorrect premature failures.

Carrying out more tests on all three materials now (i.e. 25 years later) would potentially yield even better results. Of course this argument is only based on indications rather than hard evidence.

In general, part of the reason for the existing discrepancies between prediction and test data (besides errors in the test data or manufacturing flaws) is certainly rooted in the assumptions summarized in Subsection 3.5.1. This includes in particular those pertaining to thin, flat laminates and the use of laminate and ply properties for the Poisson's calculations (rather than properties determined from the unit cells). The curing strain and Poisson's ratio calculations used for the predictions are based on this assumption, whereas the actual specimens were cylindrical.

Summarizing the results of this section, Onset Theory appears to be working well for laminate failure. It more or less correctly predicts ultimate failure for a variety of different materials and laminates, and also predicts matrix failure occurring before ultimate failure.

For uniaxial specimen failure in the transverse strain vs shear plane, there is no correlation between prediction and test. Since there are significant doubts associated with the test data used for comparison, no conclusions can be drawn at the present stage.

## 6.4 Comparison with Other Failure Theories

In order to examine the accuracy of Onset Theory in comparison with other failure theories, other failure criteria should also be applied to the data. Two of the most well-known ones are the Tsai-Wu polynomial and maximum strain failure criteria. Both of them will be used in this section.

### 6.4.1 Shear Strain Uniaxial Specimen Envelope

The main purpose of this subsection is to investigate the validity of Tsai-Wu's failure theory. In Subsection 6.4.2, the agreement between predictions and test results laminates tested under biaxial normal strains is found to be very poor. On the other hand, the same research group (Colvin & Swanson, 1990) which carried out that investigation did conclude that Tsai-Wu is working quite well for the unidirectional 90° specimen under transverse loading and shear used in Subsection 6.3.4 (for which significant doubts were expressed regarding the validity of the test data).

In this case, the stress-based version is used. Therefore, a closer discussion is relevant not only from the point of determining whether Tsai-Wu indeed gives accurate results for the case of a unidirectional specimen, but also to provide additional evidence regarding the conclusion that this dataset is simply not reliable. Figure 6.10 presents the plot given in the article, enhanced with additional information to highlight some of the problems found.

First of all, for compression and shear (which should be decoupled), the plots in stress and strain space should have essentially the same shape, with the exception of different axes. However, the data here shows completely different trends than the data in Figure 6.9.

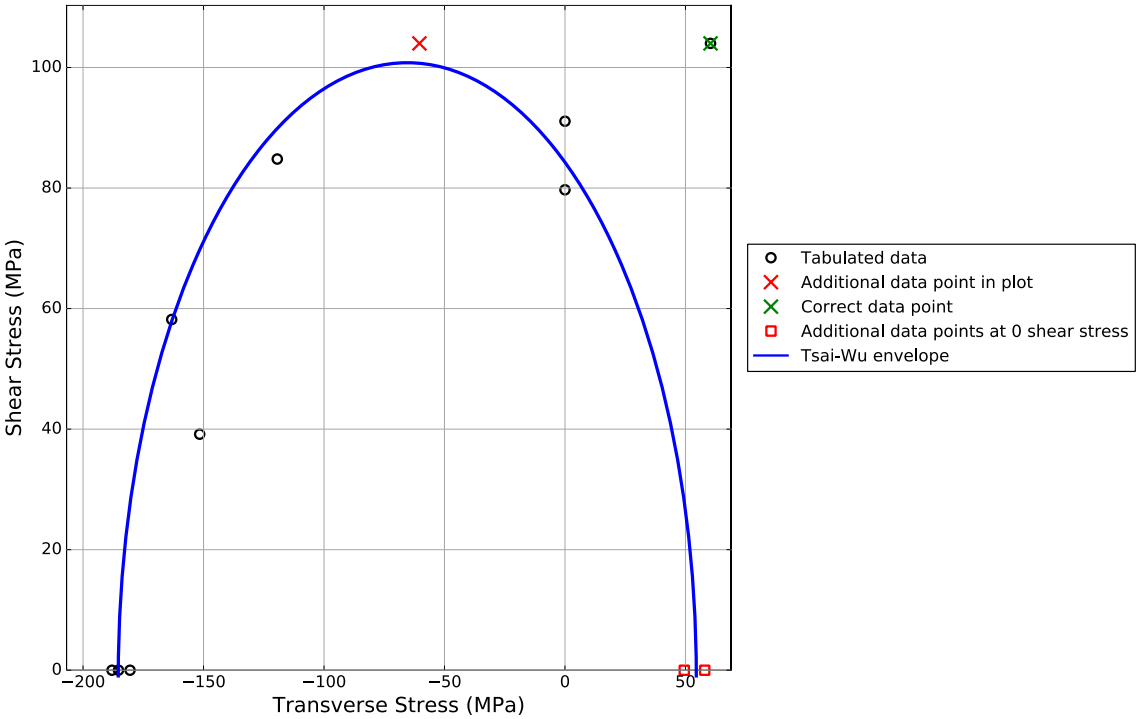


Figure 6.10: Comparison of Tsai-Wu failure envelope with lamina test data. Adapted from (Colvin & Swanson, 1990, fig. 9), also using the data in (Colvin & Swanson, 1990, Table 1)

In addition to that, the data in the plot does not match the data tabulated in the same article. Most importantly, the point at a transverse stress of 60.4 MPa is plotted at a transverse stress of −60.4 MPa. This causes the data point to be very close to the envelope, whereas the other point would be a significant outlier. For this data point, the measured strain is positive. In addition to that, the article mentions a transverse tension measurement, and this is the only point in the table where the stress is positive. Both of these support a plotting error.

Finally, additional data appears to be used at positive transverse stresses and zero shear stress. It is unclear where it stems from, since this data is not included in the tabulated values. There seems to be a disagreement with the data point at 60.4 MPa. Either way, it is clearly used as one of the anchor points for the Tsai-Wu criterion and therefore neither supports nor refutes its accuracy.

Based on the preceding discussion, it is clear that there are indeed significant issues with the stress-based test data, similar to the problems with the strain-based version discussed in Subsection 6.3.4. This means that no conclusions can be drawn regarding the validity of either Onset Theory or Tsai-Wu for unidirectional specimen failure under combinations of transverse and shear loads.

As a side note, the maximum strain criterion would not yield good results for the strain-based data (shown in Figure 6.9). As discussed in Subsection 6.3.4, the failure strains found in other literature differ significantly from the results obtained by (Colvin & Swanson, 1990). In addition to that, a vertical compressive strain limit could successfully match the failures around $\epsilon_y = -3.15\%$. However, any horizontal shear strain limit could pass through at most one of the three data points available close to $\epsilon_y = 0$. Once again this points to the data being suspect.

### 6.4.2 Biaxial Strain Laminate Envelope

For AS4/3501-6, the researchers who generated the test data carried out the comparison of both Tsai-Wu and maximum strain with the test data. Figure 6.11 shows the results they obtained. This plot is based on their original figure (Swanson & Nelson, 1986, fig. 7) and therefore only includes Tsai-Wu and maximum strain. Including Onset Theory would not be possible since their comparison took place in stress space. However, the data in this figure is the stress space version of the data used for the comparison to Onset Theory in Subsection 6.3.1. Note that the figure has been adapted by adding the suspected matrix cracking data from Table D.3.

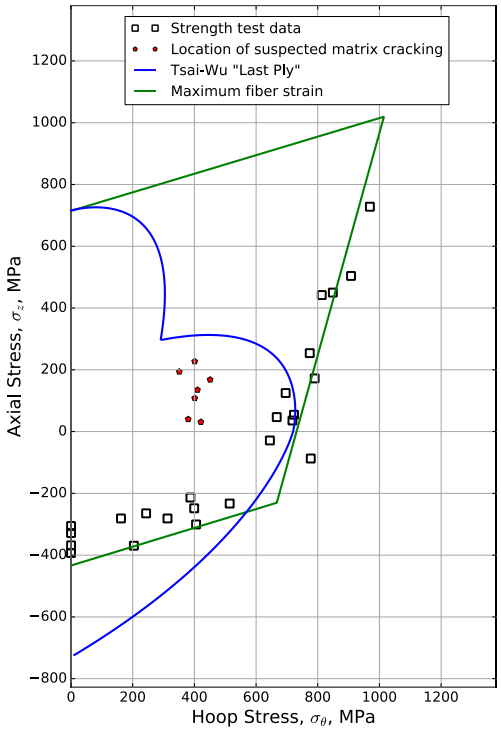


Figure 6.11: Comparison of Tsai-Wu and maximum fiber strain failure criteria with AS4/3501-6 test data. The original figure is (Swanson & Nelson, 1986, fig. 7). It has been modified by adding data points for suspected matrix cracking from Table D.3. Onset Theory is not included because this figure is shown in stress space. However, the dataset is the same as in Figure 6.4 (although there, the strain-based version was used).

Clearly, Tsai-Wu does not give useful results for the laminate envelope under biaxial strains, as the original researchers (Swanson & Nelson, 1986) also concluded. This is also discussed in (Swanson & Christoforou, 1986), reaching the same conclusion after unsuccessfully attempting a progressive failure analysis (see also Subsection 6.3.1) by setting stiffness terms to zero following “first ply failure”.

On the other hand, the maximum fiber strain criterion shows very good agreement with the ultimate failure data. For example (Hart-Smith, 2010) has argued that the maximum strain criterion (whether in its original form or the truncated version proposed by him) in fact very closely approximates the fiber failure envelope generated using Onset Theory.

Note that the agreement between maximum strain criterion and test data is, in fact, better than for Onset Theory. This is the case because the strain cutoffs have simply been selected such as to match the test data. In Subsection 6.3.1, the compression-dominated failures were argued to potentially be

examples of premature failure. This would be taken into account by a maximum strain criterion applied in this manner, but not by Onset Theory. In fact, the critical invariants used in the validation section relied on the "default" invariants found in Subsection 6.2.5, with no relation to the test data or even the material used. The following subsection discusses the reason why fine-tuning the failure cutoff is, in fact, a fatal flaw of the maximum strain criterion.

### 6.4.3 Differences between Uniaxial Lamina and Biaxial Laminate Tests

Based on the results for AS4/3501-6 in the previous subsection, it seems as if a simple maximum strain criterion (when fitted to the test data) is quite successful in predicting composite failure. Similarly, (Swanson & Qian, 1992) and (Colvin & Swanson, 1990) show good agreement between maximum fiber strain criterion and test data for T800s/3900-2 and IM7/8551-7, respectively.

However, in all cases the maximum strain is based on the test data. The authors note that there are significant differences to the ultimate strains obtained from unidirectional coupon tests. For IM7/8551-7, the values were 1.32% for laminates as opposed to 1.6% for coupons (Colvin & Swanson, 1990), while for T800s/3900-2 1.24% were found for laminates and 1.7% for coupons (Swanson & Qian, 1992). They mention this effect, acknowledging that they have no explanation for its presence. On the other hand, for AS4/3501-6, they found in essence the same failure strains for both laminates and coupons, equal to 1.46% (Swanson & Christoforou, 1986, fig. 9).

Note that due to the scatter in laminate test data in Section 6.3, it is inconclusive whether the failure occurs on a straight vertical line (truncated by a straight horizontal line once the compressive limit is exceeded), or on a curved boundary as predicted by Onset Theory (since it takes transverse strains into account). It seems more feasible to have an interaction between longitudinal and transverse strains, since failure of a composite should be related to the underlying failure modes, not to the state of strain that triggers them. In addition to that, Hart-Smith found it necessary to use a truncated maximum strain criterion (see e.g. (Hart-Smith, 2005, fig. 111). This truncation approximates the curved shape predicted by Onset Theory, as pointed out in (Hart-Smith, 2010, fig. 23).

In either case, there is apparently a difference between failure for a longitudinal laminate strain (with no applied transverse strain) and failure for a longitudinal coupon strain. Based on the development of expressions for the full state of strain in Section 3.2, this difference can be explained.

A coupon loaded uniaxially will have an additional transverse strain based on the Poisson's effects. On the other hand, loading a laminate biaxially with a pure longitudinal strain will mean that the transverse strain is forced to be zero. Since Onset Theory takes both strains into account, this results in a different failure prediction than a nonzero transverse strain.

The predicted longitudinal failure strain for the IM7/8551-7 laminate is determined by magnifying Figure 6.8. Similarly, for a uniaxial coupon the failure strain can be found using Figure 6.9 (for a 90° specimen, $\epsilon_y$-strains are in fact longitudinal strains; in addition to that, there is no coupling between normal and shear strains, meaning that for $\gamma_{yz} = 0$, the prediction is indeed identical to the one for a uniaxial coupon test). The results are 1.54% for a uniaxial coupon and 1.46% for a laminate (compared to 1.6% for coupons and 1.32% for laminates found from test data). Although the effect is smaller, the predictions clearly contain a similar trend as the test data.

Similar results are obtained for the other materials. For T800s, the 1.24% for the laminates and 1.7% for a coupon based on test data compare to between 1.38% and 1.39% for the three laminates (the difference is very small) and 1.5% for a coupon based on Onset Theory, found using the same procedure as for IM7/8551-7. Once again, the effect is smaller than in the test (in particular, it falls significantly short of the coupon test data), but a similar trend is seen.

Even more interestingly, for AS4/3501-6 (where (Swanson & Christoforou, 1986) found nearly identical values of 1.46% for laminate and coupon), Onset Theory predicts 1.54% for the laminate and 1.56% for the coupon – slightly higher than the values found in test, but indeed very similar.

This means that the full state of strain in combination with Onset Theory indeed replicates the effect of different strain allowables for laminates and uniaxial coupons, although the magnitude is smaller than found in the test data. There are three causes for this. First of all, (Colvin & Swanson, 1990) included all tests they believed to lie on a straight vertical line in the average laminate failure strain. Based on Onset Theory, this is incorrect (the envelope is predicted to be curved, meaning that failures away from $\epsilon_y = 0$ occur earlier; taking them into account lowers the average strain to failure). Another reason is the fact that measured ply properties are used, which possibly do not represent the true behavior of the composite accurately (in particular in out-of-plane direction) (see also Subsection 3.2.1). Finally, it is quite likely that improved results are obtained if the assumptions made in the derivation of the full state of strain in Section 3.2 (in particular the one of the laminate being a flat plate, whereas the real specimen is cylindrical) are discarded and the true specimen geometry (or a finite element model) is used for both laminates and coupons.

In summary, using different strain allowables for coupons and laminates (and possibly truncating the envelope generated by horizontal and vertical cutoffs) results in a good match between maximum strain criterion and data. However, this means that the strain limits depend on the specific loading condition. Uniaxial loading in place of biaxial loading invalidates the allowable, and other laminates (which differ more significantly from a quasi-isotropic laminate than having two additional 0° plies) may do so as well. This means that new tests have to be carried out for every new type of loading or laminate stacking sequence in order to generate appropriate cutoffs.

On the other hand, the full state of strain from Section 3.2, combined with the fact that Onset Theory is based on the actual physical cause of failure rather than one of many states of load that can cause failure (in other words, that it combines longitudinal and transverse strains to evaluate the distortional cutoff), means that only a single test – the critical invariant – is required to capture all loading conditions and stacking sequences, as claimed already in Section 1.2.

Note that there is an additional factor that has not been addressed yet. In the determination of the full state of strain, curing strains are calculated as well. These are included automatically if the maximum strain cutoff is based on the laminate test data, but are not present for unidirectional coupon tests. However, at least in longitudinal direction the curing strains are quite minor (for example 0.04% for the AS4/3501-6 laminate – see also Subsection 7.4.1). Therefore, even if they were taken into account in the coupon allowable for the maximum strain criterion, they would not cause a difference comparable to the difference between longitudinal lamina and coupon allowables.

# Chapter 7

# Research and Sensitivity Studies

In this chapter, various research and development efforts are carried out. Most of these are based on trends observed in Onset Theory, which (assuming Onset Theory is correct) are related to trends in composite failure in general. In addition to that, the literature contains very little information on the robustness of Onset Theory. A failure theory which is capable of generating extremely accurate predictions if the exact input data is used, but diverges completely if the input data is varied slightly, would not be very useful. This is due to both the uncertainty involved in measuring physical properties, and also due to the natural spread of the actual properties.

Section 7.1 examines the influence of the ply orientations on the resulting failure envelopes, both in strain space and also in stress space. The purpose of this investigation is to determine whether better designs are possible based on ply angles other than the 0°, ±45° and 90° plies commonly chosen, as well as investigating to what extent ply angle manufacturing inaccuracies will influence results.

In Section 7.2, the sensitivity of Onset Theory to the constituent material properties is addressed.

A real life composite does not only contain a single volume fraction, but rather a smaller or larger range, depending on the quality and consistency of the manufacturing process. The effects of this are analyzed in Section 7.3. In addition to that, (Hart-Smith, 2010) states that Onset Theory is strongly sensitive to the volume fraction, while (R. Li et al., 2003) found essentially the same strain amplification factors for volume fractions of 0.5 and 0.55. Therefore, these claims are also examined.

Section 7.4 discusses sensitivities of the failure predictions with respect to effects related to temperature. This includes the curing strains (due to a thermal expansion factor mismatch between different plies in a laminate) as well as the thermal amplification factor vector (due to a mismatch between fiber and matrix).

Finally, Section 7.5 provides an outlook into the topic of multi-cell (random fiber array) models. While these are not a core topic for this thesis, some investigation has still been carried out.

## 7.1 Effect of Ply Orientations

The purpose of this section is to show some trends in the failure envelopes related to ply orientation (in other words, to carry out a sensitivity study on ply angle). This is related to the concept of an "omni-ply" envelope, meaning an envelope valid for all laminates regardless of the exact stacking sequence or plies contained. In addition to that, it is determined whether there is room for improvement by using ply orientations other than 0°, ±45°, and 90°. This investigation also inherently addresses the topic of the sensitivity of predictions with respect to ply orientation.

### 7.1.1 Omni-Ply Envelope in Strain Space

Figure 7.1 shows the strain space envelopes for ply orientations ranging from 0° to 90°. Showing one half of the envelopes is sufficient since the effects are essentially mirrored over a line at a 45° angle passing through the origin. On the other side of this line, 0° and 90° switch place, as do 15° and 75°. The remaining couple is 30° and 60°; the 45° envelope is exactly symmetric. Note that beyond 90° the envelopes start repeating (e.g. 105° is equal to 75°, and so on).

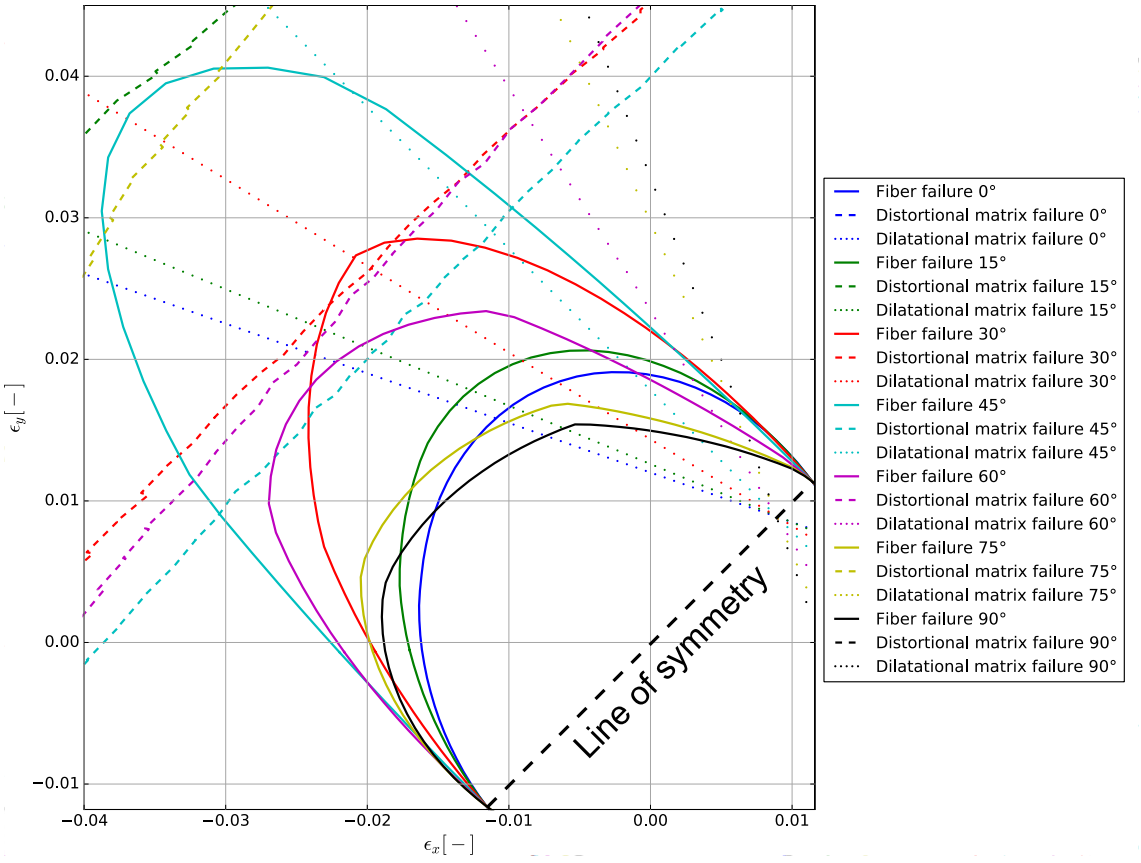


Figure 7.1: Strain space envelopes for ply orientations between 0° and 90°. Material properties as in Section D.3. No curing strains included (envelopes are for individual plies).

Based on this, several conclusions can be drawn. First of all, in strain space, fiber and dilatational matrix failure in 0° and 90° plies define the entire envelope (in other words, an omni-ply envelope can be generated based on just these two ply orientations).

It should be mentioned that curing strains are not included in these envelopes. This is due to the fact that the purpose of an omni-ply envelope is to be independent of the stacking sequence (which determines the curing strains). The curing strains only shift the failure envelope (see Subsection 3.2.4), and can be added later on. They are simply another applied global strain.

For the maximum envelope in strain space, there is no unique solution. 30°, 45° and 60° plies give maximum envelopes, depending on the state of strain. A closer investigation containing additional ply angles in this range revealed that there is no global optimum. The trend is that distortional matrix failure becomes more critical, while the fiber envelope expands. The rate of expansion is larger, meaning that the benefits associated with the larger fiber envelope probably outweigh the less significant decrease in matrix envelope.

The sensitivity of in particular the fiber envelope in strain space to varying ply orientations strongly depends on the reference angle. Deviating from a 0° or 90° ply by 15° does not cause large changes. On the other hand, deviating from the 45° ply will cause very large changes. This means that during manufacturing it is important to align plies properly with the desired directions.

### 7.1.2 Omni-Ply Envelope in Stress Space

So far, the investigation was limited to strain space. This does not provide any information about ply strength. Using this omni-ply envelope it would be possible to select a laminate based on desired stiffness properties, and to then check the resulting strains for applied loads to ensure the design does not fail. However, the same investigation should also be carried out in terms of stresses.

For this purpose, the failure envelope is converted to stress space, using the in-plane stiffness matrix derived in Eqn. (3.11). The reservations regarding this conversion (formulated in Subsection 2.2.1) related to the uncertainty in material properties still apply. However, in this context different ply orientations are compared, all using the same material properties. Even if there is some inaccuracy which would make a comparison to test data difficult, the relative results should still be valid.

Figure 7.2 shows the resulting envelopes. As for the strain-based envelopes in Figure 7.1, curing strains are excluded. Once again there is a certain correspondence between 0° and 90° envelopes (and similarly for the other pairs mentioned above). However, in this case the stiffness matrix causes the additional effect of vastly different scales in longitudinal and transverse directions. This means that for a 0° ply $\sigma_x$ should have a much larger scale than $\sigma_y$ (factor 10 in Figure 7.2), with the opposite effect for a 90° ply. A plot including both plies would therefore essentially show a horizontal and vertical line. Therefore, the stress-based envelopes are limited to the range of 0° to 45°. Even with this limitation the larger part of the envelopes for 30° and 45° has to be truncated.

A minor conclusion that can be drawn based on these envelopes is that distortional matrix failure is clearly relevant for the 45° ply, unlike for the other envelopes. What is more relevant is that the result of the rotation is to have much less load bearing capability in $\sigma_x$-direction, but increasing capability in $\sigma_y$-direction. There is no ply that has more capability in (laminate) $\sigma_x$-direction than a 0° ply, so it is not possible to obtain a better design for loads in that direction by removing the 0° ply. This corresponds to the standard wisdom of aligning ply orientations with the applied loads.

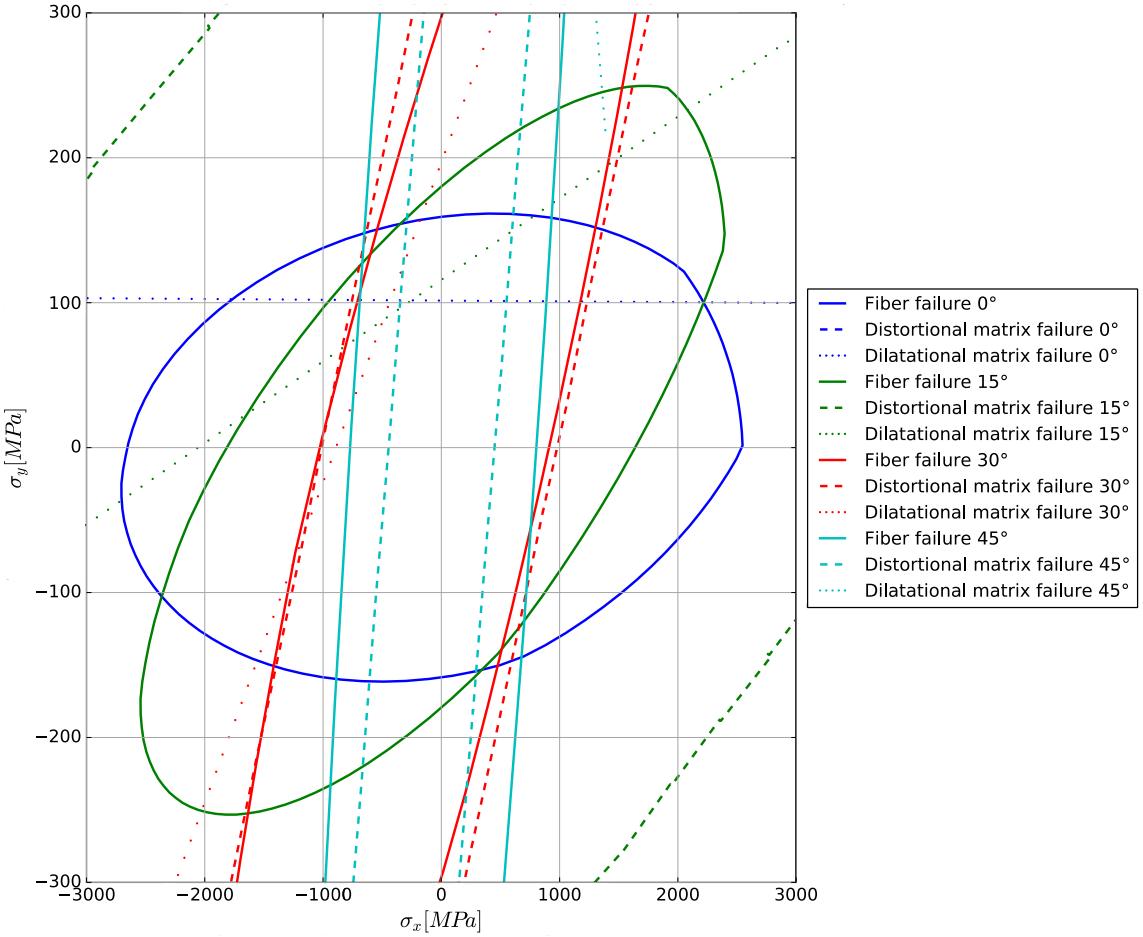


Figure 7.2: Stress space envelopes for ply orientations between 0° and 45°. Material properties as in Section D.3. No curing strains included (envelopes are for individual plies).

### 7.1.3 Optimum Quasi-Isotropic Laminate

In many structural applications, quasi-isotropic laminates are used. The reason is it that for known load paths, the fibers should be exactly aligned with the applied loads. However, for typical applications the exact states of load are not known or too numerous to take into account individually. Therefore, laminates are used which have the same properties regardless of direction. There are two "simple" quasi-isotropic laminates: $[0/90/\pm45]$s (or any shuffled version thereof; since in this thesis, only in-plane effects are considered, this is identical to for example the more common $[\pm45/0/90]$s) and $[0/60/-60]$s. Both of these are quasi-isotropic in terms of stiffness, but their strength behavior is different.

Figure 7.3 shows the envelope for a $[0/90/\pm45]$s laminate (in stress space, though the results in strain space are identical since the stiffness matrices of the two laminates are the same), while Figure 7.4 presents the $[0/60/-60]$s laminate. This is a comparison of actual laminates, so curing strains are included. The exact number of plies or their order is irrelevant, as discussed in Subsection 3.2.2.

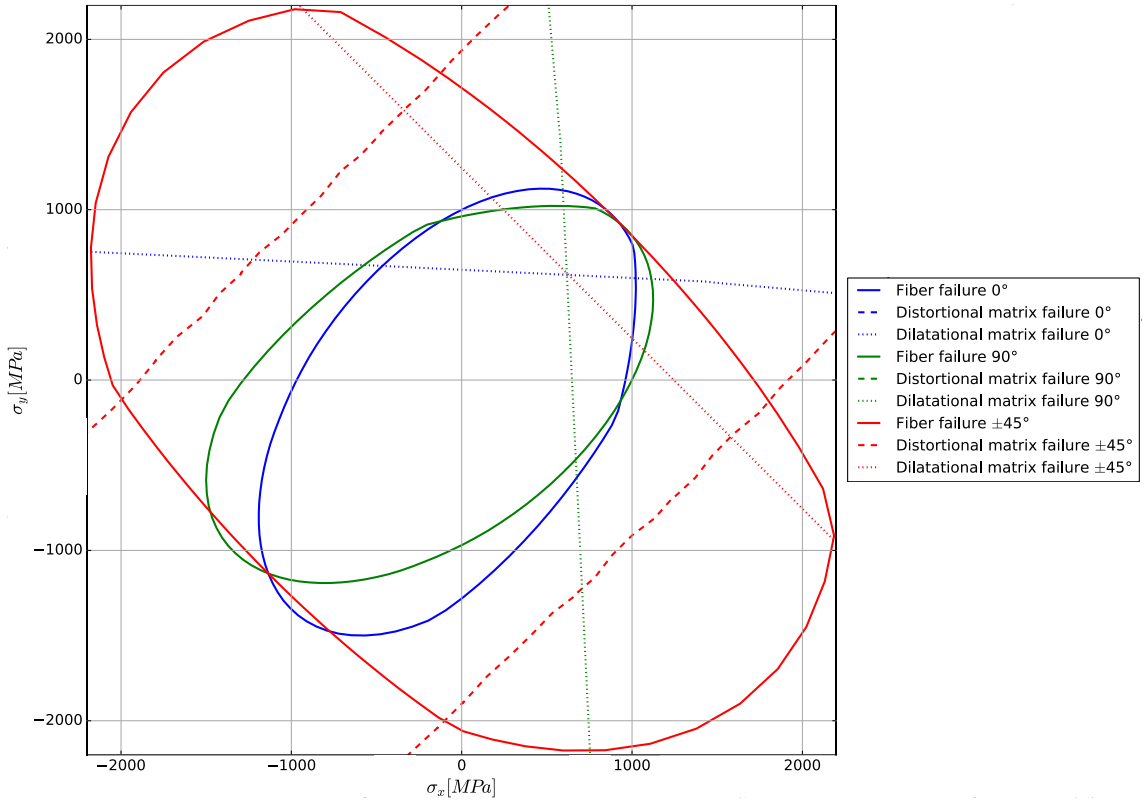


Figure 7.3: Stress-based failure envelope for a [0/90/$\pm$45]s laminate. Material properties as in Section D.3.

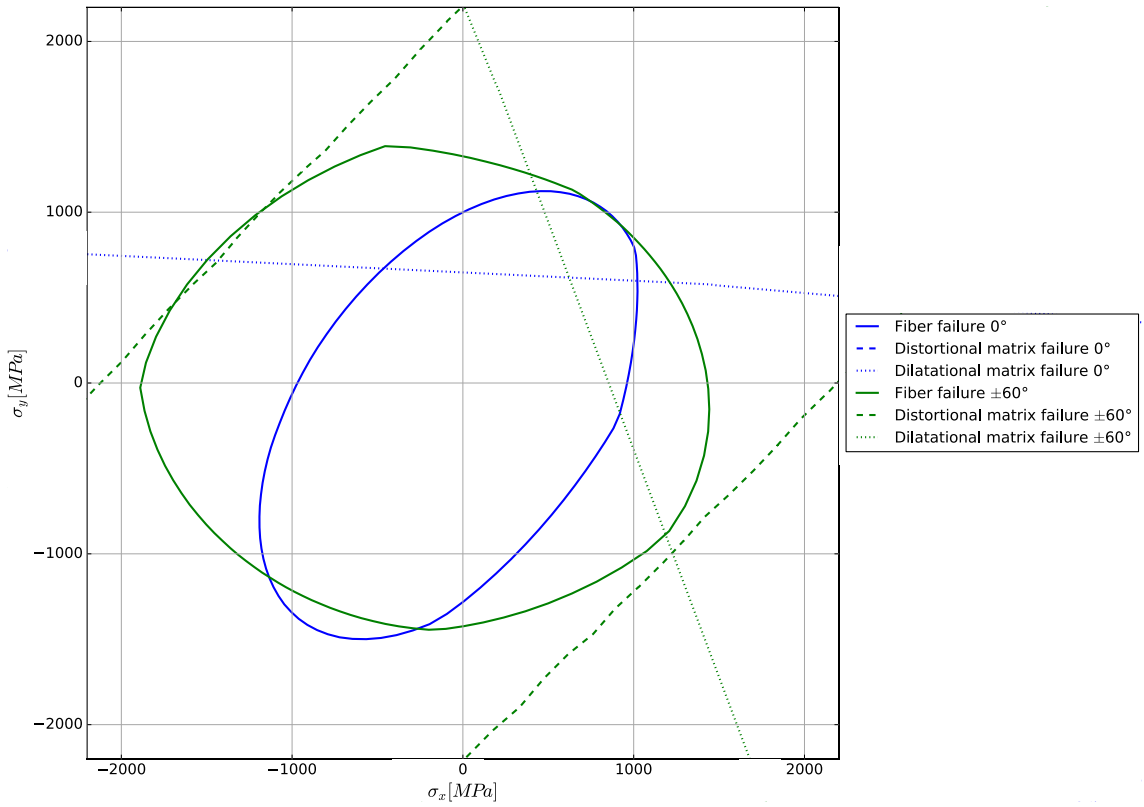


Figure 7.4: Stress-based failure envelope for a [0/60/$-60$]s laminate. Material properties as in Section D.3.

It should be mentioned that it appears as if removing e.g. the 0° ply would increase the envelope. However, this would invalidate the other envelopes since the laminate stiffness would change.

The [0/90/±45]s laminate is symmetric, whereas the [0/60/−60]s one is missing the "counter-ply" for the 0° ply. As shown in the envelopes, the result is that the [0/60/−60]s laminate offers more stress capability for compressive $\sigma_y$ over almost the entire range of $\sigma_x$.

In terms of actual load bearing capability, the stress in the three-ply laminate would be higher than the one in the four-ply laminate given the reduced thickness. However, the load bearing capability per unit weight would be the same because the [0/60/−60]s is also lighter.

Based on this, the design can be optimized further. There are many other quasi-isotropic laminates. However, all of them will involve more different ply angles. The benefit of the [0/60/−60]s laminate over the [0/±45/90]s laminate is achieved by removing the necessity of having a 90° ply. In general, the fewer plies there are the fewer strain limits have to be complied with. Evidently, this means any more complicated formulation of a quasi-isotropic laminate will not perform as well as one consisting of only 0°, 60° and −60° plies.

Another way of looking at this is that failure envelope of the [0/60/−60]s laminate is almost entirely defined by the 0° ply. The region truncated by the envelopes of other plies is very small (whereas it is significantly larger for the [0/±45/90]s laminate).

One other option would be rotating the [0/60/−60]s laminate. Since strain and stress based envelopes are identical for quasi-isotropic laminates, Figure 7.1 can be used for this purpose. For example, a [−15/45/−75]s laminate (or the same laminate with the signs reversed, or any shuffled version – note that positive and negative angles result in the same envelope) would result in some benefits in longitudinal compression. This is due to the fact that the combined envelope of 15° and 75° plies is less restrictive in that region than the 0° envelope. On the other hand, in transverse tension, the 75° envelope is more restrictive than the 0° envelope. Therefore, there would not be a significant net gain in the size of the failure envelope. Its shape would change, with its overall size remaining essentially the same.

In summary, this means that a [0/60/−60]s (or a rotated version thereof) would theoretically be the optimum design for unknown normal loads on a laminate. However, this is a rather theoretical solution since there are other factors which are in favor of the [0/±45/90]s laminate. To name just two of them, shear cases are beneficial because of the ±45° plies aligned with the shear directions; similarly, these plies also provide better buckling stability. Depending on the relative importance of these different types of loads, one type of quasi-isotropic laminate should be chosen over the other.

## 7.2 Effect of Constituent Properties

A topic of concern for Onset Theory is the use of constituent material properties. Many properties (in particular those of the fiber) cannot be measured directly. According to for example (Soden et al., 1998), this means that tests are carried out on the composite material, followed by the use of micromechanics to determine the fiber properties.

Clearly, this means that the fiber properties cannot be considered to be reliable. Similarly, the matrix properties will also differ depending on the source used due to measurement inaccuracies, test errors, and simple variations in material properties. It is therefore important to investigate how sensitive failure predictions are with respect to the constituent material properties.

A straightforward approach of doing so would be to run various analyses, using a range of values commonly found in literature. However, doing so for every single input parameter would scale too quickly to be feasible. If only three values were used for every parameter in the micromechanical analysis, the twelve fiber material properties, three matrix material properties, and the fiber volume fraction (see e.g. Subsection 3.5.4 for a list of input data) would mean $3^{12+3+1} \approx 43$ million analyses. This does not include any investigation of the lamina properties used in generating failure envelopes.

For this reason, a different approach is chosen. Comparing the materials used in Section 6.3, it is clear that for several parameters a significant range is covered, as shown in Table 7.1. Although some of the other ranges are relatively small, these are properties for different materials. It seems unlikely that values for a single material would vary more than values for different materials. Note that there is no variation on the fiber Poisson's ratios $\nu_{12}$ (and the identical $\nu_{13}$). However, for all fibers used in all rounds of the WWFE (e.g. IM7, T300, AS, S2-glass, E-glass (Kaddour & Hinton, 2012)) the reported value was 0.2. This also held true for most other sources in literature.

Table 7.1: Ranges of parameters for AS4/3501-6, IM7/8551-7, and T800s/3900-2 (see Appendix D)

| Property | Matrix material | Fiber material |
|---|---|---|
| $E_1$ [Pa] | 3.3e9 … 4.2e9 | 225e9 … 303e9 |
| $E_2$ [Pa] | | 15e9 … 19e9 |
| $E_3$ [Pa] | | 15e9 … 19e9 |
| $G_{12}$ [Pa] | 1.22e9 … 1.567e9 | 9.65e9 … 27e9 |
| $G_{13}$ [Pa] | | 9.65e9 … 27e9 |
| $G_{23}$ [Pa] | | 6.32e9 … 7e9 |
| $\nu_{12}$ [−] | 0.34 … 0.38 | 0.2 |
| $\nu_{13}$ [−] | | 0.2 |
| $\nu_{23}$ [−] | | 0.071 … 0.357 |
| $\alpha_1$ [$°C^{-1}$] | 45e-6 … 57.6e-6 | 0 … −0.4e-6 |
| $\alpha_2$ [$°C^{-1}$] | | 5.6e-6 … 15e-6 |
| $\alpha_3$ [$°C^{-1}$] | | 5.6e-6 … 15e-6 |

Comparing the envelopes for these three materials will then allow some conclusions to be drawn regarding the sensitivity of Onset Theory to the individual parameters. Note that the sensitivity of predictions with respect to the volume fraction has intentionally been excluded here, since it is covered in Section 7.3.

Figure 7.5 shows the biaxial strain envelopes for plies of all three materials, while the transverse vs shear strain envelopes are contained in Figure 7.6. Note that, as mentioned in the figure caption, all envelopes use the critical invariants from Subsection 6.2.5, meaning that any differences in envelopes are due to the micromechanical enhancement factors.

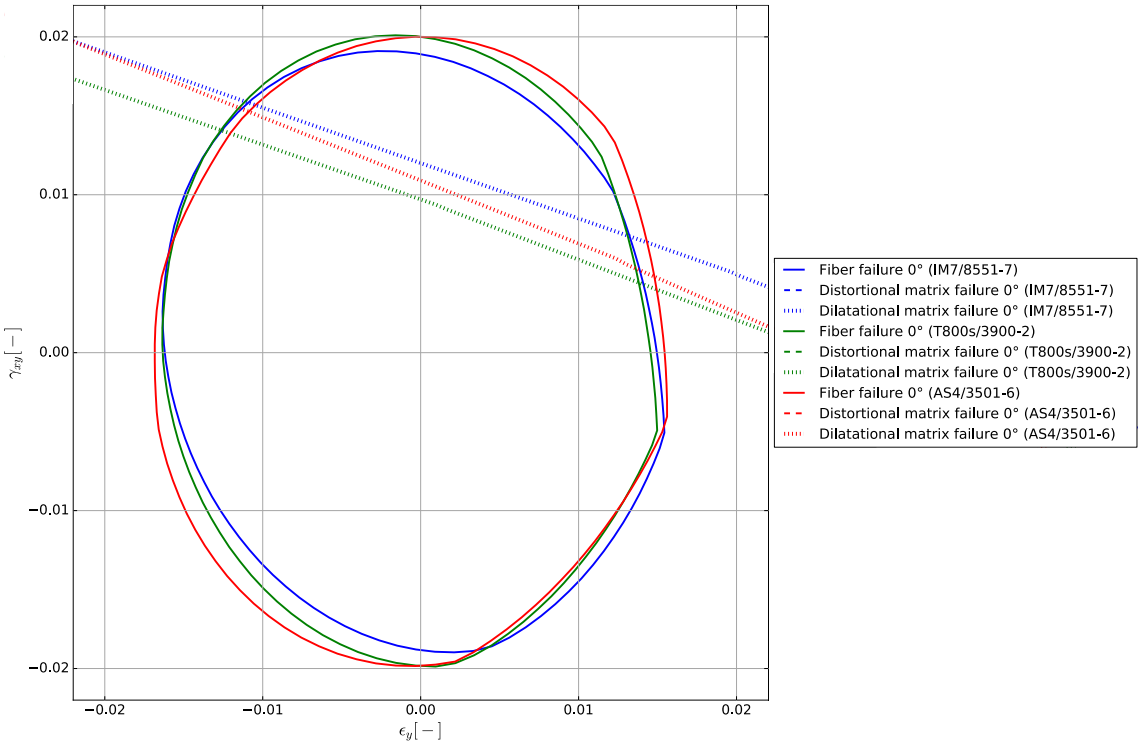


Figure 7.5: Comparison of biaxial strain ply failure envelopes for IM7/8551-7, T800s/3900-2, and AS4/3501-6. See Appendix D for input data, with the exception of $\Delta T$ for AS4/3501-6 (given as $-155°C$, but using $-157°C$ for all three materials). Invariants identical to default values from Subsection 6.2.5.

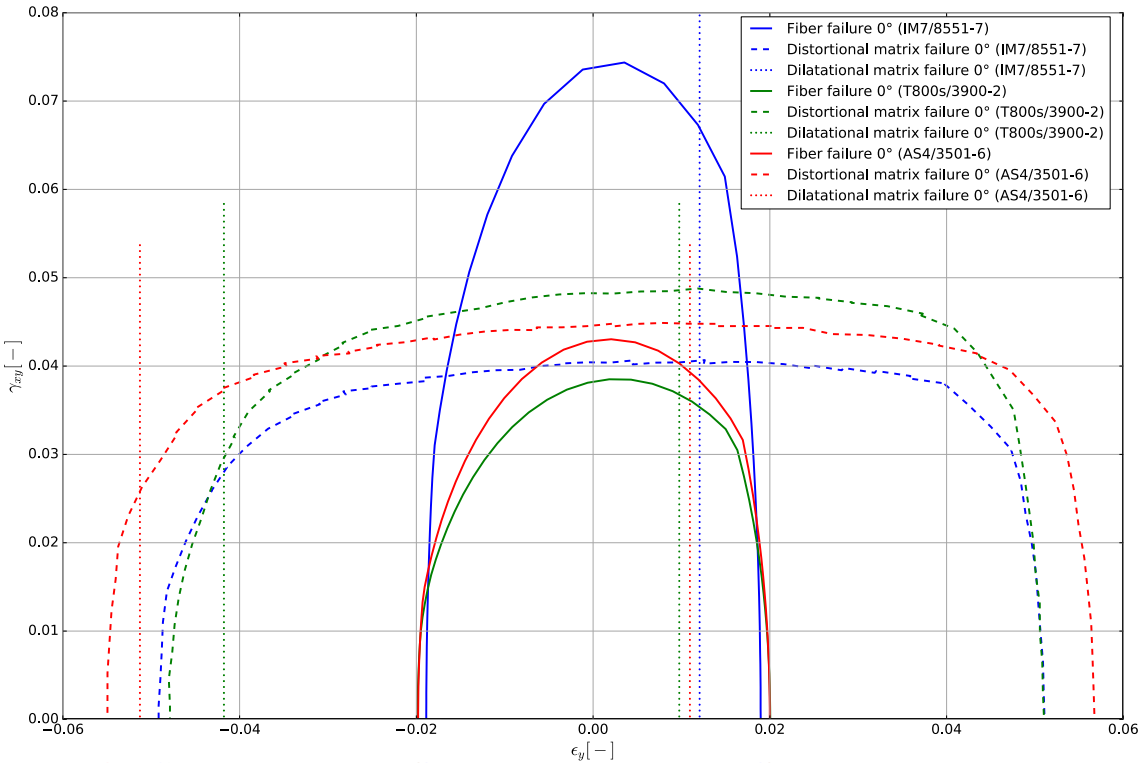


Figure 7.6: Comparison of transverse vs shear strain ply failure envelopes for IM7/8551-7, T800s/3900-2, and AS4/3501-6. Material properties and other information as in Figure 7.5.

Comparing envelopes, several rather interesting conclusions can be drawn. First of all, the biaxial strain envelopes for all three materials are very similar. The largest difference occurs in the location of the matrix cutoff, which varies between $\epsilon_x = 0.0097$ for T800s and $\epsilon_x = 0.012$ for IM7 (both for $\epsilon_y = 0$). This is a change of approximately 20%, quite comparable to the difference of transverse fiber stiffnesses (15GPa to 19GPa) and matrix stiffnesses (3.3GPa to 4.08GPa).

On the other hand, the fiber envelope for biaxial strains is not affected much. In particular, the $x$-intercepts (i.e. where there is no applied transverse strain) in strain space are very similar. This will always be the case if the same critical invariant is used, since the dominating amplification factor in longitudinal direction is 1 (see Subsection 2.1.5).

For loadings including shear, the sensitivity is much larger, in particular for the fiber failure envelope. This is most likely related to the much larger shear stiffness of the IM7 fiber (almost twice as much as for the other two fibers). A larger fiber stiffness means that for a given ply strain, the matrix will take up a larger part. Therefore, the distortional matrix envelope becomes more critical, while the fiber envelope expands. For dilatational matrix failure, the shear stiffness of the fiber does not seem to play a significant role.

In summary, this means that (with the exception of the fiber failure envelope under shear strains), the failure envelopes and cutoffs for three different carbon-epoxy composites are quite similar. Most importantly, the longitudinal stiffness of the fiber – typically one of the most distinguishing factors – does not play a significant role in longitudinal direction.

Although this does not replace a proper sensitivity study where individual parameters are varied to investigate their true influence, it seems unlikely that the sensitivity to different versions of the material properties for the same material would be excessively large.

Note that the magnitude of differences considered small in this section is similar to the magnitude considered significant in Subsection 6.4.3. There, predicted failure strains of e.g. 1.54% for coupons and 1.46% for laminates (for IM7/8551-7) were used to highlight a crucial difference between Onset Theory and the maximum strain failure criterion, namely that Onset Theory correctly captures the trend of varying failure strains. The purpose of the present section is not to discuss this type of effect, but to investigate whether Onset Theory behaves erratically if the input data is varied. This is not the case since there are no massive changes in results despite for example the fiber stiffness changing from 225GPa to 303GPa (a 35% increase). In other words, Onset Theory appears to be sufficiently robust with respect to varying constituent properties.

It should also be mentioned that only individual ply envelopes in strain space are similar. The conversion to stress space will result in vastly different envelopes since the stiffness matrices are very different. Similarly, laminate envelopes can be quite different because the curing strains and Poisson's effects are not the same for different materials.

## 7.3 Effect of Fiber Volume Fraction

Another topic of interest is the effect of the fiber volume fraction. Typical volume fractions are around 60%, but vary due to manufacturing inaccuracies. In the present section, two topics will be

investigated. First of all, an attempt is made to determine the optimum volume fraction a composite should have in order to achieve the highest possible strength (Subsections 7.3.1 and 7.3.2). Secondly, various references in literature such as (Hart-Smith, 2010, p. 4306) state that Onset Theory is quite sensitive to the fiber volume fraction, and, in particular, much more so than to the fiber array type (see also Subsection 2.2.6). This claim is examined in Subsection 7.3.3.

### 7.3.1 Approximate Relations for Lamina Properties

In order to examine the effects of the fiber volume fraction, it will be necessary to use stress-based envelopes, as also done in Subsection 7.1.2. The reason for this is that a "ply" made of pure matrix would have much larger strains to failure than a ply containing fibers (which is indeed the case, as verified during the development process). However, this of course does not mean that the pure matrix "ply" would be beneficial in terms of load bearing capability.

Lamina properties, which depend on the volume fraction, are needed for both the Poisson's effects (already present in strain space) and also for the stiffness matrix used to convert the envelope to stress space. Determining the lamina properties is a research topic of itself. In this thesis, measured ply properties are used (see Subsection 3.2.1). However, for a change in volume fraction these will not be accurate anymore. Therefore, a simple rule of mixture approach (summarized in Table 7.2) is used to determine lamina properties from the constituent material data. It can be found in most standard textbooks on composite materials.

Table 7.2: Summary of equations for lamina properties (Mallick, 2007, Eqns. 3.33-3.40 and 3.58-3.59)

| | | |
|---|---|---|
| $E_1 = V_f E_1^f + (1-V_f)E_1^m$ | $E_2 = \dfrac{E_2^f E_2^m}{E_2^f(1-V_f) + E_2^m V_f}$ | $E_3 = E_2$ |
| $\nu_{12} = \nu_{12}^f V_f + \nu_{12}^m (1-V_f)$ | $\nu_{13} = \nu_{12}$ | $\nu_{23} = \nu_{12}\dfrac{1-\frac{E_2}{E_1}\nu_{12}}{1-\nu_{12}}$ |
| $G_{12} = \dfrac{G_{12}^f G_{12}^m}{G_{12}^f(1-V_f) + G_{12}^m V_f}$ | $G_{13} = G_{12}$ | $G_{23} = \dfrac{E_2}{2(1+\nu_{23})}$ |
| $\alpha_1 = \dfrac{\alpha_1^f E_1^f V_f + \alpha_1^m E_1^m (1-V_f)}{E_1^f V_f + E_1^m (1-V_f)}$ | $\alpha_2 = \left(1+\nu_{12}^f\right)\dfrac{\alpha_1^f + \alpha_2^f}{2} V_f + (1-\nu_{12}^m)\alpha_1^m (1-V_f) - \alpha_1 \nu_{12}$ | |

It should be mentioned that this approach is quite inaccurate, as easily verified using any of the sets of input data found in for example Appendix D. More advanced formulations such as the Halpin-Tsai equations might yield better results. However, as for the stiffness matrix used in the conversion to stress space, inaccuracies are accepted since the purpose is not to obtain good results in comparison to test data, but to investigate relative trends. Assuming that the simple equations outlined above capture the trends in stiffness with sufficient accuracy, qualitative conclusions regarding the optimum volume fraction can still be drawn, although the exact value can at most be an indication.

One additional aspect related to this is the density of the composite. It is given by e.g. (Mallick, 2007, Eqn. 2.7) as $\rho = V_f \rho^f + (1-V_f)\rho^m$. Since the weight of the composite will also change with

the fiber volume fraction, the desired optimum volume fraction is the one that yields the highest strength to weight ratio.

### 7.3.2 Optimum Volume Fraction

The constituent properties used for this investigation are the ones for IM7/8551-7 found in Section D.3, while the lamina properties are determined using the equations presented in the previous subsection. In addition to that, the densities are $1.78\frac{g}{cm^3}$ for IM7[1] and $1.272\frac{g}{cm^3}$ for 8551-7[2].

For a volume fraction of 0.573 (the value in Section D.3), the theoretical density is $\rho_{reference} = 1.563\frac{g}{cm^3}$. In order to take into account the weight of the composite, all stresses will be divided by $\rho_{ratio} = \frac{\rho_{actual}}{\rho_{reference}}$, meaning that a larger weight will result in a penalty on the envelope. For a volume fraction of 0.573, the scaling factor is 1.

Figure 7.7 shows the failure envelopes for volume fractions of 0.4, 0.5, 0.573, 0.65, and 0.75.

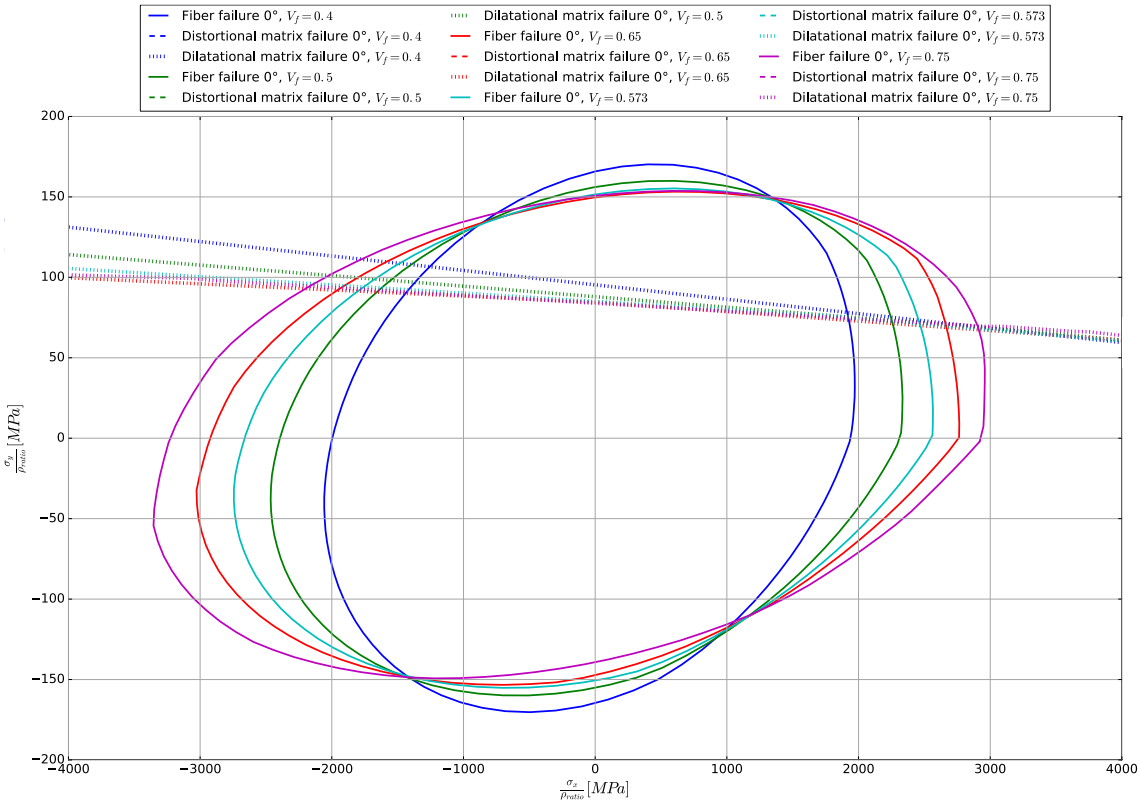


Figure 7.7: Comparison of failure envelopes (in stress space) for various volume fractions

The trends seen are essentially as expected. A larger volume fraction increases the longitudinal strength. At the same time, the transverse strength decreases, presumably because more and more of the strain is actually taken up by the fiber rather than the matrix.

[1] http://www.hexcel.com/resources/datasheets/carbon-fiber-data-sheets/im7.pdf

[2] http://www.hexcel.com/Resources/DataSheets/Prepreg-Data-Sheets/85517_us.pdf

In strain space, the opposite behavior would occur (as discussed in Subsection 7.3.1). For increasing volume fractions, the failure envelope reduces more and more. Section 7.2 already addressed the fact that the $x$-intercept in strain space remains more or less the same regardless of the amplification factors (provided the critical invariant is the same). Therefore, the difference between these points in the stress-based envelope is due to the increase in longitudinal stiffness with volume fraction.

Another comment that should be made regards the influence of the density. For the given volume fractions, the minimum and maximum densities are $1.4752\frac{g}{cm^3}$ and $1.653\frac{g}{cm^3}$, respectively. Compared to the reference density of $1.563\,\frac{g}{cm^3}$, this constitutes an increase or decrease of slightly less than 6%. In longitudinal direction, this results in some slight scaling of the envelopes, but does not change the trends seen in Figure 7.7. On the other hand, in transverse direction the envelopes are sufficiently close to change their order. Without the weight penalty, $V_f = 0.75$ also performs best in transverse tension, and in transverse compression there is very little difference between envelopes.

Dilatational matrix failure becomes worse with increasing volume fraction. However, somewhat surprisingly this effect appears to be arrested beyond a volume fraction of 0.5. Presumably, this is due to the increase in ply stiffness, which offsets the increased strain concentrations in the matrix.

Although this is not shown in the plot because it is far outside the axes ranges, distortional matrix failure is becoming much more critical for higher volume fractions. However, a volume fraction of 0.75 is already close to the maximum one possible for the square array (see Subsection 4.2.4). It is therefore unlikely that distortional matrix failure will ever become the first failure mode for biaxial states of strain.

This means that the optimum volume fraction for the majority of the envelope is simply the maximum one achievable, with the exception of cases where transverse stresses are very important. In Section 7.2, the strain-space envelope for intermediate modulus, high strength carbon fibers was found to not vary much with the material combination. In order to increase the strength of such a composite, its longitudinal stiffness should be increased. This section showed that one feasible way of doing so is to increase the fiber volume fraction.

### 7.3.3 Sensitivities to Volume Fraction and Fiber Array Type

Comparing the envelopes for volume fractions of 0.5, 0.573 and 0.65 in Figure 7.7, there are no unexpected changes. The differences between envelopes seem to behave rather linearly in the sense of equally large changes for equally large differences in volume fraction. In particular, there is no asymptotic behavior that would invalidate the use of Onset Theory if there are minor uncertainties in the volume fraction. The largest changes occur in longitudinal direction. This is directly related to stiffness differences, as discussed above. Using the material properties from Section D.3, the longitudinal stiffnesses for these three volume fractions are 140GPa, 160GPa and 181GPa, which cause the common intercept in strain space of about 1.5% to result in the different intercepts in stress space shown in Figure 7.7. These correspond to slightly more than 10% strength changes.

The sensitivity of the strength of a composite to the fiber volume fraction is therefore essentially the same as the sensitivity to the stiffness. Since this effect is not unrealistically large even for the

simplistic equations in Subsection 7.3.1, Onset Theory seems to be sufficiently stable within the range of typical volume fractions encountered due to for example manufacturing inaccuracies.

Regarding the claim by (Hart-Smith, 2010) that the strength is very sensitive to the volume fraction, it is not possible to provide a definite verdict since this depends on the definition of "very sensitive". However, a relative comparison can be carried out regarding the statement that the sensitivity with respect to the fiber volume fraction is larger than the sensitivity with respect to the fiber array. According to Hart-Smith, this increases confidence in the method. If there were drastic changes in the results for a different assumed fiber array, then the process of using unit cells would be very questionable (see also the discussion in Subsection 2.2.6), and the method would not be reliable.

Figure 7.8 shows the failure envelopes for square and hexagonal arrays at a volume fraction of 0.573, as well as complete failure envelopes for volume fractions of 0.5, 0.573 and 0.65. "Complete" in this context means that all rotation angles (see Subsection 3.3.4) and both fiber array types are taken into account, while the envelopes for square and hexagonal only contain one fiber array without any rotations. For all envelopes, the full set of interrogation points (Subsection 3.4.3) is used.

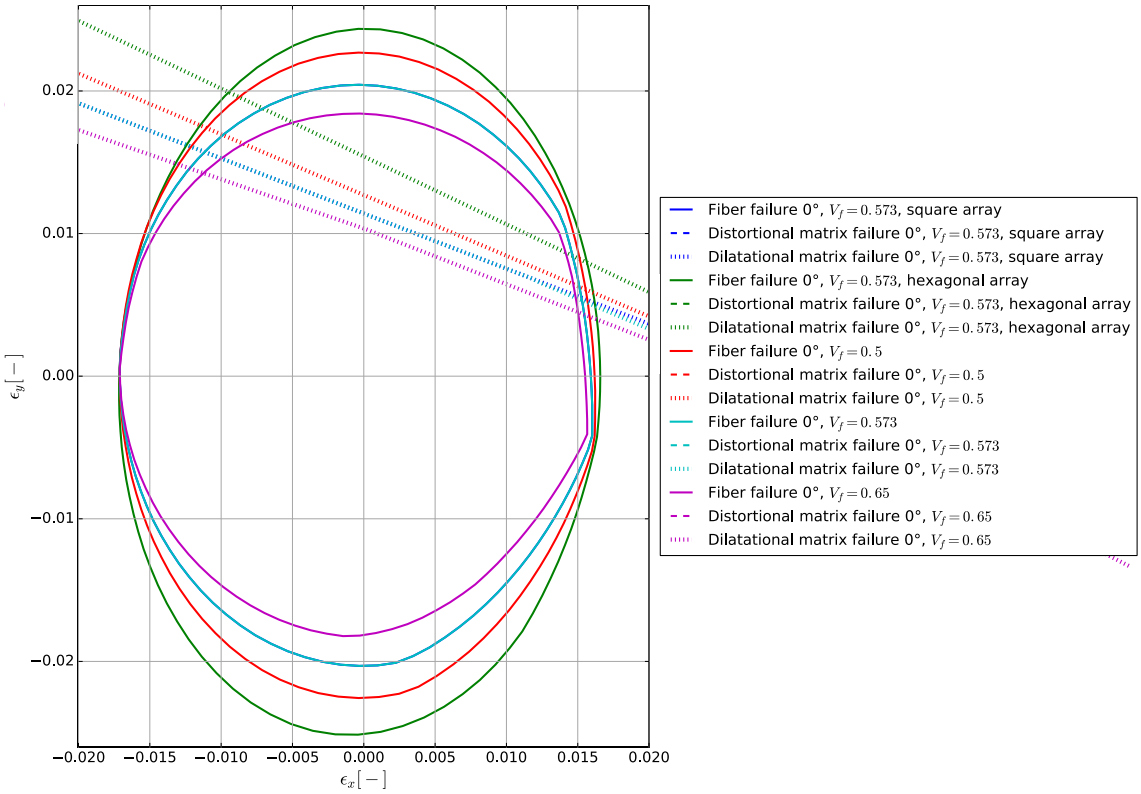


Figure 7.8: Comparison of sensitivities to fiber array type and volume fraction. The envelope for the square array at $V_f = 0.573$ overlaps with full envelope at that volume fraction.

Note that the envelope for the square array for a volume fraction of 0.573 is identical to the full conservative envelope. This once again supports the findings in Subsection 3.3.4 that a square array (and sometimes also hexagonal arrays) typically provide conservative envelopes.

Regarding Hart-Smith's claim, at least for this case the sensitivity with respect to the fiber array type is of similar magnitude as the sensitivity with respect to fiber volume fraction. The difference

between green and blue (overlapped by cyan) lines in Figure 7.8 is quite similar to the difference between red and magenta lines. In other words, changing the fiber array is comparable to an increase or reduction of the fiber volume fraction by about 7.5 percent points.

In stress space, the situation is not completely clear. If the relations in Subsection 7.3.1 are used, the trends become a little more involved since the volume fraction now plays an additional role in the stiffness matrix, but the overall conclusion remains the same (changing the fiber array results in similar differences as changing the volume fraction). However, at the current state of development the stiffness matrices for square and hexagonal array are the same (see also Subsection 3.2.1). If the stiffness properties for the actual fiber arrays are used, this conclusion may change.

Summarizing the preceding discussion, at this stage Hart-Smith's claim (that the sensitivity to the fiber volume fraction is larger than the sensitivity to the fiber array) has been refuted in strain space. In stress space, it cannot be fully investigated, although results point towards it being incorrect. Regarding the sensitivity of predictions to the volume fraction in general, Onset Theory seems to be sufficiently robust.

## 7.4 Effect of Temperature

A very important topic in the analysis of composites are residual strains due to temperature effects. As discussed in Subsection 3.2.4, there is both a mismatch between ply and laminate thermal expansion factors (the curing strains) and a mismatch between fiber and matrix thermal expansion factors (captured by the thermal amplification factor vector $\boldsymbol{A}$).

As discussed at various occasions throughout this thesis, residual strains are commonly assumed to relax over time. The following subsections will cover the magnitude of the two temperature dependent effects in order to determine how this relaxation will influence failure predictions.

### 7.4.1 Curing Strains

Using the procedure in Subsection 3.2.2, significant curing strains are developed in the laminate. For example, for the quasi-isotropic AS4/3501-6 laminate in Subsection 6.3.1, the strains are $(\epsilon_x, \epsilon_y) \approx (-0.00041, 0.0038)$ (in the ply coordinate system). Since the laminate is identical in longitudinal and transverse direction, the same values are found for all plies. Since the curing strains are pre-strains on the plies, they simply shift the envelope, as discussed in Subsection 3.2.4.

Note that the magnitude of in particular the transverse strain is quite significant. In Figure 6.4, fiber failure on the horizontal axis occurs at a strain of about $\epsilon_x = 0.015$ in the 0° ply. Not including the curing strains would mean that the envelope moves to the left by 0.00041. This is hardly a relevant change. However, for the 90° ply, the horizontal axis is the longitudinal direction. This means that the envelopes – including the matrix failure cutoff – would shift by 0.0038. Currently, matrix failure is predicted to occur exactly when observed in the test, namely at approximately $\epsilon_x = 0.007$. Excluding the curing strains, the prediction would be 0.0108, which is vastly unconservative. The influence of the curing strains is thus to take up more than half of the dilatational capability of the matrix. This was also found by (Hart-Smith, 2010, p. 4324).

As discussed above, typically the curing strains in transverse direction are much larger than those in longitudinal direction (of the individual ply – not of the envelope; note that the envelope is actually elongated in transverse direction of the ply, which can lead to some confusion at first). To explain the impact of this result, Figure 6.4 is used. If there were no curing strains, the main effect (neglecting the longitudinal curing strains altogether) would be that the envelope for the 0° ply shifts up, while the envelope for the 90° ply shifts to the right. Therefore, the fiber failure envelope will not change significantly, since that part of the laminate envelope is defined by longitudinal compression. On the other hand, the part of the laminate envelope defined by matrix failure is due to transverse strains (in the ply coordinate system). Since the transverse curing strains are very large, there will be significant changes for this type of failure. Therefore, for laminates with plies in multiple directions, the fiber failure envelope will typically not change much if curing strains are included. On the other hand, dilatational matrix failure will be affected significantly. Note that there are some changes for biaxial strains due to a change in location at which failure in one ply switches to failure in another ply. However, this effect is still relatively small.

Regarding curing strains relaxing over time, the overall effect will most likely be beneficial, since it increases the dilatational strain the matrix is capable of withstanding. One explanation for the relaxation is moisture ingression, which is not investigated in this thesis (see Subsection 2.2.2). Since this would lead to swelling of the matrix, it is very plausible that it is possible to apply larger tensile strains. The correct predictions will be somewhere between the extremes of having no curing strains and having full curing strains for the application temperature. At least for the laminate in Subsection 6.3.1, the tests seem to have occurred before there was any significant relaxation of curing strains.

The curing strains are related to the difference between the thermal expansion coefficient of the ply and that of the laminate (which, in turn, depends on stacking sequence and ply stiffness matrix). This means that a brief investigation of these three parameters should be carried out as well.

Regarding the stacking sequence, it was already mentioned in Subsection 6.3.2 that adding or removing $\pm 45°$ plies does not change the curing strains since the effect in longitudinal and transverse directions is identical. Adding plies with other orientations reduces the curing strains in plies of the same orientation, at the cost of increased strains in all other plies.

The magnitude of the ply thermal expansion coefficients is directly related to the resulting curing strains. In general, the closer to zero the thermal expansion coefficients are, the lower the resulting curing strains. The only exception are quasi-isotropic laminates, where identical nonzero thermal expansion coefficients also do not cause any curing strains.

Finally, differences in the ply longitudinal and transverse stiffness related to similar differences in resulting curing strains. For increased stiffness in a certain direction, the curing strains in that direction will reduce, while the curing strains in the other direction increase (due to the increased stiffness in that direction of other ply orientations).

### 7.4.2 Thermal Amplification Factors

For the curing strains discussed in the previous subsection, there is clearly a significant influence of temperature, since according to Eqn. (3.15) they scale linearly with temperature. This means that the temperature will certainly be very relevant for the failure predictions. The other temperature dependent term is the thermal amplification factor vector $\boldsymbol{A}$. In order to investigate its effect, the failure envelope for the AS4/3501-6 laminate from Subsection 6.3.1 has been generated including curing strains, but without the thermal amplification vector.

The results are very similar to those shown in Subsection 5.2.3. Figure 5.2 contains the thermal amplification factor vector, whereas in Figure 5.3 this effect has been removed (from the fiber failure envelope only). This results in minor changes for the fiber failure envelope: the shape changes somewhat (in particular, the envelope obtains an axis of symmetry), but there is no significant influence on failure predictions.

For the dilatational matrix cutoff, the effect is comparable to the curing strains. The thermal amplification factors result in a shift in transverse direction such that the achievable strains are reduced. However, the magnitude of the effect is smaller (removing the thermal amplification factors results in a 15% increase, compared to the more than 50% found when removing the curing strains in the previous subsection).

The same conclusions can be drawn as for the curing strains. Temperature effects are usually assumed to reduce over time. Once again this can be explained as being due to swelling of the matrix due to moisture ingression, since the trend of the effect is the same (larger dilatational strains are possible). In this case, the difference between predictions with and without temperature effects is smaller, but the true behavior will still be somewhere in between.

## 7.5 Random Arrays

So far in this thesis, regular unit cells have been used, assumed to repeat indefinitely throughout the composite. However, the real microstructure of a composite is of course far from this idealized arrangement, as visible for example in Figure 2.1.

In general, it should be mentioned that a significant amount of randomness is included already because of the use of interrogation points throughout the unit cell (Subsection 3.4.3), for various rotation angles of both square and hexagonal arrays (Subsection 3.3.4). Several thousand combinations of these parameters are taken into account. In addition to that, the sensitivity with respect to the fiber volume fraction seemed to be quite modest and mostly related to the stiffness of the composite, as discussed in Subsection 7.3.2. Together, these points will already cover a large part of the possible arrangements found in a real, random microstructure.

Another argument for the usability of regular unit cells is that based on the investigation in Section 3.3 the square fiber array is typically most conservative for fiber failure (this was also indicated in Subsection 7.3.3). Therefore, the fiber failure envelope will be defined by the square fiber array. In a real composite, other, less critical fiber array types and rotation angles will be present. Therefore, the square array does form a conservative lower limit for the composite behavior, as also

claimed by (Hart-Smith, 2010). In reality, if there are few square arrays, failures originating from this fiber array type may even be arrested by other fiber arrays, leading to overconservative predictions (although this was not typically the case in Section 6.3).

However, two important questions remain. First of all, the regular unit cells assume every fiber to be surrounded by a significant amount of matrix. However, in reality this will not always be the case. Quite often, fibers are (almost) touching. The question is whether there is a minimum distance of fibers below which the behavior suddenly turns asymptotic, with severe strain concentrations leading to failure much earlier than otherwise predicted. If this is the case, then premature failures could occur if there is a significant amount of fibers in close proximity.

Secondly, one of the main assumptions in the use of unit cells is that the strain in a unit cell is the same as the strain in the lamina, as discussed in Subsection 2.1.6. For a random fiber array, this assumption does not hold anymore. The second focus of research will therefore be to what extent a random array deviates from this assumption.

### 7.5.1 Fibers in Close Proximity

In Figure 7.7, a sensitivity study regarding the fiber volume fraction was carried out. The largest value investigated was 0.75. Based on Subsection 4.2.4, this is very close to the maximum possible volume fraction of the square fiber array (0.785) at which the fibers would be touching each other. Nevertheless, no sudden asymptotic behavior of any kind was observed.

Figure 7.9 shows a square unit cell at $V_f = 0.75$. Clearly, the fiber is nearly touching the edge of the unit cell. Note that the number of elements in the critical region is very large already for approximately 256 000 nodes. At 512 000 nodes, meshing failed.

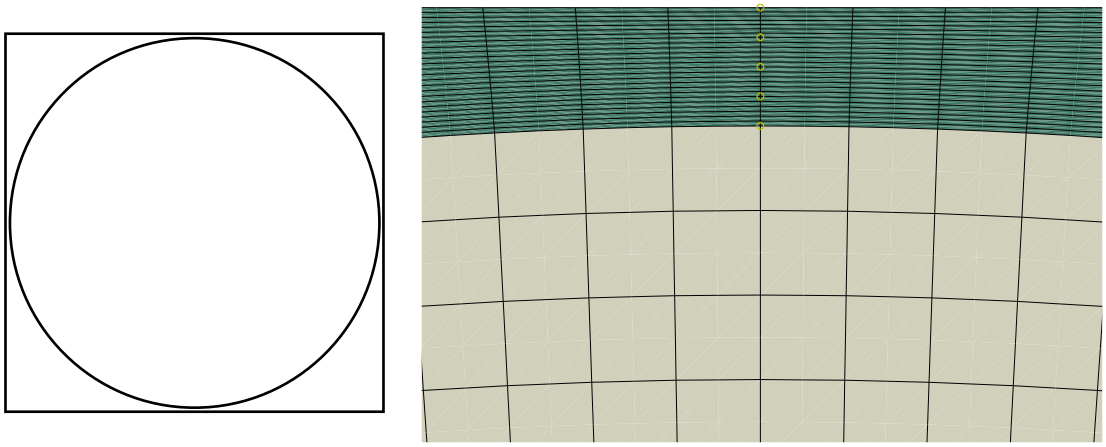

Figure 7.9: Square unit cell at a volume fraction of 0.75. Left: overview of entire unit cell (original dimensions); right: close up of mesh at of location where fibers are closest together (approximately 256 000 nodes).[1]

[1] Right part of the figure: the thin white lines visible on some screens / print outs are caused by a rendering problem in the Abaqus vector graphics export and do not carry any meaning.

According to the criteria put forth in Subsection 4.2.5, the mesh at approximately 256 000 nodes was not converged. However, a closer look revealed that the maximum difference in any amplification factor, when compared to the mesh at about 128 000 nodes, was 2.42% (which would in fact be converged even according to the strict criteria used in this thesis). Element averaging resulted in a maximum error of 7.75%, just outside of the 5% maximum limit selected in Subsection 4.2.5. While this means that technically the mesh is not converged, it is highly unlikely that for a fully converged mesh the behavior would suddenly become asymptotic. In addition to that, the convergence issues do (interestingly enough) not occur at the location where fibers are almost touching, but at locations close to the interstitial location (see e.g. Figure 2.9), where they are furthest apart.

In summary, this means that close proximity does not result in sudden asymptotic behavior. Although the strain-space failure envelope shrinks with increasing fiber volume fraction, this will be a local effect in a random microstructure. As discussed in Subsection 7.3.2, the additional stiffness provided by the higher volume fraction will in fact result in a larger stress-space failure envelope.

### 7.5.2 Equivalence of Ply and Unit Cell Strains

The other issue is related to the assumption of identical unit cell and ply strains (as discussed in Subsection 2.1.6). For a true composite, this will not be the case because the stiffness changes continuously, meaning that there will be regions with larger and smaller strains. In order to carry out a preliminary investigation into this topic, the multi-cell model shown in Figure 7.10 was used.

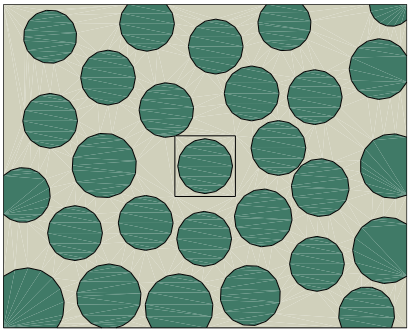

Figure 7.10: Multi-cell model used in preliminary investigation of random fiber arrays[1]

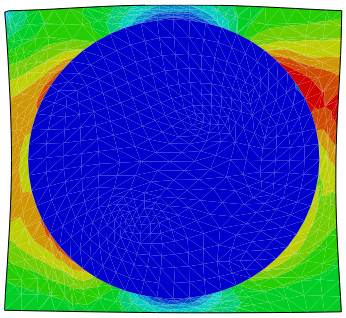

Figure 7.11: Deformed shape for unit cell extracted from multi-cell model[1]

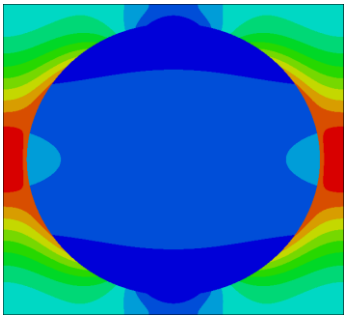

Figure 7.12: Deformed shape for single unit cell

[1] The thin white lines visible on some screens / print outs are caused by a rendering problem in the Abaqus vector graphics export and do not carry any meaning.

During this investigation, it was found that the main problem with random arrays will be that the boundaries of the center cell are not fixed anymore. This means that they do not remain straight during loading; in addition to that, they move (which invalidates the fixed boundary conditions discussed in Section 3.1).

In order to quantify the impact, using the material properties for AS4/3501-6 and applied transverse strain of 0.001 was applied. The resulting strains in Figure 7.11 range from 5.938e-4 to 1.884e-3. On the other hand, for the single unit cell model in Figure 7.12, the range is 5.811e-4 to 2.202e-3.

Apparently, for this particular region in the multi-cell model, the single unit cell is in fact more conservative. In order to determine whether this is a general trend, the strains in the entire multi-cell model are investigated. The resulting range of strains was 4.109e-4 to 2.441e-3. In other words, the minimum strain in the single unit cell is higher than the minimum strain in the multi-cell model; however, the single unit cell does fall approximately 10% short of the true maximum strain.

Obviously, this is only a very preliminary investigation. Much more work on this topic is needed. Only a single amplification factor is compared; only one random array is investigated; and it was not ensured that the mesh used in the multi-cell model was properly converged. Most importantly, only a non-rotated square fiber array is taken into account (rather than multiple rotations of square and hexagonal arrays). However, this investigation does provide an indication that unit cells should not give vastly different results than larger, multi-cell models. Based also on the validation results in Section 6.3, it seems as if using representative volume elements is a reasonable solution for the current state of development.

# Chapter 8

# Conclusions and Recommendations

The basic motivation for the development of Onset Theory was the lack of reliable composite failure criteria, as evident for example during the first WWFE. This results in the necessity to carry out very extensive and expensive test programs for every new composite design.

First and foremost, the conclusion of this thesis is that there are indeed major benefits associated with Onset Theory, which is able to generate quite accurate predictions of composite laminate failure, including predicting non-catastrophic matrix failure prior to ultimate failure without requiring a complex (and sometimes rather arbitrary) progressive failure analysis. It also reproduces other trends seen in composite tests, using a single set of strength data for all cases. The benefits of Onset Theory are summarized in more detail in Section 8.1.

In order to apply Onset Theory correctly, a consistent approach to Onset Theory had to be developed. This included deriving a method to generate failure envelopes using analytical expressions for the full state of strain. Both of these goals were reached successfully, with the complete approach having been summarized already in Section 3.5.

The reason for the necessity to develop a consistent approach was the fact that different research groups presented contradicting opinions on the steps required to apply the theory correctly. Section 8.2 summarizes the results regarding those contradictions, obtained during the development of the consistent approach.

Following automation of the entire approach, additional research activities and sensitivity studies were carried out. Their results are contained in Section 8.3. A very important conclusion is that the critical invariants used in Onset Theory seem to be identical for various materials. In addition to that, Onset Theory was found to be sufficiently robust with respect to the various input parameters.

Finally, Section 8.4 presents an overview of and some preliminary thoughts on the various topics which could not be addressed properly during this thesis.

## 8.1 Conclusions Regarding Onset Theory

Based on Sections 6.3 and 6.4, there are two main benefits associated with Onset Theory in combination with the full state of strain derived in Section 3.2. First of all, it provides quite accurate predictions of composite laminate failure under biaxial strains, unlike commonly used criteria such as Tsai-Wu (see Subsection 6.4.2). In addition to that, although the magnitude of the effect was somewhat underpredicted, there is a clear difference between lamina and laminate failure strains for those materials where this is also found in the test data, while nearly identical values are predicted for a material where this is not the case (Subsection 6.4.3).

Secondly, in order to do so, only a single critical value is required for each of the three failure modes used in Onset Theory. This is a significant benefit compared to criteria such as maximum strain, which also showed good agreement with failure under biaxial loads, but requires new allowables for every new set of loading conditions and stacking sequence. In fact, at least for the cases in this thesis, no strength tests whatsoever were necessary for the application of Onset Theory. Using the same default critical invariants (summarized in Subsection 6.2.5) for all materials gave both good predictions for laminate failure and captures the trends regarding the differences between lamina and laminate failure. The focus for the validation cases in Section 6.3 was on intermediate modulus carbon fibers in combination with thermoset untoughened resins. However, the default critical invariants also included glass fibers with no indication of any significant differences.

Regarding the value of the failure criterion, the fact that it matches the best tests means that Onset Theory appears to indeed be the correct failure criterion for composites. Although a variety of further research is suggested (as discussed in Section 8.4), it will mostly be concerned with extending the scope of applicability of the theory. This will in particular be related to properly determining the full state of strain in a ply, as well as improving the process of determining the local constituent strains. The foundation of Onset Theory – using the dilatational and distortional strain invariants as independent indicators for failure – is clearly supported using the results of this thesis.

For the cases for which Onset Theory is already applicable, the primary focus should be an improvement of the way tests are carried out, rather than making more or less arbitrary adjustments to the theory as done by other failure criteria. The result would be erratic behavior with predictions which are sometimes correct and sometimes incorrect. Instead, the tests have to be improved as much as possible (which would also lead to a better understanding of how to prepare specimens and structures such as to achieve optimum performance). Only then can flaws be included in the theory in a well-defined manner.

## 8.2 Findings Related to Literature Claims

In Section 3.5 the consistent approach to Onset Theory was summarized. During its development during this thesis, a variety of contradicting claims found in literature had to be resolved. This section contains details on the results obtained.

First of all, contrary to the choice made by Hart-Smith (see Subsection 5.2.6) fixed boundary conditions need to be used (Section 3.1), unless significant modifications are made to the applied strains.

Secondly, the various fiber array types can indeed be obtained through rotation; however, the diamond array used by many researchers does not appear to be relevant. For this thesis, it was decided to employ several rotation angles in order to ensure conservative predictions.

Regarding the required interrogation points, the interstitial location claimed to be very important by many researchers, including Gosse (the original author of SIFT), does not appear to be relevant. However, as for the rotation angles a large number of interrogation points is taken into account to ensure conservatism.

In terms of the sensitivity to the input parameters, Hart-Smith's claim that the sensitivity with respect to the volume fraction is far more relevant than the sensitivity with respect to the fiber array type could not be confirmed (Subsection 7.3.3). However, it can be confirmed that there is indeed a very strong influence of temperature on failure predictions, in particular regarding the dilatational matrix cutoff. This topic was addressed in Section 7.4.

Finally, some outright errors were found in literature. In particular, Gosse appears to be using an incorrect scaling factor for the long direction of the hexagonal array according to the verification of the strain amplification factors (Subsection 5.1.2). As stated above, Hart-Smith is using incorrect boundary conditions, and at least in the verification of the failure envelopes (Subsection 5.2.4) is neglecting curing strains.

## 8.3 Results of Research and Sensitivity Studies

One of the most important conclusions of this thesis is the fact that the critical invariants for a variety of different materials appear to be identical (see Subsection 6.2.5). Although this may not hold for example for thermoplastic resins, it did enable successful failure predictions for a variety of different cases, as discussed in the introduction to this section.

Regarding ply angles, it was found that the common wisdom of aligning plies with applied loads is also predicted by Onset Theory. While a [0/60/−60]s laminate (or a rotated version) would be a theoretical optimum for pure longitudinal and transverse loads, for most cases a [0/90/±45]s (or any shuffled version thereof) laminate is preferable (Section 7.1).

For intermediate modulus / high strength fiber carbon-epoxy composites, the ply failure envelopes were found to be quite similar, as discussed in Section 7.2. However, given the different stiffnesses of those composites, stress-space or laminate envelopes will vary significantly. A similar investigation should be carried out for composites involving other fiber and matrix material types, such as high modulus fibers, glass fibers, or thermoplastic resins. In Subsection 6.2.5, it was found that for all materials investigated (including glass fibers) the critical invariants were quite similar. It would be very interesting to determine whether this also translates into comparable strain-space failure envelopes. Since glass fibers fail at much higher strains than carbon fibers (see e.g. (Soden et al., 1998)), this will most likely not be the case.

Although the strain to failure decreases, based on a simple rule of mixture approach the highest strength of a composite will be obtained by increasing the volume fraction (Section 7.3). This means that the stiffness increase outweighs the decrease in strain space envelope. However, since the effects

in general are kind of minor, based on the purely straightforward strength/stiffness approach in this theses maintaining a constant volume fraction should not necessarily be a priority for manufacturers (a larger volume fraction with more variation will be better than a smaller volume fraction with less variation). Of course this disregards all other effects at play requiring more stringent constant volume fractions.

In general, it was found that the strength of carbon/epoxy composites seems to be more strongly related to the ply stiffness than to any other parameter. This result was found both for different materials (Section 7.2) and for different fiber volume fractions (7.3). The stiffness is far more important than the very similar or even decreasing ply strain envelopes. In addition to that, it also has a strong influence on the curing strains, as discussed in Subsection 7.4.1.

The combined effect of curing strains and thermal amplification factors is relatively minor for the fiber. For the dilatational matrix cutoff, it is very important to take this effect into account, with the curing strains amounting to almost half of the dilatational capability of the matrix (while the thermal amplification factors have a similar effect, but of smaller magnitude). Both of these effects were discussed in Section 7.4. In general, low curing strains are beneficial for matrix failure. For manufacturers, this means that an effort should be made to obtain low thermal expansion coefficients. Similarly, for designers this means that laminates should be selected where the curing strains are low for the plies loaded in transverse tension.

In summary, this means that based on the various sensitivity studies in Chapter 7, Onset Theory seems to be sufficiently robust with respect to ply orientations, constituent material properties, fiber volume fraction, and temperature effects.

In addition to that, the assumptions involved in using unit cells (already summarized in Subsection 3.5.1) do not seem to have an overly large detrimental effect, as examined briefly in Section 7.5. Particularly, fibers in close proximity do not result in asymptotic behavior of the matrix failure envelopes. Including different orientations of both square and hexagonal array (as done in this thesis) should mean that unit cells provide a reasonable approximation of the behavior of the random array microstructure. However, much more work is required on this topic, as also discussed in Subsection 8.4.1.

Given the fact that Onset Theory is quite successful in predicting laminate failure and also manages to capture the trends regarding the differences between lamina and laminate failures, it is already more accurate and robust than other composite failure criteria. The further research suggested in the following subsection will only make this comparison more favorable.

## 8.4 Suggested Further Research

Throughout this thesis, a variety of topics were discovered which went beyond the scope of research as outlined in Section 1.5 or were otherwise infeasible in terms of time and effort required. Although Onset Theory showed very promising results in this thesis, as stated in Section 1.4 the present work is at most a starting point for further research by both ATG Europe and TU Delft.

The present section provides a summary, and, where available, some preliminary thoughts and discussion on some of the topics that were not investigated and are believed to be important next steps in the development of Onset Theory.

### 8.4.1 Removing Assumptions and Limitations

Based on the list of assumptions and limitations in Subsection 3.5.1, various tasks can be defined. First of all, a progressive failure analysis should be carried out. This is discussed in detail in Subsection 8.4.3.

Secondly, ply interface failures such as delaminations (or other failure modes starting at the interface between plies) should be investigated. This will require analyzing unit cells containing multiple fiber directions. Unit cells for all combinations of ply orientations that are present in the laminate need to be analyzed. Then, the local strains at the interface need to be obtained by following a procedure equivalent to the one used in this thesis, but based on global interface strains and strain amplification factors for the particular interface under investigation. Note also that in this case the strain amplification factors are not constant through the thickness anymore. This topic has been addressed partly by (Hart-Smith, 2010), although his results are questionable (see e.g. Subsection 5.2.6).

The stiffness properties of the ply should be determined using analyses of the unit cell, rather than measured properties. However, as discussed in Subsection 3.2.1, it should be investigated whether this is indeed beneficial.

Some authors claim that nonlinear analyses are required, despite the claims found in other literature (see Subsection 2.1.6). One of these sources is (Mishra & El-Hajjar, 2012). (Jiazhen, 2014) also carried out significant research on this topic. In the future, these approaches should be investigated to determine whether nonlinear analysis results in improved predictions compared to linear analysis.

This nonlinear analysis is somewhat related to the variation of input parameters with temperature. Currently, all material properties are assumed to be independent of this factor. A full analysis would involve some form of nonlinear curing simulation of the unit cell with changing material properties to determine the correct residual strains (i.e. thermal amplification vector). In addition to that, the mechanical amplification factors would also change if the material properties change. Technically, for every application temperature a set of strain amplification factors based on a micromechanical model with the appropriate constituent properties should be used, although the variation of some properties can probably be safely neglected given the relatively small difference between curing and application temperatures. Finally, the question is whether the critical invariants themselves also change with temperature. For $J_1^*$ of adhesives, this was investigated by (Tsai et al., 1999), who concluded that the critical invariant was independent of temperature. This is also related to Subsection 8.4.4.

Further research should be carried out on the topic of multi-cells random fiber array) models in order to investigate the equivalence of strains in a unit cell and the ply. This has only briefly been examined in Section 7.5. Some examples include stochastic analysis of various random fiber arrays (see for example the work by (Mendoza-Jasso, 2012)), or introducing various modifications to the unit cells, such as moving the center fiber or changing its size (for the hexagonal array).

Related to this is an analysis of non-circular fibers. In a real composite, the fibers may for example by elliptical. This should be taken into account in form of another sensitivity study related to the deviation of the fiber cross section from the idealized circular shape.

As discussed in Subsection 2.2.2, moisture absorption and chemical shrinkage were neglected, although the evidence in favor of this was somewhat sparse. Therefore, the effects of possibly beneficial swelling should be investigated to determine whether the current predictions are overconservative. On the other hand, the effect of chemical shrinkage on the distortional invariant needs to be taken into account to avoid possible unconservatism.

The possible dilatational failure mode of the fiber should be investigated further by examining fracture planes of composites. Although (Hart-Smith, 2010) states that for glass fibers it is not clear whether this failure mode occurs or not, there was no source in literature that examined $J_1$-failure for this case.

Finally, although for more complex cases very quickly finite element models will be required, an effort should be made to derive analytical expressions for the full state of strain in plies and laminates that are loaded in bending or do not adhere to the infinitely large, flat plate assumption used in Section 3.2.

### 8.4.2 Extending the Field of Applicability of Onset Theory

In this thesis, only quasi-static loads applied to laminates made of unidirectional tape material were considered. Typically, the resins considered were untoughened thermosets (with the exception of Cycom 970, as discussed in Subsection 6.2.2). However, this is only a limited subset of the possible types of loads and materials.

Dynamic loads should not be problematic as long as the strain-based test data is used, as discussed in Subsection 2.2.1. On the other hand, fatigue loads would be a very interesting research topic. Fatigue of composites is not very well understood. Given the fact that Onset Theory appears to be one of the few failure criteria able to actually predict matrix failure, a further investigation into this topic could lead to new insights. It seems plausible that part of the problem with predicting fatigue failure in composites is due to actual matrix failure occurring, which is not captured by other failure theories. For example, (Gosse & Christensen, 2001) determined dilatational (i.e. tensile) matrix failure under compressive loads due to the micromechanical enhancement process. This might be a reason for the fact that composites fatigue far more severely in compression than can plausibly be explained otherwise.

Regarding the types of materials, thermoplastic resins will presumably have very different critical invariants than the thermosets discussed in Section 6.2. In particular, $J_1^*$ would be expected to far exceed the values found in this thesis. However, the general process of applying Onset Theory should remain the same.

Another topic are fabric materials. The research groups at the University of New South Wales and the National University of Singapore did quite some work on this, as found in for example (Pearce & Kelly, 2012) or (Jiazhen, 2014). In essence their approaches employ a second micromechanical

(possibly more accurately classified as mesomechanical) enhancement process, during which the ply strain is localized to the individual tows of the fabric before being localized to the constituent level.

Currently, Onset Theory only includes true material failures (dilatational and distortional). Given the problems with compression-dominated loads (see e.g. Subsection 6.3.5), it seems useful to include fiber kinking and compression microbuckling. Although these are (micro)structural failure modes rather than material failure modes, they might remove some of the remaining discrepancies between prediction and test data. These additional failure modes would not be interacted with the other criteria, but merely create additional cutoffs in strain space. Note that (Gosse & Christensen, 2001) claim that fiber kinking is triggered by dilatational failure in the matrix (which is already included in Onset Theory), leading to a loss of support for the fiber. This topic should be investigated further.

Finally, all analyses in this thesis assume a pristine material, excluding voids or existing damage. However, there may very well be cases where this assumption is simply not valid anymore. Voids and existing damage may or may not influence failure of the material, depending on whether they cause escalating failure due to local strain concentrations. If this is not the case, then the failure will eventually be arrested in the vicinity of the void without causing noticeable widespread failure. Note that clearly, the analysis of composites with preexisting damage is closely related to the investigation of composite fatigue discussed above.

The effect of voids is partially captured because in situ properties are used to determine the critical values (see also Subsection 8.4.4). However, a proper investigation would require mesomechanical analyses comparable to the way a fabric is suggested to be analyzed (see above). This would mean constructing models of individual fibers, surrounded by resin, with empty spaces in the model. If typical void dimensions are significantly larger than individual fibers, this approach may also be modified to contain homogenized blocks of fiber and matrix. Either way, a mesomechanical enhancement process should be carried out to determine the strains in the vicinity of the void, followed by a micromechanical enhancement process to determine individual constituent strains. The investigation should be preceded by in-depth literature and microscopy studies on typical void size, content, and distribution.

### 8.4.3 Progressive Failure Analysis

One topic that has been discussed in some detail already in Subsection 6.3.1, as well as hinted at in various sections throughout this thesis, is progressive failure analysis.

Currently, no progressive failure analysis is carried out since exclusively strain-based data is used. With the exception of curing strains, the state of strain in a ply does not depend on the other plies in the laminate. Therefore, the failure prediction for a ply does not change if another ply fails.

Some comments can be made regarding this topic. First of all, the curing strains certainly depend on the presence of other plies. This means that some form of post-first-ply-failure curing strain analysis would be needed. For example, for a [0/90]s laminate, matrix cracks in the 90° ply will reduce the residual compressive strains in the 0° ply. Quantifying this reduction will be extremely challenging. In addition to that, matrix cracking (due to a transverse strain) in a ply is predicted to eventually be followed by fiber failure (due to a larger transverse strain) in the same ply (see any

of the figures in Section 6.3). However, it seems rather questionable whether it is still possible to load the fibers in transverse direction after matrix cracking occurred. For an individual ply, the matrix cracking would constitute catastrophic failure. In a laminate, these failures will be bridged by the plies with different orientations. To what extent this is sufficient to still transmit transverse strains into the fibers is unknown.

In summary, this means that – although the agreement with test data in Section 6.3 is quite good, even for portions of the failure envelope preceded by matrix cracking – the only part of the envelope that can be predicted with relative certainty is up to the first occurrence of failure, even if this failure is not catastrophic. This is in line with the standard definition of ultimate failure for composites used in aerospace.

Moving one step further, a thought experiment can be carried out regarding the degradation of properties commonly used in "progressive failure analysis". The starting point is to assume that (neglecting the arguments above) the strain space failure envelope for each ply and failure mode is indeed independent of failures in other plies or failure modes. Based on this, using strain-based test data a straightforward comparison is possible. However, quite commonly test data is only available in stress space. This information is more valuable to some extent since it provides knowledge about the load bearing capacity of the laminate. In strain space, a ply that has completely failed and only consists of air will have an extremely large failure envelope, even though it is obviously not able to carry any load anymore.

Therefore, the following procedure seems like an interesting starting point. Assuming the strain-based failure envelopes to be constant, the conversion to stress space is made using the laminate stiffness matrix. Once the first failure occurs, the laminate stiffness matrix is updated depending on the type of damage. (Gosse, 2004b, Slide 19) contains some suggestions. For $J_1$-failure, $E_{22}$ and $E_{33}$ of the ply are set to zero, while for distortional matrix failure the shear moduli are set to zero. If the fiber fails, $E_{11}$ is zeroed out. (Obviously, this can be modified to changing them to a value of 0.1 times their original value, or any other factor of choice. Note also that it may be interesting to see how predictions change if failure is only assumed to occur once a certain percentage of interrogation points predicts failure.) Based on this, the portion of the stress space failure envelope that succeeds the first failure is redrawn until the next failure is reached. The strain based envelope will remain the same throughout this process. However, in stress space eventually all remaining failure modes for all plies will collapse into a single envelope, constituting ultimate failure of the laminate.

Note that this procedure would still not be tracking failure within a ply. It is still assumed that a ply completely fails the instant one of the critical invariants is exceeded. Doing a sub-ply level progressive failure analysis would most certainly require detailed finite element analysis and is beyond the scope of even this discussion. Some information can be found in (Gosse, 2004a) or (Tay, Tan, & Tan, 2005).

### 8.4.4 Determining Critical Invariants

The final topic that should be addressed is determining critical invariants. This is related to various (sometimes partially proven) hypotheses found in this thesis. First of all, the independence of critical

invariants (resulting in non-interactive failures modes), which is one of the central assumptions of Onset Theory as discussed in Subsection 1.3.2, should be investigated by carrying out tests on the standard set of off-axis tension coupons. This choice will be discussed in more detail below.

Secondly, invariants for different material combinations should be compared, as done by (Z. Li et al., 2011). Subsection 6.2.1 presented their proof of the independence of the matrix invariants from the fiber material, and vice versa.

In addition to that, invariants should be measured at different temperatures to verify the assumption that there is no temperature dependence (addressed in detail in Subsection 8.4.1).

Finally, the "standard" invariants derived in Section 6.2 should be confirmed by determining the invariants for materials which currently form outliers. As postulated in that section, it is believed that this may be related to incorrect measurements or procedure. In particular, it needs to be ensured to avoid premature failure of 90° tension coupons, or to use accurate measurement equipment to determine non-catastrophic matrix failure in laminates. Options could include acoustic emission sensors, changes in the slope of the stress/strain curve, load/unload tests, or loading specimens to various load levels and performing tomographical measurements on each of them. In case compressive tests are also included, structural buckling and microstructural effects such as fiber kinking have to be avoided (or should be included in the theory, as discussed in Subsection 8.4.2).

For the procedure of determining critical invariants, different options are possible. They all have in common that the critical invariants are measure in situ (in other words for the actual composite, rather than fiber or matrix in isolation). There are several reasons for this, having been discussed in many sources such as for example (Hart-Smith, 2010). Most importantly, individual fiber failures due to manufacturing flaws or microdamage are bridged by the matrix in a real composite. This effect also has to be present in the tests used to determine the critical invariants. Similarly, the constraining environment of the fibers is needed for the matrix invariants. Finally, using the composite ensures that the right curing cycles is used.

The standard way of determining the critical invariants is by testing a series of off-axis tension coupons, ranging from 0° to 90°. Subsequently, plots in accordance with Figure 1.1 can be generated to determine the critical invariants. There are several reasons for these coupons. First of all, the onset of failure in a particular failure mode is the same as ultimate failure of the coupon, meaning that it can be detected easily. Secondly, according to (Hart-Smith, 2010, p. 4302) these coupons behave linear until failure, facilitating their analysis. Typically, finite element models of these coupons are created to determine the critical invariants. The standard source is (Pipes & Gosse, 2009), who describe the process of ensuring convergence and the locations in the coupon where the critical invariant is sampled in detail. (Tran, 2012) discusses the use of oblique end tabs to avoid coupling between normal and shear loads for the unsymmetric laminates (all angles except 0° and 90°).

As mentioned above, the 90° coupon in particular tends to fail far below the actual capability of the material. In order to alleviate this issue, a very specific (non-standard) coupon is used, much thicker than regular coupons. A description of the coupons can be found for example in (Hart-Smith, 2010, sec. 6.1). It might be valuable to contact Gosse, the original author of Onset Theory, to determine whether there is an updated or improved coupon design, given the fact that Hart-Smith

has not been involved in the development for quite some years, and errors were found in his article (as discussed for example in Subsection 5.2.6).

Based on the developments in this thesis, in particular related to the automatic generation of failure envelopes, there is also another possibility. Since the effect of the critical invariant is only to scale the failure envelopes, it can be determined simply by matching the failure envelope for any given laminate to the measured failure strains. This is not the same as the "fine-tuning" to the test data that commonly occurs for other failure theories since only a single parameter is involved. If Onset Theory is correct, any test (where failure occurred in the failure mode under investigation) can be used to determine the critical invariant, and all other tests should confirm this value. In other failure theories, the number of data points used to determine the failure envelope is typically much larger (for example longitudinal and transverse tension and compression strengths), resulting in essence in an interpolation of available data rather than a failure prediction.

Note that for the off-axis specimens, this procedure is likely not feasible since finite element models need to be created to capture boundary effects and possible normal/shear strain couplings.

# References


Bergmann, H. W. (1998). *Evaluation of Failure Criteria for Thin-Walled Fiber-Reinforced Composites*. Braunschweig.

Buchanan, D. L., Gosse, J. H., Wollschlager, J. A., Ritchey, A. J., & Pipes, R. B. (2009). Micromechanical enhancement of the macroscopic strain state for advanced composite materials. *Composites Science and Technology*, *69*(11–12), 1974–1978. http://doi.org/10.1016/j.compscitech.2009.04.022

Caruthers, J. M., & Medvedev, G. A. (2009). Nonlinear Viscoelastic Behavior of Glassy Polymers and Its Effect on the Onset of Irreversible Deformation of the Matrix Resin in Continuous Fiber Composites. In *17th International Conference on Composite Materials (ICCM-17)*. Edinburgh, UK.

Chowdhury, N. T., Wang, J., Chiu, W. K., & Yan, W. (2016). Matrix failure in composite laminates under compressive loading. *Composites: Part A*, *84*, 103–113. http://doi.org/10.1016/j.compositesa.2016.01.007

Colvin, G. E., & Swanson, S. R. (1990). Mechanical Characterization of IM7/8551-7 Carbon/Epoxy Under Biaxial Stress. *Journal of Engineering Materials and Technology*, *112*, 61–67.

Eng, C. H. (2007). *Compressive Failure of Open-Hole Carbon Composite Laminates*. National University of Singapore.

Gosse, J. H. (2004a). A Damage Functional Methodology for Assessing Post-Damage Initation Environments in Composite Structure. In *45th AIAA/ASME/ASCE/AHS/ASC Structures, Structural Dynamics & Materials Conference*. Palm Springs. http://doi.org/10.2514/6.2004-1788

Gosse, J. H. (2004b). Strain Invariant Failure Theory: Failure Theory and Methodologies for Implementation.

Gosse, J. H., & Christensen, S. (2001). Strain invariant failure criteria for polymers in composite materials. In *42nd AIAA/ASME/ASCE/AHS/ASC Structures, Structural Dynamics, and Materials Conference and Exhibit*. Anaheim, CA. http://doi.org/10.2514/6.2001-1184

Gosse, J. H., Christensen, S., Tuttle, M., Lin, K. Y., Flinn, B. D., & Feraboli, P. (2007). Analysis of Composite Failure. In *AMTAS Spring 2007 Meeting*. Seattle, WA.

Ha, S. K., Jin, K. K., & Huang, Y. (2008). Micro-Mechanics of Failure (MMF) for Continuous Fiber Reinforced Composites. *Journal of Composite Materials*, *42*(18), 1873–1895. http://doi.org/10.1177/0021998308093911

Harman, A., Risborg, A., & Wang, C. H. (2008). Experimental testing of BMI laminates with stress concentrations and the evaluation of SIFT to predict failure. *Composite Structures*, *86*, 85–95. http://doi.org/10.1016/j.compstruct.2008.03.035

Hart-Smith, L. J. (1989). *A New Approach to Fibrous Composite Laminate Strength Prediction.*

Hart-Smith, L. J. (1991). The Role of Biaxial Stresses in Discriminating Between Meaningful and Illusory Composite Failure Theories. In *9th DOD/NASA/FAA Conference on Fibrous Composites in Structural Design* (pp. 1507–1528).

Hart-Smith, L. J. (2005). An Account of One Engineer's Long-Term Involvement with Aerospace Applications of Composite Structures. In *37th ISTC SAMPE Meeting*. Seattle.

Hart-Smith, L. J. (2007). Explanation of SIFT Composite Failure Criteria. Huntington Beach: Lecture slides for Boeing In-House Training Class.

Hart-Smith, L. J. (2010). Application of the strain invariant failure theory (SIFT) to metals and fiber-polymer composites. *Philosophical Magazine*, *90*(31–32), 4263–4331. http://doi.org/10.1080/14786435.2010.510450

Hart-Smith, L. J. (2014). Is There Really No Need to be Able to Predict Matrix Failures in Fibre-Polymer Composite Structures? Part 1: Explanation of Fatal Flaws in Existing Theories. *Australian Journal of Mechanical Engineering*, *12*(2), 139–159.

Hinton, M. J., Kaddour, A. S., & Soden, P. D. (2002). A comparison of the predictive capabilities of current failure theories for composite laminates, judged against experimental evidence. *Composites Science and Technology*, *64*, 1725–1797. http://doi.org/10.1016/S0266-3538(03)00226-4

Hobbiebrunken, T., Hojo, M., Jin, K. K., & Ha, S. K. (2008). Influence of non-uniform fiber arrangement on microscopic stress and failure initiation in thermally and transversely loaded CF/epoxy laminated composites. *Composites Science and Technology*, *68*(15–16), 3107–3113. http://doi.org/10.1016/j.compscitech.2008.07.006

Holmberg, J. A., Lundmark, P., & Mattsson, D. (2008). Micromechanical vs lamina based failure theories. In *13th European Conference on Composite Materials (ECCM-13)*. Stockholm, Sweden.

Hrstka, O., Kučerová, A., Lepš, M., & Zeman, J. (2003). A competitive comparison of different types of evolutionary algorithms. *Computers and Structures*, *81*(18–19), 1979–1990. http://doi.org/10.1016/S0045-7949(03)00217-7

Huang, Y., Jin, K. K., & Ha, S. K. (2008). Effects of Fiber Arrangement on Mechanical Behavior of Unidirectional Composites. *Journal of Composite Materials*, *42*(18), 1851–1871. http://doi.org/10.1177/0021998308093910

Jiazhen, M. (2014). *A multiscale modeling approach for the progressive failure analysis of textile composites*. National University of Singapore.

Jin, K. K., Huang, Y., Lee, Y.-H., & Ha, S. K. (2008). Distribution of Micro Stresses and Interfacial Tractions in Unidirectional Composites. *Journal of Composite Materials*, *42*(18), 1825–1849. http://doi.org/10.1177/0021998308093909

Jin, K. K., Oh, J. H., & Ha, S. K. (2007). Effect of Fiber Arrangement on Residual Thermal Stress

Distributions in a Unidirectional Composite. *Journal of Composite Materials*, *41*(5), 591–611. http://doi.org/10.1177/0021998306065290

Kaddour, A. S., & Hinton, M. J. (2012). Input data for test cases used in benchmarking triaxial failure theories of composites. *Journal of Composite Materials*, *46*(19–20), 2295–2312. http://doi.org/10.1177/0021998312449886

Kaddour, A. S., & Hinton, M. J. (2013). Maturity of 3D failure criteria for fibre-reinforced composites: Comparison between theories and experiments: Part B of WWFE-II. *Journal of Composite Materials*, *47*(6–7), 925–966. http://doi.org/10.1177/0021998313478710

Kaddour, A. S., Hinton, M. J., Smith, P. A., & Li, S. (2013). A comparison between the predictive capability of matrix cracking, damage and failure criteria for fibre reinforced composite laminates: Part A of the third world-wide failure exercise. *Journal of Composite Materials*, *47*(20–21), 2749–2779. http://doi.org/10.1177/0021998313499476

Kassapoglou, C. (2013). *Design and Analysis of Composite Structures* (Second Edi). Chichester, West Sussex, PO19 8SQ, UK: John Wiley & Sons Ltd.

Kim, M., Park, S., Park, J., Lee, W., & Kim, M. (2013). Micro-mechanical Failure Prediction and Verification for Fiber Reinforced Composite Materials by Multi-scale Modeling Method. *Journal of The Korean Society for Aeronautical and Space Sciences*, *41*(1), 17–24.

Koerber, H., Xavier, J., & Camanho, P. P. (2010). High strain rate characterisation of unidirectional carbon-epoxy IM7-8552 in transverse compression and in-plane shear using digital image correlation. *Mechanics of Materials*, *42*(11), 1004–1019. http://doi.org/10.1016/j.mechmat.2010.09.003

Lee, D., & Yoshioka, K. (2015). Distortional Deformation of Matrix in Open-Hole Tension Composites: Experimental Investigation. In *20th International Conference on Composite Materials (ICCM-20)*. Copenhagen.

Li, R., Kelly, D. W., & Mikulik, Z. (2007). A SIFT Approach for Analysing Failure by Delamination and Disbonding in Composite Structures. *5th Australasian Congress on Applied Mechanics, ACAM*.

Li, R., Kelly, D. W., & Ness, R. (2003). Application of a First Invariant Strain Criterion for Matrix Failure in Composite Materials. *Journal of Composite Materials*, *37*(22), 1977–2000. http://doi.org/10.1177/002199803036268

Li, X., Guan, Z., Li, Z., & Liu, L. (2014). A new stress-based multi-scale failure criterion of composites and its validation in open hole tension tests. *Chinese Journal of Aeronautics*, *27*(6), 1430–1441. http://doi.org/10.1016/j.cja.2014.10.009

Li, X., Guan, Z., Liu, L., & Li, Z. (2013). Damage simulation of composite materials based on strain invariant failure theory. *Journal of Beijing University of Aeronautics and Astronautics*, *39*(2), 190–195.

Li, Z., Guan, Z., & He, W. (2011). Strain invariant failure theory invariant properties of domestic carbon fiber/resin composites. *Acta Materia Compositae Sinica*, *28*(5), 192–196.

Lim, S. H., Pearce, G. M., Kelly, D. W., Prusty, B. G., & Crosky, A. (2013). New Developments in Onset Theory for Onset of Resin Failure in Fibre Reinforced Composites. In *19th International Conference on Composite materials (ICCM-19)*. Montreal, Canada.

Liu, G. (2007). *Damage Progression in Open-Hole Tension Composite Laminates by the Element-Failure Method*. National University of Singapore.

Lu, S. (2015). Compressive damage simulation of carbon fiber reinforced polymer matrix composite laminate open-hole structures based on strain invariant failure theory. *Acta Materia Compositae Sinica*, *32*(6), 1573–1580.

Mallick, P. K. (2007). *Fiber-Reinforced Composites: Materials, Manufacturing, and Design* (Third Edit). CRC Press.

Mao, Y. (2011). *Micromechanical Modelling for Failure of Fibre Reinforced Composite Materials*. The University of New South Wales.

Mayes, J. S., & Hansen, A. C. (2004). Composite laminate failure analysis using multicontinuum theory. *Composites Science and Technology*, (March). http://doi.org/10.1016/B978-008044475-8/50019-6

McNaught, S. (2009). *Implementation of the Strain Invariant Failure Theory for Failure of Composite Materials*. The University of New South Wales.

Mendoza-Jasso, A. J. (2012). *Study of Uncertainty in the Application of the Micromechanical Enhancement Method to Predict Failure Initiation of Fiber Composites*. Purdue University.

Mishra, K. D., & El-Hajjar, R. F. (2012). Non-linear strain invariant failure approach for fibre reinforced composite materials. *International Journal Materials and Structural Integrity*, *6*(2/3/4), 284–296.

Ng, S. J., Felsecker, A., & Meilunas, R. (2004). SIFT Analysis of IM7/5250-4 Composites. In *36th International SAMPE Technical Conference*. San Diego, CA.

Oh, J. H., Jin, K. K., & Ha, S. K. (2006). Interfacial Strain Distribution of a Unidirectional Composite with Randomly Distributed Fibers under Transverse Loading. *Journal of Composite Materials*, *40*(9), 759–778. http://doi.org/10.1177/0021998305055546

Paris, F. (2001). *A Study of Failure Criteria of Fibrous Composite Materials*. Retrieved from http://alpha.tamu.edu/public/2001-cr210661.pdf

Pearce, G. M., & Kelly, D. W. (2012). Pull-Through Failure Prediction for Composite Bolted Joints Using Onset Theory. In *15th European Conference on Composite Materials (ECCM-15)*. Venice, Italy.

Pipes, R. B., & Gosse, J. H. (2009). An Onset Theory for Irreversible Deformation in Composite Materials. In *17th International Conference on Composite Materials (ICCM-17)*. Retrieved from http://www.iccm-central.org/Proceedings/ICCM17proceedings/Themes/Behaviour/ANALYSIS FOR FLIGHT CERT/F2.3 Byron Pipes.pdf

Puck, A., Kopp, J., & Knops, M. (2002). Guidelines for the determination of the parameters in Puck's action plane strength criterion. *Composites Science and Technology*, *62*(3), 371–378. http://doi.org/10.1016/S0266-3538(01)00202-0

Ritchey, A. J. (2012). *Recovery of Microfields in Fiber-Reinforced Composite Materials: Principles and Limitations*. Purdue University.

Ritchey, A. J., Dustin, J. S., Gosse, J. H., & Pipes, R. B. (2011). Self-Consistent Micromechanical

Enhancement of Continuous Fiber Composites. In B. Attaf (Ed.), *Advances in Composite Materials - Ecodesign and Analysis* (pp. 607–624). InTech. Retrieved from http://www.intechopen.com/books/advances-in-composite-materials-ecodesign-and-analysis/self-consistent- micromechanical-enhancement-of-continuous-fiber-composites

Soden, P. D., Hinton, M. J., & Kaddour, A. S. (1998). Lamina Properties, Lay-Up Configurations and Loading Conditions for a Range of Fibre-Reinforced Composite Laminates. *Composites Science and Technology*, *58*, 1011–1022. http://doi.org/10.1016/B978-008044475-8/50003-2

Soden, P. D., Hinton, M. J., & Kaddour, A. S. (2002). Biaxial test results for strength and deformation of a range of E-glass and carbon fibre reinforced composite laminates: failure exercise benchmark data. *Composites Science and Technology*, *62*, 1489–1514. http://doi.org/10.1016/B978-008044475-8/50004-4

Sun, C. T., Quinn, B. J., Tao, J., & Oplinger, D. W. (1996). *Comparative Evaluation of Failure Analysis Methods for Composite Laminates. U.S. Department of Transportation*. Retrieved from http://trid.trb.org/view.aspx?id=523207

Sun, C. T., & Vaidya, R. S. (1996). Prediction of composite properties from a representative volume element. *Composites Science and Technology*, *56*(2), 171–179. http://doi.org/10.1016/0266-3538(95)00141-7

Sun, X. S., Tan, V. B. C., & Tay, T.-E. (2011). Micromechanics-based progressive failure analysis of fibre-reinforced composites with non-iterative element-failure method. *Computers and Structures*, *89*(11–12), 1103–1116. http://doi.org/10.1016/j.compstruc.2010.12.003

Swanson, S. R., & Christoforou, A. P. (1986). Response of Quasi-Isotropic Carbon/Epoxy Laminates to Biaxial Stress. *Journal of Composite Materials*, *20*(5), 457–471. http://doi.org/10.1177/002199838602000504

Swanson, S. R., & Nelson, M. (1986). Failure Properties of Carbon/Epoxy Laminates under Tension-Compression Biaxial Stress. In K. Kawata, S. Umekawa, & A. Kobayashi (Eds.), *Composites '86: Recent Advances in Japan and the United States* (pp. 279–286). Tokyo: Proceedings of the Third Japan-US Conference on Composite Materials.

Swanson, S. R., & Qian, Y. (1992). Multiaxial characterization of T800/3900-2 carbon/epoxy composites. *Composites Science and Technology*, *43*, 197–203.

Tan, S. H. N. (2005). *Modeling Damage in Composites Using the Element-Failure Method*. National University of Singapore.

Tay, T.-E., Tan, S. H. N., Tan, V. B. C., & Gosse, J. H. (2005). Damage progression by the element-failure method (EFM) and strain invariant failure theory (SIFT). *Composites Science and Technology*, *65*(6), 935–944. http://doi.org/10.1016/j.compscitech.2004.10.022

Tay, T.-E., Tan, V. B. C., & Liu, G. (2006). A new integrated micro-macro approach to damage and fracture of composites. *Materials Science and Engineering B: Solid-State Materials for Advanced Technology*, *132*(1–2), 138–142. http://doi.org/10.1016/j.mseb.2006.02.023

Tay, T.-E., Tan, V. B. C., & Tan, S. H. N. (2005). Element-Failure: An Alternative to Material Property Degradation Method for Progressive Damage in Composite Structures. *Journal of Composite Materials*, *39*(18), 1659–1675. http://doi.org/10.1177/0021998305051113

Tran, T. D. (2012). *Development of Micromechanical Modelling Procedures using the Onset Theory*

*for Failure of Composites*. University of New South Wales.

Tran, T. D., Kelly, D. W., Prusty, B. G., Gosse, J. H., & Christensen, S. (2012). Micromechanical modelling for onset of distortional matrix damage of fiber reinforced composite materials. *Composite Structures*, *94*(2), 745–757. http://doi.org/10.1016/j.compstruct.2011.09.009

Tran, T. D., Kelly, D. W., Prusty, B. G., & Pearce, G. M. (2011). Micromechanical Modelling of Test Specimens for Onset of Dilatational Damage of Polymer Matrix in Composite Materials. In *18th International Conference on Composite Meaterials (ICCM-18)*.

Tran, T. D., Kelly, D. W., Prusty, B. G., Pearce, G. M., & Gosse, J. H. (2013). A micromechanical sub-modelling technique for implementing Onset Theory. *Composite Structures*, *103*, 1–8. http://doi.org/10.1016/j.compstruct.2013.03.016

Tran, T. D., Simkins, D., Lim, S. H., Kelly, D. W., Pearce, G. M., Prusty, B. G., … Christensen, S. (2012). Application of a scalar strain-based damage onset theory to the failure of a complex composite specimen. In *28th International Congress of the Aeronautical Sciences*. Retrieved from http://www.icas.org/ICAS_ARCHIVE/ICAS2012/PAPERS/923.PDF

Tsai, H. C., Alper, J., & Barrett, D. (1999). Failure Analysis of Composite Bonded Joints. In *41st Structures, Structural Dynamics, and Materials Conference and Exhibit*. http://doi.org/10.2514/6.2000-1428

Tsai, H. C., & Elmore, J. (2003). SIFT Analysis of TiGr Laminates. In *35th International SAMPE Technical Conference*. Dayton, OH.

Wang, C. H. (2005). Progressive multi-scale modeling of composite laminates. In *Multi-Scale Modelling of Composite Material Systems* (1st Editio, pp. 259–277). Woodhead Publishing. http://doi.org/10.1533/9781845690847.259

Wang, J., & Chiu, W. K. (2011). Enhancing Prediction Accuracy in SIFT Theory. In *18th International Conference on Composite Materials (ICCM-18)*.

Xia, Z., Zhang, Y., & Ellyin, F. (2003). A unified periodical boundary conditions for representative volume elements of composites and applications. *International Journal of Solids and Structures*, *40*(April), 1907–1921. http://doi.org/10.1016/S0020-7683(03)00024-6

Yudhanto, A. (2005). *Effects of Micromechanical Factors in the Strain Invariant Failure Theory for Composites*. National University of Singapore.

Yudhanto, A., Tay, T.-E., & Tan. (2006). Micromechanical Characterization Parameters for a New Failure Criterion for Composite Structures. *Key Engineering Materials*, *306–308*, 781–786. http://doi.org/10.4028/www.scientific.net/KEM.306-308.781

# Appendix A

# Additional Software Description Figures[1]

This appendix contains flowcharts and sample input files for the two software tools developed, namely the micromechanical enhancement software (Section 4.2) and the failure envelope prediction software (Section 4.3). In addition to that, the process used to determine failure envelopes for individual and multiple interrogation points (Subsections 4.3.1 and 4.3.2) is visualized.

The purposes of the flowcharts is to give an overview of the relation of various parts of the software. Dark blue boxes containing white text refer to individual methods. Lighter blue boxes with black text refer to the modules and submodules into which the software is divided. Boxes with black text and white background refer to the data flows between methods. Note that only the essential steps are contained. The flowcharts do not provide a full overview of all capabilities of the software, or of all interconnections between functions. For example, for the micromechanical enhancement software verification capabilities such as plotting convergence graphs (see Appendix C) are excluded.

## A.1 Micromechanical Enhancement Software

For the micromechanical enhancement software, the distribution of flowcharts is as follows: Figure A.1 contains the main file (where the input data is set up), as well as the only task required – initiating the convergence study. Subsequently, Figure A.2 shows some of the details involved in automatically running the convergence study, as well as how a single fiber array type and mesh size is analyzed. This requires calling the dispatch functions that delegate tasks to the Abaqus-internal Python interpreter. The details of that process, as well as generating the model and extracting the results from the ODB, are outlined briefly in Figure A.3.

Finally, Figure A.4 contains the relevant parts of an example input file to show the simplicity of performing the micromechanical enhancement using the software tool developed.

[1] Credit is due to Thijs Papenhuijzen for helping to develop a backronym for the initial placeholder for the title of this appendix (“asdf”).

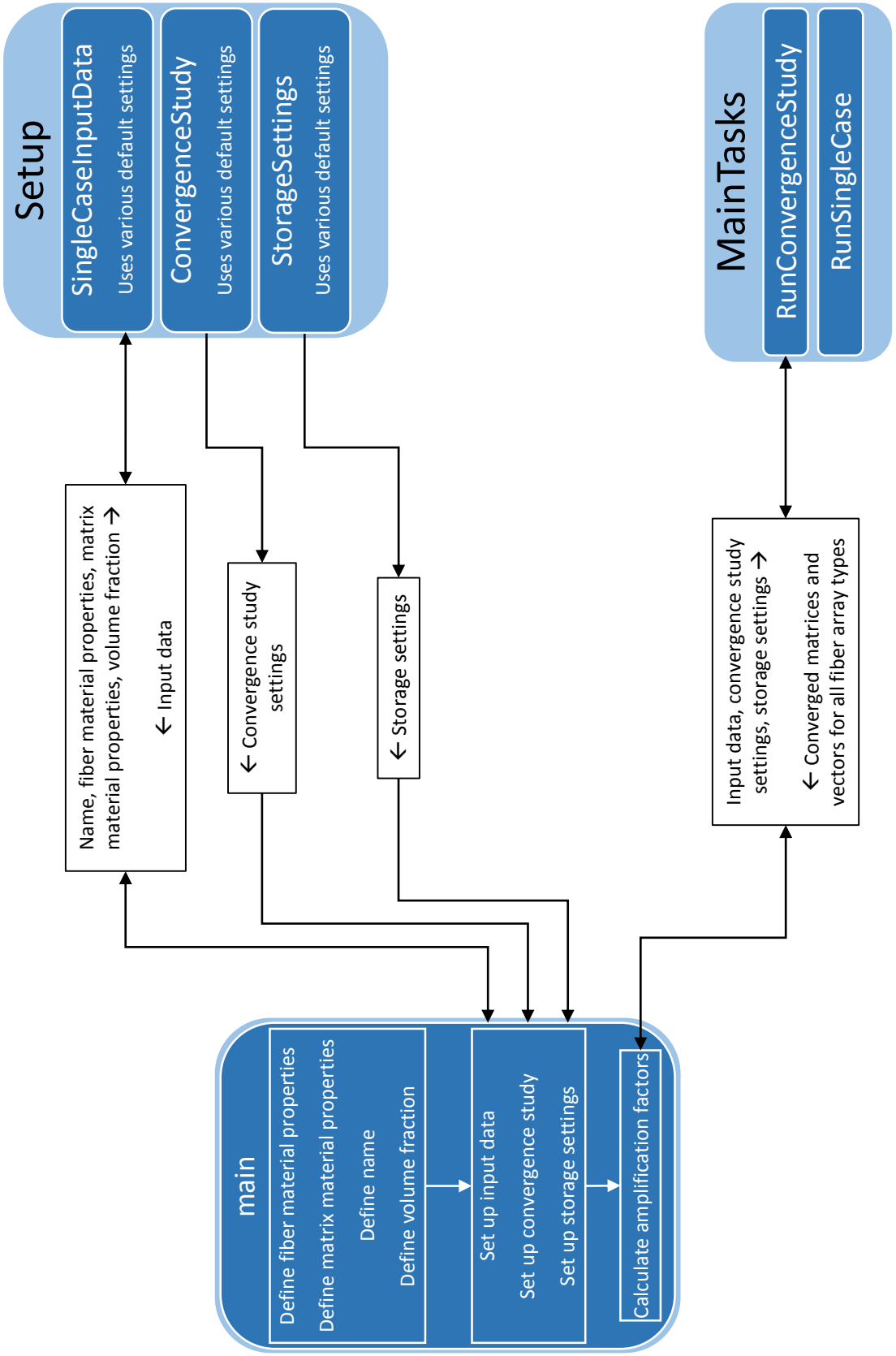


Figure A.1: Micromechanical enhancement software flowchart, part 1

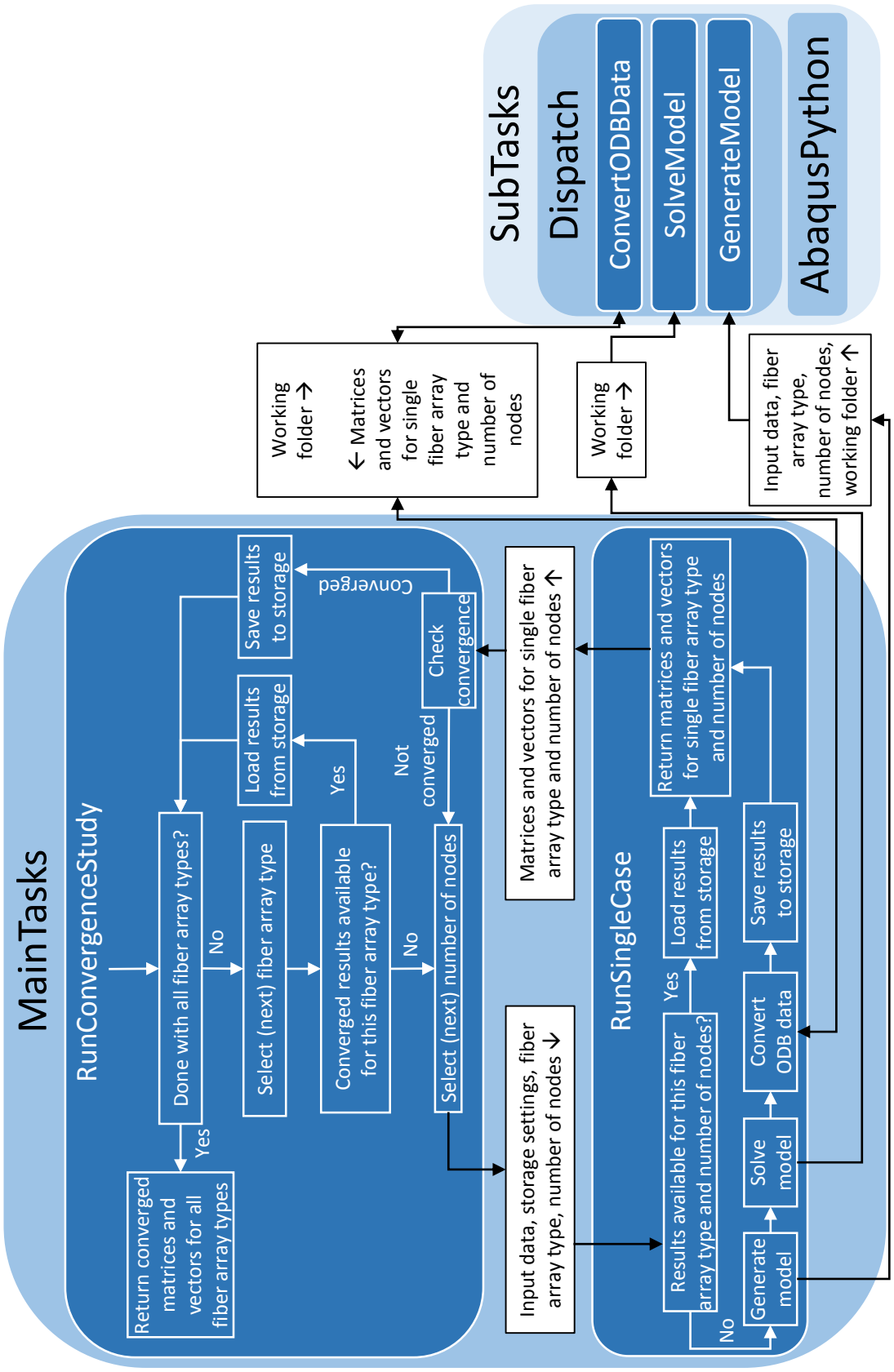


Figure A.2: Micromechanical enhancement software flowchart, part 2

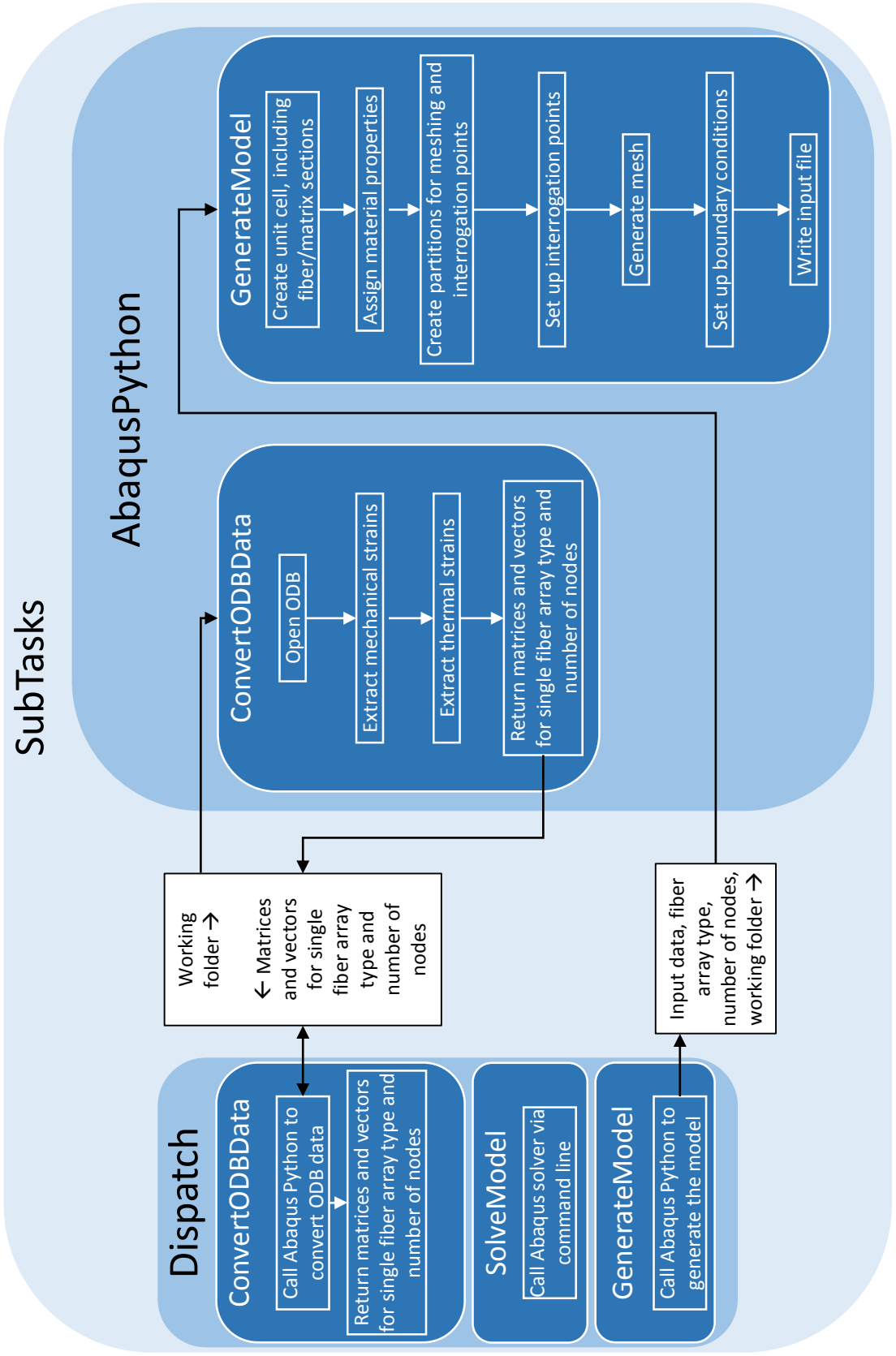


Figure A.3: Micromechanical enhancement software flowchart, part 3

```
# Fiber material properties
fiberMaterialProperties = DataStorage.MaterialProperties.Orthotropic(
    name = "IM7",
    E11 = 276e9,
    E22 = 19.5e9,
    E33 = 19.5e9,
    nu12 = 0.28,
    nu13 = 0.28,
    nu23 = 0.7,
    G12 = 70e9,
    G13 = 70e9,
    G23 = 5.74e9,
    alpha11 = -0.4e-6,
    alpha22 = 5.6e-6,
    alpha33 = 5.6e-6
)

# Matrix material properties
matrixMaterialProperties = DataStorage.MaterialProperties.Isotropic(
    name = "Epoxy8552",
    E = 4.76e9,
    nu = 0.37,
    alpha = 64.8e-6,
)

# Fiber volume fraction
volumeFraction = 0.6

# Resulting input data
inputData = Setup.SingleCaseInputData.CreateWithDefaultSettings(
    name = "VerificationRitchey",
    fiberMaterialProperties = fiberMaterialProperties,
    matrixMaterialProperties = matrixMaterialProperties,
    volumeFraction = volumeFraction)

# Set up convergence study
convergenceStudySetup = Setup.ConvergenceStudy.CreateWithDefaultSettings()

# Storage settings
storageSettings = Setup.StorageSettings.CreateWithDefaultSettings()

# Run mesh convergence
finalMatrices, finalVectors, converged, interrogationPoints = \
    MainTasks.RunConvergenceStudy(convergenceStudySetup, inputData, storageSettings)
```

Figure A.4: Micromechanical enhancement software sample main file (for the verification case in Subsection 5.1.2)

## A.2 Failure Envelope Prediction Software

As for the micromechanical enhancement software, flowcharts (Figures A.5 and A.6) and a sample input file (Figure A.7) are given. In addition to that, the process used to determine failure envelopes and cutoffs numerically is shown in Figures A.8 to A.10.

In the flowcharts, “GetCuringStrainsAndPoissonsEffects”, “GetLocalStrains” and “GenerateAmplificationFactors” are the core parts the software. The former two implement the procedure described in Subsection 3.5.3, while the latter applies the rotated unit cells (Section 3.5.2).

For the visualizations of the numerical approach, pseudo-examples are used, similar to the ones shown in Subsection 2.1.5. It should be mentioned that in reality the resolution is much finer, meaning that the resulting envelope or cutoff is (almost) identical to the real one. Note also that for the envelope in Figure A.8 only part of the data point determination is shown. The process is continued for the full 360° envelope.

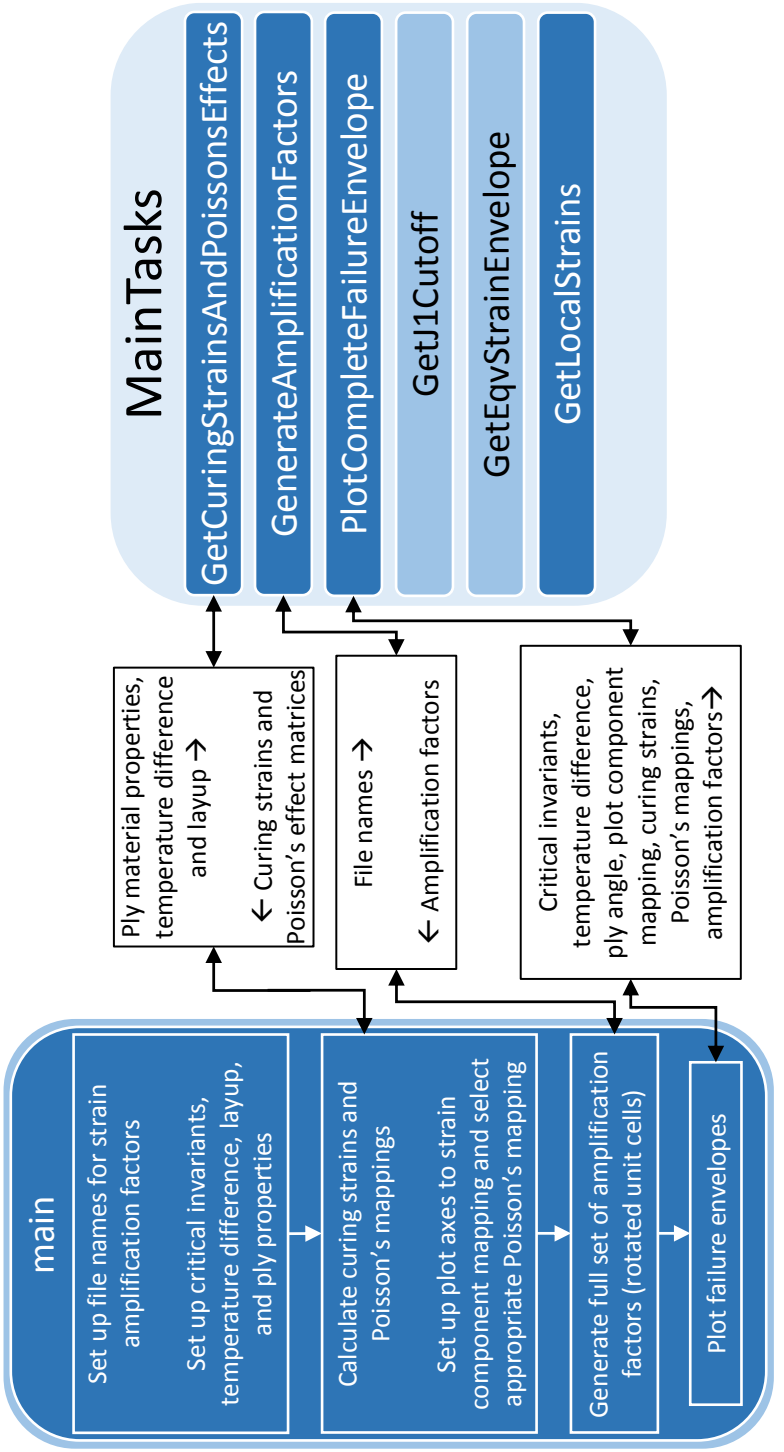


Figure A.5: Failure envelope prediction software flowchart, part 1

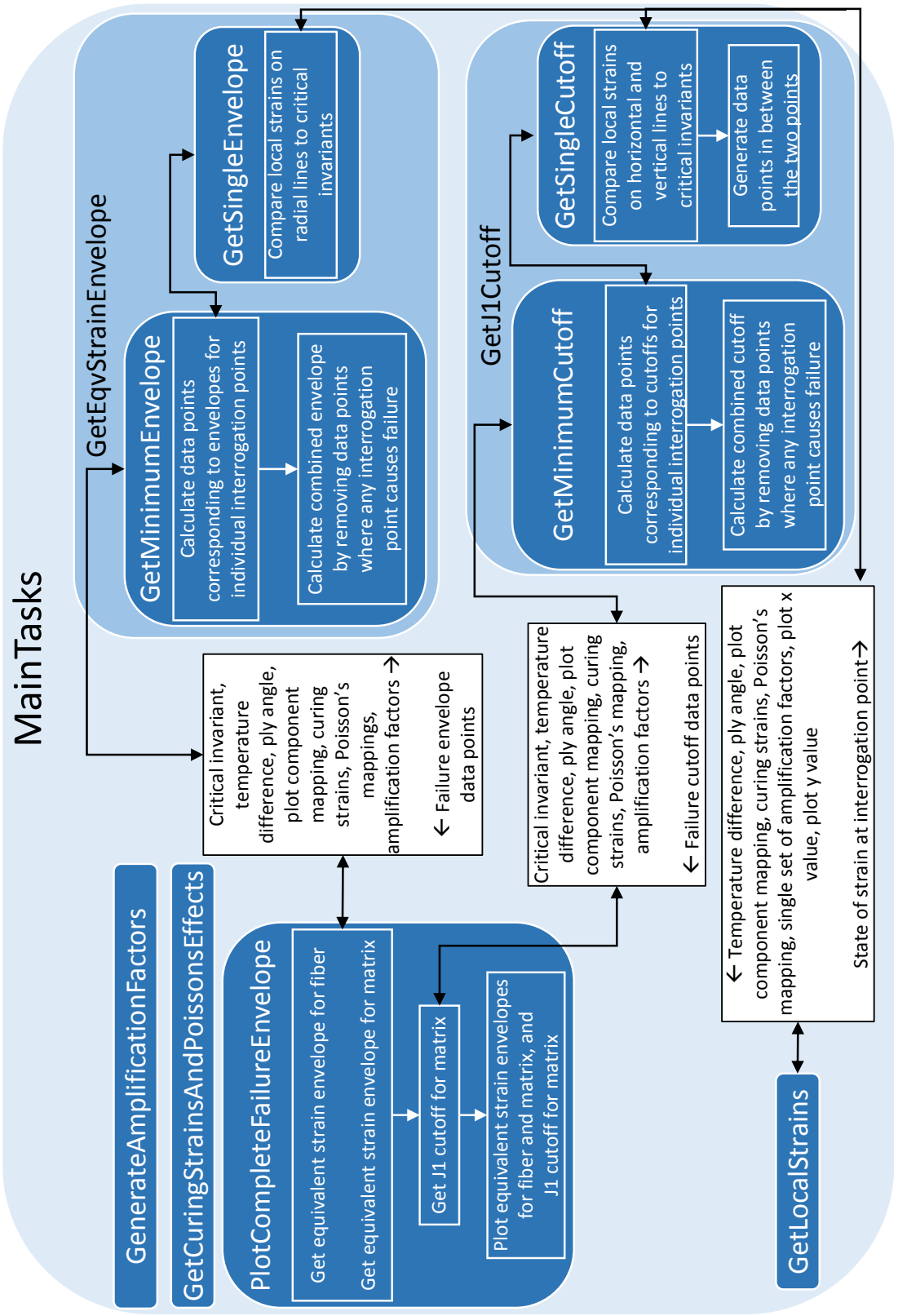


Figure A.6: Failure envelope prediction software flowchart, part 2

```
# Set up amplification factor data files
# File names should be <name><fiber array type><Matrices>.pkl and
# <name><fiber array type><Vectors.pkl>
# e.g. AS4_Epoxy3501_6HexagonalFiberArrayMatrices.pkl
inputDataFolder = "Input Data"

name = "T800s_Epoxy3900_2"

# Set up input data
epsEqvCritFiber = 0.02

epsEqvCritMatrix = 0.118

j1CritMatrix = 0.0225

dT = -140

layup = [0, 90, 45, -45, -45, 45, 90, 0]

# Calculate curing strains and Poisson's effects
curingStrains, PIbiaxialOutOfPlane, PIbiaxialInPlane, PIepsxOutOfPlane, PIepsxInPlane, \
PIepsyOutOfPlane, PIepsyInPlane = MainTasks.GetCuringStrainsAndPoissonsEffects(
    E1 = 152e9,
    E2 = 8e9,
    E3 = 8e9,
    G12 = 4e9,
    G13 = 4e9,
    G23 = 2.75e9,
    nu12 = 0.34,
    nu13 = 0.34,
    nu23 = 0.45,
    alpha1 = 3.6e-8,
    alpha2 = 37.8e-6,
    DeltaT = dT,
    layup = layup)

# Set up mapping from plot axes to strains
plotToGlobalStrainMapping = matrix([[1, 0],   # First column = x, second = y.
                                    [0, 1],   # Typically a column contains a single 1.
                                    [0, 0],   # (For triaxial strains, there may be two)
                                    [0, 0],   # A row should contain at most a single 1.
                                    [0, 0],
                                    [0, 0]])

# Set up Poisson's mapping for applied strains
outOfPlanePoissonsMapping = PIbiaxialOutOfPlane
inPlanePoissonsMapping = PIbiaxialInPlane

# Settings for sensitivity studies
ignoreFiberVariation = True
ignoreMatrixDistortionalVariation = True
ignoreMatrixDilatationalVariation = True

# Create figure
ion()

fig = figure("T800s/3900-2 failure envelope")
axes = fig.gca()

axes.axis("square")

# Generate full set of amplification factors
fiberMatrices, fiberVectors, matrixMatrices, matrixVectors = \
    MainTasks.GenerateAmplificationFactors(inputDataFolder, name)

# Plot failure envelope
with Pool(cpu_count() - 1) as pool:
    for angle in list(set(layup)):
        MainTasks.PlotCompleteFailureEnvelopeParallel(pool, axes, str(angle) + "°",
                                                      inputDataFolder, epsEqvCritFiber,
                                                      epsEqvCritMatrix, j1CritMatrix, dT,
                                                      angle, plotToGlobalStrainMapping,
                                                      curingStrains[angle],
                                                      outOfPlanePoissonsMapping,
                                                      inPlanePoissonsMapping,
                                                      fiberMatrices, fiberVectors,
                                                      matrixMatrices, matrixVectors,
                                                      ignoreFiberVariation,
                                                      ignoreMatrixDistortionalVariation,
                                                      ignoreMatrixDilatationalVariation)

    pool.close()
    pool.join()
```

Figure A.7: Failure envelope prediction software sample main file (for the [0/45/-45/90]s laminate in Subsection 6.3.2). Note that the stacking sequence in the example is shuffled. This is not relevant, as discussed in Subsection 3.2.2.

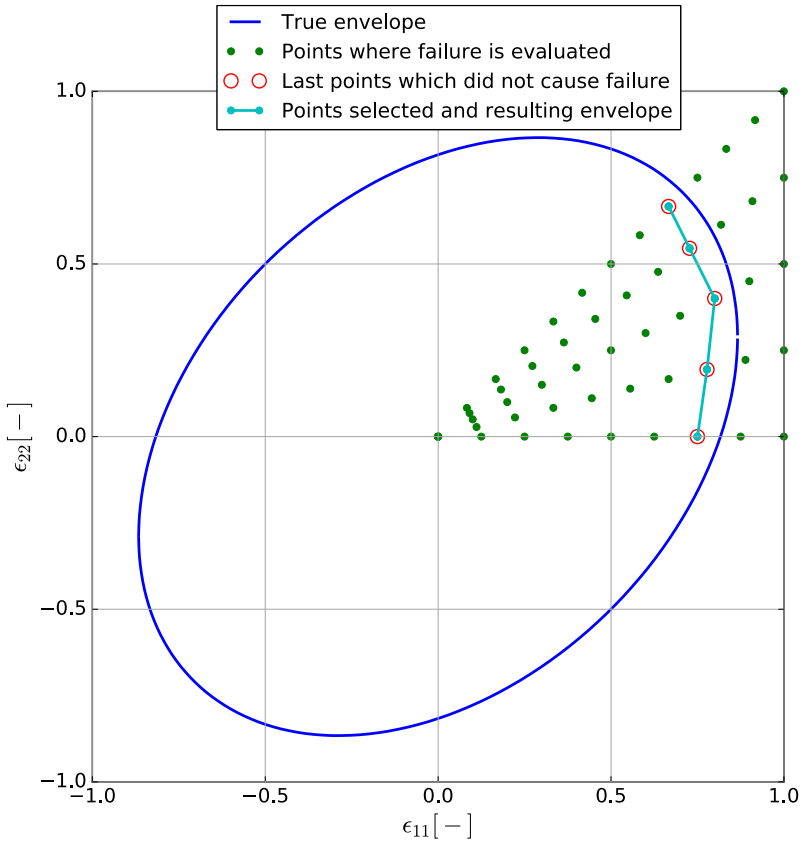


Figure A.8: Visualization of approach to determine the failure envelope numerically

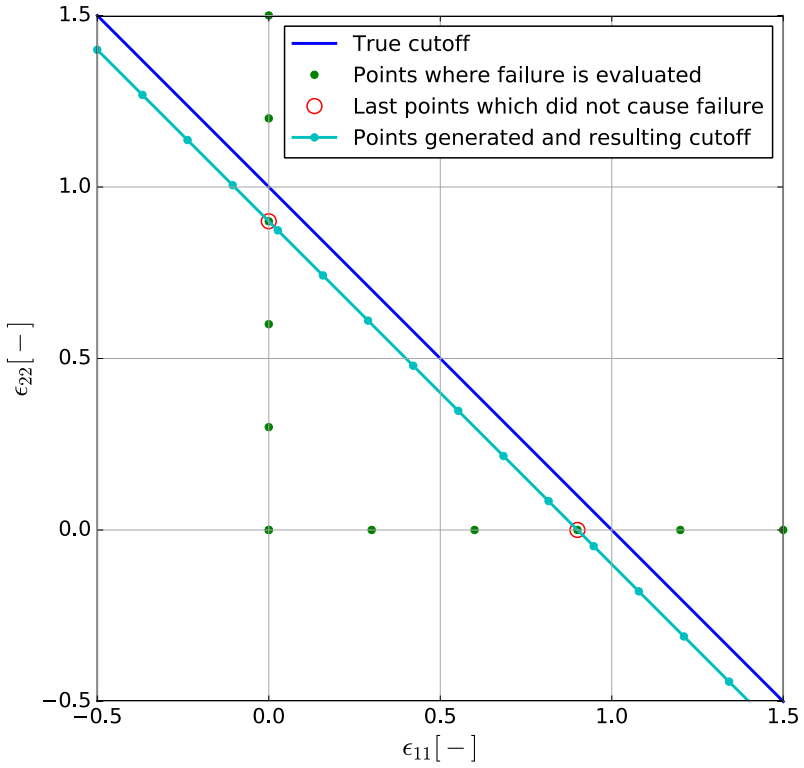


Figure A.9: Visualization of approach to determine the failure cutoff numerically

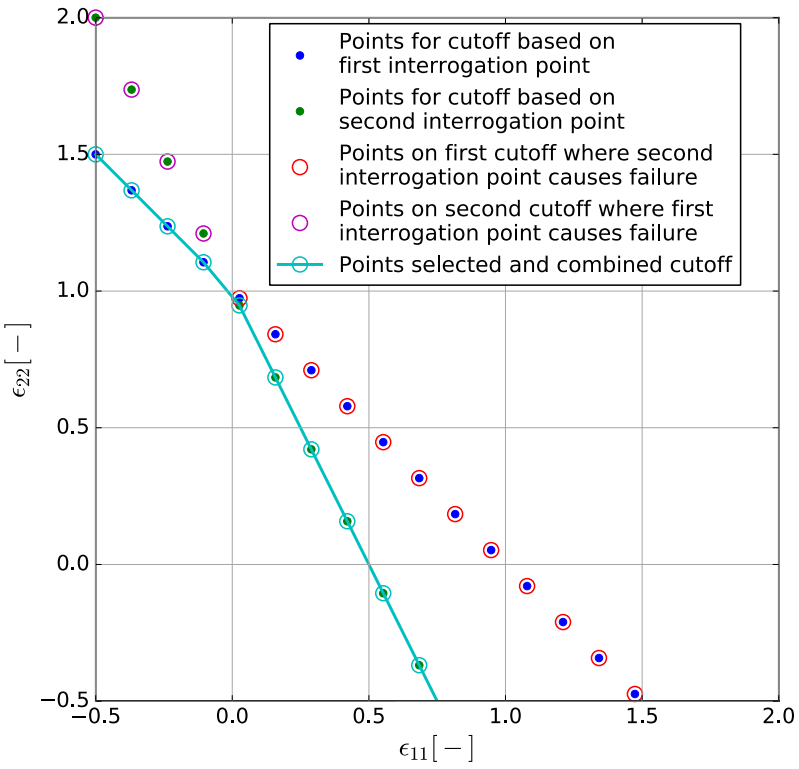


Figure A.10: Visualization of approach to determine the most conservative cutoff for multiple interrogation points

# Appendix B

# Data for Software Verification

This appendix contains the full data for the software verification carried out in Chapter 5.

## B.1 Matrix Amplification Factors for Square Fiber Array

The data used to verify the matrix amplification factors for the square fiber array is taken from (Buchanan et al., 2009). Table B.1 contains the material properties of fiber and matrix (the type of material is not given). Note that the stated shear moduli for the matrix are based on the relationship for isotropic materials, $G = \frac{E}{2(1+\nu)}$. In literature, they are given to be $G_{12} = G_{13} = G_{23} = 1.4\text{GPa}$, in other words twice the calculated value. Presumably this is due to the usage of engineering rather than true shear strains.

Table B.1: Input data for verification of the matrix amplification factors for the square fiber array (Buchanan et al., 2009, Table 2). Note use of relationship for isotropic materials to determine the matrix shear moduli.

| Property | Matrix material | Fiber material |
|---|---|---|
| $E_1$ [Pa] | 2e9 | 303e9 |
| $E_2$ [Pa] | | 15.2e9 |
| $E_3$ [Pa] | | 15.2e9 |
| $G_{12}$ [Pa] | (0.74e9) | 9.6e9 |
| $G_{13}$ [Pa] | | 9.6e9 |
| $G_{23}$ [Pa] | | 6.3e9 |
| $\nu_{12}$ [−] | 0.35 | 0.2 |
| $\nu_{13}$ [−] | | 0.2 |
| $\nu_{23}$ [−] | | 0.2 |
| $\alpha_1$ [$°C^{-1}$] | 58e-6 | 0 |
| $\alpha_2$ [$°C^{-1}$] | | 8.2e-6 |
| $\alpha_3$ [$°C^{-1}$] | | 8.2e-6 |
| | $V_f = 0.6$ | |

(Buchanan et al., 2009) obtain the data shown in Matrices B.1 to B.6. The definitions of IF1, IS and IF2 are the same as shown in Figure 2.9. The thermal amplification factors are scaled to the standard temperature difference of $\Delta T = 1°C$ (unlike the factor $\Delta T = -100°C$ chosen in literature).

The amplification factors at IF1 and IF2 are identical (except for a different arrangement of terms), as expected given the symmetry of the unit cell and loading. However, based on the results reported for IS, it is clear that the mesh is not fully converged. At that location the behavior of the unit cell in $y$- and $z$-directions should be identical. However, for example terms (2,1) and (2,2) of Matrix B.3 are not identical, and neither are terms (3,2) and (2,3) or terms (2,2) and (3,3). Even more obvious is the large difference between the second and third terms of Matrix B.4, which should also be identical. However, it seems plausible that this is an error in print given the magnitude of the difference and the fact that, for example, "380" could quite easily be mistyped as "308".

$$\begin{bmatrix} 1 & 0 & 0 & 0 & 0 & 0 \\ 0.435 & 3.81 & 0.125 & 0 & 0 & 0 \\ -0.135 & -0.52 & 0.61 & 0 & 0 & 0 \\ 0 & 0 & 0 & 2.7 & 0 & 0 \\ 0 & 0 & 0 & 0 & 0.258 & 0 \\ 0 & 0 & 0 & 0 & 0 & 5.45 \end{bmatrix}$$

Matrix B.1: Square array matrix mechanical strain amplification factors at IF1 from literature (Buchanan et al., 2009, Table 4)

$$\begin{bmatrix} -5755 \\ 11444 \\ -6871 \\ 0 \\ 0 \\ 0 \end{bmatrix} \cdot 1\text{e-}8$$

Matrix B.2: Square array matrix thermal strain amplification factors at IF1 from literature (Buchanan et al., 2009, Table 7)

$$\begin{bmatrix} 1 & 0 & 0 & 0 & 0 & 0 \\ 0.09 & 1.07 & 0.537 & 0 & 0 & 0 \\ 0.092 & 0.546 & 1.08 & 0 & 0 & 0 \\ 0 & 0 & 0 & 2.55 & 0 & 0 \\ 0 & 0 & 0 & 0 & 1.8 & 0 \\ 0 & 0 & 0 & 0 & 0 & 1.8 \end{bmatrix}$$

Matrix B.3: Square array matrix mechanical strain amplification factors at IS from literature (Buchanan et al., 2009, Table 5)

$$\begin{bmatrix} -5749 \\ 390 \\ 308 \\ 0 \\ 0 \\ 0 \end{bmatrix} \cdot 1\text{e-}8$$

Matrix B.4: Square array matrix thermal strain amplification factors at IS from literature (Buchanan et al., 2009, Table 7)

$$\begin{bmatrix} 1 & 0 & 0 & 0 & 0 & 0 \\ -0.135 & 0.61 & -0.52 & 0 & 0 & 0 \\ 0.435 & 0.125 & 3.81 & 0 & 0 & 0 \\ 0 & 0 & 0 & 2.7 & 0 & 0 \\ 0 & 0 & 0 & 0 & 5.45 & 0 \\ 0 & 0 & 0 & 0 & 0 & 0.258 \end{bmatrix}$$

Matrix B.5: Square array matrix mechanical strain amplification factors at IF2 from literature (Buchanan et al., 2009, Table 6)

$$\begin{bmatrix} -5755 \\ -6871 \\ 11444 \\ 0 \\ 0 \\ 0 \end{bmatrix} \cdot 1\text{e-}8$$

Matrix B.6: Square array matrix thermal strain amplification factors at IF2 from literature (Buchanan et al., 2009, Table 7)

Using the software tool developed during this thesis, the data shown in Matrices B.7 to B.12 is obtained. Contrary to the literature results, these results point towards a fully converged mesh, with all terms that should be the same indeed being identical (including the results at IS).

$$\begin{bmatrix} 1 & 0 & 0 & 0 & 0 & 0 \\ 0.4235 & 3.79 & 0.07776 & 0 & 0 & 0 \\ -0.1325 & -0.5039 & 0.6064 & 0 & 0 & 0 \\ 0 & 0 & 0 & 2.625 & 0 & 0 \\ 0 & 0 & 0 & 0 & 0.2608 & 0 \\ 0 & 0 & 0 & 0 & 0 & 5.395 \end{bmatrix}$$

Matrix B.7: Square array matrix mechanical strain amplification factors at IF1

$$\begin{bmatrix} -5711 \\ 11450 \\ -6929 \\ 0 \\ 0 \\ 0 \end{bmatrix} \cdot 1\text{e-}8$$

Matrix B.8: Square array matrix thermal strain amplification factors at IF1

$$\begin{bmatrix} 1 & 0 & 0 & 0 & 0 & 0 \\ 0.08933 & 1.079 & 0.5258 & 0 & 0 & 0 \\ 0.08933 & 0.5258 & 1.079 & 0 & 0 & 0 \\ 0 & 0 & 0 & 2.598 & 0 & 0 \\ 0 & 0 & 0 & 0 & 1.808 & 0 \\ 0 & 0 & 0 & 0 & 0 & 1.808 \end{bmatrix}$$

Matrix B.9: Square array matrix mechanical strain amplification factors at IS

$$\begin{bmatrix} -5711 \\ 404.8 \\ 404.8 \\ 0 \\ 0 \\ 0 \end{bmatrix} \cdot 1\text{e-}8$$

Matrix B.10: Square array matrix thermal strain amplification factors at IS

$$\begin{bmatrix} 1 & 0 & 0 & 0 & 0 & 0 \\ -0.1325 & 0.6064 & -0.5039 & 0 & 0 & 0 \\ 0.4235 & 0.07776 & 3.79 & 0 & 0 & 0 \\ 0 & 0 & 0 & 2.625 & 0 & 0 \\ 0 & 0 & 0 & 0 & 5.395 & 0 \\ 0 & 0 & 0 & 0 & 0 & 0.2608 \end{bmatrix}$$

Matrix B.11: Square array matrix mechanical strain amplification factors at IF2

$$\begin{bmatrix} -5711 \\ -6929 \\ 11450 \\ 0 \\ 0 \\ 0 \end{bmatrix} \cdot 1\text{e-}8$$

Matrix B.12: Square array matrix thermal strain amplification factors at IF2

## B.2 Matrix Amplification Factors for Hexagonal Fiber Array

The data used to verify the matrix amplification factors for the square fiber array is taken from (Ritchey et al., 2011). Table B.2 contains the material properties of fiber and matrix.

Table B.2: Input data for verification of the matrix amplification factors for the hexagonal fiber array (Ritchey et al., 2011, Table 1)

| Property | Matrix (8552) | Fiber (IM7) |
|---|---|---|
| $E_1$ [Pa] | 4.76e9 | 276e9 |
| $E_2$ [Pa] | | 19.5e9 |
| $E_3$ [Pa] | | 19.5e9 |
| $G_{12}$ [Pa] | 1.74e9 | 70e9 |
| $G_{13}$ [Pa] | | 70e9 |
| $G_{23}$ [Pa] | | 5.74e9 |
| $\nu_{12}$ [−] | 0.37 | 0.28 |
| $\nu_{13}$ [−] | | 0.28 |
| $\nu_{23}$ [−] | | 0.28 |
| $\alpha_1$ [$°C^{-1}$] | 64.8e-6 | -0.4e-6 |
| $\alpha_2$ [$°C^{-1}$] | | 5.6e-6 |
| $\alpha_3$ [$°C^{-1}$] | | 5.6e-6 |

$$V_f = 0.6$$

(Ritchey et al., 2011) report the strain amplification factors at a point corresponding to IF2 for the hexagonal array in Figure 2.9. However, they use a hexagonal unit cell with the $y$-direction being the shorter of the two sides. Because the software tool uses a unit cell where the $y$-direction refers to the long side, the literature results have to be rotated by 90° before the comparison can take place. This procedure has been discussed in Section 3.3 and, given the rotation angle of 90°, only results in swapping several terms of the matrix (and correspondingly also of the vector). The resulting mechanical and thermal amplification factors are shown in Matrices B.13 and B.14. Note that they appear to have been rounded to one decimal.

$$\begin{bmatrix} 1 & 0 & 0 & 0 & 0 & 0 \\ -0.2 & 0.6 & -0.5 & 0 & 0 & 0 \\ 0.6 & 0.3 & 2.8 & 0 & 0 & 0 \\ 0 & 0 & 0 & 1.4 & 0 & 0 \\ 0 & 0 & 0 & 0 & 4.7 & 0 \\ 0 & 0 & 0 & 0 & 0 & 0.3 \end{bmatrix}$$

Matrix B.13: Hexagonal array matrix mechanical strain amplification factors at IF2 from literature (Ritchey et al., 2011, Table 4)

$$\begin{bmatrix} -64 \\ -60 \\ 90 \\ 0 \\ 0 \\ 0 \end{bmatrix} \cdot 1\text{e-}6$$

Matrix B.14: Hexagonal array matrix thermal strain amplification factors at IF2 from literature (Ritchey et al., 2011, Table 5)

From the software tool, the results shown in Matrices B.15 and B.16 are obtained. It should be mentioned that the convergence study did not conclude, even at a mesh size of 510 985 nodes. However, using the command line output (see also Appendix C) this could be traced to points unrelated to the point of interest. This is a typical case of results oscillating around the numerical cutoff described in Subsection 4.2.6, both in terms of element result averaging and also in terms of mesh convergence from one mesh size to the next. Even though the automatic approach failed to converge, the results are still usable because the lack of convergence is limited to a small region of the unit cell, and, in fact, will not even have a large effect there because the problematic values are small.

$$\begin{bmatrix} 1 & 0 & 0 & 0 & 0 & 0 \\ -0.1503 & 0.9514 & -0.5344 & 0 & 0 & 0 \\ 0.5983 & 0.5277 & 2.793 & 0 & 0 & 0 \\ 0 & 0 & 0 & 1.404 & 0 & 0 \\ 0 & 0 & 0 & 0 & 4.684 & 0 \\ 0 & 0 & 0 & 0 & 0 & 0.3124 \end{bmatrix}$$

Matrix B.15: Hexagonal array matrix mechanical strain amplification factors at IF2

$$\begin{bmatrix} -64.39 \\ -59.01 \\ 87.01 \\ 0 \\ 0 \\ 0 \end{bmatrix} \cdot 1\text{e-}6$$

Matrix B.16: Hexagonal array matrix thermal strain amplification factors at IF2

Since the literature results have been rounded to one decimal, the same process was carried out for the results obtained from the software tool. Matrices B.17 and B.18 show the results.

$$\begin{bmatrix} 1 & 0 & 0 & 0 & 0 & 0 \\ -0.2 & 1 & -0.5 & 0 & 0 & 0 \\ 0.6 & 0.5 & 2.8 & 0 & 0 & 0 \\ 0 & 0 & 0 & 1.4 & 0 & 0 \\ 0 & 0 & 0 & 0 & 4.7 & 0 \\ 0 & 0 & 0 & 0 & 0 & 0.3 \end{bmatrix}$$

Matrix B.17: Rounded hexagonal array matrix mechanical strain amplification factors at IF2

$$\begin{bmatrix} -64 \\ -59 \\ 87 \\ 0 \\ 0 \\ 0 \end{bmatrix} \cdot 1\text{e-}6$$

Matrix B.18: Rounded Hexagonal array matrix thermal strain amplification factors at IF2

## B.3 Fiber Amplification Factors for Square Fiber Array

The data used to verify the matrix amplification factors for the square fiber array is taken from (McNaught, 2009). Table B.3 contains the material properties of fiber and matrix. For the fiber, properties such as $G_{13}$ or $G_{23}$ are not given. Isotropy is assumed to obtain a full set of input data.

Table B.3: Input data for verification of the fiber amplification factors for the square fiber array (McNaught, 2009, Table 6-1). Note that isotropy is assumed for fiber material properties.

| Property | Matrix (RTM6) | Fiber (E-glass) |
|---|---|---|
| $E_1$ [Pa] | 2.8e9 | 45e9 |
| $E_2$ [Pa] | | 12e9 |
| $E_3$ [Pa] | | 12e9 |
| $G_{12}$ [Pa] | 1e9 | 5.5e9 |
| $G_{13}$ [Pa] | | (5.5e9) |
| $G_{23}$ [Pa] | | (5.5e9) |
| $\nu_{12}$ [−] | 0.38 | 0.28 |
| $\nu_{13}$ [−] | | (0.28) |
| $\nu_{23}$ [−] | | (0.28) |
| $\alpha_1$ [$°C^{-1}$] | 54e-6 | 7.1e-6 |
| $\alpha_2$ [$°C^{-1}$] | | (7.1e-6) |
| $\alpha_3$ [$°C^{-1}$] | | (7.1e-6) |

$$V_f = 0.6$$

(McNaught, 2009) reports values corresponding to locations at the center of the fiber and in the fiber on the fiber/matrix boundary at 0° and 90° (corresponding to e.g. points F3 and F5 of Figure 2.10). In addition to that, data for IF1, IF2 and IS (as shown in Figure 2.9) are also given. Since this part of the verification effort is concerned with fiber amplification factors, only the points at the center of the fiber and at 0° and 90° are included here (see Matrices B.19 to B.21). The order of shear amplification factors has been switched to adhere to the standard convention (see Subsection 2.1.4). Note that the results show the expected features. At the fiber center, $y$- and $z$-directions are identical, while at 0° and 90° results are identical except for a different arrangement of terms.

The results obtained using the software tool developed in this thesis are reported in Matrices B.22 to B.27. The thermal amplification factors are also included for reference purposes, although they cannot be verified due to a lack of literature data.

$$\begin{bmatrix} 1 & 0 & 0 & 0 & 0 & 0 \\ -0.0487 & 0.771 & -0.046 & 0 & 0 & 0 \\ -0.0487 & -0.046 & 0.796 & 0 & 0 & 0 \\ 0 & 0 & 0 & 0.44 & 0 & 0 \\ 0 & 0 & 0 & 0 & 0.54 & 0 \\ 0 & 0 & 0 & 0 & 0 & 0.54 \end{bmatrix}$$

Matrix B.19: Square array fiber mechanical strain amplification factors at the center of the fiber from literature (McNaught, 2009, Appendix A)

$$\begin{bmatrix} 1 & 0 & 0 & 0 & 0 & 0 \\ -0.0688 & 0.55 & 0.085 & 0 & 0 & 0 \\ -0.0235 & 0.042 & 0.834 & 0 & 0 & 0 \\ 0 & 0 & 0 & 0.61 & 0 & 0 \\ 0 & 0 & 0 & 0 & 0.73 & 0 \\ 0 & 0 & 0 & 0 & 0 & 0.44 \end{bmatrix}$$

Matrix B.20: Square array fiber mechanical strain amplification factors at 0° on the fiber/matrix boundary from literature (McNaught, 2009, Appendix A)

$$\begin{bmatrix} 1 & 0 & 0 & 0 & 0 & 0 \\ -0.0235 & 0.834 & 0.042 & 0 & 0 & 0 \\ -0.0688 & 0.085 & 0.55 & 0 & 0 & 0 \\ 0 & 0 & 0 & 0.61 & 0 & 0 \\ 0 & 0 & 0 & 0 & 0.44 & 0 \\ 0 & 0 & 0 & 0 & 0 & 0.73 \end{bmatrix}$$

Matrix B.21: Square array fiber mechanical strain amplification factors at 90° on the fiber/matrix boundary from literature (McNaught, 2009, Appendix A)

$$\begin{bmatrix} 1 & 0 & 0 & 0 & 0 & 0 \\ -0.04848 & 0.7985 & -0.04671 & 0 & 0 & 0 \\ -0.04848 & -0.04671 & 0.7895 & 0 & 0 & 0 \\ 0 & 0 & 0 & 0.325 & 0 & 0 \\ 0 & 0 & 0 & 0 & 0.5486 & 0 \\ 0 & 0 & 0 & 0 & 0 & 0.5486 \end{bmatrix}$$

Matrix B.22: Square array fiber mechanical strain amplification factors at the center of the fiber

$$\begin{bmatrix} 2085 \\ 2008 \\ 2008 \\ 0 \\ 0 \\ 0 \end{bmatrix} \cdot 1\text{e-}9$$

Matrix B.23: Square array fiber thermal strain amplification factors at the center of the fiber

$$\begin{bmatrix} 1 & 0 & 0 & 0 & 0 & 0 \\ -0.06521 & 0.5542 & 0.09984 & 0 & 0 & 0 \\ -0.02291 & 0.04314 & 0.8353 & 0 & 0 & 0 \\ 0 & 0 & 0 & 0.4831 & 0 & 0 \\ 0 & 0 & 0 & 0 & 0.7204 & 0 \\ 0 & 0 & 0 & 0 & 0 & 0.4219 \end{bmatrix}$$

Matrix B.24: Square array fiber mechanical strain amplification factors at 0° on the fiber/matrix boundary

$$\begin{bmatrix} 2085 \\ -5353 \\ 13260 \\ 0 \\ 0 \\ 0 \end{bmatrix} \cdot 1\text{e-}9$$

Matrix B.25: Square array fiber thermal strain amplification factors at 0° the on fiber/matrix boundary

$$\begin{bmatrix} 1 & 0 & 0 & 0 & 0 & 0 \\ -0.02291 & 0.8353 & 0.04314 & 0 & 0 & 0 \\ -0.06521 & 0.09984 & 0.5542 & 0 & 0 & 0 \\ 0 & 0 & 0 & 0.4831 & 0 & 0 \\ 0 & 0 & 0 & 0 & 0.4219 & 0 \\ 0 & 0 & 0 & 0 & 0 & 0.7204 \end{bmatrix}$$

Matrix B.26: Square array fiber mechanical strain amplification factors at 90° on the fiber/matrix boundary

$$\begin{bmatrix} 2085 \\ 13260 \\ -5353 \\ 0 \\ 0 \\ 0 \end{bmatrix} \cdot 1\text{e-}9$$

Matrix B.27: Square array fiber thermal strain amplification factors at 90° the on fiber/matrix boundary

## B.4 Fiber Amplification Factors for Hexagonal Fiber Array

Table B.4 contains the input data used by (Yudhanto, 2005). It seems noteworthy here that Yudhanto states the material combination as IM7/Epoxy, while Tran gives virtually identical material properties for T800s/3900-2 (see Section D.2).

Based on this, Yudhanto reports amplification factors for four unique locations: the center of the fiber, and points at 0°, 45° and 90° on the fiber boundary (points F9, F3, F2, and F1, respectively, in Figure 2.13). Other points are mirror images of F1, F3, and F2 and do not carry any added value. As stated in the introduction to Section 5.1, the only terms that can be compared are the diagonal terms of the mechanical amplification factors. Matrices B.28 to B.31 contain Yudhanto's results.

The order of shear components has been switched to follow the standard convention (Subsection 2.1.4).

Table B.4: Input data for verification of the fiber amplification factors for the hexagonal fiber array (Yudhanto, 2005, Table 4-1)

| Property | Matrix (epoxy) | Fiber (IM7) |
|---|---|---|
| $E_1$ [Pa] | 3.31e9 | 303e9 |
| $E_2$ [Pa] | | 15.2e9 |
| $E_3$ [Pa] | | 15.2e9 |
| $G_{12}$ [Pa] | 1.23e9 | 9.65e9 |
| $G_{13}$ [Pa] | | 9.65e9 |
| $G_{23}$ [Pa] | | 6.32e9 |
| $\nu_{12}$ [−] | 0.35 | 0.2 |
| $\nu_{13}$ [−] | | 0.2 |
| $\nu_{23}$ [−] | | 0.2 |
| $\alpha_1$ [$°C^{-1}$] | 57.6e-6 | 0 |
| $\alpha_2$ [$°C^{-1}$] | | 8.28e-6 |
| $\alpha_3$ [$°C^{-1}$] | | 8.28e-6 |

$$V_f = 0.5$$

$$\begin{bmatrix} 1 & & & & & \\ & 0.477 & & & ? & \\ & & 0.506 & & & \\ & & & 0.564 & & \\ & ? & & & 0.394 & \\ & & & & & 0.348 \end{bmatrix}$$

Matrix B.28: Hexagonal array fiber mechanical strain amplification factors at the center of the fiber from literature (Yudhanto, 2005, Appendix A)

$$\begin{bmatrix} 1 & & & & & \\ & 0.579 & & & ? & \\ & & 0.531 & & & \\ & & & 0.462 & & \\ & ? & & & 0.343 & \\ & & & & & 0.396 \end{bmatrix}$$

Matrix B.29: Hexagonal array fiber mechanical strain amplification factors at 0° on the fiber/matrix boundary from literature (Yudhanto, 2005, Appendix A)

$$\begin{bmatrix} 1 & & & & & \\ & 0.58 & & & ? & \\ & & 0.638 & & & \\ & & & 0.332 & & \\ & ? & & & 0.391 & \\ & & & & & 0.344 \end{bmatrix}$$

Matrix B.30: Hexagonal array matrix mechanical strain amplification factors at 45° on the fiber/matrix boundary from literature (Yudhanto, 2005, Appendix A)

$$\begin{bmatrix} 1 & & & & & \\ & 0.565 & & & ? & \\ & & 0.563 & & & \\ & & & 0.468 & & \\ & ? & & & 0.368 & \\ & & & & & 0.369 \end{bmatrix}$$

Matrix B.31: Hexagonal array fiber mechanical strain amplification factors at 90° on the fiber/matrix boundary from literature (Yudhanto, 2005, Appendix A)

Full results for those points, including the entire amplification factor matrix (rather than just the diagonal terms) and the thermal amplification factors using the correct boundary conditions, are reported in Matrices B.32 to B.39, although they cannot be verified using literature results. It should be mentioned that the results at F2 are not exactly at 45° but at a slightly different location due to the automatic generation of interrogation point locations. This causes small deviations everywhere, including for example the introduction of the (6,5) and (5,6) terms of Matrix B.34.

$$\begin{bmatrix} 1 & 0 & 0 & 0 & 0 & 0 \\ -0.03117 & 0.4841 & 0.1607 & 0 & 0 & 0 \\ -0.02843 & 0.1641 & 0.521 & 0 & 0 & 0 \\ 0 & 0 & 0 & 0.5441 & 0 & 0 \\ 0 & 0 & 0 & 0 & 0.3898 & 0 \\ 0 & 0 & 0 & 0 & 0 & 0.3463 \end{bmatrix}$$

Matrix B.32: Hexagonal array fiber mechanical strain amplification factors at the center of the fiber

$$\begin{bmatrix} 691.2 \\ 2207 \\ 4837 \\ 0 \\ 0 \\ 0 \end{bmatrix} \cdot 1\text{e-}9$$

Matrix B.33: Hexagonal array fiber thermal strain amplification factors at the center of the fiber

$$\begin{bmatrix} 1 & 0 & 0 & 0 & 0 & 0 \\ -0.028425 & 0.5763 & 0.099845 & -0.05952 & 0 & 0 \\ 0.03115 & 0.1082 & 0.5369 & 0.049925 & 0 & 0 \\ 0 & -0.09573 & 0.101 & 0.4358 & 0 & 0 \\ 0 & 0 & 0 & 0 & 0.3467 & 0.0038465 \\ 0 & 0 & 0 & 0 & 0.00322 & 0.3899 \end{bmatrix}$$

Matrix B.34: Hexagonal array fiber mechanical strain amplification factors at 0° on the fiber/matrix boundary

$$\begin{bmatrix} 691.2 \\ 4842 \\ 2226 \\ 445.4 \\ 0 \\ 0 \end{bmatrix} \cdot 1\text{e-}9$$

Matrix B.35: Hexagonal array fiber thermal strain amplification factors at 0° on the fiber/matrix boundary

$$\begin{bmatrix} 1 & 0 & 0 & 0 & 0 & 0 \\ -0.03117 & 0.5802 & 0.06462 & 0 & 0 & 0 \\ -0.02836 & 0.03998 & 0.6369 & 0 & 0 & 0 \\ 0 & 0 & 0 & 0.3468 & 0 & 0 \\ 0 & 0 & 0 & 0 & 0.3907 & 0 \\ 0 & 0 & 0 & 0 & 0 & 0.3466 \end{bmatrix}$$

Matrix B.36: Hexagonal array fiber mechanical strain amplification factors at 45° on the fiber/matrix boundary

$$\begin{bmatrix} 691.2 \\ 2210 \\ 4905 \\ 0 \\ 0 \\ 0 \end{bmatrix} \cdot 1\text{e-}9$$

Matrix B.37: Hexagonal array fiber thermal strain amplification factors at 45° on the fiber/matrix boundary

$$\begin{bmatrix} 1 & 0 & 0 & 0 & 0 & 0 \\ -0.02978 & 0.5635 & 0.09711 & 0 & 0 & 0 \\ -0.02978 & 0.09706 & 0.5636 & 0 & 0 & 0 \\ 0 & 0 & 0 & 0.4671 & 0 & 0 \\ 0 & 0 & 0 & 0 & 0.3684 & 0 \\ 0 & 0 & 0 & 0 & 0 & 0.3684 \end{bmatrix}$$

Matrix B.38: Hexagonal array fiber mechanical strain amplification factors at 90° on the fiber/matrix boundary

$$\begin{bmatrix} 691.2 \\ 3539 \\ 3539 \\ 0 \\ 0 \\ 0 \end{bmatrix} \cdot 1\text{e-}9$$

Matrix B.39: Hexagonal array fiber thermal strain amplification factors at 90° on the fiber/matrix boundary

## B.5 Hart-Smith's Failure Envelopes

Table B.5 summarizes the input data given by (Hart-Smith, 2007), used in Subsections 5.2.3 to 5.2.5. Figure B.1 contains an additional plot referenced in Subsection 5.2.4.

Table B.5: Input data for verification of failure envelopes (Hart-Smith, 2007, Slides 17-20). Note use of imperial units. As discussed in Subsection 6.2.3 ${\epsilon^*_{eqv}}^m$ is probably using an incorrect definition of the distortional invariant.

| Property | Matrix material | Fiber material | Lamina |
|---|---|---|---|
| $E_1$ [psi] | 5.5e5 | 3.93e7 | 23 800 000 |
| $E_2$ [psi] | | 2.5e6 | 1 033 835 |
| $E_3$ [psi] | | 2.5e6 | 1 033 835 |
| $G_{12}$ [psi] | 2.05e5 | 4e6 | 475 914 |
| $G_{13}$ [psi] | | 4e6 | 475 914 |
| $G_{23}$ [psi] | | 1.2e6 | 407 960 |
| $\nu_{12}$ [−] | 0.34 | 0.32 | 0.328 |
| $\nu_{13}$ [−] | | 0.32 | 0.328 |
| $\nu_{23}$ [−] | | 0.2 | 0.256 |
| $\alpha_1$ [$°F^{-1}$] | 3.2e-5 | -6e-7 | -2.99e-7 |
| $\alpha_2$ [$°F^{-1}$] | | 4.6e-6 | 1.56e-5 |
| $\alpha_3$ [$°F^{-1}$] | | 4.6e-6 | 1.56e-5 |

$V_f = 0.6$ $\quad \Delta T = -300°F$

$J_1^{*m} = 0.023$ $\quad {\epsilon^*_{eqv}}^m = 0.103$ $\quad {\epsilon^*_{eqv}}^f = 0.0182$

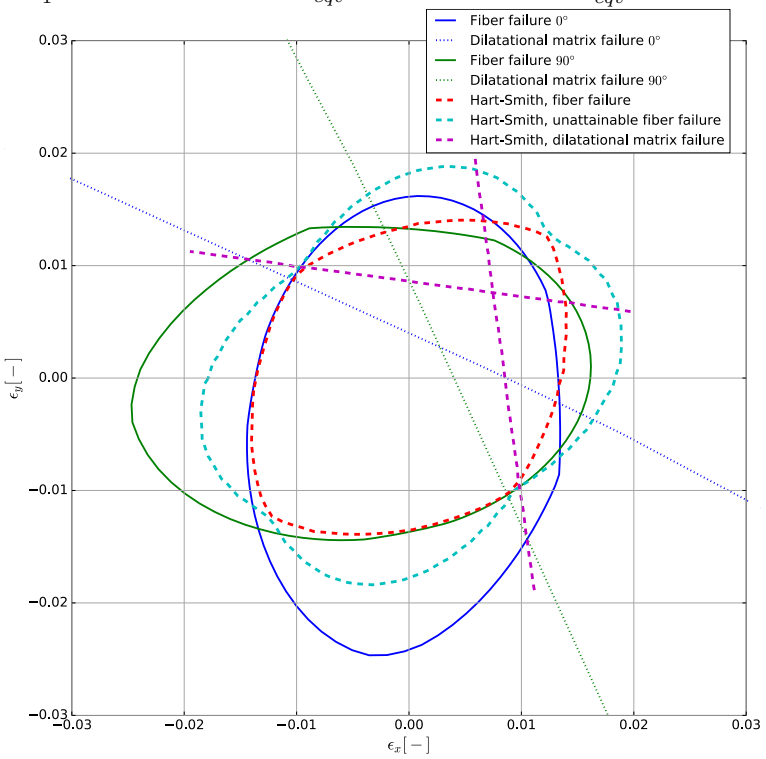


Figure B.1: Comparison of correct normal strain [0/90/90/0] laminate failure envelope with Hart-Smith's envelope (Hart-Smith, 2010, fig. 23). See also Subsection 5.2.4.

# Appendix C

## Example Convergence Study

This appendix contains an example convergence study for the verification case presented in Subsection 5.1.1. As stated in Subsection 4.2.5, where the process of performing an automated convergence study has been introduced, this task is actually carried out in the background for every set of amplification factors used in this thesis. Reporting the details every time would be unfeasible. However, it is useful to provide one example to show the extent of tasks carried out automatically.

Figure C.1 shows the convergence study for the mechanical amplification factors at IS (defined in accordance with Figure 2.9), while Figure C.2 contains the same information for the thermal amplification factors. Clearly, the mesh is fully converged at this point for all mesh sizes. This means that the interrogation point at IS are not the driving factor for the convergence study. However, a number of interesting features can be pointed out.

First of all, the first mesh (on which the difference for the mesh containing 135 203 nodes is based), contains 66 419 nodes. The number of nodes is automatically determined to be close to the initial target of 64 000 nodes (and subsequent factor two increases of that number).

The vertical scales are different for every plot. Not also that due to the use of differences, there is no monotonically decreasing convergence curve, as discussed in Subsection 4.2.5

Note also that in the software a much larger number of interrogation points is used than the three specified by (Buchanan et al., 2009) (IF1, IS, and IF2). The interrogation point at IS is internally referred to as IP174Matrix: it is the $174^{th}$ interrogation point defined in the software, and it refers to matrix elements. Typically, at each interrogation point there will be exclusively matrix or fiber elements. However, at points on the fiber/matrix interface, there will actually be two interrogation points: IP<xyz>Matrix and IP<xyz>Fiber. This was also discussed in Subsection 4.2.5. The exact numbering of the interrogation points is usually irrelevant, except for when looking at the results at an individual interrogation point. This is not usually the case except for verification activities.

Convergence at IF1 and IF2 is similarly uneventful. In order to trace back the driving factors behind the increase to 252 003 nodes before convergence is achieved, the relevant parts of the command line output of the micromechanical amplification factor software are presented in Figure C.3.

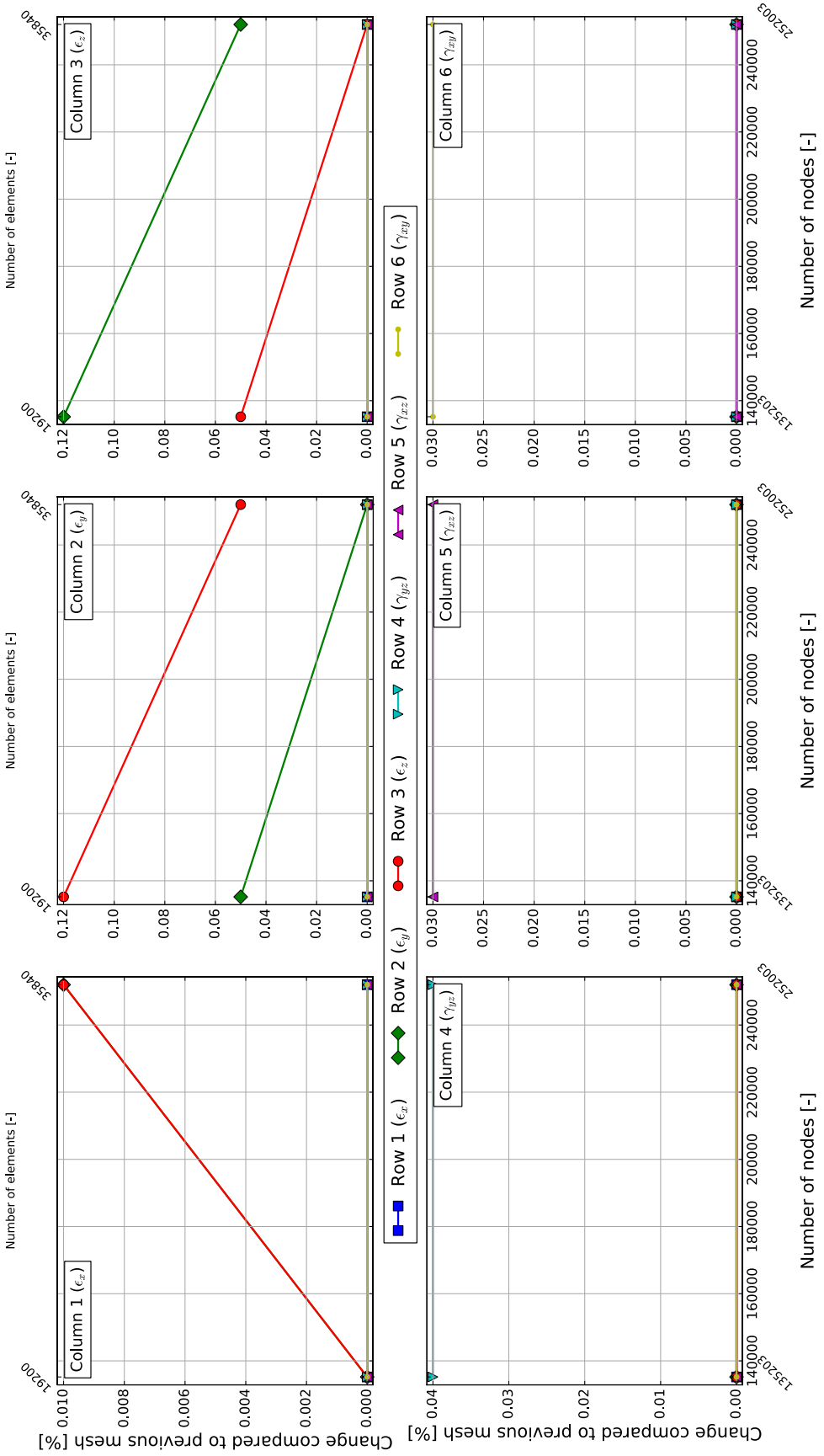


Figure C.1: Convergence study for mechanical amplification factors at IS (internally: IP174Matrix)

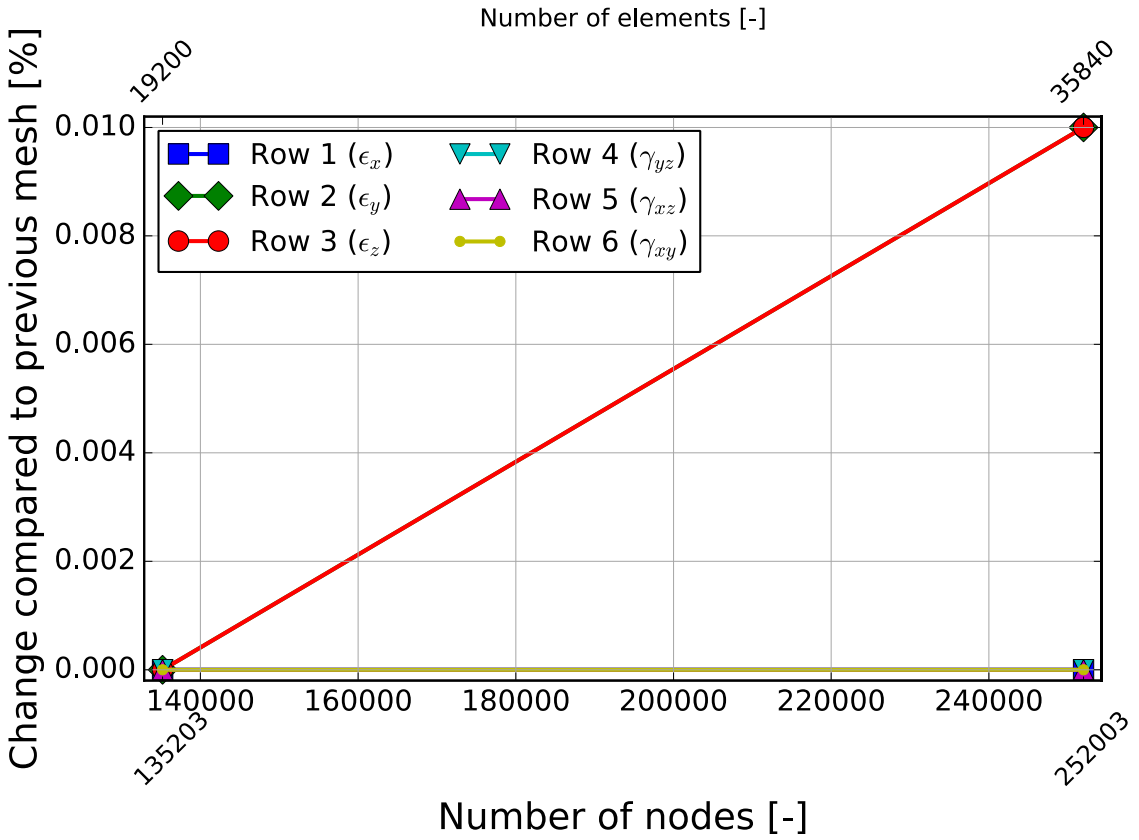


Figure C.2: Convergence study for thermal amplification factors at IS (internally: IP174Matrix)

```
Actual mesh size: 66419 nodes.

     Matrix averaging error too large at IP30Matrix (6.0%)

     Matrix averaging error too large at IP122Matrix (6.0%)

     There is/are 0 subsequent acceptable meshes.


Actual mesh size: 135203 nodes.

     Max difference between the meshes with 64000 and 128000 nodes is
     7.7% in the matrix for IP130Matrix

     There is/are 1 subsequent acceptable meshes.


Actual mesh size: 252003 nodes.

     Max difference between the meshes with 128000 and 256000 nodes is
     2.8% in the matrix for IP38Matrix

     There is/are 2 subsequent acceptable meshes.


Convergence study concluded.
```

Figure C.3: Relevant command line output during automatic convergence study

Based on the command line output in Figure C.3, two reasons for the lack of convergence at 135 203 nodes can be identified. First of all, element result averaging at IP30Matrix and IP122Matrix fails, resulting in a 6% error each for the first mesh. This means that the mesh with 66 419 nodes is not acceptable. Since two subsequent acceptable meshes should be converged, the convergence study progresses to the analysis of a mesh of approximately 128 000 nodes (in this case 135 203 nodes). At this mesh refinement level, there are no matrix averaging problems anymore.

Figure C.4 shows the local mesh at IP122Matrix, located at the red dot in the upper right of the picture. It is surrounded by elements with relatively sharp corners. This type of situation has been identified as a typical issue requiring rather fine meshes. The situation at IP30Matrix is identical. It refers to the same point as IP122Matrix, but mirrored to the upper left quarter of the unit cell.

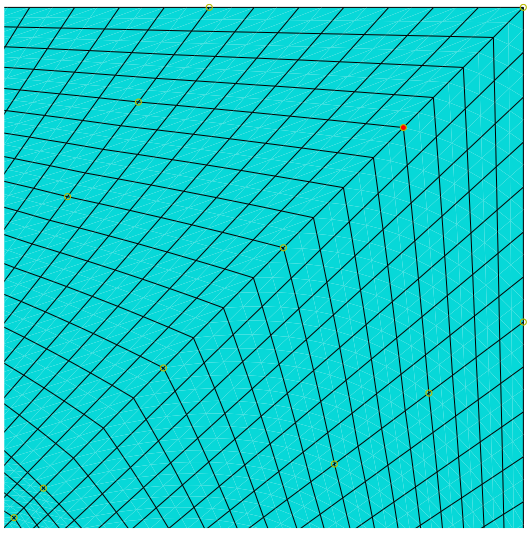

Figure C.4: Location of IP122Matrix in the unit cell.[1]

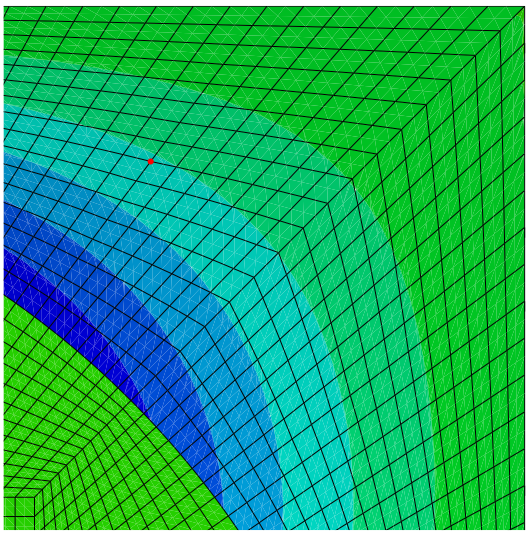

Figure C.5: Strains at IP38Matrix.[1]

Even if the first mesh had been acceptable, the convergence study would still have continued to 252 003 nodes. This is due to the lack of convergence at IP130Matrix and IP38Matrix. The strains at IP38Matrix is shown in Figure C.5 ($\gamma_{13}$ for applied $\gamma_{12}$). IP130Matrix refers to the same location in the opposite quarter of the unit cell. These points lie in a high gradient zone, meaning that the change in results from a mesh with 66 419 nodes to one with 135 203 nodes is too large.

Figure C.6 contains the convergence study for the mechanical amplification factors at IP130Matrix, while the thermal amplification factor convergence is presented in Figure C.7. The results for IP38Matrix would be identical except for a change in signs.

As seen in Figure C.3 the convergence study concluded at 252 003 nodes. The total runtime for this case was slightly under ten minutes on the system described in the introduction to Chapter 4. This is a fairly typical value, showing the strength and simplicity of obtaining fully converged strain amplification factors using the automated software tool.

[1] The thin white lines visible on some screens / print outs are caused by a rendering problem in the Abaqus vector graphics export and do not carry any meaning.

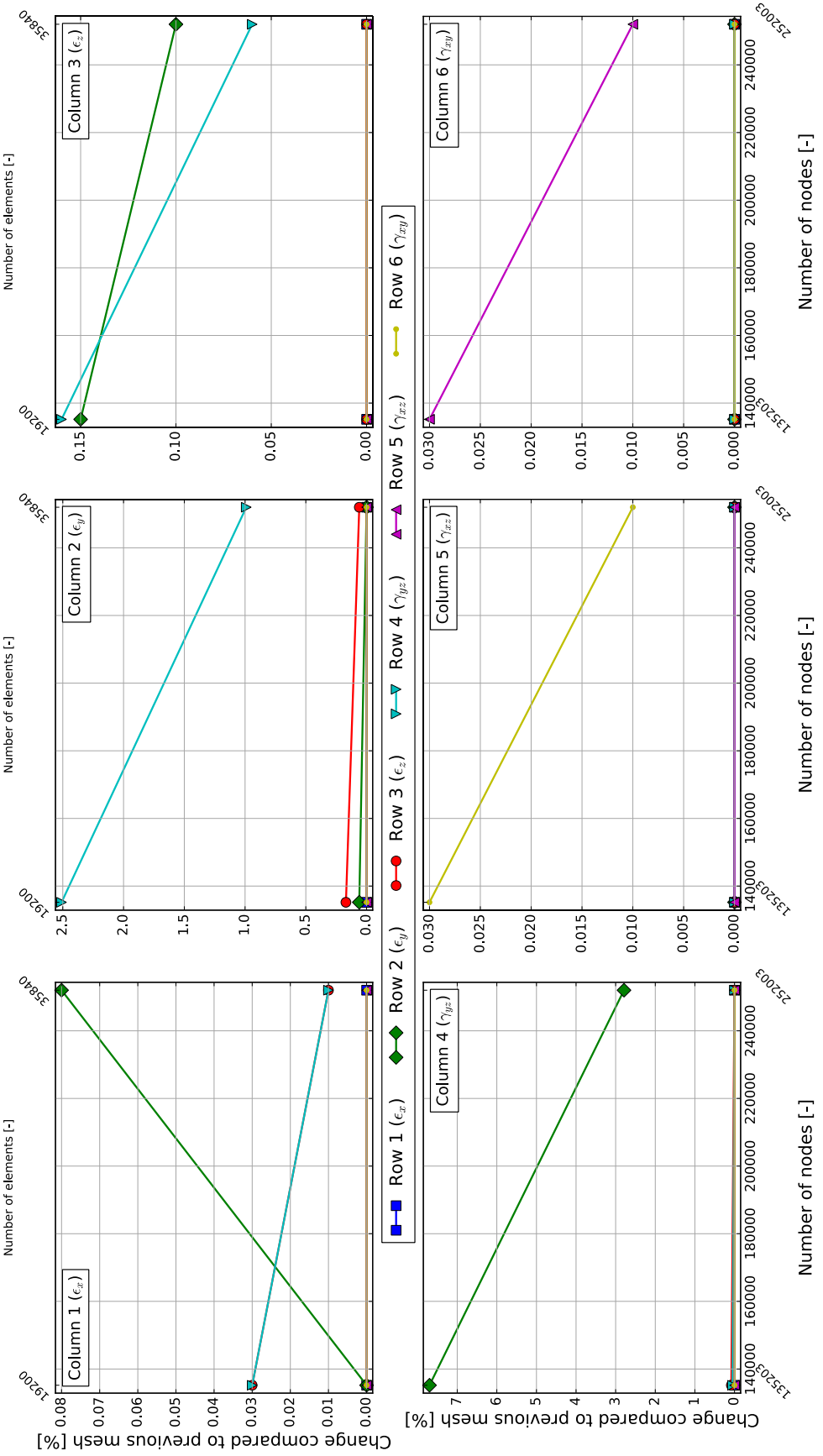


Figure C.6: Convergence study for mechanical amplification factors at IP130Matrix

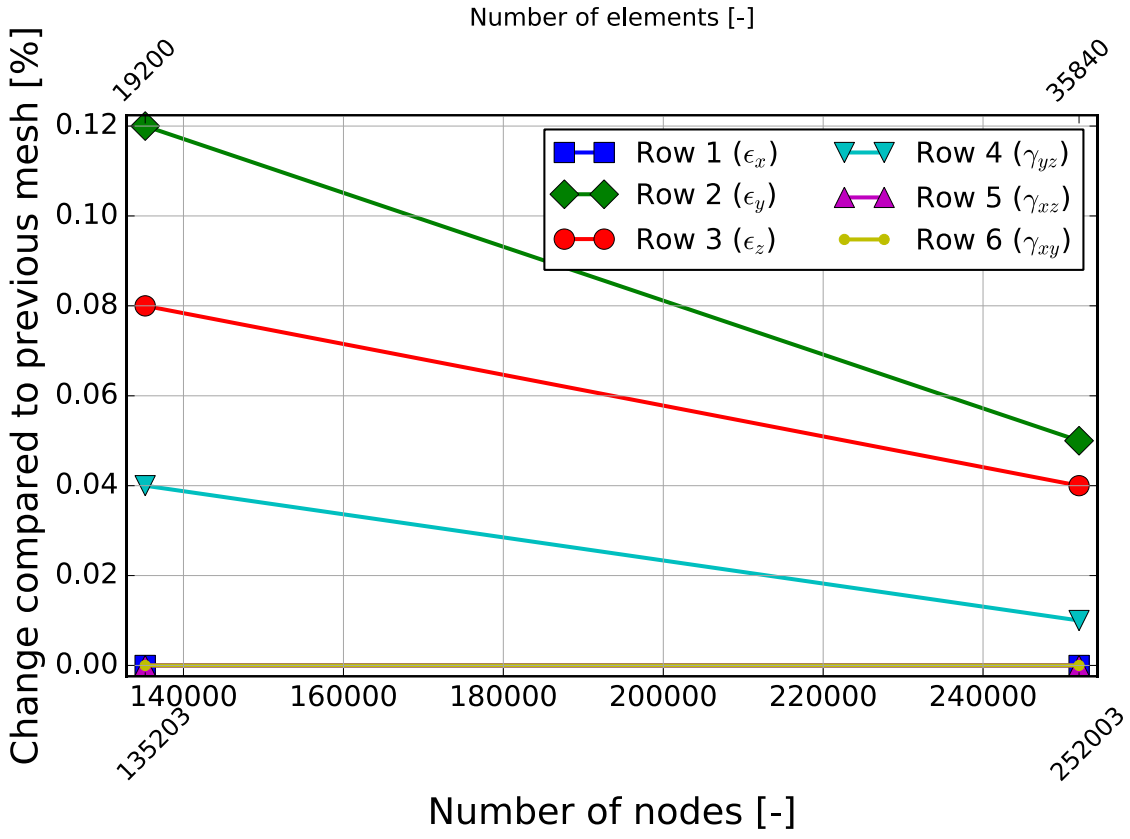


Figure C.7: Convergence study for thermal amplification factors at IP130Matrix

# Appendix D

# Input Data for Validation and Research

This appendix contains the available test data mentioned in Section 6.1 in tabulated form for reference purposes. In addition to that, it contains the input data required to determine the micromechanical enhancement factors and generate failure envelopes (see Subsection 3.5.4).

## D.1 AS4/3501-6

Table D.1 the constituent and lamina material properties required for the micromechanical enhancement calculations and fiber envelope generation. Properties in 2- and 3-directions are assumed to be identical (e.g. $E_3 = E_2$ or $G_{13} = G_{12}$). $\nu_{23}$ is calculated based on the relationship for isotropic materials ($G = \frac{E}{2(1+\nu)} \rightarrow \nu = \frac{E}{2G} - 1$), using $G_{23}$ and $E_2 = E_3$.

Table D.1: Constituent and lamina material properties for AS4/3501-6 (Soden et al., 1998, Tables 1-3). Values in brackets are assumed or calculated.

| Property | Matrix material | Fiber material | Lamina |
|---|---|---|---|
| $E_1$ [Pa] | 4.2e9 | 225e9 | 126e9 |
| $E_2$ [Pa] | | 15e9 | 11e9 |
| $E_3$ [Pa] | | (15e9) | (11e9) |
| $G_{12}$ [Pa] | 1.567e9 | 15e9 | 6.6e9 |
| $G_{13}$ [Pa] | | 15e9 | (6.6e9) |
| $G_{23}$ [Pa] | | 7e9 | (3.93e9) |
| $\nu_{12}$ [−] | 0.34 | 0.2 | 0.28 |
| $\nu_{13}$ [−] | | 0.2 | 0.28 |
| $\nu_{23}$ [−] | | (0.071) | 0.4 |
| $\alpha_1$ [$°C^{-1}$] | 45e-6 | −0.5e-6 | −1e-6 |
| $\alpha_2$ [$°C^{-1}$] | | 15e-6 | 26e-6 |
| $\alpha_3$ [$°C^{-1}$] | | (15e-6) | (26e-6) |

No volume fraction is given in either of the two sources used for test data. Therefore, the value found in (Soden et al., 1998, Table 1) – $V_f = 0.6$ – is used. (Swanson & Christoforou, 1986) give a curing temperature of $175°C$, resulting in $\Delta T = -155°C$.

Biaxial failure strains for various versions of quasi-isotropic laminates are given. Note that sometimes multiples (e.g. [0/±45/90/0/±45/90]s) or shuffled versions of the laminates are used. However, as discussed in Subsection 3.2.2, this does not matter for the resulting curing strains.

Part of the data has been digitized from a figure using the WebPlotDigitizer available at http://arohatgi.info/WebPlotDigitizer/app/ since no tabulated data was available.

The 0° ply is aligned with the $x$-direction, although this is irrelevant for quasi-isotropic laminates (which are rotation-symmetric for every increment of 45°). The digitized data is a superset of the tabulated data. Given the good agreement between tabulated and digitized data, only the digitized data will be used for the comparison.

It should also be mentioned that the axial load specimens (the last four entries in the data digitized from the plot, where $\epsilon_x$ is between 0.21 and 0.28) appear to use a [0/90]s layup according to (Swanson & Nelson, 1986). However, as also mentioned in Subsection 6.3.2 adding ±45° plies does not change the curing strains because their effect is identical in both directions. Therefore, all data can be included in the same plot.

Table D.2: Failure strains of AS4/3501-6 for a quasi-isotropic laminate

| [90/±45/0]s, tabulated data (Swanson & Christoforou, 1986, Table 2) | | [0/±45/90]s, digitized from plot (Swanson & Nelson, 1986, fig. 6) | |
|---|---|---|---|
| $\epsilon_x$ [%] | $\epsilon_y$ [%] | $\epsilon_x$ [%] | $\epsilon_y$ [%] |
| 1.23 | −0.341 | 1.2 | −0.34 |
| 1.44 | −0.16 | 1.4 | −0.16 |
| 1.455 | −0.363 | 1.4 | −0.36 |
| 1.52 | −0.225 | 1.5 | −0.22 |
| 1.4 | −0.275 | 1.4 | −0.27 |
| 1.33 | −0.043 | 1.3 | −0.033 |
| 1.34 | 0.31 | 1.3 | 0.31 |
| 1.44 | 0.34 | 1.4 | 0.35 |
| 1.4 | 0.42 | 1.4 | 0.43 |
| 1.43 | 0.787 | 1.4 | 0.8 |
| | | 1.5 | −0.35 |
| | | 1.7 | −0.54 |
| | | 1.4 | −0.46 |
| | | 1.3 | −0.75 |

| [90/±45/0]s, tabulated data (Swanson & Christoforou, 1986, Table 2) | | [0/±45/90]s, digitized from plot (Swanson & Nelson, 1986, fig. 6) | |
|---|---|---|---|
| $\epsilon_x$ [%] | $\epsilon_y$ [%] | $\epsilon_x$ [%] | $\epsilon_y$ [%] |
| | | 1.4 | −0.82 |
| | | 0.99 | −0.77 |
| | | 0.69 | −0.66 |
| | | 1 | −1.1 |
| | | 0.75 | −0.86 |
| | | 0.75 | −0.97 |
| | | 0.21 | −0.61 |
| | | 0.25 | −0.8 |
| | | 0.28 | −0.94 |
| | | 0.24 | −0.87 |

For the critical invariants of AS4/3501-6, (Lu, 2015, Table 4) reports values of $J_1^{*m} = 0.0301$, ${\epsilon^*_{eqv}}^m = 0.198$, and ${\epsilon^*_{eqv}}^f = 0.021$. On the other hand, (C. H. Wang, 2005, Table 8.4) reports ${\epsilon^*_{eqv}}^f = 0.021$. Both values are very close to the "default" value of ${\epsilon^*_{eqv}}^f = 0.02$ found in Subsection 6.2.4, which will be used for the initial investigation in Subsection 6.3.1. Similarly, ${\epsilon^*_{eqv}}^m$ is very close to the "default" value of 0.02, which will be used as well. The final required input parameter is $J_1^{*m}$. For this value, the reported value differs significantly from the range $J_1^{*m} = 0.024 \pm 15\%$ suggested in Subsection 6.2.5. This topic is investigated in Subsection 6.3.1.

In (Soden et al., 2002, fig. 10), the authors note the location of suspected matrix failure (in stress space). A change in slope of the stress/strain curve was used as the sole indicator, which is not necessarily a very accurate way of determining failure. This data is converted to strain space, notwithstanding the issues of using stress-based data as discussed in Subsection 2.2.1. Table D.3 contains the data sampled from (Soden et al., 2002, fig. 10).

Table D.3: Suspected matrix cracking for AS4/3501-6 (in stress space)

| $\sigma_x$ [$Pa$] | $\sigma_y$ [$Pa$] |
|---|---|
| 401e6 | 227e6 |
| 351e6 | 194e6 |
| 451e6 | 168e6 |
| 410e6 | 135e6 |
| 401e6 | 108e6 |
| 380e6 | 40e6 |
| 421e6 | 31e6 |

Using Eqn. (3.11), the laminate in-plane stiffness matrix can be determined to be

$$\boldsymbol{Q}_{laminate} = \begin{bmatrix} 55.8 & 16.3 & 0 \\ 16.3 & 55.8 & 0 \\ 0 & 0 & 19.8 \end{bmatrix} \cdot 1e9\ [Pa].$$

By carrying out the multiplication $\boldsymbol{Q}^{-1}_{laminate} \cdot [\sigma_x \quad \sigma_y \quad 0]^T$ for each of these data points, the suspected matrix cracking data is converted to strain space. Table D.4 shows the resulting information.

Table D.4: Suspected matrix cracking for AS4/3501-6 (in strain space)

| $\epsilon_x$ [%] | $\epsilon_y$ [%] |
|---|---|
| 0.66 | 0.22 |
| 0.58 | 0.18 |
| 0.79 | 0.07 |
| 0.73 | 0.03 |
| 0.72 | −0.02 |
| 0.72 | −0.14 |
| 0.81 | −0.18 |

## D.2 T800s/3900-2

For T800s/3900-2, the required input data is given in Table D.5. Note that these material properties are almost identical to the ones given by Yudhanto for IM7/Epoxy (see Section B.4).

Table D.5: Constituent and lamina material properties for T800s/3900-2 (Tran, 2012, Table 3-3)

| Property | Matrix material | Fiber material | Lamina |
|---|---|---|---|
| $E_1$ [Pa] | 3.3e9 | 303e9 | 152e9 |
| $E_2$ [Pa] | | 15.2e9 | 8e9 |
| $E_3$ [Pa] | | 15.2e9 | 8e9 |
| $G_{12}$ [Pa] | 1.22e9 | 9.65e9 | 4e9 |
| $G_{13}$ [Pa] | | 9.65e9 | 4e9 |
| $G_{23}$ [Pa] | | 6.32e9 | 2.75e9 |
| $\nu_{12}$ [−] | 0.35 | 0.2 | 0.34 |
| $\nu_{13}$ [−] | | 0.2 | 0.34 |
| $\nu_{23}$ [−] | | 0.2 | 0.45 |
| $\alpha_1$ [$°C^{-1}$] | 57.6e-6 | 0 | 3.6e-8 |
| $\alpha_2$ [$°C^{-1}$] | | 8.3e-6 | 37.8e-6 |
| $\alpha_3$ [$°C^{-1}$] | | 8.3e-6 | 37.8e-6 |

(Swanson & Qian, 1992) do not state the volume fraction. Based on the manufacturer datasheet (http://www.toraycfa.com/pdfs/T800SDataSheet.pdf), a volume fraction of $V_f = 60\%$ is used. The same source mentions a curing temperature of $177°C$, resulting in an assumed applied temperature difference to room temperature of $\Delta T = -157°C$.

Biaxial failure strains for three different laminates are available, shown in Table D.6. As in Section D.1, sometimes multiples of the laminates are used. For the two cases where the failure strain is given as exceeding a certain value (e.g. >0.8), that value will be used.

The 0° ply is aligned with the $x$-direction. For [0/±45/90]s and [0/$(\pm45)_2$/90]s, this is not relevant since they are symmetric with respect to a 90° rotation. However, for the laminate containing additional 0° plies, the alignment of the laminate is important.

Table D.6: Failure strains of T800s/3900-2 for three different laminates

| [0/±45/90]s (Swanson & Qian, 1992, Table 3) | | [$0_3$/±45/90]s (Swanson & Qian, 1992, Table 4) | | [0/$(\pm45)_2$/90]s (Swanson & Qian, 1992, Table 5) | |
|---|---|---|---|---|---|
| $\epsilon_x$ [%] | $\epsilon_y$ [%] | $\epsilon_x$ [%] | $\epsilon_y$ [%] | $\epsilon_x$ [%] | $\epsilon_y$ [%] |
| 1.145 | −0.361 | 1.169 | −0.314 | 1.175 | −0.525 |
| 1.321 | −0.511 | 1.235 | −0.358 | 1.294 | −0.615 |
| 1.348 | −0.436 | 1.068 | −0.324 | 1.237 | −0.521 |
| 1.299 | 0.828 | 1.173 | 0.805 | 1.25 | 0.539 |
| 1.28 | 0.838 | 1.149 | >0.75 | 1.032 | 0.507 |
| 1.368 | >0.8 | 1.498 | 1.094 | 1.298 | 0.586 |
| 1.213 | −0.755 | 1.052 | 0.838 | 1.277 | −1.053 |
| 1.342 | −0.744 | 1.024 | −0.812 | 1.218 | −1.003 |
| 1.301 | −0.722 | 0.961 | −0.831 | 0.983 | −0.857 |
| 1.005 | −1.334 | 1.024 | −0.863 | | |
| 1.084 | −1.084 | | | | |
| 0.99 | −1.101 | | | | |

Regarding the critical invariants, in Subsection 6.2.2 a very large spread of values was reported for the critical dilatational invariant of the matrix. This spread coincided almost exactly with the default range of values suggested. Therefore, $J_1^{*m} = 0.024$ will be used. For ${\epsilon^*_{eqv}}^m$, the values found in Subsection 6.2.3 were almost identical to the default value of 0.2. Therefore, the default value will be used. Finally, for ${\epsilon^*_{eqv}}^f$ no data is available. Once again the default value will be used, in this case 0.02.

In summary, this means that the default values suggested in Subsection 6.2.5 will be used for all three critical invariants.

## D.3 IM7/8551-7

Table D.7 shows the constituent and lamina material properties for IM7/8551-7. As for AS4/3501-6 in Section D.1, properties in 2- and 3-directions are assumed identical, and the relationship for isotropic materials is used to calculate unknown properties.

Table D.7: Constituent and lamina material properties for IM7/8551-7 (Kaddour & Hinton, 2012, Tables 1-3). Values in brackets are assumed or calculated.

| Property | Matrix material | Fiber material | Lamina |
|---|---|---|---|
| $E_1$ [Pa] | 4.08e9 | 276e9 | 165e9 |
| $E_2$ [Pa] | | 19e9 | 8.4e9 |
| $E_3$ [Pa] | | 19e9 | 8.4e9 |
| $G_{12}$ [Pa] | 1.478e9 | 27e9 | 5.6e9 |
| $G_{13}$ [Pa] | | (27e9) | 5.6e9 |
| $G_{23}$ [Pa] | | 7e9 | 2.8e9 |
| $\nu_{12}$ [−] | 0.38 | 0.2 | 0.34 |
| $\nu_{13}$ [−] | | 0.2 | 0.34 |
| $\nu_{23}$ [−] | | (0.357) | 0.5 |
| $\alpha_1$ [$°C^{-1}$] | 46.7e-6 | −0.4e-6 | −1e-6 |
| $\alpha_2$ [$°C^{-1}$] | | 5.6e-6 | 18e-6 |
| $\alpha_3$ [$°C^{-1}$] | | 5.6e-6 | 18e-6 |

(Colvin & Swanson, 1990) give a volume fraction of 57.3%. Note that this disagrees with the volume fraction for which the lamina properties are given (60%). However, the differences should be minor. This is investigated in Section 7.3. A stress-free temperature of $177°C$ is used based on (Kaddour & Hinton, 2012), resulting in a difference to room temperature of $\Delta T = -157°C$.

Two sets of test data are available, as summarized in Table D.8. One set consists of biaxial ($\epsilon_x$ vs $\epsilon_y$) test data for a [90/45/-45/0]s laminate, whereas the other one contains transverse strain vs shear data for a 90° uniaxial test specimen. As in Section D.1, sometimes multiples of the laminate are used, which does not affect the failure predictions in any way. 0° is aligned with the $x$-direction.

Table D.8: Failure strains of IM7/8551-7 for one laminate and one ply

| [90/±45/0]s (Colvin & Swanson, 1990, Table 3) | | 90° uniaxial (Colvin & Swanson, 1990, Table 1) | |
|---|---|---|---|
| $\epsilon_x$ [%] | $\epsilon_y$ [%] | $\epsilon_y$ [%] | $\gamma_{xy}$ [%] |
| 1.352 | −0.424 | −3.14 | 0.04 |
| 1.316 | −0.372 | −3.24 | 0.05 |
| 1.337 | 0.312 | −3.13 | 0.05 |
| 1.359 | 0.335 | −3.07 | 4.25 |
| 1.403 | −0.735 | −3.21 | 1.42 |
| 1.12 | −0.862 | −0.71 | 2.69 |

| [90/±45/0]s (Colvin & Swanson, 1990, Table 3) | | 90° uniaxial (Colvin & Swanson, 1990, Table 1) | |
|---|---|---|---|
| $\epsilon_x$ [%] | $\epsilon_y$ [%] | $\epsilon_y$ [%] | $\gamma_{xy}$ [%] |
| 1.336 | −1.035 | −0.18 | 5.04 |
| 1.054 | −1.118 | −3.54 | 4.5 |
| 1.109 | −1.119 | 0.49 | 7.29 |
| 0.275 | −0.935 | | |
| 0.387 | −1.295 | | |

For IM7, the critical invariant was found in Subsection 6.2.4 to be very close to the "default" value of ${\epsilon^*_{eqv}}^f = 0.02$. Since for 8551-7 no data is available, the default values summarized in Subsection 6.2.5 will be used for the matrix as well, meaning $J_1^{*m} = 0.024$ and ${\epsilon^*_{eqv}}^m = 0.2$.

# Appendix E

## List of Critical Invariants

This appendix contains the list of all critical invariants found in literature, as discussed in Section 6.2. The source(s), material combination, and potential comments are included, as well as the definition used for the critical distortional invariant (see Subsection 2.1.1). In addition to that, sources are numbered by an entry number in order to reduce the amount of text in the axis labels in Figures 6.1 to 6.3. Content missing for a particular entry (for example the definition number in case no equivalent strain results are available) is left blank. The order is essentially chronologically.

The general structure of each entry is shown in Table E.1, while Table E.2 contains the full list of critical invariants.

Table E.1: Example structure of entry in list of critical invariants

| Source(s) | Entry # | Material combination |
|---|---|---|
| Critical dilatational matrix invariant | Critical distortional matrix invariant | Critical distortional fiber invariant |
| Comments | | Definition used for distortional invariants |

Table E.2: List of critical invariants

| | | |
|---|---|---|
| (Gosse & Christensen, 2001, Table 1) | [1] | IM7/5250-4 |
| 0.016 or 0.0171 | | |
| The critical dilatational matrix invariant is given separately for tests of two different laminates. | | |
| (Gosse & Christensen, 2001, Table 2) | [2] | IM7/PETI-5 or 977-3 |
| 0.0216 or 0.0205 (twice) or 0.0194 | | |
| In the body of the text, PETI-5 is mentioned as the resin. However, the table heading states 977-3. | | |
| $J_1^{*m}$ is given separately for tests of four different laminates. | | |

| | | |
|---|---|---|
| (Gosse & Christensen, 2001, Table 3) | [3] | T300/5208 |
| 0.0105 | 0.0339 or 0.0331 | |
| The critical distortional matrix invariant is given separately for tests of a uniaxial coupon at two different off-axis tension angles. | | Definition #1 |
| (Tsai & Elmore, 2003, Section 4.2) | [4] | IM7/977-3 |
| 0.0244 | 0.11 | 0.02 |
| The equations for the invariants are not stated. | | Definition #? |
| (Ng et al., 2004, Table 5) | [5] | IM7/5250-4 |
| 0.014 or 0.0142 or 0.015 or 0.0155 | 0.16 | 0.0204 |
| The critical dilatational invariant is given for different off-axis tension tests. | | Definition #1 |
| (Hart-Smith, 2010, fig. 24; Tan, 2005, p. 76; Tay, Tan, Tan, et al., 2005, Section 5) | [6] | IM7/977-3 |
| 0.023 | 0.103 | 0.0182 |
| All references cite (personal communication with) Gosse as the source for the critical invariant.<br>There is a typo in the article by (Tay, Tan, Tan, et al., 2005); it states that the critical distortional matrix invariant is 0.013.<br>Note that the critical distortional invariants are identical to the values in entry [14], while the critical dilatational invariant is different. On the other hand, the critical invariant is identical to the one given by Gosse in entry [13], although the material stated there is IM7/K3B. | | Definition #1 |
| (C. H. Wang, 2005, Table 8.4) | [7] | AS4/3501-6 |
| | | 0.019 |
| The critical value is determined based on strength test data. | | Definition #1 |
| (C. H. Wang, 2005, Table 8.4) | [8] | T300/BSL914C |
| | | 0.0133 |
| See previous entry for comments. | | Definition #1 |
| (C. H. Wang, 2005, Table 8.4) | [9] | E-glass 21xK43/LY556 |
| | | 0.0266 |
| See previous entry for comments. | | Definition #1 |
| (C. H. Wang, 2005, Table 8.4) | [10] | E-glass 1200tex/MY750 |
| | | 0.0349 |
| See previous entry for comments. | | Definition #1 |

| | | |
|---|---|---|
| (Yudhanto et al., 2006, Table 1) | [11] | IM7/K3B |
| | | 0.0195 |
| Critical invariants cited from an article by Gosse which could not be found. | | Definition #1 |

| | | |
|---|---|---|
| (Yudhanto et al., 2006, Table 1) | [12] | IM7/977-3 |
| 0.0272 | 0.179 | |
| See comment for previous entry. | | Definition #1 |
| Note also that entry [14] reports a very similar value of the critical dilatational invariant for the same material, while the value of the critical distortional matrix invariant differs by approximately a factor of $\sqrt{3}$. This corresponds to the difference between definitions #1 and #2. | | |

| | | |
|---|---|---|
| (Gosse et al., 2007, Slide 16) | [13] | IM7/K3B |
| 0.023 or 0.0224 | | |
| The critical dilatational invariant is given separately for 0° and ±10° compression coupons. | | |

| | | |
|---|---|---|
| (Eng, 2007, Table 1; Liu, 2007, Table 3.1; Yudhanto, 2005, Table 3-1) | [14] | IM7/977-3 |
| 0.0274 | 0.103 | 0.0182 |
| All references cite (personal communication with) Gosse as the source for the critical invariant. | | Definition #1 |
| Note that the critical distortional invariants are identical to the values in entry [6], while the critical dilatational invariant is different. | | |
| See also comment in entry [12]. | | |

| | | |
|---|---|---|
| (Holmberg, Lundmark, & Mattsson, 2008, Table 1) | [15] | E-glass/MY750 |
| 0.0297 | 0.036 or 0.0313 | 0.0194 |
| The critical distortional matrix invariant is based on two separate tests, one transverse compression test and one in-plane shear test. | | Definition #1 |
| An attempt is made to modify the procedure by implicitly including manufacturing strains in the invariants. The set of invariants reported here does not contain this modification. The authors also consider a separate compression invariant for the fiber (its value is found to be 0.0125). All in all their procedure seems somewhat suspect. | | |

| | | |
|---|---|---|
| (McNaught, 2009, Table 6-3) | [16] | E-glass/RTM6 |
| 0.011694 | 0.020069 | 0.022434 |
| | | Definition #1 |

| | | |
|---|---|---|
| (Pipes & Gosse, 2009, Tables 1 and 2) | [17] | Carbon/glassy polymer |
| 0.0242 (twice) or 0.0233 or 0.0238 or 0.0226 or 0.024 or 0.0237 | 0.1144 or 0.1124 or 0.1164 or 0.114 | |
| The invariants are determined based on different off-axis tension tests. | | Definition #2 |
| (Mao, 2011, Table 5-11) | [18] | E-glass/MTM57 |
| 0.0208 or 0.021 or 0.0212 or 0.0215 or 0.0217 | 0.1472 | 0.0189 |
| The strain amplification factors could not be reproduced (see Subsection 5.1.3). | | Definition #1 |
| The critical distortional invariant for the fiber is estimated based on the trend of the data. | | |
| The critical dilatational invariant is based on different off-axis tension tests. | | |
| Mao's gives nearly identical values using one definition of the critical distortional matrix invariant, but then obtains vastly different values using the standard definition. Only the main value (which could be confirmed) is reported here. | | |
| (Tran et al., 2011, Table 3) | [19] | T300/Cycom 970 |
| 0.0224 or 0.0233 | | |
| The two values correspond to different modeling strategies. | | |
| The values are quite different from the ones in entry [23] for Cycom 970, but very similar to the ones in entry [24] for 3900-2. | | |
| (Z. Li et al., 2011, Table 3) | [20] | CCF300/5228 |
| 0.0191 | 0.144 | 0.017 |
| It seems that a factor $\frac{1}{\sqrt{2}}$ is missing in the definition for the critical distortional invariant. However, (X. Li, Guan, Liu, & Li, 2013) contains the same critical invariants and uses the correct definition. Therefore, it is assumed that the missing factor is simply a mistake in the article. | | Definition #1 |
| This paper is in Chinese. | | |
| (Z. Li et al., 2011, Table 3) | [21] | CCF300/5428 |
| 0.0319 | 0.195 | 0.018 |
| See previous entry for comments. | | Definition #1 |
| (Z. Li et al., 2011, Table 3) | [22] | T700/5428 |
| 0.0313 | 0.202 | 0.023 |
| See previous entry for comments. | | Definition #1 |
| (Tran, 2012, Table 5-2) | [23] | T300/Cycom 970 |
| 0.036 or 0.035 or 0.033 (twice) | 0.118 (twice) | |
| Data is from different off-axis tension specimens. | | Definition #2 |

| | | |
|---|---|---|
| (Tran, 2012, Table 5-3) | [24] | T800s/3900-2 |
| 0.023 (3 times) or 0.027 or 0.02 or 0.021 | 0.119 or 0.117 or 0.113 | |
| Data is from different off-axis tension specimens. | | Definition #2 |
| (Tran, Kelly, et al., 2012, Table 4) | [25] | T300/Cycom 970 |
| | 0.1125 or 0.1186 or 0.1184 | |
| Data is from different modeling strategies for 10° and 20° off-axis tension specimens. | | Definition #2 |
| (Tran et al., 2013, Tables 4 and 5) | [26] | T300/Cycom 970 |
| 0.0335 or 0.0347 or 0.0348 | 0.118 or 0.121 or 0.122 | |
| Data corresponds to different modeling strategies. | | Definition #2 |
| (Tran et al., 2013, Tables 4 and 5) | [27] | T800s/3900-2 |
| 0.0229 or 0.0244 or 0.02445 | 0.119 or 0.117 or 0.118 | |
| Data corresponds to different modeling strategies. | | Definition #2 |
| (Tran, Simkins, et al., 2012, Table 2) | [28] | T800s/3900-2 |
| 0.0225 | 0.117 | |
| | | Definition #2 |
| (Kim, Park, Park, Lee, & Kim, 2013, Table 3) | [29] | T700/CU200NS |
| 0.00398 | 0.04919 | 0.01495 |
| This paper is in Korean. | | Definition #1 |
| (Lim, Pearce, Kelly, Prusty, & Crosky, 2013, Section 3) | [30] | T800s/3900-2 |
| 0.0225 | 0.119 | |
| | | Definition #2 |
| (Lee & Yoshioka, 2015, Section 4.1) | [31] | T800s/3900-2 |
| 0.02489 | 0.03434 | |
| | | Definition #4 |
| (Lu, 2015, Table 4) | [32] | AS4/3501-6 |
| 0.0301 | 0.198 | 0.021 |
| This paper is in Chinese. | | Definition #1 |